TIME-RESOLVED OPTICAL STUDY OF QUASIPARTICLE AND COLLECTIVE DYNAMICS IN IRON PNICTIDES

Anna Pogrebna

Doctoral Dissertation
Jožef Stefan International Postgraduate School
Ljubljana, Slovenia

Supervisor: Asst. Prof. Dr. Tomaž Mertelj, »Jozef Stefan« Institute, Ljubljana, Slovenia

Evaluation Board:
Prof.Dr. Victor Kabanov, Chair, »Jozef Stefan« Institute, Ljubljana, Slovenia
Dr. Alexey Kimel, Member, Institute of Molecules and Materials, Radboud University, Nijmegen, The Netherlands
Prof. Dr. Denis Arčon, Member, »Jozef Stefan« Institute, Ljubljana, Slovenia

MEDNARODNA PODIPLOMSKA ŠOLA JOŽEFA STEFANA
JOŽEF STEFAN INTERNATIONAL POSTGRADUATE SCHOOL



Anna Pogrebna

TIME-RESOLVED OPTICAL STUDY OF QUASIPARTICLE AND COLLECTIVE DYNAMICS IN IRON PNICTIDES

Doctoral Dissertation

ČASOVNO-LOČLJIVE OPTIČNE RAZISKAVE KVAZIDELČNE IN KOLEKTIVNE DINAMIKE V ŽELEZOVIH PNIKTIDIH

Doktorska disertacija

Supervisor: Asst. Prof. Dr. Tomaž Mertelj

Ljubljana, Slovenia, September 2015

To my brother...

Acknowledgments

First of all I would like to express my deepest gratitude to my adviser Prof. Tomaz Mertelj. I appreciate a lot of his infinite patience in listening to all of my ideas, an enormous enthusiasm in answering to all questions and strong motivation in demanding a high quality of work. I am very thankful for each and every debate we had, that ultimately sharpened my mind and broadened my horizons.

My sincere thanks also go to Prof. Dragan Mihailovic, who provided me an opportunity to join the team, and who gave an access to the laboratory facilities, which I couldn't even dream about before. Without his precious support it would not be possible to conduct this research.

Thank to Prof. T. Mertelj, Prof. D. Mihailovic, Prof. V. Kabanov, Prof. A.Mertelj and Prof. B. Majaron for precious time we spent within coffee-breaks, where they shared their ideas, opinions and philosophies about science, research, being scientist and about life in general.

Many thanks to those, without whom my life would turn to chaos, to the administration team: Natasa, Sabina and Martina. You took the most difficult work and let us to concentrate on science

I would like to thank to all colleagues from the department F7. Thank you for being my true friends, encouraging me and helping me with every obstacle in my research years. Thank you Jure Strle, Martin Strojnik, Ljupka Stojchevska, Joze Buh, Andrej Kovic, Peter Topolovsek and Matej Prijatelj for making our office the best office ever with a very friendly and willing environment. Thanks to Ljupka, Jure and Joze for being very patient in correcting my Slovenian. Thank you Vladimir Baranov, Igor Vaskivskyi, Gleb Veryasov, Tanja Borzda, Jure Novak and Zala Lenarcic for a strong support in personal life and for many great time spent together. Special thanks to Ivan Madan, who supported me a lot in each and every situation, was always willing to listen and to help. I appreciate all fruitful discussions about physics, philosophy and humanity.

Last but not the least, I would like to thank my family: my parents and to my brother for inspiring me and supporting spiritually throughout writing this thesis and my life in general.

Abstract

This work presents investigations of the ultrafast quasiparticle dynamics in $A\mathrm{Fe_2As_2}$ iron pnictides by means of the ultrafast time-resolved optical spectroscopy. Probing the quasiparticle relaxation in different regions of the phase diagram enables us to get a comprehensive view of the nature of the relaxation processes in the spin density wave (SDW), nematic, superconducting and ferromagnetic states in the iron pnictides.

We present the first all-optical spectrally-resolved transient reflectivity study in $A\mathrm{Fe_2As_2}$ in the SDW state. The behavior of the SDW response is analyzed in the framework of the relaxation-bottleneck model. We propose the magnon to be the most appropriate candidate for the bottleneck boson. A relation of the observed relaxation to the magnetostructural order parameter relaxation is discussed.

Also we show the possibility of the non-thermal destruction of the SDW state by ultrafast laser pulses. For the first time the evolution of the SDW order through the non-equilibrium phase transition is investigated by means of the ultrafast optical three-pulse technique. The evolution of the systems has a two-step character. Firstly, the electronic order recovers in a non-equilibrium fashion on a ps timescale, after that the quasi-equilibrium heat diffusion follows. The data suggest proportionality of the response to the coherently driven order parameter.

We present the systematic study of the isovalently doped $\mathrm{BaFe_2(As_{0.7}P_{0.3})_2}$ superconductor in low and in high excitation regimes. We show that the presence of nodes in the superconducting gap does not influence the quasiparticle relaxation. From the comparison of the effective magnitude of the superconducting gap of ~ 5 meV obtained from the low excitation data fits with the ARPES data we establish that the γ-hole Fermi surface gives the largest contribution to the optical response. In the strong excitation regime the pump-probe response is equal to the difference in reflectivity between normal and gapped states as described by the Mattis-Bardeen theory, implying complete photodestruction of the superconductivity. The photodestruction energy density is found to scale with T_c^2.

We report ultrafast magnetooptic dynamics of $\mathrm{Eu^{2+}}$ spins in $\mathrm{EuFe_2As_2}$ compounds with different levels of dopings. We show that the coupling between $\mathrm{Eu^{2+}}$ spins and Fe derivative d-bands is weak, implying the possibility of the coexistence of the singlet superconductivity with the long-range ferromagnetic order. Remarkably, the polarization analysis of the coherently excited spin wave response points towards a ferromagnetic ordering of spins with two distinct types of ferromagnetic domains.

Povzetek

Doktorsko delo obravnava ultrahitro dinamiko kvazidelcev v železovih pniktidih $A\mathrm{Fe_2As_2}$ s femtosekundno optično spektroskopijo. Merjenje relaksacije kvazidelcev na različnih območjih faznega diagrama omogoča celovit pogled na naravo relaksacijskih procesov v stanju vala spinske gostote (VSG) ter v nematskem, superprevodnem in feromagnetnem stanju v železovih pniktidih.

Večpasovna narava železovih pniktidov omogoča številne relaksacijske poti za fotovzbujene kvazidelce. Predstavljamo sistematično optično spektralno ločlivo študijo tranzentne reflektivnosti v $A\mathrm{Fe_2As_2}$ v stanju VSG. Obnašanje odziva, ki je zelo občutljivo na magnetno-strukturni fazni prehod, smo analizirali v okviru modela ozkega grla, ki vključuje magnone. Rezultate primerjamo s prejšnjimi rezultati časovno-ločljive kotne fotoemisijske spektroskopije in razpravljamo o možnih alternativnih razlagah relaksacije.

Raziskali smo netermalno uničenje stanja VSG z ultrahitrimi laserskimi sunki. V bližini faznega prehoda smo opazili kritično upočasnitev. Razvoj ureditve VSG skozi neravnovesni fazni prehod smo raziskali s pomočjo ultrahitre optične trisunkovne tehnike. Sistem se razvija v dveh korakih. Najprej se elektronski sistem vrne v osnovno stanje na časovni skali pikosekund, potem sledi toplotna difuzija. Eksperimentalni podatki kažejo na koherentno vzbuditev parametra reda.

Zaradi razkritja morebitnih učinkov superprevodnih vozelnih črt na relaksacijo fotovzbujenih kvazidelcev se je sistematična femtosekundna optična študija v optimalno isovalentno-dopiranem $\mathrm{BaFe_2(As_{0.7}P_{0.3})_2}$ izvajala v nizkem in visokem režimu vzbujanja. Relaksacijski procesi ozkega grla skozi režo v vrzelnem žepu Fermijeve površine prevladujejo v nizkem režimu vzbujanja. V močnem režimu vzbujanja pa je signal posledica razlike med normalnim stanjem in stanjem z režo. Gostota energije optičnega uničenja se obnaša linearno s T_c^2.

Raziskali smo ultrahitro magneto-optično dinamiko spinov $\mathrm{Eu^{2+}}$ v spojinah $\mathrm{EuFe_2As_2}$ z različnimi stopnjami dopiranja. Pokazali smo, da je sklopitev med spini $\mathrm{Eu^{2+}}$ in d-pasove, ki izhajajo iz Fe, šibka, kar pomeni sožitje dolgoročnega feromagnetnega reda s superprevodnostjo. Analiza polarizacije odziva koherentno vzbujenih valov gostote spina kaže proti preprostemu feromagnetnemu redu spinov z dvema različnima tipoma feromagnetnih domen.

Contents

List of Figures **xvii**

List of Tables **xxi**

Abbreviations **xxiii**

1 Introduction **1**
1.1 Thesis Structure . . . 1
1.2 Iron pnictides and high-temperature superconductivity . . . 3
1.2.1 General properties of iron pnictide superconductors . . . 3
1.2.2 Historical view on the problem of high-T_c superconductors . . . 5
1.2.3 High-temperature superconductivity in iron pnictides . . . 7
1.2.4 Optical properties of iron pnictides . . . 8
1.3 Spin density waves . . . 10
1.3.1 Spin density waves in solids: general theory . . . 10
1.3.2 Magnetic long-range order in pnictides . . . 13
1.4 Competing and coexisting phases in iron pnictides . . . 14
1.4.1 Coexistence of superconductivity and magnetism: general view . . . 15
1.4.2 Superconductivity and Fe magnetism in iron pnictides . . . 15
1.4.3 Superconductivity and Eu magnetism in iron pnictides . . . 16
1.5 Ultrafast optical spectroscopy: theory and experiments . . . 17
1.5.1 Transient reflectivity . . . 18
1.5.2 Electron-phonon interactions: two-temperature model and beyond . . . 19
1.5.3 Rothwarf-Taylor model . . . 20
1.5.4 Temperature dependence of the quasiparticle density and the relaxation time . . . 22
1.5.5 Optical response at strong photoexcitation . . . 23
1.5.6 Order parameter dynamics . . . 23
1.5.7 Magnetization dynamics excited by ultrafast laser pulses . . . 25
1.5.8 Time-resolved spectroscopy in iron pnictides: overview . . . 25
1.5.8.1 All-optical experiments . . . 25
1.5.8.2 Other ultrafast techniques . . . 28

2 Experimental details **31**
2.1 Standard pump-probe setup . . . 31
2.2 Broadband probe experiments . . . 32
2.3 Magnetic measurements . . . 33
2.4 Three-pulse technique . . . 33
2.5 Samples . . . 35

3 Ultrafast transient reflectivity in 122 iron pnictides **37**
3.1 General pump-probe features of the signal . . . 37

3.2 Normal state response and coherent phonons . . . 37
3.3 Polarization properties and nematic phase fluctuations . . . 40
3.4 Spin density wave response . . . 41
3.4.1 SDW suppression upon doping . . . 42
3.5 Superconducting response . . . 44
3.6 Summary and conclusions . . . 44

4 Spectrally-resolved femtosecond reflectivity relaxation dynamics in undoped SDW 122 pnictides 47
4.1 Search for additional relaxation processes . . . 47
4.2 Spectral dependence of transient reflectivity . . . 48
4.3 Singular value decomposition . . . 50
4.3.1 General principles . . . 50
4.3.2 Decomposition of experimental data . . . 50
4.4 Temperature dependence . . . 52
4.5 Bottleneck model fits . . . 53
4.6 Discussion . . . 54
4.7 Summary and conclusions . . . 57

5 Spin density wave destruction 59
5.1 SDW destruction . . . 59
5.2 Pump fluence dependence . . . 59
5.3 Saturation model . . . 60
5.4 Calculation of the destruction energy . . . 62
5.5 Thermal destruction energy . . . 64
5.6 Relaxation time behaviour . . . 65
5.7 Summary and conclusions . . . 65

6 Amplitude recovery dynamics through the photoinduced SDW phase transition 67
6.1 Destruction pulse arrives after pump . . . 67
6.2 Destruction pulse arrives before pump . . . 67
6.3 Recovery dynamics . . . 69
6.3.1 Destruction fluence dependence . . . 69
6.3.2 Recovery time . . . 70
6.4 Amplitude dynamics and QP relaxation rate . . . 71
6.5 Thermal diffusion model . . . 71
6.6 Temperature dependence . . . 72
6.7 Summary and outlook . . . 74

7 Superconducting gap in $BaFe_2(As_{1-x}P_x)_2$ from temperature dependent transient optical reflectivity 75
7.1 Fluence dependence . . . 75
7.2 Destruction energy . . . 76
7.3 Temperature dependence in strong and weak excitation regimes . . . 78
7.4 Superconducting gap . . . 79
7.5 Summary and conclusions . . . 81

8 Eu^{2+} spin dynamics 83
8.1 Peculiarities of Eu-based 122 compounds . . . 83
8.2 Low-T response in Eu-based 122 iron pnictides . . . 85

8.3 Magnetic field dependence of response 86
8.4 Coherent oscillations 88
8.5 Polarization analysis of coherent oscillations 89
8.6 Magnetic order of Eu^{2+} spins 92
8.7 Strength of the coupling between Eu and FeAs layers 93
8.8 Summary and conclusions 94

9 Conclusions **97**

Appendix A Appendix **99**

References **101**

Bibliography **129**

Biography **133**

List of Figures

Figure 1.1: Schematic representation of the six homologous phases of iron-based pnictides and chalcogenides identified at present. 3
Figure 1.2: The structure and a schematic phase diagram of 122 iron pnictides. . . 5
Figure 1.3: The Fermi surfaces of $BaFe_2(As, P)_2$. 6
Figure 1.4: The real part of the optical conductivity and a band structure of iron pnictides. 9
Figure 1.5: Wavevector dependent Lindhard function. 10
Figure 1.6: The dispersion relation and the charge/spin modulation for the two sublattices for one-dimentional SDW below the phase transition. . . . 12
Figure 1.7: Various amplitude and phase excitations for a spin density wave ground state. 12
Figure 1.8: The Fermi surface of $BaFe_2As_2$. 13
Figure 1.9: The magnetic and crystal structure of Ba-122. 15
Figure 1.10: The Eu spin ordering in 122 iron pnictides. 16
Figure 1.11: A schematic diagram of the electron processes in pump-probe experiment. 17
Figure 1.12: A schematic representation of the timing of the laser pulses in three-pulse experiment. 24
Figure 1.13: The possible excitation energy transfer paths in terms of the three temperature model. 25
Figure 1.14: Temperature dependence of the photoinduced reflectivity $\Delta R/R$ for $SmFeAsO_{0.8}F_{0.2}$. 26
Figure 1.15: The photo-induced change of the optical conductivity of Ba-122. 28

Figure 2.1: A scheme of a standard pump-probe setup. 32
Figure 2.2: Schematic of the pump-broadband-probe experiment. 33
Figure 2.3: Experimental scheme for magnetooptic measurements. 34
Figure 2.4: The schematic of the three-pulse experiment. 34
Figure 2.5: Magnetic susceptibility along the c-axis as a function of the temperature in Eu-122 and EuP-122. 35

Figure 3.1: The metallic response in the transient reflectivity measured in a few investigated iron pnictides. 38
Figure 3.2: Coherent phohon oscillations in transient reflectivity signal. 38
Figure 3.3: Illustration of two models of coherent optical phonons generation: ISRS and DECP. 39
Figure 3.4: The temperature dependence of the pump-probe response for Eu-122. . 40
Figure 3.5: Anisotropy of SDW domains in Eu-122 and EuP-122. 41
Figure 3.6: T-dependent transient reflectivity measured for the orthogonal polarizations of the probe, $\mathcal{P}^-$ and $\mathcal{P}^+$ in $EuFe_2As_2$ and $EuFe_2(As_{0.81}P_{0.19})_2$. 42

Figure 3.7: The tempearture dependence of the amplitude and the relaxation time of the SDW response, obtained from a single-exponential fit of the transient reflectivity traces. 43
Figure 3.8: The phase diagram of $Eu(Fe,Co)_2As_2$. 43
Figure 3.9: Temperature dependence of transient reflectivity of superconducting $BaFe_2(As_{0.7}P_{0.3})_2$ measured at low and high pump fluences. 44

Figure 4.1: Photoinduced reflectivity transients in $EuFe_2As_2$ as a function of the probe-photon energy just below T_{SDW}. 48
Figure 4.2: Photoinduced reflectivity transients in $BaFe_2As_2$ as a function of the probe-photon energy just below and just above T_{SDW}. 49
Figure 4.3: Photoinduced reflectivity transients in $SrFe_2As_2$ as a function of the probe-photon energy just below T_{SDW}. 49
Figure 4.4: A few temporal eigenvectors with the highest singular values. 51
Figure 4.5: Spectral dependence of the three most significant SVD temporal-eigenvectors weights just below respective T_{SDW}. 51
Figure 4.6: The risetime/resolution parameter and the longest relaxation time as a function of T. 52
Figure 4.7: The amplitude of the $\Delta R/R$ transients in $BaFe_2As_2$ as a function of T. 53
Figure 4.8: The amplitude of the $\Delta R/R$ transients in $EuFe_2As_2$ as a function of T. 54
Figure 4.9: The amplitude of the $\Delta R/R$ transients in $SrFe_2As_2$ as a function of T. 55
Figure 4.10: Spectral dependence of the fit amplitudes for all three samples. 56

Figure 5.1: The photoinduced reflectivity $\Delta R/R$ in $EuFe_2As_2$ at various photoexcitation fluences. 60
Figure 5.2: The photoinduced reflectivity $\Delta R/R$ in $SrFe_2As_2$ as a function of the pump fluence. 61
Figure 5.3: The photoinduced reflectivity $\Delta R/R$ in $BaFe_2As_2$ as a function of the photoexcitation fluence. 62
Figure 5.4: The amplitude of the SDW response as a function of the pump fluence, measured at 65 K for Sr-122 and Ba-122 for two orthogonal polarizations of the probe beam. 63
Figure 5.5: The planar destruction energy of SDW order in parent undoped 122 iron pnictides as a function of square of transition temperature. 64
Figure 5.6: The change of the internal energy with T calculated for $EuFe_2As_2$ from the specific heat data. 65
Figure 5.7: Normalized transient reflectivity measured for $EuFe_2As_2$ at 68 K as a function of the pump fluence. The relaxation rate as a function of the pump fluence compared with the transient amplitude. 66

Figure 6.1: The transient reflectivity as a function of the time delay between pump (P) and probe (pr) pulses, measured as a function of the delay between the destruction (D) and pump pulses for different D fluences. 68
Figure 6.2: The transient reflectivity as a function of t_{P-pr} measured for different delays between D and P pulses, when the D pulse arrives before P. . . . 69
Figure 6.3: The transient reflectivity in three-pulse experiment as a function of pump-probe delay, measured for different D-P delays. 70
Figure 6.4: The maximum amplitude in the three-pulse experiment as a function of t_{D-P} delay, plotted for different destruction fluences. 70
Figure 6.5: The comparison of the recovery time and the relaxation time as a function of destruction and pump fluence. 71

Figure 6.6: The QP relaxation rates and the amplitude recovery dynamics as a function of delay t_{D-P} for a few different destruction fluences. 72
Figure 6.7: The comparison of the amplitude recovery dynamics and the adiabatic amplitude dynamics obtained by means of thermal diffusion model . . . 73
Figure 6.8: The SDW order parameter dynamics as a function of destruction fluence measured at different temperatures. 73

Figure 7.1: The photoinduced reflectivity transients $\Delta R/R$ in $BaFe_2(As_{0.7}P_{0.3})_2$ measured as a function of pump fluence in the superconducting and normal state. 76
Figure 7.2: The fluence dependence of the transient amplitude and the dominant relaxation time in the superconducting state. 77
Figure 7.3: The in-plane SC-state optical destruction energy density as a function of T_c^2 for some iron based pnictides compared to other layered superconductors. 77
Figure 7.4: Temperature dependence of the transient reflectivity $\Delta R/R$ at low and high pump fluence. 78
Figure 7.5: The temperature dependence of the SC response amplitude for low and high excitation density. 80

Figure 8.1: Schematic phase diagram of $EuFe_2(As_{1-x}P_x)_2$ indicating the SDW and SC phase. 84
Figure 8.2: Photoinduced reflectivity transients at low-T in Eu-122 and EuP-122 for two probe-photon polarizations. 84
Figure 8.3: The amplitude of the transient reflectivity at long delays as a function of temperature in Eu-122, and EuP-122, compared to the magnetic moment along the c-axis. 85
Figure 8.4: The transient reflectivity at low-T in $EuFe_2As_2$ as a function of probe-photon energy for the $\mathcal{P}^+$ polarization. 86
Figure 8.5: The reflectivity transients in $EuFe_2As_2$ with the magnetic field parallel to the $\mathcal{P}^-$ polarization. 87
Figure 8.6: The amplitude of the slow component as the function of the applied magnetic field measured in EuP-122 at $T = 1.5$ K. 87
Figure 8.7: The reflectivity transients in $EuFe_2(As_{0.81}P_{0.19})_2$ for $\mathcal{P}^+$ and $\mathcal{P}^-$ probe polarizations. 88
Figure 8.8: The oscillatory part of the isotropic $\Delta R/R$ component in EuP-122at low magnetic fields. The frequency, decay time and amplitude of the oscillations as functions of the magnetic field. 89
Figure 8.9: $\Delta R/R$, rotation and ellipticity in $\mu_0 H = 0.3$ T magnetic field. 90
Figure 8.10: Ellipticity and rotation upon reversal of the magnetic field. 91
Figure 8.11: The isotropic component of transient reflectivity in EuP-122 at different T and $\mathcal{F}$ in 0.3 T. 92
Figure 8.12: The doping dependence of the transient reflectivity response in EuCo-122 measured at 7 K with 7 μJ/cm^2 pump fluence. 93
Figure 8.13: The doping dependence of the rise time of the slow component in $EuFe_{2-x}Co_xAs_2$. 94
Figure 8.14: The photoexcitation of Eu^{2+}spins in iron-based pnictides is enabled through the indirect spin-lattice mechanism. 95

List of Tables

Table 2.1: Samples, which were studied in the dissertation. 35

Table 4.1: Charge gap magnitudes and the relative effective number of involved bosons. 54

Table 5.1: The destruction energy of the SDW state in $EuFe_2As_2$, $SrFe_2As_2$ and $BaFe_2As_2$ for different temperatures and polarizations. 63

Abbreviations

AFM	... antiferromagnetic
ARPES	... angle-resolved photoemission spectroscopy
BBO	... BaB_2O_4 nonlinear crystal
BCS	... Bardeen-Cooper-Schrieffer theory
CAFM	... canted antiferromagnet
CDW	... charge density wave
DECP	... displacive excitation of coherent phonon
DOS	... density of states
DW	... density wave
FC	... field cooling
FFLO	... Fulde–Ferrell–Larkin–Ovchinnikov interaction
FM	... ferromagnetic
HFB	... high frequency boson
IP	... iron pnictide
ISRS	... impulsive stimulated Raman scattering
LDA	... local-density approximation
NMR	... nuclear magnetic resonance
PG	... pseudogap
QP	... quasiparticle
RKKY	... Ruderman-Kittel-Kasuya-Yosida interaction
SC	... superconductor
SDW	... spin density wave
STM	... scanning tunneling microscopy
SV	... singular value
SVD	... singular value decomposition
SQUID	... superconducting quantum interference device
SW	... spectral weight
TDM	... thermal diffusion model
TE	... temporal eigenvector
TR–ARPES	... time-resolved angle-resolved photoemission spectroscopy
TR–MOKE	... time-resolved magneto-optical Kerr effect
TTM	... two-temperature model
ZFC	... zero field cooling

Chapter 1

Introduction

1.1 Thesis Structure

The discovery of the first class of high-temperature (high-T_c) superconductors - the copper oxides (or the cuprates) in 1986 [1] has started a new era in condensed matter physics. But even after thirty years of the intensive research the mechanism of their superconductivity remains unrevealed [2], [3]. Thus, scientists are trying to solve this problem also extensively by searching for new classes of materials which would possess high-temperature superconductivity. This way some organic, fulleride, boride and chalcogenide unconventional superconductors were discovered [4]–[8]. Due to the antagonistic relationship between superconductivity and magnetism scientists were avoiding Fe in the search for high-T_c compounds for a long time. But in 2006 Hideo Hosono's group reported [9] on a new class of high-temperature superconductors, which were based on FeAs layers, and this breakthrough discovery has started a new stage in the research of mechanisms of superconductivity. Since then, superconductivity in iron-based pnictides has become hot topic in the condensed-matter physics [10]–[16]. Great interest for this class of materials originates also from their rich phase diagram [17], which includes regions of coexistence of spin density wave (SDW), superconducting (SC) and ferromagnetic (FM) orders, opening great opportunity for experimental physicists to bring further insight into mechanisms behind electronic collective states in high-temperature superconductors.

Among iron pnictide (IP) family the most widely studied members are $A\mathrm{Fe_2As_2}$ (or 122) compounds [18], where A = Ca, Sr, Ba, Eu, Sm, La, Ce, Pr, or Th. In normal conditions these materials are multiband metals with a tetragonal structure. With decreasing temperature a structural transition to an orthorhombic state takes place and in proximity to this transition the Fe spins order antiferromagnetically (AFM). Due to nesting in the electronic band structure, the AFM order is believed to be the SDW like. This is corroborated with the opening of the partial gap in electronic density of states. Application of an external pressure or chemical doping suppresses the SDW-like AFM phase and induces the SC phase.

Ultrafast time-resolved optical spectroscopy is known to be an efficient technique for a direct study of electron-phonon dynamics, electron-spin interaction and the structure of the quasiparticle density of states [19]. To this date, extensive time-resolved studies were performed in iron pnictides, in which the quasiparticle (QP) dynamics was investigated [20], the electron-phonon coupling constant was determined for a number of 122 compounds [21], the observation of nematic phase fluctuations was reported [22], the coherent optical control on phonon modes [23] was realized, *etc.*

This thesis is dedicated to time-resolved optical studies, performed on iron pnictides in order to reveal the relaxation processes which take place in these materials after the pho-

toexcitation. Chapter 2 is dedicated to the instrumental details of experimental techniques applied for the dissertation studies. In Chapter 3 we concentrate on general properties of the transient reflectivity signal from 122 iron pnictides. The nature of the response measured by single-wavelength probe in every region of the phase diagram is going to be discussed.

The orthorhombic SDW state of the undoped parent compound is believed to be closely related to the high-T_c superconductivity in iron pnictides [17]. Therefore, substantial effort was applied to study this state by different techniques [24], [25] including the static [26], [27] and ultrafast [28] optical measurements. However, most of the published all-optical experiments were performed using narrow-band spectrally unresolved probes, so some relaxation processes could remain hidden due to their optical inactivity at the chosen wavelength. Thus, the nature and properties of photoinduced excitations in SDW state are still not completely understood. Chapter 4 is dedicated to the search for additional relaxation paths in SDW state, performed by means of the pump-broadband-probe technique.

The discovery of ultrafast lasers also enabled studies of the dynamics of the systems going through the non-equilibrium phase transitions. For example, [29] an optically-driven non-thermal destruction of the SC state in a cuprate superconductor was demonstrated. The study of a photoinduced non-thermal SDW phase transitions is presented in Chapter 5.

We present the study of the dynamics of the system through photoinduced SDW phase transition in Chapter 6 using a novel three-pulse technique, in which the introduction of an additional strong ultrafast laser pulse induces a strongly non-thermal distribution of excitations. This gives an interesting opportunity for a direct observation of the dynamics of the system evolving through a non-equilibrium phase transition. Similar studies were already performed on related phenomena, such as charge density wave (CDW) [30] and SC [31] systems. To our best knowledge, there were no such experiments conducted in a SDW system.

$BaFe_2(As_{1-x}P_x)_2$ is a unique iron-based superconductor, where the superconductivity is induced by the isovalent substitution of phosphorus for arsenic. The superconducting gap in $BaFe_2(As_{1-x}P_x)_2$ has been suggested to contain nodal lines by various experiments [32]. Nodes in the superconducting gap can strongly affect the relaxation of photoexcited carriers. The discussion of the gap symmetry influence on the quasiparticle relaxation is discussed in Chapter 7.

Another interesting aspect revealed in Eu-based 122 compounds is the coexistence of the SC state with seemingly incompatible FM phase of Eu^{2+} spins [17]. Ferromagnetism and superconductivity are antagonistic phenomena. Their coexistence implies either a modulated ferromagnetic order parameter on a lengthscale shorter than the superconducting coherence length or a weak exchange coupling between the itinerant superconducting electrons and the localized ordered spins. In some Eu-based iron pnictide superconductors the coexistence of ferromagnetism and superconductivity has been clearly demonstrated [33]. The nature of the coexistence, however, remains elusive since no clear understanding of the spin structure in the superconducting state has been reached and the reports [33], [34] on the coupling strength remain controversial. Therefore, Chapter 8 is dedicated to reveal the mechanisms of the coexistence of the Eu ferromagnetism and superconductivity in materials.

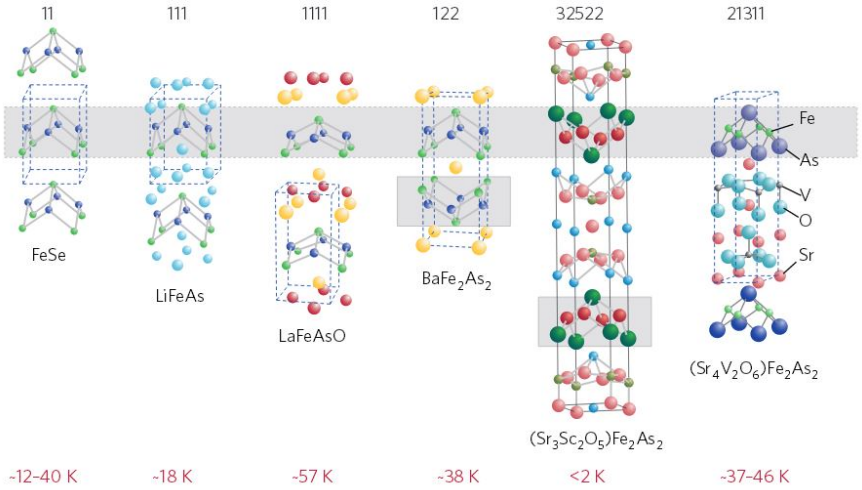


Figure 1.1: Schematic representation of the six homologous phases of iron-based pnictides and chalcogenides identified at present. Listed below each structure is the highest achieved T_c so far. Adapted from [36].

1.2 Iron pnictides and high-temperature superconductivity

1.2.1 General properties of iron pnictide superconductors

In 2008 Hideo Hosono's group [18] discovered that layered FeAs compounds synthesized with LaO show unconventional high-T_c superconductivity. Usually, the conflict between superconductivity and magnetism persuaded researchers to avoid iron in synthesis of high-temperature superconductors. That is why the discovery of iron pnictide superconductors was completely unexpected. There is a broad variety of materials which are known as iron pnictides. The majority of them is illustrated in Fig. 1.1[1]. All of them have a common two-dimensional (2D) Fe*Pn* layer, where *Pn* is a pnictogen atom, such as As, P or Sb (an atom from V group of the periodic table). Three of the most stable and thus most known and studied of them are iron pnictides, which have the so-called "11", "1111" and "122" structures, where the digits represent the indices in the respective chemical formulas. For example, FeAs is a member of the "11" class, LaFeAsO has the "1111" structure, while the typical "122" specimen has a chemical composition similar to $BaFe_2As_2$ or $EuFe_2As_2$.

All studies presented in the dissertation were performed in the compounds with 122 structure, which is a combination of FeAs layer with layers of alkali-earth-metal or rare-earth elements and has the composition AFe_2As_2 , where A refers to Ca, Sr, Ba, Eu, Sm, La, Ce, Pr or Th. In the literature they are abbreviated as 122 iron pnictides. High interest of scientists in exactly this structure is due to the fact that in the 122 iron pnictides the antiferromagnetic phase is not completely suppressed, when the material is superconducting, but these two alternative phases coexist, in contrast to, *e. g.* 1111 compounds. Another, and probably, the main, reason is a simpler synthesis of large 122 crystals of a high quality.

Undoped parent 122 iron pnictides are not superconducting but usually considered as bad quasi-2D metals. The electrical in-plane resistivity value at the room temperature is around 0.4 mΩ·cm (while for pure elemental metals like copper it is two magnitudes lower $\sim$ 1.68 $\mu\Omega$·cm). Such a high electrical resistivity results from the lower carrier density [37].

At room temperature the unit cell has a tetragonal symmetry with the lattice constants

[1] There are more related materials, which are not in the figure, but belong to the class of iron pnictides [35].

$a = 3.96$ and $c = 13.02$ for Ba-122 [38], that slightly vary from compound to compound. With decreasing the temperature below T_{nem} [39]–[42], the system spontaneously breaks the fourfold in-plane symmetry of the electronic properties in the FeAs-plane. Since, the time-reversal symmetry is preserved, in analogy to nematic liquid crystals, where molecules arrange along preferable direction, this phase in the iron pnictides is called nematic. Unlike isotropic liquid crystals, in the pnictides the director can point only either along x or y directions. This makes the nematic order parameter Ising-like, hence sometimes the name is Ising-nematic order. The nematic order [16] gives rise to anisotropies in several quantities — the electrical and thermal transport, orbital occupation, optical conductivity and magnetic susceptibility [42]–[44].

The nature of the nematic phase in the pnictides is still under debate. Firstly it was proposed that the structural transition is phonon-driven [45], but early theoretical works [46], [47] have already suggested that it may be driven by electronic rather than lattice degrees of freedom. Later it was shown that the symmetry breaking has an electronic nature. Many methods such as transport measurements [48], [49], scanning tunneling microscopy [42], [50]–[52] and angle-resolved photoemission spectroscopy (ARPES) [53] have shown strong in-plane anisotropy of the electronic states below a few hundred K. The question whether the order parameter which drives the nematic phase in iron pnictides has orbital-charge or spin nature still remains unresolved [16]. The high interest in the nematic phase is caused by the suggestion that the high-temperature superconductivity in iron pnictides is driven by the same electron fluctuations as the nematic phase [54], [55].

Preliminary studies [56] have also suggested that above the SC transition the phase diagram of the iron pnictides contains the state which is characterized by a suppression of the electronic density of states near the Fermi energy or, in analogy to the copper oxides, so-called pseudogap (PG) state. It is still unclear whether the high-T_{c} superconductivity can be universally associated with the pseudogap formation. For the copper oxides the relation between these two phases is under intense debates [57], [58]. In iron pnictides the opening of the pseudogap was suggested first theoretically [59]. Finally, the spectroscopic ellipsometry measurements [60] revealed the formation of the pseudogap at about 0.65 eV and its restriction to energies below 2 eV. The pseudogap was also observed by the infrared spectroscopy in [61] and the ARPES in [62]. The first optical pump-probe experiments also revealed an evidence of the pseudogap presence [63].

At slightly lower temperature, T_{S}, the rotational point group symmetry of the lattice is reduced and the structural transition from the tetragonal to the orthorhombic state takes place. The combination of magnetic torque measurements with synchrotron X-ray measurements [39] has suggested that the distinct difference between the transitions at T_{nem} and T_{S} is that the one at T_{nem}, signifying a true nematic transition, and the other at T_{S} ($<T_{\text{nem}}$), was shown not to be a true phase transition. But in reality the picture is much more complicated and the order and temperature of structural and nematic transitions strongly depend on doping (see Fig. 1.2).

In the proximity to the structural transition, at T_{SDW}, [64] a magnetization density oscillations form in the crystal. Iron pnictides are multiband materials with a complicated Fermi surface, which consists of a few onion-like hole pockets in the center of the Brillouin zone and electron pockets in the corner (see Fig. 1.3). It is believed that due to the nesting between the electron and hole pockets at T_{SDW} a partial gap opens and the spin density wave (SDW) modulation forms. The reader can find more about the SDW and the iron magnetism in iron pnictides in Section 1.3.

As soon as the SDW ordering is commensurate, the Fe spins in the FeAs plane order AFM in a way that alternates the direction of magnetic moments from one row of iron atoms to another, forming a stripe-like pattern (Fig. 1.2a) [66], [67]. The presence of

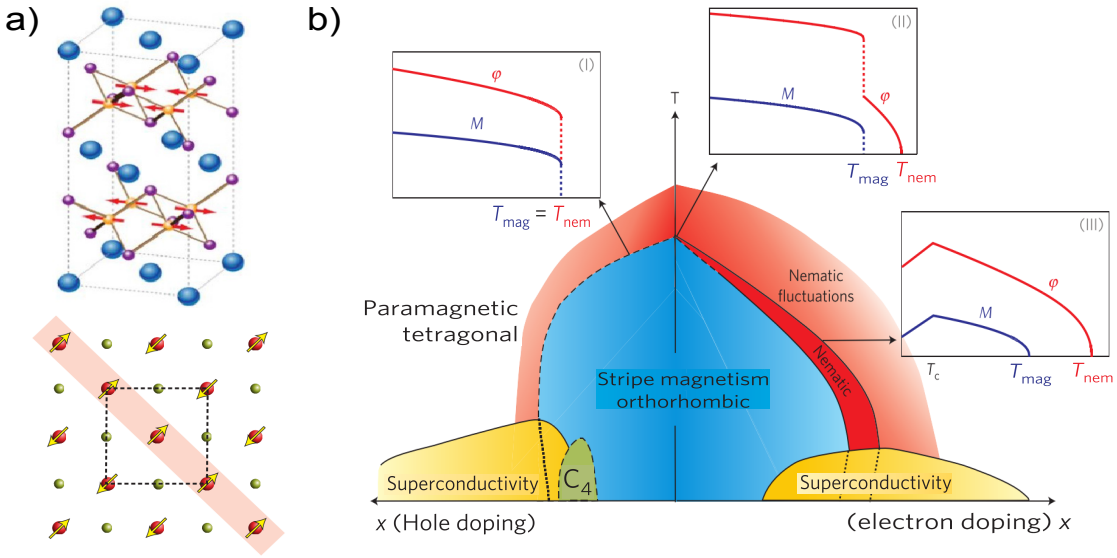


Figure 1.2: a) The structure of 122 iron pnictides, with iron ions shown in red and pnictogen ions shown in gold. Adapted from [65]. b) A schematic phase diagram of hole-doped and electron-doped iron pnictides of the 122 family. The blue area denotes the stripe-type orthorhombic magnetism, the red area denotes the nematic/orthorhombic paramagnetic order, and the yellow area superconductivity. The green area corresponds to a magnetically ordered state that preserves tetragonal symmetry. The dark red region denotes a regime with strong nematic fluctuations. The insets show the temperature-dependence of the nematic (ϕ) and magnetic (M) order parameters in different regions of the phase diagram: region (I) corresponds to simultaneous first-order magnetic and nematic transitions; region (II) corresponds to split second-order nematic and first-order magnetic transitions; and region (III) corresponds to split second-order transitions. Adapted from [16].

localized magnetism in iron pnictides was predicted by theoreticians from first principle calculations [68]–[70]. The fact that the commensurate ordering vector coincides with the nesting vector, which connects the hole and the electron pockets, it has been suggestive that the static AFM order is apparently the SDW state driven by the nesting of the Fermi surface. In the hole-doped iron pnictides structural and magnetic transitions are simultaneous and first order, while in the electron or isovalently doped compounds the transitions are second order and $T_{SDW} \leq T_S$ (Fig. 1.2b). The undoped compounds remain metallic in the whole temperature range down to zero.

The most important aspect of the phase diagram of iron pnictides is revealed with an application of the external pressure [25], [71]–[75], the chemical doping by holes [38] and electrons [40], or by the isovalent substitution [76]. This leads to the suppression of the nematic and AFM phases, and the material becomes superconducting. It is widely believed that the interaction which leads to the high-T_c superconductivity originates from the iron-arsenic layer. The overlap of the AFM/SDW and nematic states with superconductivity is a special feature of 122 systems [10], [41], [77], and one of the main challenges and motivations to study this system.

1.2.2 Historical view on the problem of high-T_c superconductors

The discovery of superconductivity is one of the major discoveries in physics of the XXth century. It was done by Kamerlingh-Onnes in 1911 [78], after he liquified helium gas,

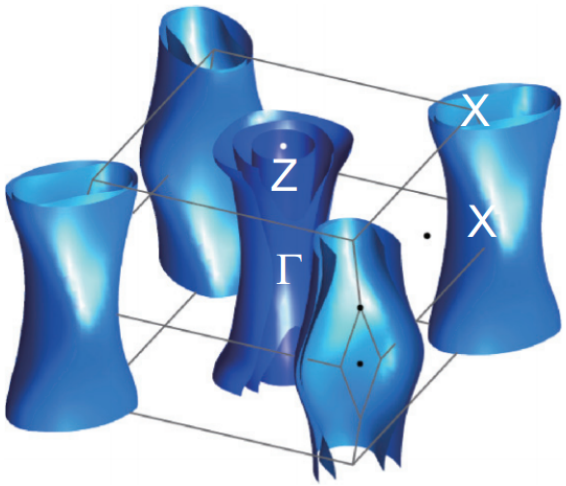


Figure 1.3: The Fermi surfaces of $BaFe_2(As, P)_2$ for x =0.30 obtained from first principle band calculations. Adapted from [62].

which becomes liquid at a very low temperature, about 4 K. This breakthrough discovery allowed Kamerlingh-Onnes to perform a set of experiments in which he was cooling different materials to very low temperatures and measured their electrical properties such as the resistance. The classical theory suggests that the resistance should slowly, gradually decrease with decreasing the temperature. But Kamerlingh-Onnes and his two assistants Cornelis Dorsman and Gilles Holst found that the resistance of mercury sharply drops to zero at the critical temperature around 4 K. This phenomenon of dropping the resistivity to zero, and thus the conductivity to infinity was named by Kamerlingh-Onnes as superconductivity [79].

Shortly after the discovery it was found that superconductors behave also as perfect diamagnets. The effect of complete expelling of the external magnetic field from a superconductor is called the Meissner effect. This effect takes place by setting up electric currents near the superconductors surface. The magnetic field of these surface currents cancels the applied magnetic field within the bulk of the superconductor. As the field is expelled or canceled, and it does not change with time, the currents producing this effect do not decay with time. The explanation for this effect was done within the framework of the London theory, which relates the current to the electromagnetic field in and around a superconductor.

But the London theory did not take into account quantum effects in superconductors. The first quantum theory appeared after discovery of superfluidity (a complete loss of viscosity) by Pyotr Kapitsa in 1937. To describe the phenomenon of the superfluidity Landau proposed a theoretical model, which was later generalized for superconductors by Landau and Ginzburg. This theory describes the evolution of the order parameter through the second order SC transition, where the effective wavefunction of the superconducting electrons $\psi(r)$ is considered as the order parameter. Nowadays, the Ginzburg-Landau theory is widely used by scientists involved in studying transport in superconductors. But in spite of all the splendor of the Ginzburg-Landau theory, it does not explain the microscopic mechanisms of superconductivity.

The first reasonable microscopic description of superconductivity was derived by Bardeen, Cooper, and Schrieffer, who created the famous BCS theory. The theory describes superconductivity as an effect caused by a condensation of pairs of correlated electrons or the

Cooper pairs into a boson-like state. Electrons near the Fermi surface may have an effective attraction, interacting with each other mediated *via* bosons. The Cooper pair can be formed by electrons with opposite spins, which move in the opposite directions and their energy differs from the Fermi energy by less than $h\omega_{\mathrm{D}}$, where ω_{D} is the Debye frequency. The remaining electrons do not interact. This feature allows the pairs to move without colliding with the lattice and the remaining electrons, *i. e.*, without any energy loss.

The BCS theory was a very reasonable explanation for microscopic processes taking place in superconductors, until it turned out that it does not always work very well [80], [81]. In 1986 Georg Bednorz and Alex Muller [1] have discovered the property of ceramics based on the copper oxide, lanthanum, and barium ($La_{2-x}Ba_xCuO_4$) to become superconductive below 30 K. It was the first step towards the high-temperature superconductivity. Since then, many related materials were discovered showing high-temperature superconductivity, the highest critical temperature being almost 160 K. An unified, general microscopic theoretical model that would describe well the observed properties of high-T_{c} superconductors, has not been discovered yet.

The first report on the discovery of a high-temperature non-cuprate superconductor was on iron-based layered superconductor $La(O_{1-x}F_x)FeAs$ ($x = 0.05 - 0.12$) [9] with $T_{\mathrm{c}} = 26$ K. It was found that the crystal structure of *Re*FeAsO, where *Re* refers to the rare-earth elements, so-called iron pnictides, is very similar to the cuprate superconductors. Similar layered structure and pronounced analogies of their phase diagram led scientists to believe that perhaps the nature of the superconductivity in the pnictides is the same as in the cuprate superconductors. To test this hypothesis, calculations were performed [82] using the BCS theory and showed that the critical temperature should not exceed 1 K, which obviously contradicts the experimental data. It looks like the BCS theory cannot describe the nature of superconductivity in these materials, and a new theory should be built. Therefore, the problem of obtaining superconductivity at room temperature still remains as one of the main problems of modern physics.

1.2.3 High-temperature superconductivity in iron pnictides

Even though the highest transition temperature so far reached for iron pnictides is 56 K [83], they are considered as a class of materials exhibiting unconventional high-temperature superconductivity. In contrast to the copper oxides, the absence of the Mott behaviour in iron pnictides excludes them from being strongly correlated electronic systems. The ultrafast time-resolved spectroscopy was shown to be a convenient instrument to estimate the electron-phonon coupling in metallic superconductors [84], [85]. For example, it was revealed that the electron-phonon constant for iron pnictides is rather small $\lambda = 0.2 - 0.3$ [86], [87], while for cuprates it is usually a bit higher, $\lambda = 0.3 - 0.5$. But still, many experiments have shown that the mechanism for superconductivity does not originate from electron-phonon coupling as in conventional metals or MgB_2, but from the electron-electron interactions [88]. Moreover, the electron-electron mechanism was speculated on a base of results of optical measurements [89]. Therefore, the iron pnictides are sometimes treated as a correlated system, and in some cases Mott physics might be relevant to its charge dynamics and magnetic properties [90]–[92].

Whether the mechanism of superconductivity in iron-based superconductors is identified with the conventional phonon mechanism or not is still an open question. Several studies [93]–[95] suggest that superconductivity at the high-T_{c} can not be explained by conventional electron-phonon interactions, but antiferromagnetic spin fluctuations. The isotope coefficient is often used as a probe for the strength of electron-phonon interactions. But isotope constant of Fe measured for iron pnictides strongly depends on the composition and synthesis procedure. For some compounds it is reported to be negative

$\alpha \simeq -(0.2-0.5)$ [96]–[98], which contradicts the electron-phonon scenario (for comparison in conventional MgB_2, $\alpha = 0.5$ [99]).

At this moment there are mostly theoretical works which propose spin fluctuations as the main mechanism of high-temperature superconductivity in iron pnictides. For instance, in works [100]–[104] the authors claim that the superconducting transition occurs with the breaking of the time-reversal symmetry as it happens during paramagnetic-antiferromagnetic transitions. However, the experimental confirmation of this theory remains open because of the difficulties to probe the time-reversal invariance in the pnictides due to the symmetry of the superconducting state[2]. [107]

It is commonly believed that the SC order parameter in iron pnictides has a $s\pm$ symmetry [68], [108], [109]. It means that the superconducting order parameter looks like an s-wave, where a phase switches by π between the two sets of the Fermi surfaces. Superconducting gap structures appear to vary substantially from family to family, and even within families as a function of doping or pressure. Moreover, the multiband nature allows the prediction of some more exotic types of superconductivity, which in some cases even breaks the time-reversal symmetry. Contrary, there are some works which predict the s wave without sign reversal [110] for orbitally driven superconductivity in iron pnictides. Theoreticians also propose coexistence of the s wave in one pocket of the Fermi surface and another singlet s [101], [102], d [111] wave, or even triplet t-wave [100] in the other. However, there are no experimental works, which would report on any of the exotic scenarios for the pairing symmetry. Conversely, Chen *et al.* [112] developed a phase-sensitive technique and report on observation of evidence for $s\pm$ symmetry in the Nd-1111 pnictide.

The most recent review of the nature of superconductivity in iron pnictides one can find in [3], and a general review of high-temperature superconductors was published in [113].

1.2.4 Optical properties of iron pnictides

The electronic band structure is one of the most important characteristics of a material, because it determines many physical properties, such as transport and optical properties, photoelectron spectra, *etc.* Despite the large variety of crystal structure and chemical compositions all IP share the same features of the electronic structure. The electronic band structure in the proximity to the Fermi energy in all IP is mostly formed by orbitals from FeAs plane and even more, calculations show that in IP only Fe d-derived bands are present near the Fermi energy.

The electronic structure of IP was calculated in a number of works [37], [115]–[118]. For example [119], the local-density approximation (LDA) calculations of the band structure for $Ba_{0.68}K_{0.32}Fe_2As_2$ in the normal state are shown in Fig. 1.4b. It can be clearly seen that this material has a multiband nature, where hole bands around the Γ point coexist with electron bands in the corners of the Brillouin zone at the M point. Such an electronic structure leads to a significant interband scattering at the nesting vector, which is believed to be the main driving force for the magnetic instability and superconductivity in iron pnictides.

In the normal state at any temperature and at any doping all 122 iron pnictides are metallic and the low-energy optical conductivity is dominated by the itinerant charge-carriers response. In the normal state the optical conductivity spectra are mainly composed from three main contributions (Fig. 1.4) in addition to the metallic Drude component in the low-energy part of the spectra [89], [120]:

1) the low-energy part originates from the contribution (the red line in Fig. 1.4a) made

[2] In contrast to cuprates, where order parameter has d-vawe symmetry.[105], [106]

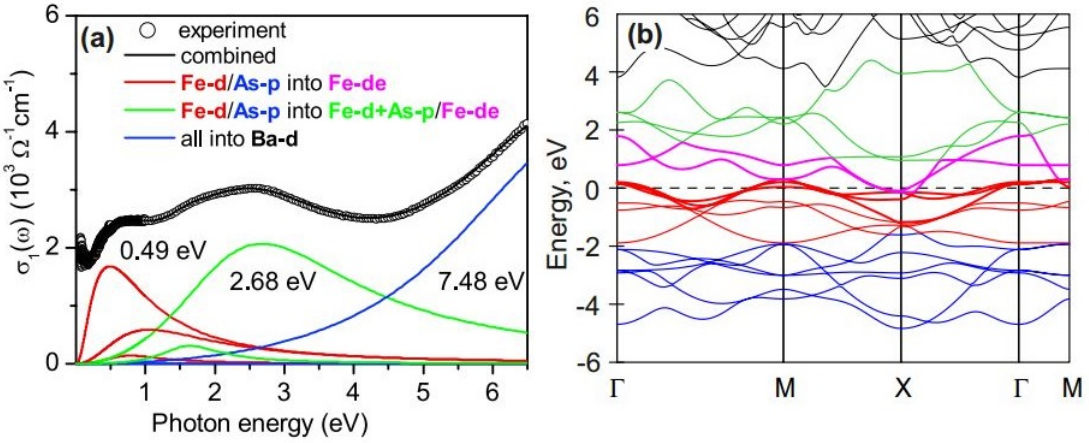


Figure 1.4: a) The real part of the optical conductivity of $Ba_{0.68}K_{0.32}Fe_2As_2$ and contributing interband transitions determined by a dispersion analysis. b) Band structure from LDA calculation. The blue and red lines correspond to weakly hybridized As-p and Fe-d states, respectively. The purple lines correspond to Fe-d bands near Fermi level. Green lines correspond to strongly hybridized Fe-d and As-p bands. The black lines correspond to Ba-d states. Adapted from [114].

by the transition from the low-energy weakly hybridized Fe d-bands and the chalcogen As p-bands below the Fermi level (red and blue lines on Fig. 1.4b) to the electronic states formed by Fe d-bands (purple lines on Fig. 1.4b) in proximity to the Fermi level (Fe-de in Fig. 1.4);

2) the intermediate energy part (the green line in Fig. 1.4a) is mainly due to the transitions from the same states to the strongly hybridized Fe d-bands and As p-bands situated above the Fermi level;

3) the high energy contribution (the blue line in Fig. 1.4a) is predominantly made by transitions from all itinerant states to A = Ca, Ba, Sr, Eu electronic levels, which are situated well above the Fermi energy. [114]

Upon lowering the temperature IP undergo a sequence of structural and magnetic phase transitions. The ~ 30 meV [57], [62] pseudogap which opens slightly above the onset of the magnetic order is associated with the appearance of an anisotropy of electronic properties due to nematic phase fluctuations [15], [121]. The multiband nature of IP caused the observation of two different SDW gaps with the ratio of $2\Delta/T_{\mathrm{SDW}} \approx 3.5$ and 9.6. In all cases IP remain metallic in the SDW state, so the optical conductivity is non-zero at low frequencies.

Opening of the superconducting gap in IP is also pronounced in the optical properties [122]. In 122 systems the optical reflectivity below 150 cm^{-1} suddenly turns to unity below T_{c}, following the BCS description [123]. In the optical conductivity a part of the Drude weight collapses into the superconducting condensate at zero frequency.

The crystal structure of the 122 iron pnictides belongs to the $I4/mmm$ space group. There are four Raman active modes including A_{1g}, B_{1g} and two E_g modes, and four infrared modes including two A_{2u} and two E_u modes. Among all the Raman-active phonon modes, the A_{1g} mode of arsenic around 200 cm^{-1} appears the most important in exploring the superconducting and SDW mechanism for Fe-based compounds [124]–[126]. Recent ultrafast THz study have shown that the modulation of this phonon by laser pulses can induce the SDW ordering above the transition temperature [23].

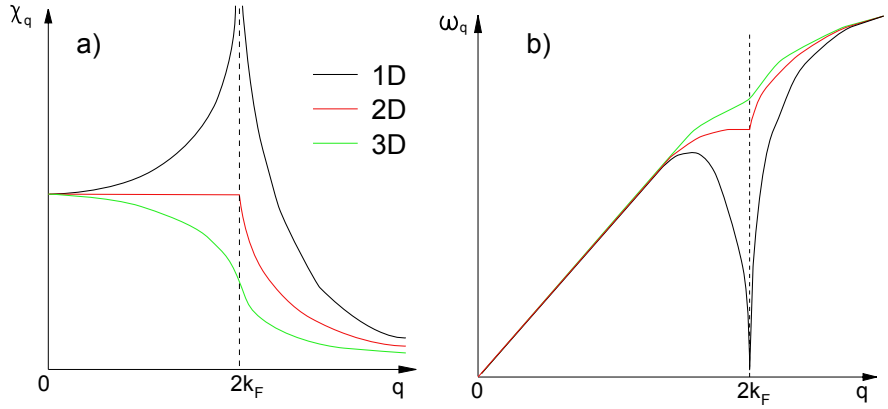


Figure 1.5: Wavevector dependent Lindhard function a) and acoustic phonon dispersion relation b) for a one-, two- and three-dimensional electron gas at zero temperature.

1.3 Spin density waves

In quasi one- and two-dimensional metals the electrons can organize themselves into regular patterns known as CDW, which are coupled to lattice, or SDW. The formation of density waves (DW) was theoretically predicted by Peierls in 1950s and first observed in 1970. The nature of the DW comes from the peculiarities of the Fermi surface of low-dimensional systems. Since then DWs were found in numerous low-dimensional structures. Theoretical and experimental evidence that SDW develops at low temperature in iron pnictides was reported almost immediately after their discovery [69].

1.3.1 Spin density waves in solids: general theory

To understand the physics of density waves in solids one should consider the Lindhard response function, which is given in d dimensions by [127]:

$$\chi(\boldsymbol{q}) = \int \frac{d\boldsymbol{k}}{(2\pi)^d} \frac{f_k - f_{k+q}}{\epsilon_k - \epsilon_{k+q}}, \tag{1.1}$$

where $f = f(\epsilon_k)$ is the Fermi-Dirac distribution function.

The Lindhard function (see Fig. 1.5) in low-dimesional systems has a singularity, which is caused by the topology of the Fermi surface. For example, in the one-dimensional electron gas the Fermi surface consists of two points, one at k_F and another at $-k_\mathrm{F}$. The dispersion relation is then given by $\epsilon(\boldsymbol{k}) = \hbar^2 k^2/2m$ and the Fermi energy is $\epsilon_\mathrm{F} = \frac{\hbar^2 k_\mathrm{F}^2}{2m_\mathrm{e}}$. It leads to a divergence of the response function when $q = 2k_\mathrm{F}$. It can also be shown that for two and three-dimensional electron gas the Lindhard response function can also have a singularity when $q = 2k_\mathrm{F}$ [127]. The divergence of the response function due to the topology of the Fermi surface is called nesting. In higher dimensions the number of states which differ at $q = 2k_\mathrm{F}$ is significantly reduced, leading to the removal of singularity.

The Lindhard function is related to the rearrangement of the charge density as: $\rho^{\mathrm{ind}}(\boldsymbol{q}) = \chi(\boldsymbol{q})\phi(\boldsymbol{q})$, where $\phi(\boldsymbol{r}) = \int_q \phi(\boldsymbol{q}) e^{iqr'} d\boldsymbol{q}$ is the response of an electron gas to a potential. The formation of the CDW modulation and gap formation in an electronic density of states can be derived if one considers an electron-phonon interaction Hamiltonian, which depends on the lattice displacements and the ionic potential, and solves the equation of motion. The divergence of the response function leads to the Peierls instability and the charges arrange into a density wave. As a result the conduction band splits to filled and empty bands, and

a gap in the electron density of states opens. If the new periodicity is a rational fraction or multiple of the lattice constant, the density wave is said to be commensurate; otherwise the density wave is termed incommensurate.

The mean field theory predicts the formation of DW state at a finite temperature. The behaviour near the transition temperature can be understood in terms of the Landau theory of phase transitions. The functional for the free energy is given as:

$$F = F_0 + n(\epsilon_{\mathrm{F}}) \int dx (a|\Delta|^2 + b|\Delta|^4 + c \left| \frac{d\Delta}{dx} \right|^2), \tag{1.2}$$

with $a_0 = f(T - T_{\mathrm{DW}})$, $b = const$ and $c = f(T, T_{\mathrm{DW}})$. The temperature dependent order parameter can be obtained from the equilibrium condition:

$$\frac{dF}{d\Delta} = 0. \tag{1.3}$$

If we neglect the spatial fluctuations of the order parameter, for $T < T_{\mathrm{DW}}$ we obtain:

$$|\Delta(T)| = (\frac{a_0}{2b})^{1/2} (T_{\mathrm{DW}} - T)^{1/2}. \tag{1.4}$$

The specific heat jump at the transition is observed for any type of density wave:

$$\Delta C = \frac{a_0^2 n(\epsilon_{\mathrm{F}})}{2bT_{\mathrm{DW}}}. \tag{1.5}$$

While the changes of the phonon modes are observed at CDW phase transition. For SDW presence of the magnetization term in Hamiltonian leads to the susceptibility is enhancement by the Stoner factor in the direction of the magnetic field [128], [129]:

$$\chi(q) = \frac{\chi_0(q)}{1 - \frac{U\chi_0(q)}{2\mu_{\mathrm{B}}^2}}. \tag{1.6}$$

The ground state for the SDW can be viewed as two sublattices of a CDW - one for spin up and one for spin down, which are spatially out of phase by π, as it is shown in Fig. 1.6

Generally, in DW there are phase and amplitude excitations of the order parameter. The oscillations of the phase cause the electronic charge redistribution with respect to the ionic positions; and consequently this mode is active in optical spectra, while the amplitude mode is expected to be Raman active. The frequency of the phason in SDW is $\omega_\phi = \upsilon_{\mathrm{F}} q$ and the frequency of the amplitude mode is given by $\omega_{\mathrm{A}} = ((2\Delta/\hbar)^2 + (\upsilon_{\mathrm{F}} q)^2)^{1/2}$. The amplitude mode is therefore expected to occur above the gap, merging with the continuum of the single particle excitations. This leads to the damping of the amplitude mode, similar to the damping of the amplitude mode of superconductors [130].

The SDW can be considered as two CDWs with the opposite spin, thus, the phason and amplitudon can appear in a complicated form of combination of these two excitations (Fig. 1.7).

Because of the magnetic character of the SDW ground state the spin excitations are also present. In the absence of spin-orbit and dipole-dipole interactions the spin degrees of freedom have a full rotational symmetry and for the two magnon branches following expression can be obtained:

$$\omega_{\mathrm{S}} = 2J_{\mathrm{eff}} \frac{\lambda_0}{2} q, \tag{1.7}$$

where J_{eff} is an effective coupling constant and $\lambda_0 = \pi/k_{\mathrm{F}}$ is the period of modulation.

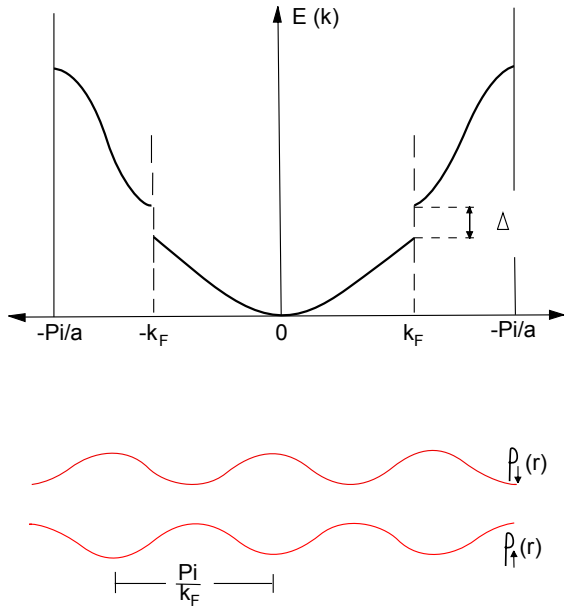


Figure 1.6: The dispersion relation and the charge/spin modulation for the two sublattices for one-dimentional SDW below the phase transition.

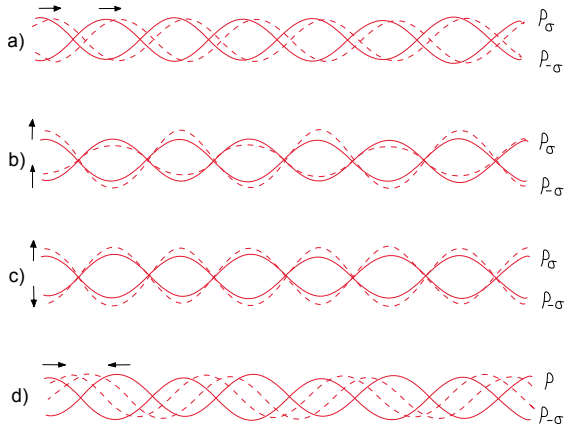


Figure 1.7: Various amplitude and phase excitations for a spin density wave ground state in the $q = 0$ limit. Each case is viewed as two CDWs - one for each spin subband - with the solid lines indicating the initial state and the dashed lines the perturbed state. Arrows show the displacement direction. a) SDW phason mode, b) time-dependent charge density (is not allowed), c) SDW amplitude mode, d) such a displacement leads to the charge buildup and, is therefore, forbidden. Adapted from [129].

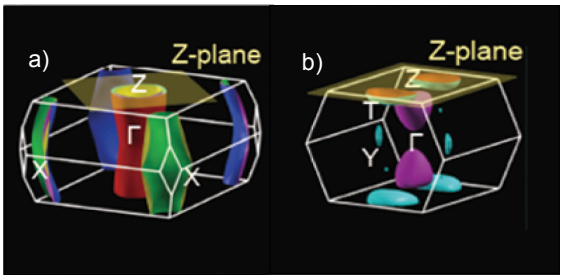


Figure 1.8: The Fermi surface of $BaFe_2As_2$, calculated for normal a) and the orthorhombic magnetically ordered SDW state b). Adapted from [138].

In the case of commensurate or nearly commensurate DW the period of the modulation is proportional to the lattice constant of the crystal. This fact has a few important consequences. The ground state becomes a periodic function of the phase ϕ, and the phase excitation develops a gap in the $q = 0$ limit. Because of the quasiperiodic dependence of the ground state on the phase, the nonlinear excitations occur in a system. In CDW most commonly this nonlinear excitation is a soliton, while in SDW, which can be considered as two CDW, complicated solitonic excitations are expected.

The experimental manifestations of the SDW [127]:

1) the gap which opens at T_{SDW} can be observed in optical conductivity measurements;

2) the transition temperature can also be estimated from the jump in specific heat at T_{SDW};

3) SDW anomaly is also seen by superconducting quantum interface device (SQUID);

4) spin polarized scanning tunneling microscopy (STM) enables capturing of the SDW images;

5) also, transport measurements are sensitive to the formation of SDW order;

6) neutron scattering experiments allow the studying of low-energy excitations in SDW as well as the static modulation.

1.3.2 Magnetic long-range order in pnictides

Magnetic fluctuations are widely believed to be responsible for the high-T_c superconductivity in iron pnictides [131], [132]. The nature of magnetism in these materials has a complex character. Some studies assume localized spins which interact *via* superexchange-like interactions [91], [133]. Other reports suggest itinerant spins, which are related to the Fermi surface [68], [109]. At a later stage, it was proposed that the truth is somewhere in between and the moments are substantially localized and large, but that they are nonetheless formed by the itinerant electrons, and are greatly reduced by fluctuations [59], [134]–[137].

As it was shown above, the DWs are fundamentally electronic phenomena, which originate from the topology of the Fermi surface. That is why consideration of the electronic band structure of iron pnictides is very crucial for understanding these two phenomena. The band structure for iron pnictides was calculated within density functional theory in [37]. The main As p-bands occur between -5.5 and -2 eV with respect to the Fermi energy, while the bands near the Fermi energy are dominated by the Fe d-bands. It was also shown that the band structure originates from the Fe-Fe interaction in FeAs plane.

The Fermi surface consists of onion-like cylindrical hole pockets around the center of the Brillouin zone and cylindrical electron pockets in corners (Fig. 1.8a). They are mostly derived from Fe d_{xz} and d_{yz} orbitals, the hole pocket also partially originate from the hybridized Fe-As orbitals.

This theoretically predicted 3D electronic band structure has been confirmed by a number of ARPES experiments on parent [139]–[143] or underdoped IP [144]–[147], and by quantum oscillations measurements on the underdoped compounds [148]–[150].

Such a band structure allows the interband nesting between the electron and hole pockets. It was shown that below T_{SDW} the electron pocket projects on the center of the Brillouin zone, causing the divergence in the Lindhard function which leads to the Peierls instability (see the section about the SDW theory). The peak in the Lindhard function together with the Stoner enhancement causes the formation of a partial gap and SDW. The fact that the phonon frequencies do not shift suggests that the gap is not CDW [69]. The reconstruction of the Fermi surface below the SDW transition is shown in Fig. 1.8b [138].

It is remarkable that in the SDW state iron pnictides remain metallic, which means that the gap is partial and there are itinerant carriers remaining. The coexistence of the partial gap and the metallic properties was observed experimentally by optical conductivity measurements [151].

The scenario of interpocket nesting is also reflected in the phase diagram of iron pnictides, where the doping leads to the suppression of SDW and rise of the SC region. When, for example, we dope a material with holes, the hole pockets become larger, while the size of the electron pockets reduces, leading consequently to the breaking of the nesting conditions, and the same in the case of electron doping. It means that doping should suppresses the SDW as it was observed experimentally. Not only doping suppresses the SDW order, but also isovalent substitution and application of a physical pressure influence the properties of material in the same way. For example, in several works, where in $BaFe_2(As_{1-x}P_x)_2$ [76], [152] or in $SrFe_2(As_{1-x}P_x)_2$ [153] arsenic is partially substituted by phosphorus, quite similar phase diagrams are demonstrated. Such substitution is not supposed to introduce any extra charge carriers. Indeed, the ARPES measurements [32] reveal that the size and shape of the electronic part of the Fermi surface do not change much even for high P concentrations, while the shape of the hole pocket changes and divides into parts.

It was suggested that changes of the unit-volume play a key role in forming SDW in iron pnictides, but the report on $Ba_{1-x}Sr_xFe_2As_2$ [154] that shows comparable shrinking of the unit cell, but no superconductivity, refuted this idea. Instead, several works [23], [38] proposed that the variation of the pnictogen height in Fe-As tetrahedra plays an important role in building up the phase diagram of iron pnictides.

1.4 Competing and coexisting phases in iron pnictides

As it was already mentioned the special feature of the 122 compounds is, that there is a part of the phase diagram where the magnetism and superconductivity overlap.

To understand the phenomenon of high-temperature superconductivity, it is important to understand the competing states to the superconducting phase. In iron pnictides same as in the cuprates, the competing states consist of various symmetry-broken phases, which interact with superconductivity in unclear ways. In the cuprates, one of the biggest puzzles is the nature of the PG phase, which envelops a large portion of the superconducting dome in the phase diagram. In iron pnictides the collinear SDW order and the nematic phase have been well established as the main competing phases to the superconducting one.

Another good candidate for competing with superconductivity in iron pnictides is the FM order of Eu spins in Eu-based compounds. Below 19 K Eu^{2+} spins order antiferromagnetically in undoped $EuFe_2As_2$, but there is no clear picture how exactly Eu spin ordering changes with doping.

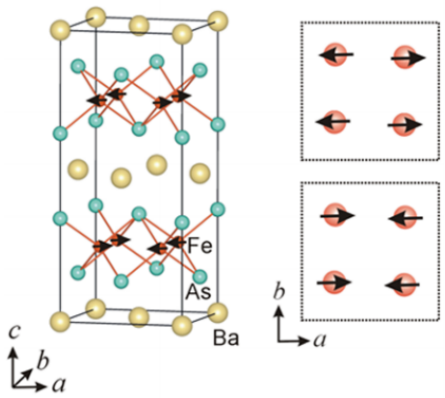


Figure 1.9: The magnetic and crystal structure of $BaFe_2As_2$. Adapted from [157].

1.4.1 Coexistence of superconductivity and magnetism: general view

Superconductivity and magnetism represent types of ordering which compete with each other, so the question whether the two types of ordering can coexist in the same crystal is not a trivial one. There are two mechanisms for the relative interaction of the magnetic moments and superconductive electrons: the electromagnetic and exchange mechanism.

The electromagnetic mechanism was first studied by Ginzburg [155], who treated the problem with the suppression of superconducting pairing by the magnetic induction in a ferromagnet. He has shown that the coexistence can be enabled only in exceptional cases, when the magnetic induction is suppressed, but in a bulk superconducting samples the ferromagnetic order cannot be realized. In later works it was shown that the long-range magnetic order is screened by the Meissner currents, if the superconducting transition occurs at a temperature above that corresponding to the magnetic transition. In this case superconductivity prevents the formation of the ferromagnetic phase by lowering the temperature at which it would appear.

In addition, in some works it was also noted that the occurrence of superconductivity in a ferromagnet is more favourable near a domain wall than inside a domain [156].

1.4.2 Superconductivity and Fe magnetism in iron pnictides

Superconductivity and ferromagnetism are two intriguing collective phenomena in condensed matter physics [158], [159]. Conventional SC is characterized by the spin-singlet *s*-wave Cooper pairing, in which the time-reversal symmetry is conserved. However, ferromagnetism breaks the time-reversal symmetry. This fundamental difference makes the two phenomena antagonistic and competitive.

The first intriguing aspect of the coexistence of superconductivity and magnetism in iron pnictides appears in underdoped samples, where at low temperatures the SDW ordering coexists with the superconducting state [14], [157]. Iron spins arrange into commensurate SDW in the parent iron-based superconductors below T_{SDW}, which makes them long-range-ordered antiferromagnets (see Fig. 1.9). In $LaO_{1-x}F_xFeAs$ the magnetic moment is $0.36(5)\mu_{\mathrm{B}}$ per iron atom at 8 K [64], while in $EuFe_2As_2$ 1.92 μ_{B} Fe local moments were calculated [160].

The μ-spin relaxation measurements, where the paramagnetic volume can be precisely extracted revealed, that, for example, in Sn-flux grown $(BaK)Fe_2As_2$, below T_{SDW}, only part of the sample ($\sim$ 50%) becomes magnetically ordered [161]–[163]. This suggests

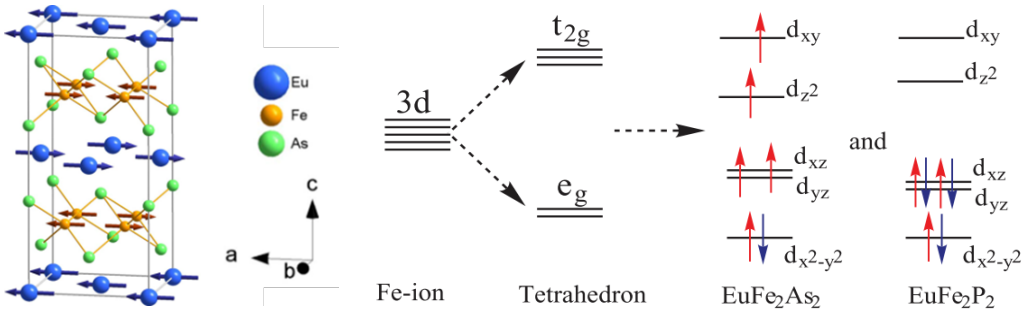


Figure 1.10: Below $T_N = 19$ K Eu^{2+} spins order antiferromagnetically. The ordering is depicted on the left side. On the right the sketch of the Fe $3d$ orbital levels for $EuFe_2As_2$ and $EuFe_2P_2$. Adapted from [160].

that the coexistence of superconductivity with Fe magnetism can be enabled through a phase separation. It means that in the sample there are some parts of the volume with the magnetic ordering neighboring with the paramagnetic islands which host the superconducting phase. On the other hand, measurements of the muon spin relaxation [164], [165], NMR [24], [166], and tunneling spectroscopy [167] revealed no phase separation on polycrystalline samples, which means that the microscopic phase coexistence is taking place. This suggestion was also proven by ARPES measurements [14].

The formation of the Fulde–Ferrell–Larkin–Ovchinnikov (FFLO) phase, when SC coexists with magnetism, was observed in heavy fermionic systems and organic superconductors [168]. But in iron pnictides it was also proposed theoretically [169] and suggested experimentally [170].

1.4.3 Superconductivity and Eu magnetism in iron pnictides

Among various parent compounds of iron pnictide superconductors $EuFe_2As_2$ stands out due to the presence of both, the SDW ordering of the itinerant carriers in the Fed-derived bands and the AFM ordering of the localized Eu^{2+}-f spins, which show a large local Eu^{2+} magnetic moments with $J = S = 7/2$. As it is shown in Fig. 1.10, the Eu^{2+} spin order ferromagnetically in plane and antiferromagnetically between planes in undoped $EuFe_2As_2$. The sketch of 3d orbital levels for undoped $EuFe_2As_2$ and fully substituted $EuFe_2P_2$, obtained by all-electron full potential linear augmented plane wave plus local orbitals method [160], are shown in Fig. 1.10. The Eu $4f$ states are localized. DOS calculations show that the unfilled Eu $4f$ states are at about 10 eV above the Fermi level [160].

The antiferromagnetic Eu^{2+}-spin order in the undoped SDW $EuFe_2As_2$ is rather well understood [17], [171]. Contrary, no coherent picture of Eu^{2+} spin ordering upon P or Co doping exists. In addition to the proposal of a SC induced helimagnetic ordering [172] in $Eu(Fe,Co)_2As_2$ a canted AFM was proposed by Zapf *et al.* [173] in superconducting $EuFe_2(As_{1-x}P_x)_2$, while a pure FM ordering at $x = 0.15$ coexisting with superconductivity was reported by Nandi *et al.* [33]. Recently, a spin-glass state over the whole P doping range was also suggested by Zapf *et al.* [173].

Upon application of an in-plane magnetic field the Eu^{2+} AFM order is destroyed above $\mu_0 H \sim 1$ T [174], [175]. There is also an indication of a metamagnetic transition with a partial spin reorientation around $\mu_0 H \sim 0.5$ T in $EuFe_2As_2$ [175]. In $EuFe_2(As_{0.81}P_{0.19})_2$ a similar field-induced spin reorientation in the ab plane is observed around $\mu_0 H \sim 0.6$ T

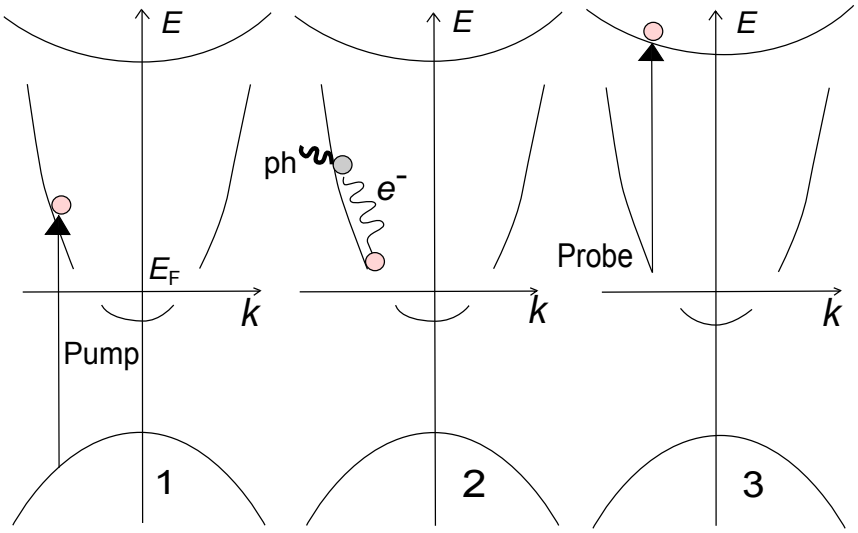


Figure 1.11: A schematic diagram of the electron processes in pump-probe experiment. In the first step the pump photoexcites quasiparticles, in the second step the quasiparticles thermalize with electrons or phonons. The last step is a detection of the photoexcited quasiparticles near the Fermi level.

[33].

The study on the Eu^{2+}spin dynamics and possible mechanisms of coexistence of Eu^{2+} spin ordering and superconductivity in $Eu(Fe,Co)_2As_2$ and $EuFe_2(As,P)_2$ by means of the ultrafast Kerr effect measurements is presented in Chapter 8.

1.5 Ultrafast optical spectroscopy: theory and experiments

The developments in ultrafast lasers have opened a new field of time-resolved spectroscopy [176]. The optical ultrafast time-resolved spectroscopy, often called pump-probe spectroscopy (see Fig. 1.11), is an experimental technique for studying dynamical properties of the condensed matter and some other systems. The main concept of the technique is splitting of the pulsed laser output into two beams. One beam is used to excite the system and it is called the pump (P). Another, the probe (p) beam is suitably delayed in time with respect to the pump. The reflectivity or transmittance changes of the probe beam reflect the changes induced in the sample by the pump excitation. This technique allows separation of different excitations by their relaxation times, which is not possible by other techniques.

The technical details of the pump-probe spectroscopy are presented in the next chapter. In the following sections the theoretical approaches which are traditionally used in the ultrafast spectroscopy are going to be discussed. We start from the discussion of processes which contribute to changes of probe reflectivity. Subsequently, we discuss the two-temperature model, which is often used to describe the electron-phonon thermalization in metals. Further, we introduce the Rothwarf-Taylor equations, which provide a successful phenomenological framework for understanding non-equilibrium dynamics in gapped systems. Finally, we discuss the bottleneck model in a weak and strong excitation regime.

1.5.1 Transient reflectivity

For small changes of the complex dielectric constant the photoinduced transient reflectivity can be written as:

$$\triangle R = a\triangle\epsilon' + b\triangle\epsilon'', \tag{1.8}$$

where ϵ' and ϵ'' are the real and imaginary parts of the complex dielectric constant, respectively, $a = \delta R/\delta\epsilon'$ and $b = \delta R/\delta\epsilon''$ are constants. In principle, to completely characterize the changes of dielectric constant one should measure both the reflectivity and transmission over the entire optical spectrum. However, a lot of information can also be obtained by measuring only the reflectivity changes at a single wavelength, as it was shown in [177].

To understand the optical response in pump-probe experiments, let us consider the dielectric constant, which is calculated by the Fermi golden rule:

$$\epsilon = \int d^3k |M_{\alpha,\beta}(\boldsymbol{k})|^2 \frac{f_\alpha(\boldsymbol{k}) - f_\beta(\boldsymbol{k})}{\epsilon_\alpha(\boldsymbol{k}) - \epsilon_\beta(\boldsymbol{k}) - h\omega_{\text{probe}}}, \tag{1.9}$$

where $|M_{\alpha,\beta}(\boldsymbol{k})|$ is the effective probe-polarization and wavelength dependent optical-dipole matrix element between an initial band α, and a final band β, $f_\alpha(\boldsymbol{k})$ and $f_\beta(\boldsymbol{k})$ are the quasiparticle distribution functions in α and β bands, respectively, $\hbar\omega_{\text{probe}}$ is the probe-photon energy.

For simplicity we assume that the energy of the final band is far from the Fermi energy, and probe energy is much higher than the thermal energy$|\epsilon_\beta(\mathbf{k}) - \epsilon_{\text{F}}| \sim h\omega_{\text{probe}} \gg k_{\text{B}}T$, so the changes of the distribution function $\Delta f_\beta(\mathbf{k})$ after the fast initial relaxation of the ultra-hot carriers can be neglected. Assuming that the transient reflectivity is proportional to the transient absorption, we obtain:

$$\delta R_{\alpha,\beta} \propto \int d^3k |M_{\alpha,\beta}(\boldsymbol{k})|^2 \delta f_\alpha(\boldsymbol{k}) g(\epsilon_\beta(\boldsymbol{k}) - \epsilon_\alpha(\boldsymbol{k}) - h\omega_{\text{probe}}), \tag{1.10}$$

where $\Delta f_\alpha(\mathbf{k})$ is the photoexcited change of the quasiparticle distribution function in the initial band, and $g(\epsilon)$ is the effective transition line-shape.

Different regions of the k-space contribute to the integral (1.10) due to the $\boldsymbol{k}$-vector selectivity of the matrix element $|M_{\alpha,\beta}(\boldsymbol{k})|$, depending on the probe polarization and photon energy. Due to contributions of several optical transitions with finite effective line-widths it is usually assumed that (1.10) smoothly samples over the relevant energy range in the vicinity of the Fermi energy and ΔR can be approximated by the total photoexcited carrier density n_{pe}, $\Delta R = \gamma n_{\text{pe}}$, [178], [179] and any change of ΔR upon change of the external parameters (T for example) is attributed to the change of n_{pe}.

However, 122 iron pnictides are characterized by the complicated electronic structure reconstruction below T_{SDW}, which may violate the assumption of a constant γ [22]. Expanding γ in terms of a temperature-dependent order parameter $\Delta(T)$, associated with the opening of the partial T-dependent gap below T_{SDW}, the changes of reflectivity can be expressed as following:

$$\Delta R = \left[\gamma_0 + \eta\frac{\Delta^2(T)}{\Delta^2(0)}\right] n_{\text{pe}}. \tag{1.11}$$

where γ_0 is a constant.

In this work we are going to discuss not only the electronic response, but also the relaxation to spin and phonon degrees of freedom, and take a look on the dynamics of the order parameter. All these processes contribute to the changes of the complex dielectric constant, and consequently to measured transient reflectivity. In order to discriminate between

aforementioned contributions comparison with different experiments is often employed. Of particular importance is a knowledge of the transition temperatures.

The timescales of relaxation processes are defined by the transition rates between states, which are dependent on the magnitude of the relevant interactions. Relaxation by electron-electron scattering, electron-phonon scattering and electron-spin scattering span a range between a few femtoseconds to a few hundred picoseconds or even longer.

1.5.2 Electron-phonon interactions: two-temperature model and beyond

The two-temperature model (TTM) was introduced to describe the relaxation of photoexcited electrons in metals *via* electron and phonon degrees of freedom [180]. The model is based on the assumption that electrons and phonons are in thermal quasi-equilibrium (the electron-phonon thermalization is much slower than electron-electron scattering), with two different time-dependent temperatures of electrons, T_e, and lattice, T_l. When the metal is excited by an ultrashort laser pulse a non-equilibrium hot electron distribution is created. Because of the large difference between the electronic (C_e) and lattice (phononic C_p) heat capacities (with $C_\mathrm{p} \gg C_\mathrm{e}$ at higher temperatures) the lattice temperature remains essentially unchanged. Then, over a time scale of a few picoseconds the electrons *via* electron-phonon interactions return to a local equilibrium at a somewhat elevated temperature, causing an equilibrium distribution of the excess energy between the electronic and lattice subsystems. Finally, a slower relaxation process dominated by heat diffusion returns the system to the ambient temperature. The rate of relaxation to the local equilibrium is governed solely by the electron-phonon processes.

The dynamics of the electron and lattice sub-systems can be described by a set of coupled differential equations given as [180]:

$$C_\mathrm{e}(T_\mathrm{e})\frac{\partial T_\mathrm{e}}{\partial t} = \frac{\partial}{\partial z}\left(k_\mathrm{e}\frac{\partial T_\mathrm{e}}{\partial z}\right) - g(T_\mathrm{e} - T_\mathrm{l}) + S(z,t), \tag{1.12}$$

$$C_\mathrm{l}(T_\mathrm{l})\frac{\partial T_\mathrm{l}}{\partial t} = g(T_\mathrm{e} - T_\mathrm{l}). \tag{1.13}$$

The first part of Equation (1.12) describes the electronic heat transport into the bulk of the sample. k_e is the thermal conductivity and its temperature dependence can be described by $k \approx k_0(T_\mathrm{e}/T_\mathrm{l})$, where k_0 can also be a temperature-dependent quantity [181]. With the assumption that the laser beam size is much larger than the electron diffusion length, only the diffusion along the direction of the surface normal z is important. The second part of Equations (1.12) and (1.13) account for the cooling of the electrons and heating of the phonons, which is characterized by the electron-phonon interaction with a coupling constant g. The $S(z,t)$ is the source term which represents the amount of the laser power absorbed in a unit volume.

The electron-phonon interaction is the main process governing the formation of the superconducting state in the BCS superconductors. The electron-phonon coupling constant describes quantitatively the strength of this interaction. If one approximates the second moment of Eliashberg spectral function with the product of a dimensionless electron-phonon constant and the square of a characteristic phonon frequency $\lambda\langle\omega^2\rangle = \lambda\omega_0^2$, then the electron-phonon coupling constant can be determined from [84]:

$$\lambda\langle\omega^2\rangle = 2\int_0^\infty \alpha^2 F(\omega)\omega d\omega. \tag{1.14}$$

Recently, the TTM model has been criticized [182], [183]. Authors argued that electron-electron thermalization rate is much smaller than the electron-phonon thermalization rate in the temperature range where most of the experiments are performed $\hbar^2\omega_{\mathrm{D}}^2/E_{\mathrm{F}} < k_{\mathrm{B}}T < \hbar\omega_{\mathrm{D}}(E_{\mathrm{F}}/\hbar\omega_{\mathrm{D}})^{1/3}$, contrary to the main assumption of the TTM model. Indeed, the e-ph thermalization rate is $\tau_{\mathrm{e-ph}}^{-1} \sim T^3/\omega_{\mathrm{D}}^2$ in the low $k_{\mathrm{B}}T < \omega_{\mathrm{D}}$ limit and $\tau_{\mathrm{e-ph}}^{-1} \sim \omega_D^2/T$ in the high $k_{\mathrm{B}}T > \omega_{\mathrm{D}}$ limit [183], where ω_{D} is the Debye frequency, and T is the equilibrium temperature. While in [183] it was demonstrated that the e-e thermalization rate $\tau_{\mathrm{e}}^{-1} \sim T^2/E_{\mathrm{F}}$, where E_{F} is the Fermi energy. Some inconsistencies of the TTM model were also shown in measurements of the relaxation time in noble metals [184], where the relaxation time does not show any pump fluence dependence, as well as in the time-resolved photoemission experiments [185]. Alternatively to the TTM model, for describing the dynamics in photoexcited metals the model [182] which represents the Bolzman's kinetic equations was proposed. It takes into account the non-equilibrium electron distribution function with the electron-electron and electron-phonon collision integrals, while assuming that phonons are at equilibrium.

Since the scattering on phonons is one of the main relaxation processes for electrons, $\lambda\langle\omega^2\rangle$ can be extracted from the electron-phonon relaxation time $\tau_{\mathrm{e-ph}}$ [186] :

$$\lambda\langle\omega^2\rangle = \frac{2\pi}{3}\frac{k_B T_{\mathrm{l}}}{\tau_{\mathrm{e-ph}}}. \tag{1.15}$$

The above formula is only applicable if the relaxation time $\tau_{\mathrm{e-ph}}$ does not depend on the pump fluence [186].

The ultrafast time-resolved spectroscopy is known is known to be one of few experimental techniques, which directly probe $\lambda\langle\omega^2\rangle$, and nicely separate the electron-phonon coupling from other effects. Expression 1.15 is applicable also if $\tau_{\mathrm{e-e}} > \tau_{\mathrm{e-ph}}$. Since $\tau_{\mathrm{e-ph}}$ is predicted to be linearly dependent on T_{l} (not T_{e} as in two-temperature model), it should be independent on the fluence. This fact can be taken as a test of the model's applicability. To determine $\tau_{\mathrm{e-ph}}$ the pump-probe signal measurements are always performed at higher temperatures, because the model is only applicable for temperatures higher than the Debye temperature.

Coupling between electrons and phonons drives the formation of the electron pairs responsible for conventional superconductivity [187]. In iron pnictides the average e-ph coupling constant has been found to be relatively weak both experimentally [28], [143], [188] and theoretically [86], [93] with $\lambda \leq 0.35$, insufficient to explain the high critical temperatures found in the pnictides within the conventional pairing scheme, similarly to the copper oxide superconductors [186], [189].

1.5.3 Rothwarf-Taylor model

In contrast to metals where the recombination of photoexcited quasiparticles is mainly governed by the electron-phonon interaction, in the gapped systems, such as SC, CDW, or SDW, one needs to take into account phonon reabsorption processes. Let us assume a simple system with a gap in electronic density of states at the Fermi energy. The most successful model used to interpret the carrier dynamics in superconductors is the Rothwarf-Taylor (RT) model [190].

When a system is excited by a laser pulse, the photoexcited electrons create quasiparticles above the gap. During the recombination the photoexcited quasiparticles relax by emitting bosons, which depending on the system can be phonons, magnons or any other kind of bosons. If these bosons remain in the system and have enough energy they can excite new quasiparticles, thus slowing down the energy relaxation of the QP system, and therefore a "bottleneck" appears in the relaxation. On the other hand, when the bosons

lose their energy with time to the low frequency bosons with energies lower than the gap size, they can not excite QP. It means that the lifetime of QP is not only governed by the intrinsic relaxation rate, but also one should consider the boson reabsorption processes, which are responsible for the "bottleneck" in the relaxation channel for quasiparticles. The model describes the evolution of the quasiparticle and high-frequency phonon populations by a set of two differential equations:

$$\frac{dn}{dt} = I_0(t) + \eta N - Rn^2, \tag{1.16}$$

$$\frac{dN}{dt} = J_0(t) - \frac{\eta N}{2} + \frac{Rn^2}{2} - \gamma(N - N_T), \tag{1.17}$$

where n and N are the concentrations of QPs and high-frequency bosons, respectively, η is the probability for pair breaking by absorption of high-frequency bosons, R is the QPs recombination rate with the creation of HFB. N_{T} is the concentration of high-frequency bosons (HFB) in the thermal equilibrium, and γ is the decay rate for HFB.

Equation (1.16) describes changes of concentration of the excited quasiparticles. The first two terms on the right side describe the increasing of the QP concentration due to the laser initial excitation I_0, and absorption of the high-frequency bosons ηN. The last term Rn^2 represents the bimolecular recombination of QPs to the superconducting condensate. The second equation describes the dynamics of bosons. Their number increases due to pumping with a laser pulse J_0 and QP relaxation, $\frac{Rn^2}{2}$. Terms $\frac{\eta N}{2}$ and $\gamma(N-N_{\mathrm{T}})$ represent the processes of reexcitation of the QP by the high-frequency bosons and their decay to the low frequency bosons, respectively. The phonon decay rate is considered as temperature independent [191].

Even though in the original paper authors considered phonons as the main channel of QPs relaxation, the model is generally applicable for many systems, which are characterized by the presence of the gap with the magnitude close to the boson frequencies, magnons for instance. The RT model is equally well applicable for CDW [19], [192], [193] and SDW [28] systems.

Depending on the way of understanding the pump-probe signal, two main approaches of using the RT model for describing ultrafast pump-probe experiments can be found in the literature.

If the phonon relaxation rate γ is small and the equilibrium between quasiparticles and HFB is established, then it is called the strong bottleneck regime, and the weak bottleneck regime in the opposite case. A detailed study of the evolution of the SC state following excitation by an ultrashort laser pulse using the RT model is presented in [191], where analytical solution of the model in the limit of a strong and a weak bottleneck is obtained. The results enable comparison to experimentally measured quantities like the SC state recovery time and the photoinduced QP density. Comparison with published data suggests that both cuprate and conventional SCs follow the RT scenario, both being in the strong bottleneck regime.

Another approach was presented in [194], where it was assumed that the initial laser pulse excites only quasiparticles. The relaxation observed in the transient reflectivity was associated with the thermalization of quasiparticles to bosons in the so-called pre-bottleneck regime. In this case the bosons contribution to the first equation is small and ηN can be neglected. Thus, the number of the photoexcited quasiparticles changes with time as $n \sim \frac{n_0}{n_0+Rt}$. In [194] it was assumed that the measured reflectivity change is related to an exponentially weighted average of the non-equilibrium quasiparticle density. This model was used to describe time-resolved photoinduced reflectivity experiments in the cuprate superconductor $YBa_2Cu_3O_{6.5}$ [194]. The approximation of this approach to

Rothwarf-Taylor model is based on the assumption that the laser pulse mainly influences the quasiparticle bath, which excites phonons when thermalized. However, there are studies [177] which suggest that the quasiparticle dynamics arises from the fact that the photoexcitation is initially followed by energy relaxation to high-frequency phonons instead of, as commonly assumed, e-e thermalization.

1.5.4 Temperature dependence of the quasiparticle density and the relaxation time

In this section we review the work by Kabanov et al. [195], in which temperature dependence of the photoinduced quasiparticle density and its relaxation time is theoretically studied.

When the system is only weakly perturbed by the laser pulse and the photoexcited carrier density is substantially smaller than the total carrier density, the gap can be considered as unperturbed. Under the bottleneck conditions the photoexcited quasiparticles thermalize with HFB and can be characterized by the temperature T'. The non-equilibrium phonon (N_ω) and quasiparticle (f_ϵ) distributions can be approximated as:

$$N_\omega = \begin{cases} \frac{1}{\exp\left(\frac{\hbar\omega_q}{k_\mathrm{B}T}\right)-1}, \hbar\omega_\mathrm{q} < 2\Delta \\ \frac{1}{\exp\left(\frac{\hbar\omega_q}{k_\mathrm{B}T'}\right)-1}, \hbar\omega_\mathrm{q} > 2\Delta \end{cases}; \tag{1.18}$$

$$f_\epsilon = \frac{1}{\exp\left(\frac{\epsilon}{k_\mathrm{B}T'}\right)+1}, \tag{1.19}$$

where T is the lattice temperature, T' is the temperature of quasiparticles and high-frequency phonons with $\hbar\omega_\mathrm{q} > 2\Delta$, ω_q phonon frequency and Δ is the energy gap. In the strong bottleneck regime, when the equilibrium between QPs and phonons is established, the number of excited quasiparticles can be determined from the energy conservation condition. Then, for the temperature independent gap the number of photoexcited quasiparticles is given [178] by:

$$\Delta R/R \sim n_\mathrm{pe} \sim \frac{E_i/\Delta}{1 + g_\mathrm{ph}\exp(-\Delta/k_\mathrm{B}T)}. \tag{1.20}$$

In the case of temperature dependent BCS gap the expression is:

$$\Delta R/R \sim n_\mathrm{pe} \sim 1/\left[\left(\frac{2\Delta(T)}{k_\mathrm{B}T_\mathrm{c}}+\frac{T}{T_\mathrm{c}}\right)\left(1+g_\mathrm{ph}\sqrt{\frac{k_\mathrm{B}T}{\Delta(T)}}\exp\left(-\frac{\Delta(T)}{k_\mathrm{B}T}\right)\right)\right], \tag{1.21}$$

where $g_\mathrm{ph} = \frac{2\nu}{N(0)\hbar\Omega_C}$ represents the relative effective number of the involved boson degrees of freedom, $N(0)$ is the density of states at the Fermi energy, Ω_C is phonon energy cut off, ν is the number of phonons involved in the bottleneck formation. The notable difference in Equations (1.20) and (1.21) is the presence of the tail in the signal in the case of T-independent gap, while in the temperature-dependent gap case the signal drops to zero. Another peculiar distinction is a small peak close to $T/T_\mathrm{c} \approx 0.7$, which is predicted in the temperature-dependent case, but not always present, depending on g_{ph}.

In the bottleneck model the relaxation rate of photoinduced QPs is determined by the energy transfer from the high-frequency to the low frequency bosons. This is described by the Bolzman kinetic equations, with phonon-phonon scattering integral. The final expression for the T-dependence of the relaxation rate in the high-T limit leads:

$$\frac{1}{\tau_\mathrm{ph}} = 12\Gamma_\omega\Delta(T)^2/\hbar\omega^2\ln\left[1/\{1/2N(0)\Delta(0)^2+\exp\left(-\frac{\Delta(T)}{k_\mathrm{B}T}\right)\}\right], \tag{1.22}$$

where Γ_ω is the Raman phonon frequency. The rate at which phonons lose their energy increases with the energy gap size. It explains the divergence of the relaxation time as T approaches to T_c from below .

1.5.5 Optical response at strong photoexcitation

The physics described above is applicable only in the low excitation regime, where $n \ll n_T$, $N \ll N_T$ and where the pump-probe signal linearly depends on the pump fluence. With increasing the pump fluence the transient reflectivity amplitude deviates from the linear dependence and saturates [29]. This corresponds to the complete destruction of the ordered state. The magnitude of the transient reflectivity is simply the difference of the dielectric constant between the gapped and the normal state. The Mattis-Bardeen formula, which was derived to explain the anomalous skin effect of superconductors, [196] gives the ratio between the optical conductivity in superconducting and normal states $(\sigma_S - \sigma_N)/\sigma_N$ calculated for a single-band model. In the limit of photon energies $\hbar\omega$ being much higher than the gap $\Delta(T)$ the following expression for the amplitude of reflectivity change is derived in [29]:

$$A(T) \propto \left(\frac{\Delta(T)}{\hbar\omega}\right)^2 \ln\left(\frac{3.3\hbar\omega}{\Delta(T)}\right). \tag{1.23}$$

This equation is in a good agreement with experimental data for copper oxide superconductors [29], [197] and iron pnictides [198].

1.5.6 Order parameter dynamics

Changes of the order parameter (OP) can be observed in the reflectivity changes:

$$\delta R(t) = \frac{\partial R}{\partial \psi}\delta\psi(t). \tag{1.24}$$

The first attempt to observe the order parameter dynamics through the phase transition in electronic systems was reported in [199], where femtosecond time- and angle-resolved photoelectron spectroscopy were used (trARPES) to observe the transient charge density wave melting, excited collective vibrations in $TbTe_3$. The study of the temporal evolution of systems undergoing symmetry breaking phase transitions started from the paper of Yusupov *et al.* [30]. Authors have employed a novel three-pulse ultrafast technique (Fig. 1.12a) for a high-time-resolution study of the evolution of both the bosonic and fermionic excitations through an electronic charge-ordering phase transition. The main idea realized in the report is to quench the system into the high-symmetry state with intense 'destruction' (D) laser pulses and then monitor the time evolution through the phase transition by measuring the resulting reflectivity oscillations with a pump– probe (P–p) sequence.

The critical slowing down of the order parameter dynamics near the phase transition was explained in the terms of the Ginzburg-Landau theory. The time evolution of the potential energy of the system U is shown schematically in Fig. 1.12b. Before the arrival of the destruction pulse the system is ordered and the amplitude of the order parameter does not change. After the D pulse, the double-well potential disappears in favor of a single energy minimum. After some time delay two minima emerge and start to attract the system, breaking the symmetry.

The first measurements of the trajectory of the superconducting order parameter $\psi(t)$ through the normal-to-superconductor transition in $La_{1.9}Sr_{0.1}CuO_4$ under ultrafast quench conditions are reported in [200].

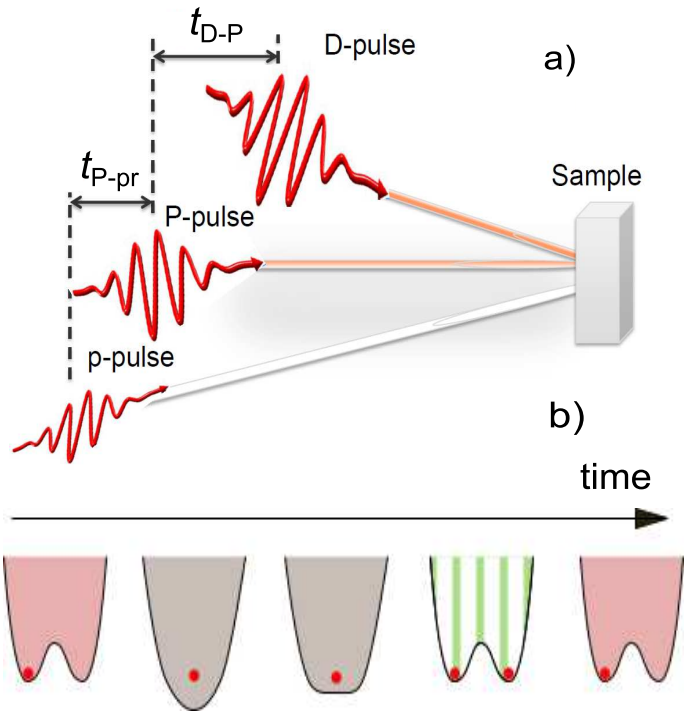


Figure 1.12: a) A schematic representation of the timing of the laser pulses: a destruction (D) pulse is absorbed within the penetration depth and quenches the system, and a pump–probe (P–pr) sequence probes the reflectivity at a later time $\triangle t_{P-pr}$. b) The evolution of the potential U as a function of time, described in terms of time-dependent Ginzburg-Landau theory. The system is in the high-symmetry state (gray) for very short times after the quench. The red dot signifies the state of the system, and the blue/orange potential signifies a topologically mixed broken-symmetry state.

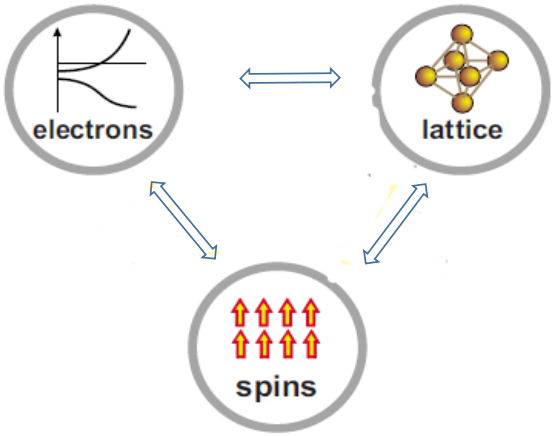


Figure 1.13: The possible excitation energy transfer paths in terms of the three temperature model.

1.5.7 Magnetization dynamics excited by ultrafast laser pulses

In the recent years it was shown that ultrashort laser pulses can be used to affect different types of magnetic materials [201], [202]. Magnetization dynamics can be excited in media thermally [203], by fast heating, or nonthermally *via* magneto-optic processes. Thermal ultrafast demagnetization is usually described in terms of the three-temperature model, where in contrast to TTM, beside the electron and lattice, the spin degrees of freedom are also included. Generally speaking, the laser pulse can affect any of the reservoirs, depicted in Fig. 1.13. The spin reservoir can be excited directly [204], [205] or through indirect electron-spin or spin-lattice interactions. Recent experiments [206], [207] demonstrated the possibility of considerable non-thermal excitation of spin fluctuations by laser pulses. Such excitations are possible because of the fact that the impact of short (effective length is 200 fs) laser pulses of circularly polarized light on transparent AFM is equivalent to the generation of the pulsed magnetic field due to the inverse Faraday effect. These field pulses are characterized by the duration of the order of the optical pulse length and field strength up to 1 T. This allows to significantly manipulate the magnetization on time scale of the order of picoseconds, without significant heating of the sample [208]. In this case, the excitation of the spin system is realized through interaction of the field pulse with a weak ferromagnetic moment, which is present in the ground state of the material due to its symmetry properties.

1.5.8 Time-resolved spectroscopy in iron pnictides: overview

1.5.8.1 All-optical experiments

The first time-resolved optical spectroscopy experiments in the superconducting pnictides were reported by Mertelj *et al.* in 2009 [63]. Afterwards, a number of studies on the competition between the ground states by systematic experiments as a function of doping and temperature were reported. This section is devoted to a short overview of ultrafast experiments performed in iron pnictides.

In [63] authors investigate the quasiparticle relaxation in nearly optimally doped superconducting $SmFeAsO_{0.8}F_{0.2}$ with $T_c = 49.5$ K. Multiple relaxation processes were observed

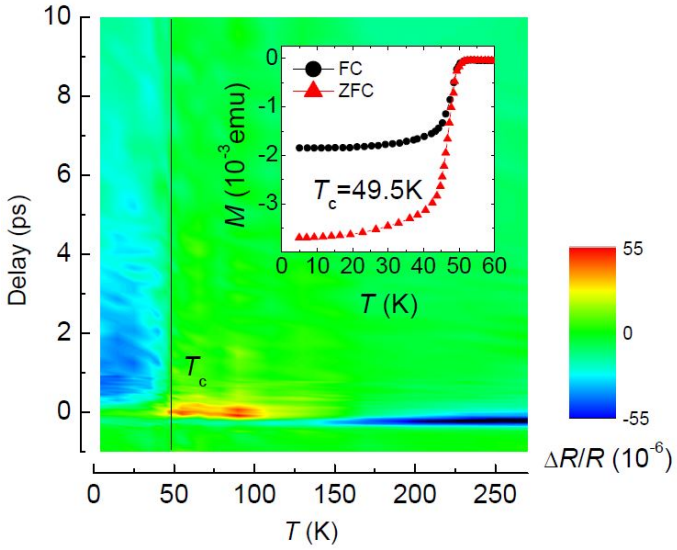


Figure 1.14: Temperature dependence of the photoinduced reflectivity $\Delta R/R$ for $SmFeAsO_{0.8}F_{0.2}$ reveals two distinct relaxation processes. Below T_c, the response of the superconducting state is clearly seen. Another component is assigned as a response from a pseudogap. In the inset, the temperature dependence of the magnetization in the superconducting state is shown. Adapted from [63].

(Fig. 1.14). Below T_c the response is dominated by the difference between the reflectivity in the superconducting and normal state, which authors describe with Mattis-Bardeen model. The "pseudogap" feature was observed with an onset below 180 K and relatively well described by a temperature independent gap with magnitude $\Delta = 61 \pm 9$ meV. The saturation fluence was measured for both components and it is found to be 4 and 40 $\mu J/cm^2$, respectively.

In the undoped $SmFeAsO_{0.8}$ single crystals a single relaxation process is reported in [209]. The signal shows a remarkable critical slowing down of the QP relaxation dynamics at the SDW transition temperature $T_{SDW} = 125$ K. From the pump-photon energy dependence authors conclude that the SC state and PG relaxation channels are independent, implying the presence of two separate electronic subsystems. Authors discuss the data in terms of spatial inhomogeneity and multiband scenarios, finding that the latter is more consistent with the present data.

Furthermore, Mansart *et al.* [188] investigated the photoexcited electron energy relaxation in the same material focusing on the possibility of preferential relaxation to different phonon baths. Separating the phonon baths into a high-frequency phonon bath and a low frequency bath, and using a three-temperature model [185], they attribute the faster relaxation component to preferential scattering of the electrons with only a subset of the lattice vibration modes with a second moment of the Eliashberg function $\lambda\langle\omega^2\rangle = 264$ meV^2. The simultaneous excitation of a strong fully symmetric A_{1g} optical phonon corroborates this conclusion and makes it possible to deduce the value of $\lambda = 0.12$. This small value for the electron-phonon coupling suggests that a phonon-mediated process cannot be the only mechanism leading to the formation of superconducting pairs in this family of iron pnictides. Another work on time-resolved study of coherent phonons in Ca-based IP was done by Kumar *et al.* [210]. The doping dependence of the quasiparticle relaxation dynamics in $(Ba,K)Fe_2As_2$ is reported by Chia *et al.* [211]. In optimally doped, underdoped, and undoped regimes. In the underdoped sample SDW order forms at ~ 85 K, followed

by superconductivity at ~ 25 K. They find an emergence of a normal-state order which suppresses SDW at a temperature $T* = 60$ K and argue that this normal-state order is a precursor to superconductivity.

Stojchevska *et al.* [28] investigated the quasiparticle relaxation and low-energy electronic structure in undoped $SrFe_2As_2$ exhibiting SDW ordering using optical pump-probe femtosecond spectroscopy. A remarkable critical slowing down of the quasiparticle relaxation dynamics at the SDW transition temperature $T_{SDW} = 200$ K is observed. From the temperature dependence of the transient reflectivity amplitude authors determine the SDW-state charge gap magnitude, $2\triangle_{SDW}/k_B T_{SDW} = 7.2 \pm 1$. The second moment of the Eliashberg function, $\lambda \left\langle (\hbar\omega)^2 \right\rangle = 110$ meV^2, determined from the relaxation time above T_{SDW}.

In [22] authors systematically investigated the photoexcited QP relaxation and the low-energy electronic structure in electron doped $Ba(Fe_{1-x}Co_x)_2As_2$ single crystals as a function of Co doping, $0 < x < 0.11$. Remarkably, the evolution of the photoinduced reflectivity transients with x proceeds with no abrupt changes as the sample composition changes the ground state from a SDW to a superconductor. In the SDW state, a bottleneck associated with a partial charge-gap opening is detected, similar to previous reports in different SDW iron pnictides [209], [211]. In the SC state, an additional relaxation component appears due to a partial (or complete) destruction of the SC state on a sub-0.5-picosecond timescale. From the SC component saturation behaviour the optical SC-state destruction energy, $U_p/k_B = 0.3\,\mathrm{K/Fe}$, was determined near the optimal doping.

Band-dependent quasiparticle dynamics in $Ba_{0.6}K_{0.4}Fe_2As_2$ ($T_c = 37$ K) measured using ultrafast pump-probe spectroscopy is reported by Torchinsky *et al.* [212]. In the superconducting state, they observe two distinct relaxation processes: a fast component with decay rate increasing linearly with excitation density and a slow component with an excitation density independent decay rate. Authors argue that these two components reflect the recombination of quasiparticles in the two hole bands through intraband and interband processes. The authors also find that the thermal recombination rate of quasiparticles increases quadratically with temperature. The temperature and excitation density dependence of the decays indicates fully gapped hole bands and nodal or very anisotropic electron bands. A more detailed study of quasiparticle dynamics of Ba-122 on both electron and hole doped sides is reported in [213]. In the $Ba(Fe_{0.94}Co_{0.06})_2As_2$ samples, dependence of the recombination rate on quasiparticle density at low doping is suppressed upon submergence of the inner hole band, and quasiparticle relaxation occurs in a slow, density-independent manner.

Employing the momentum sensitivity of time- and angle-resolved photo-emission spectroscopy Rettig *et al.* [21] demonstrated the analysis of ultrafast single- and many-particle dynamics in antiferromagnetic $EuFe_2As_2$. Authors find a strong difference in electron and hole dynamics induced by the SDW order (they call it AFM), which allows us to separate the SDW order parameter dynamics from single-particle dynamics. In the SDW phase, the restricted phase space for relaxation of electrons and a spin-relaxation bottleneck lead to a slow recovery of the SDW ordering within 800 fs, while the e-ph scattering is more than four times faster. Analysis of the leading edge midpoint of time-resolved angle-resolved photoemission spectroscopy (TR-ARPES) spectra suggests that the initial loss of spin order is dominated by purely electronic processes, followed by a structural reorientation on a slower time scale of 100 fs.

Kumar *et al.* [214] report on ultrafast study of superconducting $Ca(Fe_{0.944}Co_{0.056})_2As_2$ single crystals. They have estimated the zero-temperature charge gap value in the superconducting state to be $\sim 1.8 k_B T_c$ and an electron-phonon coupling constant $\lambda = 0.1$ in the normal state that signifies weak electron-phonon coupling in iron pnictides.

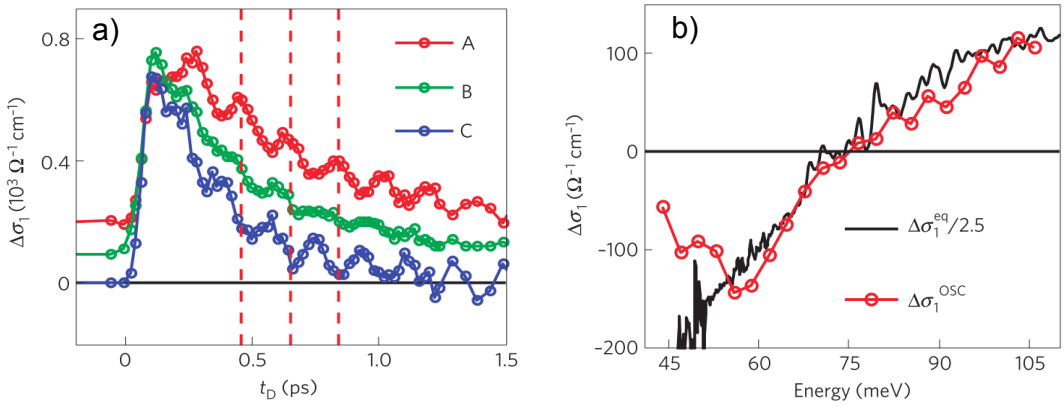


Figure 1.15: a) The photo-induced change averages of the optical conductivity at $T_L = 134$ K and $\Phi = 530\ \mu J/cm^2$. A, B, and C correspond to the spectral regions below, around, and above the SDW gap edge. The red dashed lines at the maxima/minima emphasize the out-of-phase oscillations in different frequency regions. b) Comparison of the dispersion of the oscillatory signal $\Delta\sigma_1^{osc}$ with the one of the SDW-induced changes in the equilibrium state $\Delta\sigma_1^{eq} = \sigma_1^{100K} - \sigma_1^{140K}$. $\Delta\sigma_1^{osc}$ is obtained from the difference spectrum between averages of maxima and minima in the interval of time delays between 0.28 ps and 1.12 ps after subtracting an exponential decay component of the electronic signal. Adapted from [23].

Authors of a recent study [15] reveal critical nematic fluctuations in an unstrained $Ba(Fe_{1-x}Co_x)_2As_2$. The ultrafast polarization spectroscopy allowed the observation of relaxation dynamics of the Ising-nematic-order parameter following a non-equilibrium photoexcitation. Authors distinguish two different dynamics in the anisotropic signal and associate them with the relaxation of the long-range magnetic order and nematic fluctuations. This observation suggests the existence of independent electronic nematic degrees of freedom, which differs from the magnetic and structural orders.

1.5.8.2 Other ultrafast techniques

The application of THz spectroscopy has allowed Kim *et al.* [23] to examine the coupling of the spin density wave gap Δ_{SDW} to the coherently generated phonon oscillations of the collective amplitude mode, showing that the Δ_{SDW} closely follows the phonon oscillations and is nearly adiabatically modulated by them. Authors distinguish three distinct spectral regions below (A), around (B), and above (C) the gap edge, as indicated in Fig. 1.15. The oscillations in spectral regions A and C (red and blue circles, respectively) are out of phase with each other, whereas the oscillatory response is strongly suppressed in region B (green circles). A quantitative analysis of the oscillatory component reveals that it closely matches the change in the optical conductivity that is induced in the equilibrium state by the SDW. It indicates that even in the normal state well above $T_{SDW} = 120$ K the coherently driven A_{1g} phonon periodically induces the SDW. As the coherent phonon oscillations modulate the Fermi surface pockets, they modulate the nesting wavevector which is the origin of the SDW instability. The implication of this observation is that in spite of the relatively weak electron-phonon coupling indicated by band structure calculations and photoelectron energy relaxation [188], there is a strong influence of the collective nuclear motion on the spin ordering.

It was suggested in a few works [215] that the shape of FeAs tetrahedra is a key to the

puzzle of iron pnictide phase diagram. To verify this, the time-resolved x-ray diffraction study on structural dynamics of coherently excited A_{1g} phonon mode parent Ba-122 iron pnictide was recently reported [216]. The fluence dependent intensity oscillations of two specific Bragg reflections with distinctly different sensitivity to the pnictogen height in the compound allows authors to quantify the coherent modifications of the Fe-As tetrahedra, indicating a transient increase of the Fe magnetic moments. By comparison with time-resolved photoemission data, they derive the electron-phonon deformation potential for this particular mode. The observed experiment value is comparable with theoretical predictions and demonstrates the importance of this degree of freedom for the electron-phonon coupling in the Fe pnictides.

Also, it should be mentioned that there are also TR-ARPES studies performed on IP [21], [143], where authors demonstrate the analysis of ultrafast single- and many-particle dynamics and estimate the electron-phonon coupling constants for a number of iron-based pnictides.

In [217] authors analyze the response of the electronic structure of the 122 Fe-pnictide parent compounds $Ba/EuFe_2As_2$ and optimally doped $BaFe_{1.85}Co_{0.15}As_2$ near the Γ point with the optical excitation by an infrared femtosecond laser pulse. Pronounced changes of the electron population within several 100 meV above and below the Fermi level are explained as a combination of (i) coherent lattice vibrations, (ii) a hot electron and hole distribution, and (iii) transient modifications of the chemical potential. Employing a transient three-temperature model the author deduces momentum-averaged electron-phonon coupling quantified by values of $\lambda \langle \omega^2 \rangle$ between 30 and 70 meV^2. The chemical potential generates pronounced transient changes reaching a maximum of 15 meV about 0.6 ps after optical excitation and is modulated by the coherent phonons.

The global oscillation of the Fermi level, at the frequency of the A_{1g} phonon mode observed in $BaFe_2As_2$ is reported in [218]. It is argued that this behaviour reflects a modulation of the effective chemical potential in the photoexcited surface region that arises from the high sensitivity of the band structure near the Fermi level to the A_{1g} phonon mode combined with a low electron diffusivity perpendicular to the layers. The results establish a novel way to tune the electronic properties of iron pnictides: coherent control of the effective chemical potential.

Chapter 2

Experimental details

In recent years femtosecond time-resolved spectroscopy was used as a powerful instrument for elucidating the nature of electronic excitations in high-temperature superconductors. This technique is widely used to examine the nature of superconductivity. In this chapter we will describe the experimental details of the results presented in the dissertation. First, the standard pump-probe technique is going to be introduced, including the new spectrally resolved pump-broadband-probe and three-pulse techniques. Since one chapter of the dissertation is dedicated to the magneto-optic measurements, technical details on Kerr effect measurements will also be discussed. At the end of this chapter we will also discuss some details about the sample preparation procedure.

2.1 Standard pump-probe setup

The conceptual scheme of the ultrafast time-resolved reflectivity measurements is shown in Fig. 2.1. A beam from a Ti-sapphire (Ti:Al_2O_3) laser is divided into two beams by a beam splitter. The pump (P) beam is stronger, and used for exciting the sample. The second, weaker beam is suitably delayed in time with respect to the pump beam. Changes excited in a sample by the pump are probed by this weaker, probe beam (pr). The signal we measure can be expressed as a relative change in the reflected probe intensity, measured by the photodetector. The lock-in amplification [219] allows the reduction of noise level down to 10^{-6}.

Measurements of the transient photoinduced reflectivity, $\Delta R/R$, were performed using 50-fs optical pulses from a 250-kHz Ti:Al_2O_3 regenerative amplifier seeded with a Ti:Al_2O_3 oscillator. We used the pump photons with both, the laser fundamental ($\hbar\omega_P = 1.55$ eV) and the doubled ($\hbar\omega_P = 3.1$ eV) photon energy, and the probe photons with the laser fundamental 1.55 eV photon energy. When using the doubled photon energy the scattered pump photons were rejected by long-pass filtering, while the analyzer was oriented perpendicularly to the pump beam polarization for rejection in the case of the degenerate pump and probe-photon energies. The pump and probe beams were nearly perpendicular to the cleaved sample surface (001) with polarizations perpendicular to each other and oriented with respect to the crystals to obtain the maximum/minimum amplitude of $\Delta R/R$ at low temperatures. The beam diameters were accurately identified by measuring the ratio of beam power before and after the set of fine pinholes, as it was described elsewhere [29]. The pump beam diameters were, depending on experimental conditions, in the $50-100$ μm range with somewhat smaller probe beam diameters.

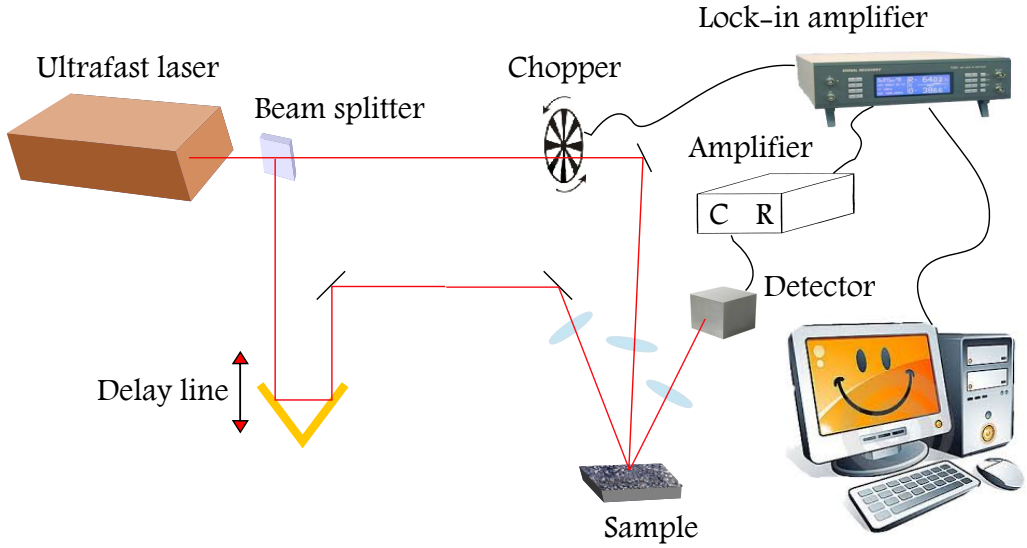


Figure 2.1: A scheme of a standard pump-probe setup. The beam from a Ti-sapphire laser is divided into two beams: the pump and the probe. The probe beam is suitably delayed in time with respect to the pump beam. The transient reflectivity induced in a sample by the pump is probed by this weaker beam. The signal we measure can be expressed as a relative changes of the reflectivity $\frac{\Delta R}{R} = \frac{R_{\mathrm{pump}} - R_0}{R_0}$, where R_{pump} and R_0 are reflectivities of the probe beam in the presence and absence of the pump beam, respectively.

2.2 Broadband probe experiments

The single-wavelength ultrafast spectroscopy enables the detection of very small signals by rejecting the laser noise by the lock-in detection. But on the other hand, use of broadband optical pulses can provide an additional spectral information.

Measurements of the probe-photon energy ($\hbar\omega_{\mathrm{pr}}$) dependent photoinduced reflectivity, $\Delta R/R$, (Fig. 2.2) were performed using a standard pump-probe technique, similar as described above. The pump photons with energy $\hbar\omega_{\mathrm{P}} = 3.1$ eV were derived by the frequency doubling in a barium borate (BaB_2O_4 – BBO) nonlinear crystal. The probe photons were derived from a supercontinuum generated in a 2.5 mm thick Al_2O_3 plate. Schott glass filter was used to suppress the strong spectral density around 1.55 eV resulting in the useful spectral density within the 1.65−2.55 eV band. The polarization of the probe photons with respect to the crystal was controlled by a broadband half-wave waveplate and the beam was focused on the sample by a pair of achromatic lenses. The reflected probe beam was collimated, dispersed by a transmissive optical grating and focused on a 48-channel silicon PIN diode array. The array was connected to an in-house built 64-channel integrating analog-to-digital converter that was synchronized to the laser and synchronously drove an optical chopper inserted in the pump beam.

The broadband light generation and the fact that the different wavelengths of probe pulse will travel through air and optical elements media for a different time, cause the time-delay between different frequencies, which is called chirp. In our system the supercontinuum pulse chirp is bout 2 ps long. It was calibrated from measurements of the samples at the room temperature, where the relaxation dynamics is comparable [22], [220] to the temporal resolution of the setup of about $\sim 200 - 300$ fs, depending on the probe-photon energy.

The pump beam diameters were, depending on experimental conditions, in a 300 μm

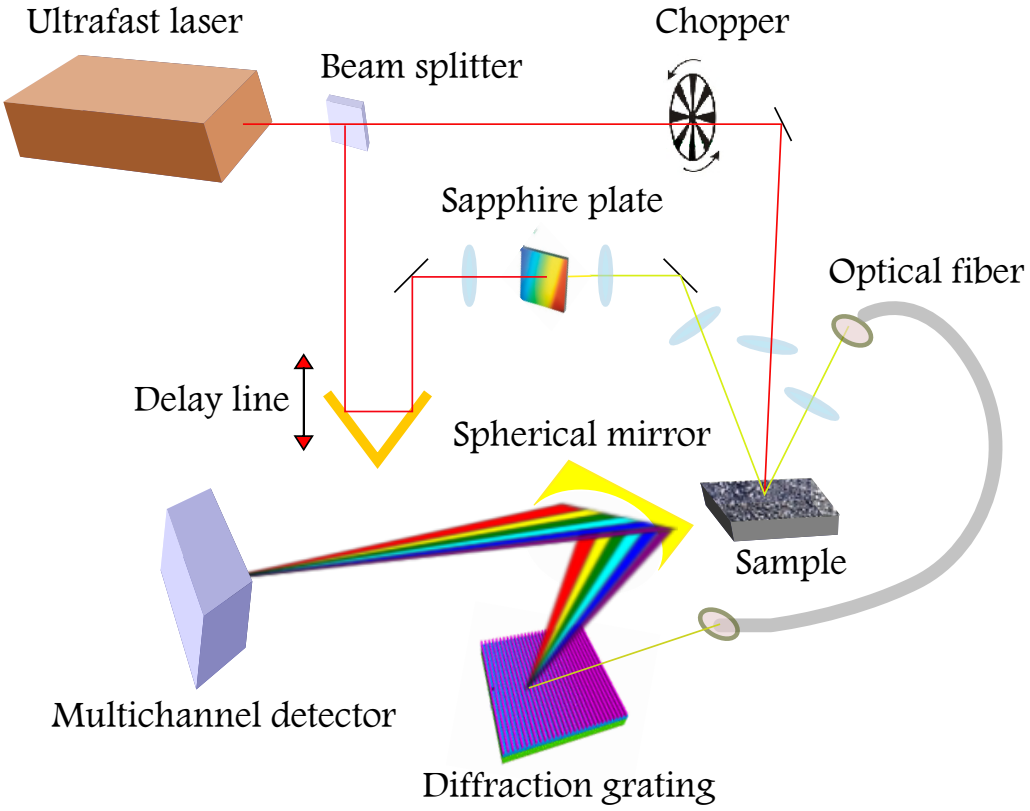


Figure 2.2: Schematic of the pump-broadband-probe experiment. A sapphire plate was inserted into the path of the probe beam in order to generate the 1.65−2.55 eV band. The reflected light was collected with a lens in an optical fiber. After the optical fiber the beam was diffracted on a diffraction grating and focused on the multichannel detector with a spherical mirror.

range with a smaller probe beam diameter of ~ 50 μm.

2.3 Magnetic measurements

Time-resolved magneto-optical Kerr angles were measured using a balanced detector scheme using a Wollaston prism [221] and a standard homodyne modulation technique in a 7-T split-coil optical superconducting magnet. Two $\lambda/2$ waveplates were inserted in front of the sample into the pump and probe beams in order to control the polarization. The reflected probe beam was directly (without mirrors) sent to the detector. The reflected probe beam was analyzed with a Wollaston prism and a pair of balanced photodiodes using standard lock-in techniques. The transient Kerr angle was determined as the difference between transient signals from the two balanced photodetectors.

To measure the ellipticity, η_{K}, a $\lambda/4$ waveplate was inserted in front of the Wollaston prism. In order to minimize the pollution of the Kerr signals with the photoinduced reflectivity signal, the detector was carefully balanced prior to each scan.

2.4 Three-pulse technique

In contrast to the standard pump-probe technique, an additional “destruction” pulse is introduced [30]. The destruction (D) laser pulse at 800 nm excites a cold sample into the

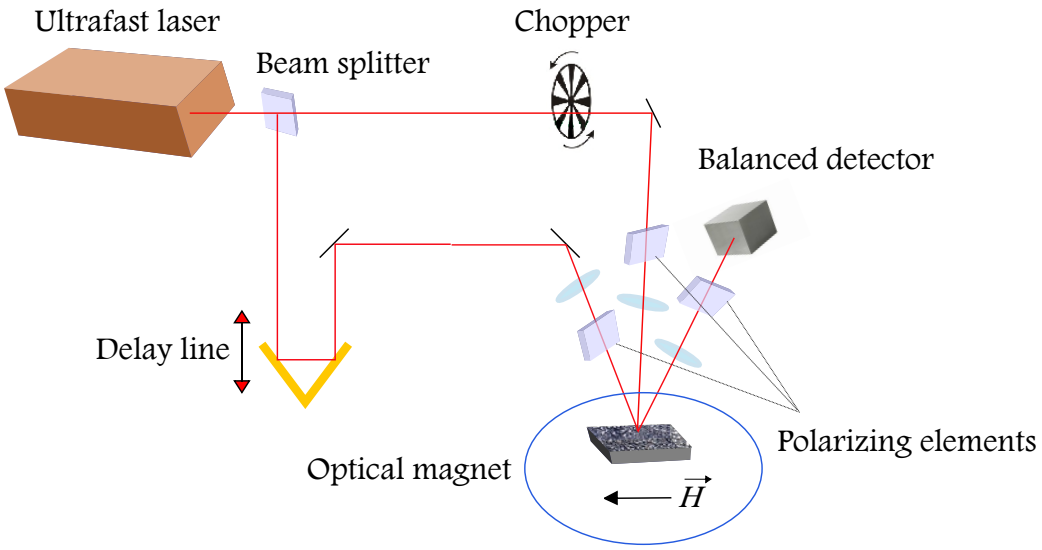


Figure 2.3: For Kerr rotation angle measurements the sample was inserted into a superconducting magnet which allows the application of magnetic fields up to 7 T. The polarization of pump and probe beams was controlled by polarizing elements. The Kerr angle measurements were performed by two phototedectors balanced by the Wollaston prism.

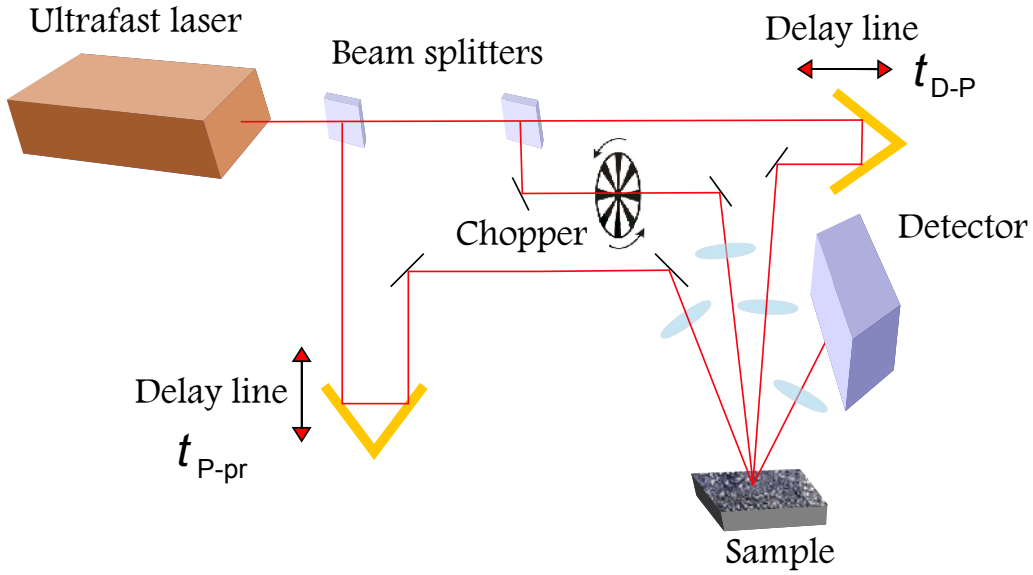


Figure 2.4: The schematic of the three-pulse experiment. Beside the pump and probe beam, a strong destruction beam is introduced. The D-pulses are suitably delayed in time with respect to the P-beam by means of an additional delay-line.

Sample name	Abbr.	T_c	T_S/T_{SDW}	Origin	T_N/T_C (Eu^{2+})
$EuFe_2As_2$	Eu-122	non-SC	190 K	*	18.5 K
$EuFe_2(As_{0.81}P_{0.19})_2$	EuP-122	22.7 K	-	*	18 K
$Eu(Fe_{0.83}Co_{0.17})_2As_2$	-	20.5 K	-	**	16.5 K
$Eu(Fe_{0.813}Co_{0.187})_2As_2$	-	8.5 K	-	**	17 K
$Eu(Fe_{0.685}Co_{0.315})_2As_2$	-	non-SC	-	**	18 K
$BaFe_2As_2$	Ba-122	non-SC	134 K	***	-
$BaFe_2(As_{0.7}P_{0.3})_2$	-	30 K	-	@	-
$BaFe_2(As_{0.5}P_{0.5})_2$	-	non-SC	-	@	-
$SrFe_2As_2$	Sr-122	non-SC	203 K	@@	-

Table 2.1: Samples, which were studied in the dissertation. *G. Cao, Z. Xu, Zhejiang Univ., Hangzhou, China; **Z. Bukowski, N. Zhigadlo, Polish Academy of Sciences, Warsaw, Poland; ***J.-H. Chu, I. R. Fisher, Stanford Univ., Stanford, USA; @D. L. Feng, Fudan Univ, Shanghai, China; @@X. Lin, G. Cao, Z. Xu, Zhejiang Univ., Hangzhou, China.

disordered state, breaking up the order. We then monitor the evolution of the transient reflectivity $\Delta R/R$ excited with a weaker pump (P) pulse as a function of time delay t_{D-P} between the D and P pulses. The D pulse fluence is adjusted to be above the threshold for causing the destruction of the ordered state.

2.5 Samples

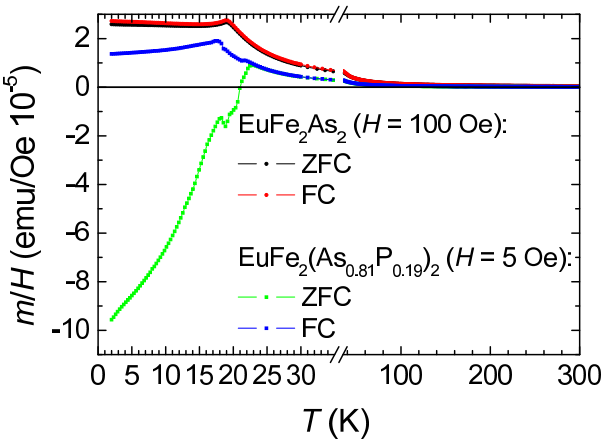


Figure 2.5: Magnetic susceptibility along the c-axis as a function of the temperature in Eu-122 and EuP-122.

Single crystals of $EuFe_2As_2$ and $SrFe_2As_2$ were grown by the flux method at Zhejiang University, similar to a previous report [222]. Small Eu chunks and powders of Fe, As (Alfa Aesar, >99.9 %) were mixed together in the molar ratio of Eu:Fe:As = 1:5:5 and sealed in an evacuated quartz ampoule. After heating the mixture up to 973 K for 24 hours, the obtained precursor was thoroughly ground before being loaded into an alumina

crucible. The crucible was then sealed by arc wielding in a tube made of stainless steel under atmosphere of argon, and then heated up to 1573 K over 10 hours in a muffle furnace filled with argon. After holding at 1573 K for 5 hours, the furnace was cooled down to 1223 K at the rate of 5 K/h, followed by switching off the furnace. In this way, large crystals with size up to $4\times4\times0.6$ mm^3 could be harvested.

The as-grown crystals were characterized by X-ray diffraction, which showed good crystallinity as well as single "122" phase. The exact composition of the crystals was determined by energy-dispersive X-ray spectroscopy (EDS) affiliated to a field-emission scanning electron microscope (FEI Model SIRION). The measurement precision was better than 5% for the elements measured.

The out-of-plane magnetic susceptibilities for Eu-122 and EuP-122 shown in Fig. 2.5 are consistent with previous results. [173], [175] From the susceptibility we infer Eu^{2+} spin ordering temperatures $T_N = 19$ K and $T_C = 17.6$ K in Eu-122 and EuP-122, respectively. EuP-122 also shows the onset of superconductivity at T_c =22.7 K.

Single crystals of $BaFe_2(As_{0.7}P_{0.3})_2$ were grown from a self flux at Fudan university and characterized as described previously.[22], [223] Sample showed the onset of superconductivity below $T_c = 30$ K.

For optical measurements all the crystals were glued onto a copper sample holder and cleaved by a razor before mounting in an optical liquid-He flow cryostat.

Chapter 3

Ultrafast transient reflectivity in 122 iron pnictides

3.1 General pump-probe features of the signal

As mentioned in Introduction the iron pnictides bear many different properties which have electronic, phononic or spin nature. To certain extent all of them are coupled to the dielectric constant of the material and, therefore, they can be studied by optical techniques. Since 2008, many experimentalists attempted to investigate the nature of intriguing iron pnictide features. Also, many ultrafast experiments were performed (see Introduction), which demonstrated striking features of relaxation dynamics in metallic, SDW and SC states.

In this chapter we will discuss the relaxation dynamic observed in optical transient reflectivity measurements presented in this thesis through the whole phase diagram. First, we will start from the metallic response at 300 K and then go down with temperature and explain all the features observed in the signal, like the excitation of coherent phonons or observation of nematic phase fluctuations. Excitations in the SDW state are going to be discussed in details in the next chapter, so here we will just mention them. Also, the influence of the doping on the pump-probe signal, when the SDW state is suppressed and the superconductivity emerges, are going to be discussed in this chapter.

3.2 Normal state response and coherent phonons

As we have mentioned in the Introduction, at room temperature all iron pnictides are metals. The transient reflectivity is believed to be dominated by the thermalization of hot electrons (Fig. 3.1) [184], [224], [225].

In some experiments, where the signal-noise ratio was the best, at high temperatures and high pump fluences oscillations with a frequency of 5.5 THz were observed on top of the metallic response (see Fig. 3.2). The frequency of the oscillations corresponds to the optical phonon frequency of the A_{1g} mode of As (see Fig. 1.15), observed before in Raman [226] and in THz experiments [23]. As it is expected, the frequency of observed oscillations does not depend on the pump fluence (see Fig. 3.2a) and their amplitude changes linearly with the fluence up to $\mathcal{F} = 400$ μJ/cm^2 and then saturates (Fig. 3.2b).

Phonons with such a frequency can not be directly excited by photons with energy 3.1 eV (corresponds to 750 THz). Two types of mechanisms are considered for the generation of coherent phonons: the impulsive stimulated Raman scattering (ISRS) and the displacive excitation of coherent phonons (DECP) [227].

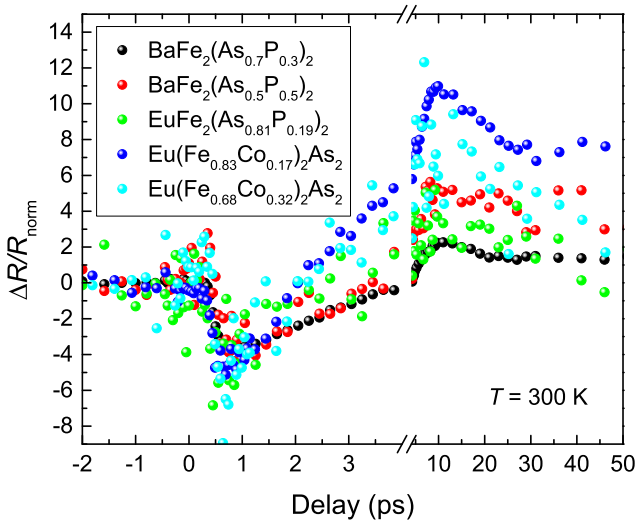


Figure 3.1: The metallic response in the transient reflectivity measured in a few investigated iron pnictides. The pump fluence for all curves is below 50 μJ/cm^2.

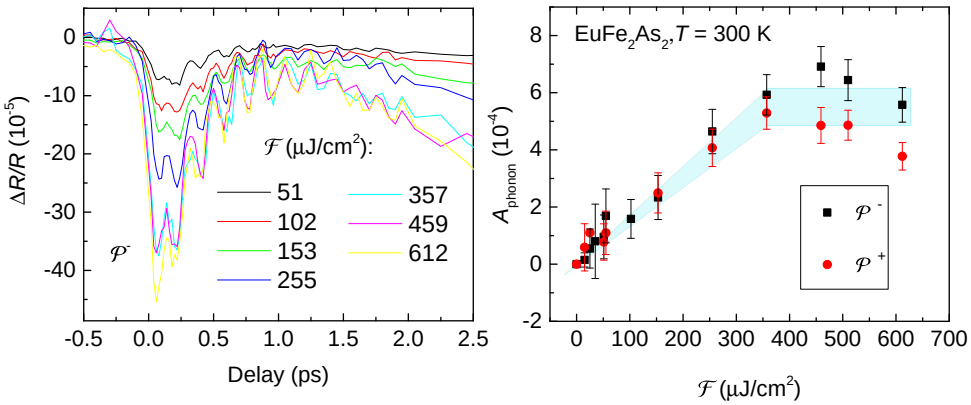


Figure 3.2: a) The coherent phonon oscillations measured at 300 K as a function of the pump fluence. b) Amplitude of the phonon oscillations as a function of the pump fluence for the two orthogonal polarizations of probe $\mathcal{P}^+$ and $\mathcal{P}^-$.

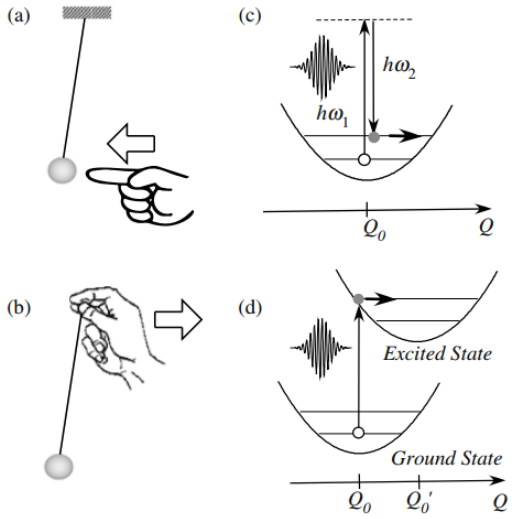


Figure 3.3: Two models of coherent optical phonons generation. a), c) impulsive stimulated Raman scattering (ISRS). b), d) displacive excitation of coherent phonons. a) and b) illustrate the driving forces in ISRS and DECP, respectively. Adapted from [228].

In ISRS the excitation is produced *via* Raman scattering and the ions oscillate in the ground state around the equilibrium coordinate Q_0 (Fig. 3.3a). The driving force depends on the Raman tensor and on the two components of the field involved in the Raman process. In the case of a short pulse it is an impulsive force and the initial phase of the motion is sine-like.

The electronic population excited upon light absorption, instead, originates from DECP (Fig. 3.3b). Indeed the photoexcited electronic density modifies the electron-ion potential instantaneously, thereby exerting a force on the lattice. Thus, the system evolves on a new potential curve, where the equilibrium $Q*$ is displaced with respect to the original coordinate. This sets oscillations of the ions around the new equilibrium coordinate. The change in the potential occurs step-wise and the oscillations begin at the maximum, in a cosine-like motion.

Both mechanisms cause the nuclear displacement Q, which induces a change of optical properties of the material through the refractive index n and the susceptibility χ:

$$\Delta R \approx \frac{\partial R}{\partial \chi}\frac{\partial \chi}{\partial Q}Q(t). \tag{3.1}$$

Because $\partial\chi/\partial Q$ is the first order Raman tensor, only Raman active modes can be observed in linear optical experiments. It was already shown in a number of compounds that the laser pulses whose duration is shorter than the period of a lattice vibration may excite coherent phonons [229]–[231].

Since the Raman intensity is normally linear with the excitation density, the saturation behaviour of the amplitude of the observed coherent phonon suggests that the displacive excitation mechanism is enabled.

There are also many studies which suggest that the secret of high-temperature superconductivity is hidden in the angle configuration of the Fe-As tetrahedra [232], but there is still no recipe how to make the room temperature superconductor. As it was shown in a few recent works, the phonons might indeed play one of the key roles in forming the properties of high-temperature superconductors. For example, in [23] it was shown that the coherent modulation of the A_{1g} phonon with ultrafast THz laser pulses can generate the SDW order

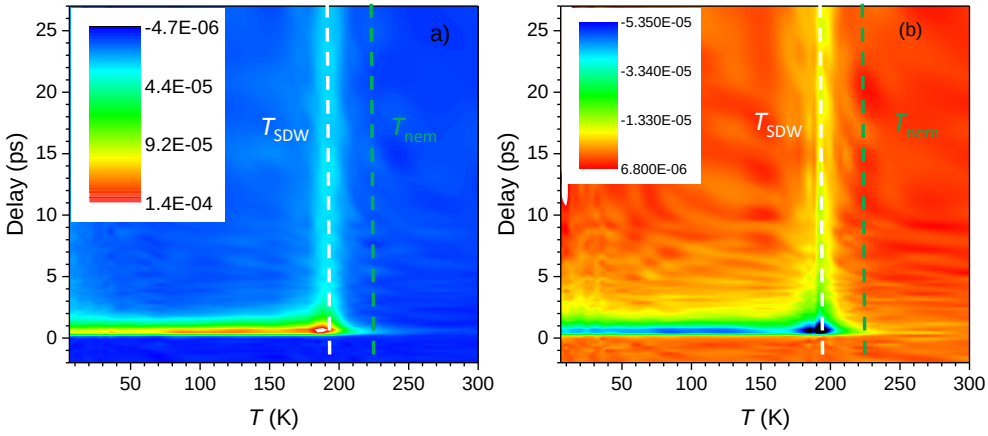


Figure 3.4: The temperature dependence of the pump-probe response for Eu-122. a) and b) correspond to two orthogonal polarizations of the probe beam. At $T_{\mathrm{SDW}} = 190$ K the divergency of relaxation time is observed.

in the parent $BaFe_2As_2$ in the normal state, at temperatures far above T_{SDW}. It is also possible that phonons can play an important role in generation of superconductivity, as was shown for the copper oxides [233].

3.3 Polarization properties and nematic phase fluctuations

In contrast to the high-temperature metallic response, which is isotropic with respect to the probe polarization, at lower temperatures the situation changes. Despite the fact, that there is no deliberate unaxial strain applied, below T_{nem} most of the samples show a twofold in-plane rotational anisotropy with respect to the probe polarization.

In Fig. 3.4 we plot the temperature dependence of the photoinduced reflectivity ($\Delta R/R$) transients for the parent $EuFe_2As_2$. At 195 K the divergence of the relaxation time indicates SDW, which coincides with the structural transition to the orthorhombic state. The structural transition breaks the rotational symmetry and the sample shows a twofold in-plane rotational anisotropy with respect to the probe polarization. In the orthorhombic state, the anisotropy indicates a preferential ordering of the orthorhombic twin domains in the probed volume.

But one can notice that the signal is anisotropic also above $T_{\mathrm{S}}/T_{\mathrm{SDW}}$. The anisotropy of the transient reflectivity above the structural transition in iron pnictides was associated with the presence of nematic phase fluctuations [22].

Let us discuss which mechanisms are responsible for observation of anisotropy of the pump-probe signal. If one assumes in Eq. (1.10) that $|M_{\alpha,\beta}|^2$ depends on the angle in the vicinity to the Fermi energy, then the polarization of probe absorption can easily be derived [179]. Expressing $|M_{\alpha,\beta}(\theta,\epsilon)|^2 = M_x^2\sin^2(\theta) + M_y^2\cos^2(\theta)$, where in general case $M_x \neq M_y$ in the orthorhombic state, we obtain a qualitative description of the angular dependence of the transient reflectivity:

$$\triangle R \sim (M_x^2\sin^2(\theta) + M_y^2\cos^2(\theta))\triangle n_{\mathrm{pe}}. \tag{3.2}$$

In the orthorhombic state the anisotropy slightly varies along the surface of the sample

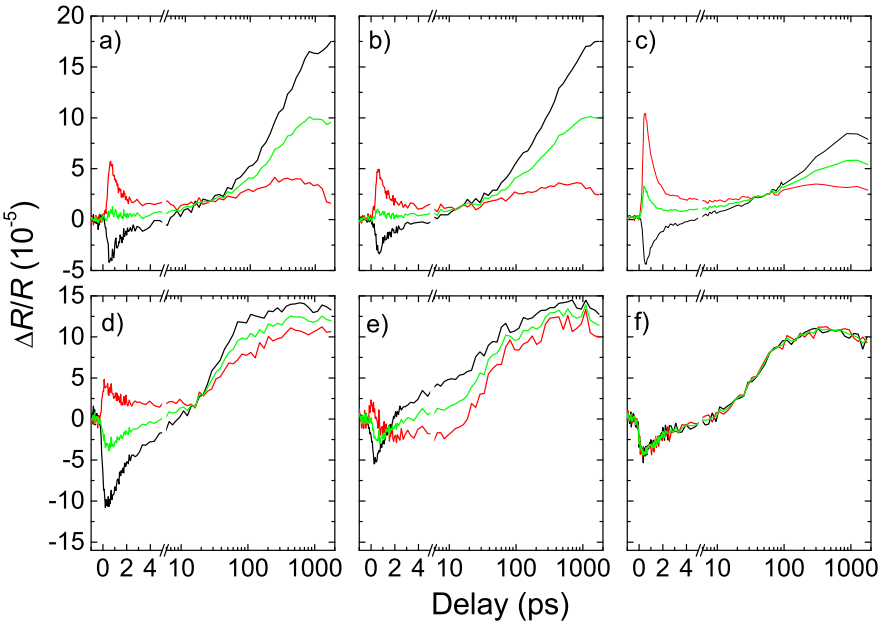


Figure 3.5: Transient reflectivity for a-c) Eu-122, d-f) EuP-122 measured at 7 K at different points at the same conditions. Black and red lines correspond to two orthogonal probe polarizations, the green line corresponds to their average.

due to the domain structure on the length scale of the probe beam diameter of ∼50 µm (see Fig. 3.5). The transients of the less anisotropic spots are consistent with a linear combination of the most anisotropic transients. This indicates that the variation is not due to the sample inhomogeneity but due to the spatially inhomogeneous detwinning. In the absence of information which crystallographic directions correspond to the two different orthogonal probe polarization, we denote the polarization according to the low-temperature photoinduced-reflectivity ($\Delta R/R$) sub-picosecond peak sign: $\mathcal{P}^-$ and $\mathcal{P}^+$.

In experiments described in the following chapters we therefore tried to measure the single domain response by choosing the position on the sample surface with the maximal anisotropy.

3.4 Spin density wave response

In Fig. 3.6 we show the temperature dependence of the transient reflectivity in the parent $EuFe_2As_2$ and superconducting $EuFe_2(As_{0.81}P_{0.19})_2$, measured at the two orthogonal polarizations. In both samples at low temperatures the sub-picosecond relaxation component is present. The amplitude of this component increases at the respective SDW transition temperature and drops to almost zero at room temperature.

In this case the rise time of the transient reflectivity signal is associated with establishment of the thermal quasi-equilibrium between the photoexcited quasiparticles and the high-frequency bosons. It depends on photoexcitation processes and in low excitation experiments it is usually limited by the laser pulse length ∼ 50 fs.

The presence of the fast component in the orthorhombic/SDW state was previously associated with the bottleneck in relaxation due to opening of the partial charge gap in the electronic density of states [22]. Indeed, above $T_{SDW} = 35$ K for $EuFe_2(As_{0.81}P_{0.19})_2$ (Fig. 3.7a) and $T_{SDW} = 195$ K for $EuFe_2As_2$ (Fig. 3.7b), the amplitude of the signal strongly drops (see Fig. 3.7). The remaining twofold rotational anisotropy of the response above

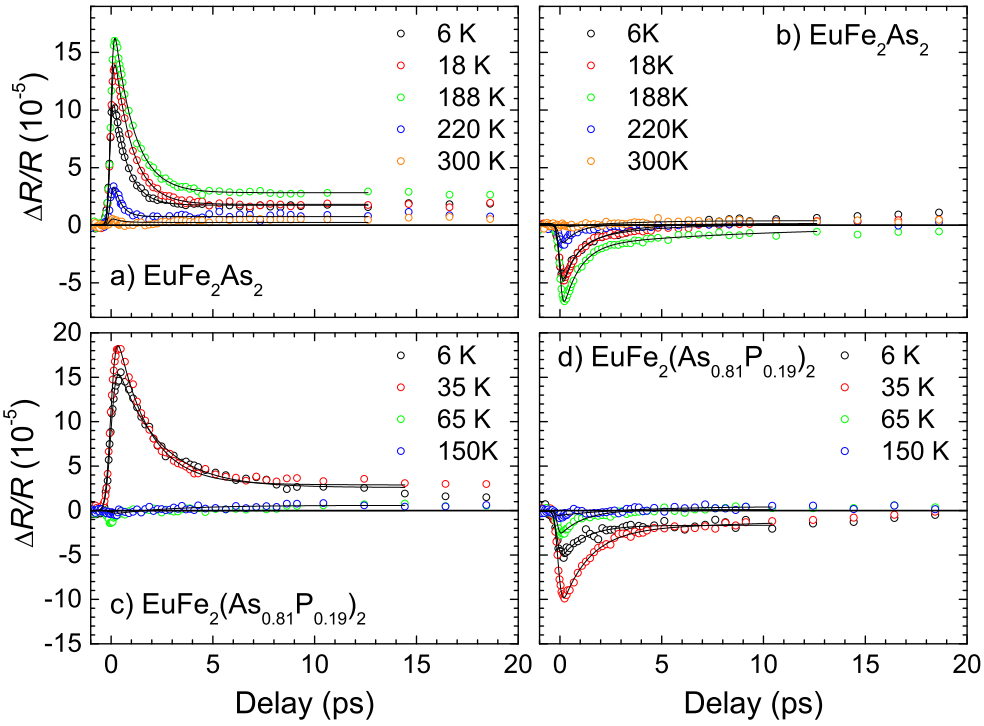


Figure 3.6: T-dependent transient reflectivity measured for the orthogonal polarizations of the probe, $\mathcal{P}^-$ and $\mathcal{P}^+$ in $EuFe_2As_2$ a), b) and $EuFe_2(As_{0.81}P_{0.19})_2$ c), d), respectively. The pump fluence is $\mathcal{F} = 36$ μJ/cm^2. Black lines correspond to exponential fits.

T_{SDW} is attributed to the fluctuations of the nematic order as discussed previously [22] in $Ba(Fe,Co)_2As_2$. In Figs. 3.7c,d we plot the temperature dependence of the relaxation time for the optimally doped and parent compound, respectively. The relaxation time is obtained from a single exponential fit. The data are consistent with previous results, reported in [22], [28].

3.4.1 SDW suppression upon doping

Visually, phase diagrams of iron pnictides and copper oxides are very similar. In both classes of materials there is an antiferromagnetic order in the parent compounds, which is suppressed with doping. For example, Fig. 3.8 illustrates the phase diagram of $Eu(Fe,Co)_2As_2$ and the temperature dependence of the amplitude of the pump-probe response for a wide range of doping.

In the parent compound with $x = 0$ the transition to the SDW state is observed as an abrupt change in the amplitude of the transient reflectivity signal at $T = 190$ K. By doping the sample with $x = 0.17$ of Co the transition temperature is decreased to $T = 158$ K, which is well observed in our experiment (Fig. 3.8). Further doping completely suppresses the antiferromagnetic ordering (see left panel of Fig. 3.8), the samples become metallic and the signal almost does not depend on the temperature and doping (see $x = 0.182$ and $x = 0.315$).

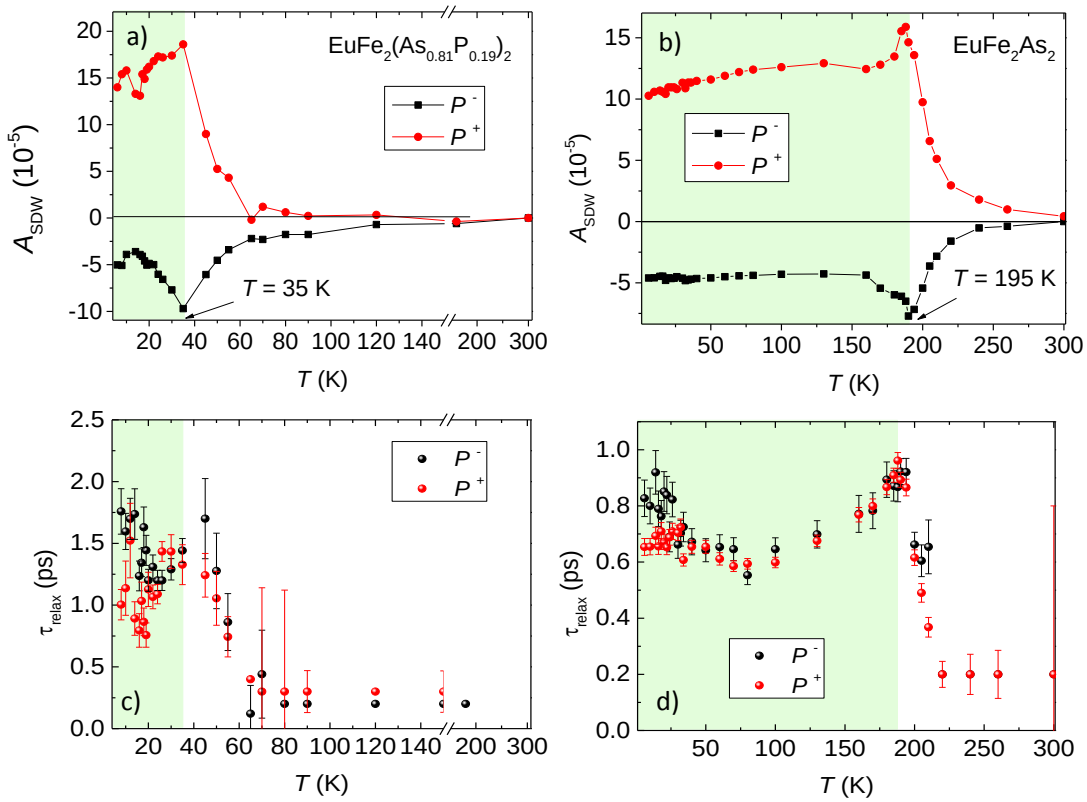


Figure 3.7: The temperature dependence of the amplitude and the relaxation time of the SDW response, obtained from a single-exponential fit of the transient reflectivity traces shown in Fig. 3.6. Shaded area corresponds to the temperature region, where the sample is in the SDW state.

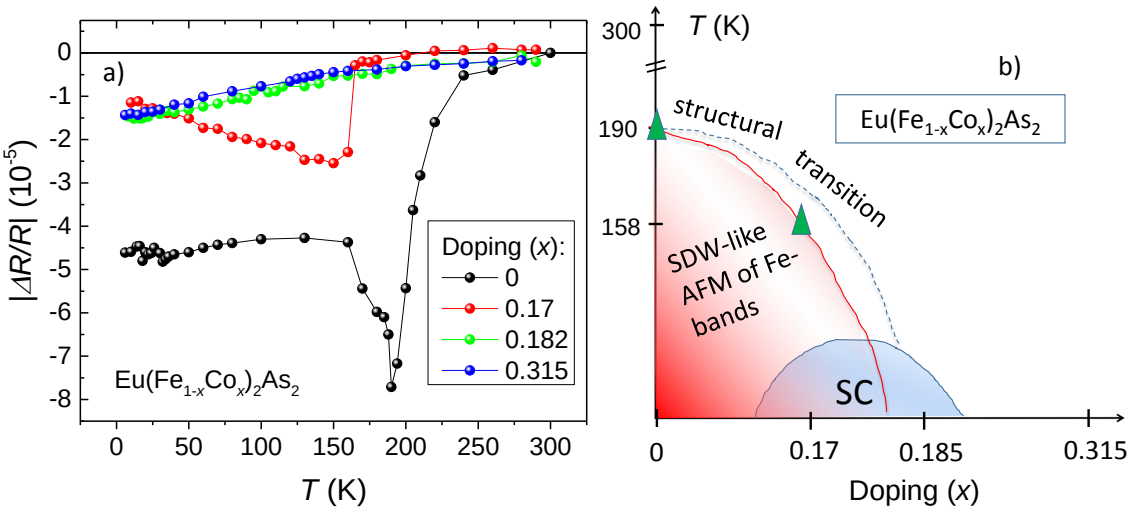


Figure 3.8: a) The amplitude of the transient reflectivity as a function of the temperature for $Eu(Fe_{1-x}Co_x)_2As_2$, where $x = 0$; 0.17; 0.182 and 0.315. b) The phase diagram of $Eu(Fe,Co)_2As_2$. Green triangles represent the poins obtained from the data shown in a).

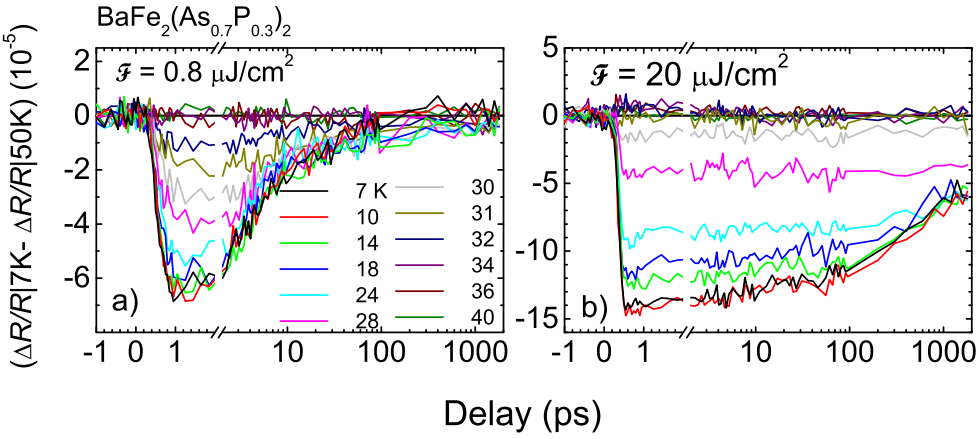


Figure 3.9: Temperature dependence of transient reflectivity of superconducting $BaFe_2(As_{0.7}P_{0.3})_2$ measured at low $\mathcal{F} = 0.8$ μJ/cm^2 a) and high $\mathcal{F} = 20$ μJ/cm^2 b) pump fluences.

3.5 Superconducting response

With doping parent iron pnictides become superconducting. It was shown before in the high-T_c superconductors [234] that the amplitude of the transient reflectivity signal gradually increases when the sample is cooled down below the critical temperature. As it was explained in the introduction, such an observation is associated with the opening of a superconducting gap and the amplitude of the pump-probe signal is proportional to the number of excited superconducting pairs.

According to BCS theory, if the T_c is small, then the density of electronic states near the Fermi level is also low. The T_c is usually less than 40 K for 122 compounds. Also, it was shown [11], [235] that some 122 iron pnictides do not possess bulk superconductivity, but the superconductivity is present in a form of nodes, which can also influence the signal. Another technical problem in measuring signals from systems with a small gap is related to the destruction energy. In [29] it was shown that ultrafast laser pulses can nonthermally destroy the gapped state which makes it sometimes really tricky to measure the superconducting response in iron pnictides. Thus, the superconductive component in pump-probe can be very weak and sometimes it might be difficult to resolve them due to the signal/noise relation [22].

In [22] the superconducting signal was measured in $Ba(Fe,Co)_2As_2$. The destruction fluence is only 0.43 μJ/cm^2 and thus the observed signal was not due to bottleneck relaxation, but was showing the difference between the normal and superconducting states. In Fig. 3.9 we show the superconducting signal measured for the first time in both low and high excitation regimes. The Chapter 7 is dedicated to the research of the SC signal in $BaFe_2(As_{0.7}P_{0.3})_2$.

3.6 Summary and conclusions

The ultrafast spectroscopy is a very powerful technique, which allows the observation of the real-time dynamics of excitations, which represent every region of the rich phase diagram of 122 iron pnictides.

(i) We investigate the normal state response at room temperature, which is produced by the thermalization of hot electrons.

(ii) The coherent phonon oscillations of the A_{1g} As mode, which plays an important role in forming properties of the pnictides, are observed on top of the metallic signal.

(iii) The temperature dependence and anisotropy analysis of transient reflectivity amplitude allows the observation of the nematic fluctuations phase.

(iv) The SDW transition temperature at different dopings is precisely determined using the transient reflectivity measurements.

(v) Excitations in the superconducting state can also be studied in iron pnictides.

Chapter 4

Spectrally-resolved femtosecond reflectivity relaxation dynamics in undoped SDW 122 pnictides

4.1 Search for additional relaxation processes

Time-domain optical spectroscopy has been, among other spectroscopies, very instrumental in elucidating the nature of the superconducting and unusual normal states in novel superconductors and related materials by virtue of the fact that different components in the low-energy excitation spectrum could be distinguished by their lifetimes.[22], [63], [70], [195], [211], [212], [234], [236]–[241] Unfortunately, all-optical techniques lack the momentum resolution so assignments of the relaxation processes are indirect, based on model-predicted temperature and fluence dependencies.[178], [194], [242]. Despite the indirect assignments no inconsistencies with the previous all-optical based results were found for the cuprates by the recent TR-ARPES [243], [244] experiments.

Most of the published all-optical time-resolved experiments were performed using relatively narrow-band spectrally unresolved probes (see Subsection 1.5.8). Since narrow-band probes can be rather selective, probing only a limited subset of the relevant low-energy electronic states, and laser TR-ARPES suffers from surface sensitivity and limited momentum range, broadband spectrally-resolved all-optical transient experiments are necessary to complement both probes and elucidate information about any additional relaxation processes, that might have been missed due to the limitations.

In the cuprates a few such experiments have been performed [31], [245], [246] indicating no additional low-temperature relaxation processes to the previously observed by all-optical narrow-band probes and associated to the pseudogap and the superconducting states.[31] In iron-based superconductors, to our best knowledge, no broad-band time-resolved spectroscopy data exists, except in the THz region.[23] Similarly to the cuprates however, the narrow-band all-optical time-resolved spectroscopy indicates a limited number of distinctive relaxation components.[22], [63], [211], [212], [220]

The multiband nature of iron-based pnictides offers a possibility of additional photoexcited quasiparticle relaxation pathways that might remain undetected by the narrow-band optical and the momentum constrained laser TR-ARPES [21] probes. In the absence of broad-band time-resolved spectroscopy data in iron-based pnictides and in order to check about existence of additional processes, we therefore performed a systematic spectrally-resolved visible broad-band probe transient-reflectivity study of the SDW state in three related undoped parent compounds: $A\mathrm{Fe_2As_2}$ (A-122) with A = Ba, Sr and Eu.

In the previous chapter it was shown that in the SDW state a single ~ 1 ps relaxation

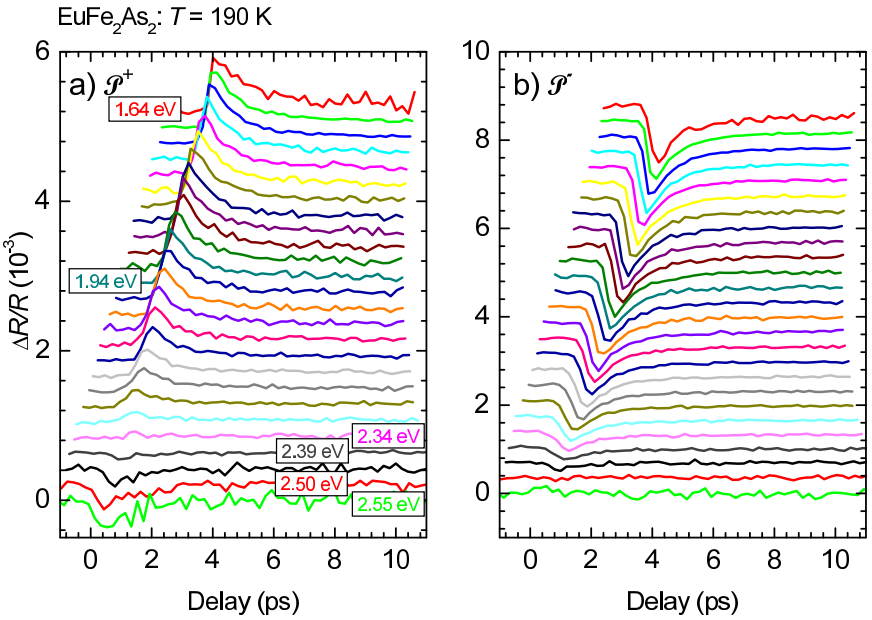


Figure 4.1: Photoinduced reflectivity transients in $EuFe_2As_2$ as a function of the probe-photon energy just below T_{SDW}. a) and b) correspond to the $\mathcal{P}^+$ and $\mathcal{P}^-$ polarizations, respectively. The traces are vertically and horizontally offset for clarity.

component dominates the near-infrared narrow-band optical response, while TR-ARPES experiments [21] indicate at least two distinct relaxation processes, with the longest relaxation time similar to the one observed in the optical response.

We found that in all three compounds the transient-reflectivity consists of no more than two fast relaxation components. One is faster than the experimental temporal resolution of ~ 200 fs and compatible with the fastest component measured by TR-ARPES[21], while the slower component shows a divergent-like relaxation time at the respective magneto-structural transition temperatures.

4.2 Spectral dependence of transient reflectivity

In Fig. 4.1 the probe-photon energy dependence of $\Delta R/R$ at and above T_{SDW} is shown for the two orthogonal polarizations. The linearity of the responses with respect to both, the pump and the probe fluences was checked, to ensure that experiments were performed in the weak excitation regime. In the absence of information about the orientation of the crystallographic axes we denote the polarizations $\mathcal{P}^+$ and $\mathcal{P}^-$ according to the sign of the response at the lowest probe-photon energy. With increasing $\hbar\omega_{pr}$ the response for the $\mathcal{P}^+$ polarization changes its sign at $\hbar\omega_{pr} \sim 2.35$ eV. The signal for the $\mathcal{P}^-$ polarization, on the other hand, changes sign at a slightly larger $\hbar\omega_{pr} \sim 2.5$ eV, almost at the edge of our experimental spectral range.

The behaviour is similar in Sr-122 (see Fig. 4.3), where the zero crossing is slightly lower, at $\hbar\omega_{pr} \sim 2.23$ eV, for the $\mathcal{P}^+$ polarization and slightly higher, just at the edge of the spectral window, at $\hbar\omega_{pr} \sim 2.56$ eV, for the $\mathcal{P}^-$ polarization.

In Ba-122 the signal is less anisotropic below T_{SDW} [22] so only the $\mathcal{P}^-$ polarization was measured, that shows no indication of the sign change below T_{SDW} as shown in Fig. 4.2.

In all three samples the spectral dependence of the transients does not change qualitatively through the transition.

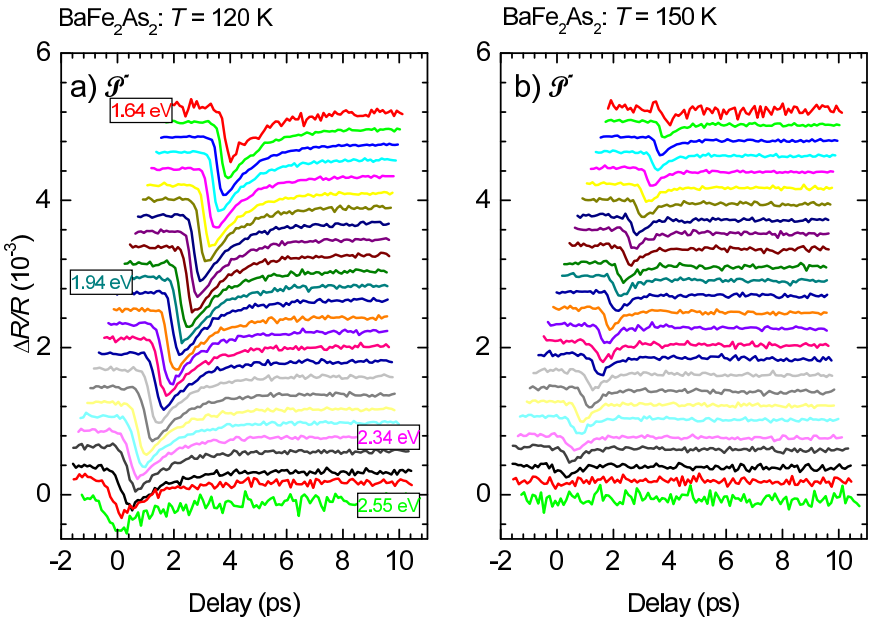


Figure 4.2: Photoinduced reflectivity transients in $BaFe_2As_2$ as a function of the probe-photon energy just below and just above T_{SDW} a) and b), respectively. The traces are vertically and horizontally offset for clarity.

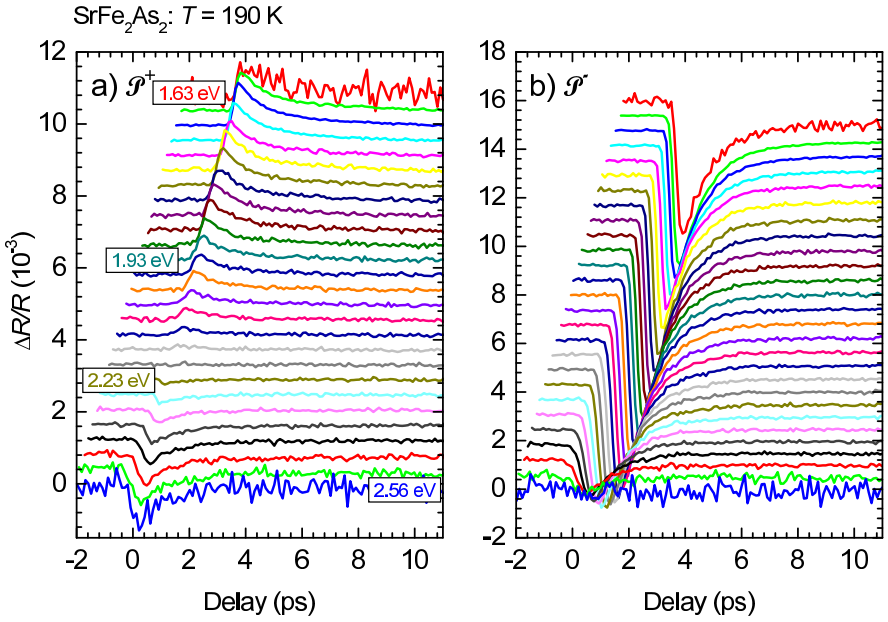


Figure 4.3: Photoinduced reflectivity transients in $SrFe_2As_2$ as a function of the probe-photon energy just below T_{SDW}. a) and b) correspond to the $\mathcal{P}^+$ and $\mathcal{P}^-$ polarizations, respectively. The traces are vertically and horizontally offset for clarity. $\mathcal{F} = 3.2\ \mu J/cm^2$.

4.3 Singular value decomposition

When large arrays of data describing some multicomponent dependency should be analyzed, singular value decomposition (SVD) can be a very efficient instrument. The main idea is in the search of the set of basic orthogonal vectors whose linear combination can well describe all the experimental data as a function of changing parameter.

4.3.1 General principles

Mathematically SVD is written as:

$$X = USV^T \tag{4.1}$$

where X is a $m \times n$ matrix of experimental data x_{ij} (for us it is going to be transient reflectivity at a certain delay i and probe photon energy j), U is an $m \times n$ matrix, S is a diagonal matrix, and V^T is also $m \times n$ matrix. The columns of U are called the left singular vectors, and form an orthogonal basis. The rows of V^T contain the elements of right singular vectors, and also form an orthogonal basis. The elements of S are non-zero only on the diagonal, and are called singular values.

To calculate the SVD one should first calculate V^T and S by diagonalizing $X^TX = VS^2V^T$, and then calculate $U = XVS^{-1}$.

In our case we have the data of the transient reflectivity as a function of the probe wavelength. To decompose them we first write the matrix $X \equiv \frac{\Delta R(\omega_{\mathrm{pr},i},t_j)}{R(\omega_{\mathrm{pr},i})}$ in which every row represents the transient reflectivity changes as a function of time delay for one wavelength, while every column represents the transient reflectivity at a certain delay for different probe wavelength. Afterwards, using the above system of equations, we get the resulting U and V^T matrices. In our case the right singular vectors will represent the independent relaxation components and left singular vectors will represent the spectral components.

Here one very important point should be noted. The obtained relaxation components can not be treated as the relaxation components which correspond to the real physical processes. One should remember that SVD is only a mathematical instrument, which forces singular vectors to be orthogonal, while the real relaxation processes are usually not. But this fact does not cancel the beauty of SVD, because (i) it is one of the best methods to understand how a few independent components can describe the whole data set, (ii) discarding non-informative components with low weight will significantly reduce the noise level, (iii) and the main advantage is that the linear combination of components can describe the whole set of experimental data, which significantly reduces the array of data to be analyzed. The last will be shown in the following subsection.

4.3.2 Decomposition of experimental data

The measured data points at each temperature can be arranged into a rectangular matrix and decomposed using the standard SVD, as described above:

$$\begin{aligned} \frac{\Delta R(\omega_{\mathrm{pr},i},t_j)}{R(\omega_{\mathrm{pr},i})} &= \sum w_k u_{ik} v_{jk} \\ &= \sum A_k(\hbar\omega_{\mathrm{pr},i}) r_k(t_j). \end{aligned} \tag{4.2}$$

In analogy to previous subsection w_k, u_{ik} and v_{jk} are the singular values (SV), the left singular eigenvectors and the right singular eigenvectors, respectively. With the above

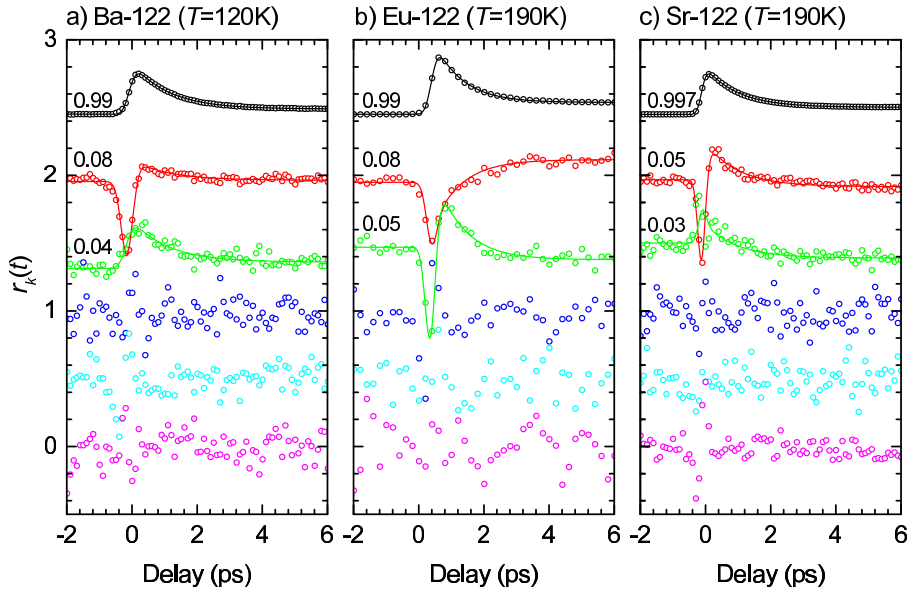


Figure 4.4: A few temporal eigenvectors with the highest singular values. The lines are exponential fits (4.3) for the three most significant temporal eigenvectors. The numerical labels are the normalized singular values, $w_l/\sqrt{\sum w_k^2}$.

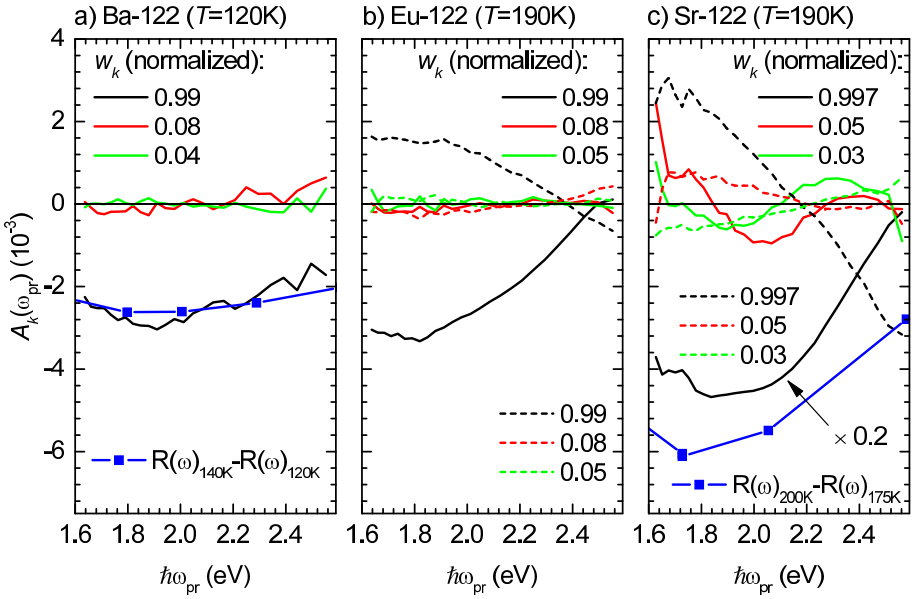


Figure 4.5: Spectral dependence of the three most significant SVD temporal-eigenvectors weights just below respective T_{SDW}. The numerical labels are normalized singular values. The thermal reflectivity difference from [247] for Ba-122 in Sr-122 is shown for comparison.

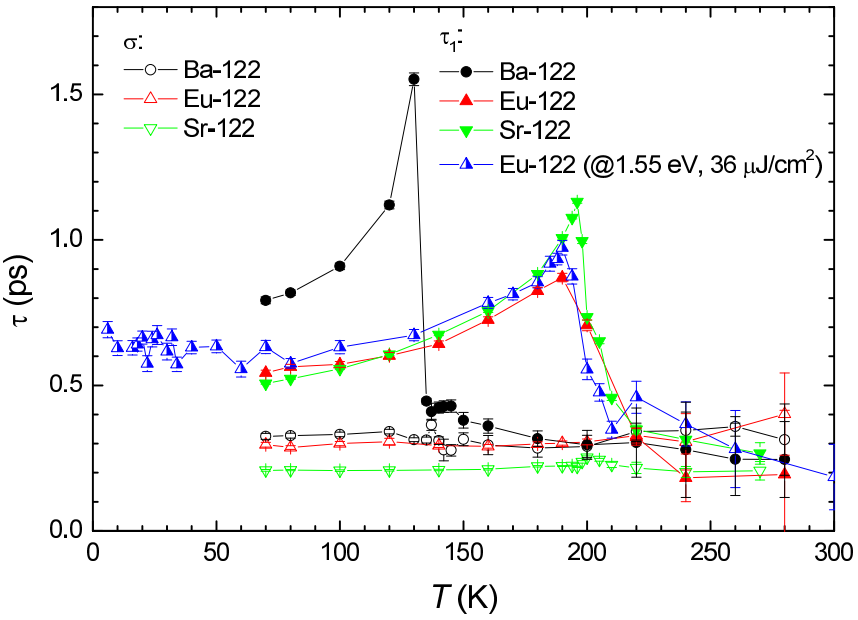


Figure 4.6: The risetime/resolution parameter and the longest relaxation time, τ_{B}, as a function of T. The shortest relaxation time, τ_{C}, is shorter than σ, so it was kept constant at 50 fs for all fits. The 1.55-eV probe result in Eu-122 is also shown for comparison.

matrix arrangement we define the SVD spectral weights (SW) as weighted left singular eigenvectors $A_k(\omega_{\mathrm{pr},i}) = w_k u_{ik}$, while the right singular eigenvectors correspond to the orthonormal temporal eigenvectors (TEv): $r_k(t_j) = v_{jk}$.

In Fig. 4.4 we plot a few most significant TEv for each sample at temperatures just below T_{SDW}.[1] It is obvious, that for each sample only the three most significant TEv contain the coherent response, while the rest represent noise only. SW corresponding to the three most significant TEv are shown in Fig. 4.5. The TEv with the largest SV clearly dominates the spectral response in all compounds. In Ba-122 and Eu-122 the SW of the next two TEv are near the noise level while in Sr-122 they are almost comparable to the first TEv SW for the $\mathcal{P}^+$ polarization.

The spectral dependence of the most intensive component SW is very similar to the static reflectivity change when crossing the magneto-structural transition [247] in Ba-122. In Sr-122 however, the similarity is only in the peak position at ~ 1.7 eV with a large difference between the positions of the zero crossings.

4.4 Temperature dependence

The three largest SV TEv can be rather well fit by a double exponential relaxation model with a finite risetime/resolution and a finite long delay value (see Fig. 4.4):

$$r_k(t) = \sum_{m\in\{\mathrm{A,B}\}} \frac{A_{m,k}}{2} \mathrm{e}^{-\frac{t-t_0}{\tau_m}} \operatorname{erfc}\left(\frac{\sigma^2 - 4(t-t_0)\tau_m}{2\sqrt{2}\sigma\tau_m}\right) + \\ + \frac{A_{\mathrm{C,k}}}{2} \operatorname{erfc}\left(-\frac{\sqrt{2}(t-t_0)}{\sigma}\right). \tag{4.3}$$

[1] For Sr-122 and Eu-122 we performed SVD decomposition joining together the data for both polarizations at each T.

Here the risetime/resolution parameter σ and relaxation times τ_m are shared among the three TEv, while the amplitudes $A_{m,k}$ are kept independent.

The fits yield virtually T-independent σ of 200−300 fs shown in Fig 4.6 indicating that it corresponds to the instrumental resolution.[2] One of the relaxation times, τ_A, was found significantly shorter than σ so it was kept constant at 50 fs for all fits. The second relaxation time τ_B shows a marked T-dependence with a divergent like behaviour at T_{SDW}. In Ba-122 it sharply drops above T_{SDW}, while in Eu-122 and Sr-122 the drop is somewhat less steep. At T significantly above T_{SDW} it becomes comparable to the experimental temporal resolution.

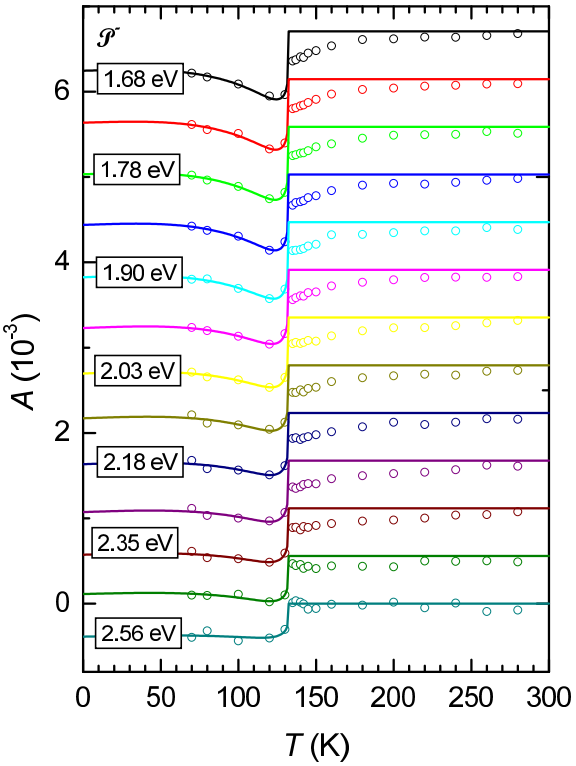


Figure 4.7: The amplitude of the $\Delta R/R$ transients in $BaFe_2As_2$ as a function of T. The thin lines are the bottleneck-model (Eq. (4.4)) fits discussed in text. The traces are vertically offset for clarity.

4.5 Bottleneck model fits

To analyze the anisotropic T dependence of the $\Delta R/R$ amplitude in AFe_2As_2, we use the approach presented in Introduction (Eq. (1.10)), where we assume that γ is temperature dependent and expand it in terms of an order parameter. The order parameter can be associated with the opening of a partial T-dependent charge gap $\Delta(T)$ upon the Fermi surface reconstruction below T_{SDW}.[248] Assuming a complex BCS-like order parameter with the magnitude $\Delta(T)$ below T_{SDW} we use:

$$\Delta R = \left[\gamma_0 + \eta \frac{\Delta^2(T)}{\Delta^2(0)}\right] n_{pe}. \tag{4.4}$$

[2]Somewhat larger σ in Ba-122 and Eu-122 might be attributed to a slightly worse chirp compensation.

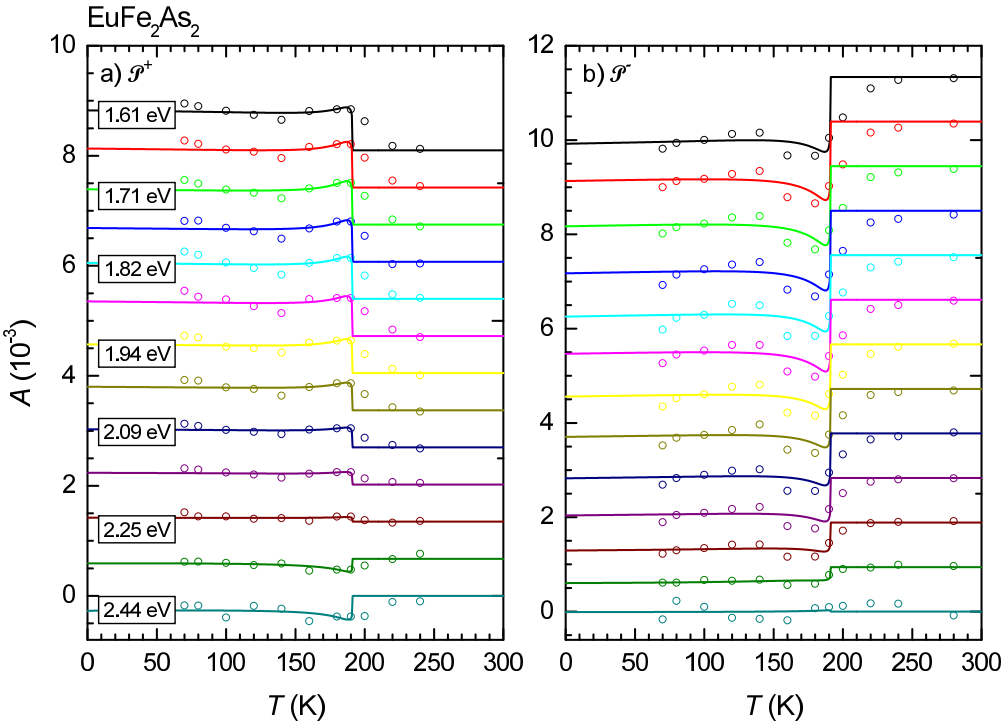


Figure 4.8: The amplitude of the $\Delta R/R$ transients in $EuFe_2As_2$ as a function of T. a) and b) correspond to $\mathcal{P}^+$ and $\mathcal{P}^-$ polarizations, respectively. The thin lines are the bottleneck-model (Eq. (4.4)) fits discussed in text. The traces are vertically offset for clarity.

sample	$2\Delta(0)/k_BT_{SDW}$	g_{ph}
Ba-122	8 ± 6	3.2 ± 1.1
Eu-122	13 ± 8	2.8 ± 1.4
Sr-122	8 ± 3	2.7 ± 0.8
$YBa_2Cu_3O_{7-\delta}$ [195]	10	200

Table 4.1: Charge gap magnitudes and the relative effective number of involved bosons as obtained from the fits of (4.4) to the data shown in Figs. 4.7, 4.8, 4.9. The results of a fit to the data in $YBa_2Cu_3O_{7-\delta}$ superconductor ($T_c = 93$ K) are shown for comparison.

To describe the T-dependence of n_{pe} we use the bottleneck model from Kabanov *et al.* [178] (see Eq. (1.21)). Using the BCS temperature dependent gap we can obtain a good fit of Equation (4.4) to the $\Delta R/R$ amplitude for both probe polarizations (see Figs. 4.7, 4.8, 4.9). The relative gap magnitudes are consistent (see Table 4.1) with previously reported values [22], [220] and the highest of the two gaps observed in the optical conductivity [151], [247], with a larger discrepancy for Eu-122 [249].

4.6 Discussion

The bottleneck model (1.21) is based on assumption that on a certain timescale a quasi-equilibrium is achieved between a gapped quasiparticle population and a boson population with the characteristic energy of $\hbar\omega = 2\Delta(T)$. This assumption is valid when the energy relaxation between different energy scales is sufficiently slow, even if the system is not fully gapped as is the case of the investigated SDW iron pnictides, that remain metallic

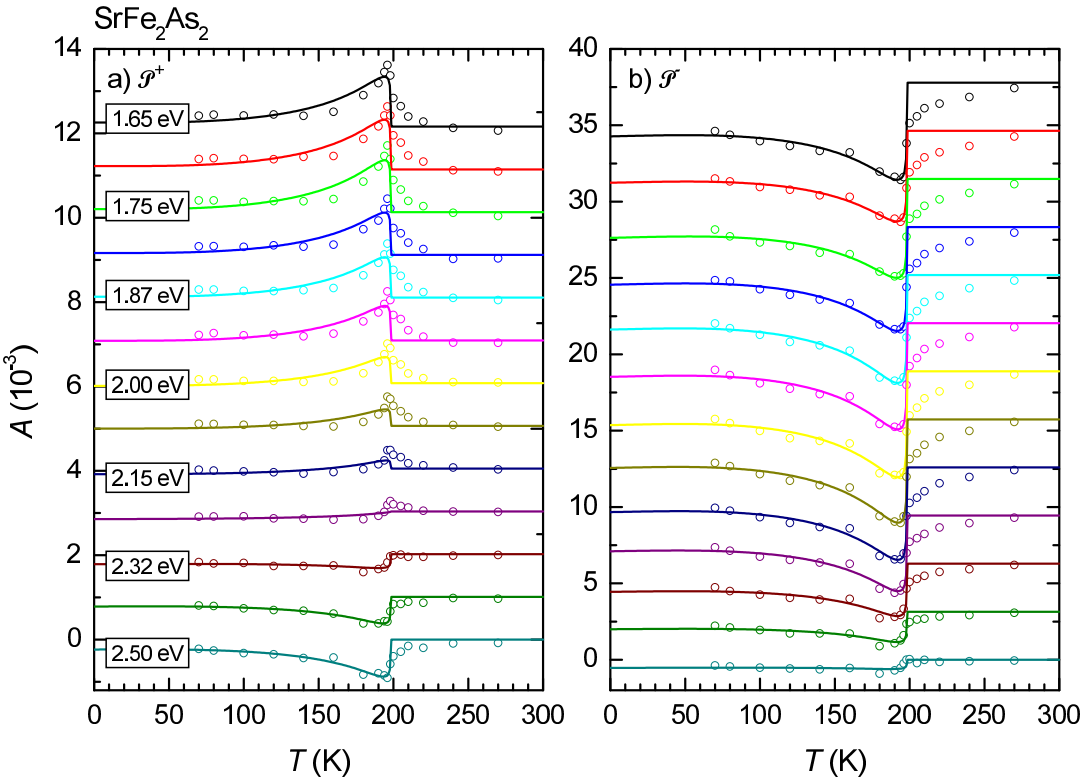


Figure 4.9: The amplitude of the $\Delta R/R$ transients in $SrFe_2As_2$ as a function of T. a) and b) correspond to $\mathcal{P}^+$ and $\mathcal{P}^-$ polarizations, respectively. The thin lines are the bottleneck-model (Eq. (4.4)) fits discussed in text. The traces are vertically offset for clarity.

below T_{SDW}. The quasi-equilibrium is achieved on a timescale of ~ 200 fs and the energy relaxation time is in the $0.5 - 1.5$ ps range. Based on the room-T relaxation times, [22], [220] where the relaxation is governed by the electron-phonon interaction, [245], [250] the risetime is long enough for establishing a quasi-equilibrium between the quasiparticle and high-frequency phonon populations. On the other hand, the characteristic boson energies obtained from the fits are in the range $\sim 100 - 200$ meV and significantly exceed the maximum phonon energy that is < 50 meV, [251] so the phonon bottleneck is not possible.

Another possible boson reservoir are antiferromagnetic magnons with maximum energies exceeding ~ 200 meV. [252]–[254] The number of magnon degrees of freedom is however much smaller than the number of phonon degrees of freedom and should be reflected in g_{ph}. Indeed, the obtained values of g_{ph} are significantly smaller than in the cuprate superconductor $YBa_2Cu_3O_{7-\delta}$ (see Table 4.1), where the phonon bottleneck was clearly established.

The bottleneck model therefore consistently describes the data and the obtained gap parameters are consistent with results obtained by means of the steady state optical spectroscopy [151], [247].

Comparison of our data with the TR-ARPES results in Eu-122 [21] reveals agreement between the relaxation time of the resolution-limited fast component observed in our case and the T-dependent hole relaxation time of $\sim 200 - 300$ fs observed by TR-ARPES. Contrary, the T-dependent relaxation-time of the dominant slower component observed in our case differs from the slower TR-ARPES electron-relaxation time beyond the combined error bars of the experiments. While the low T optical value of 650 fs is just slightly smaller than the TR-ARPES value of 800 fs, at T_{SDW} the optical relaxation time shows

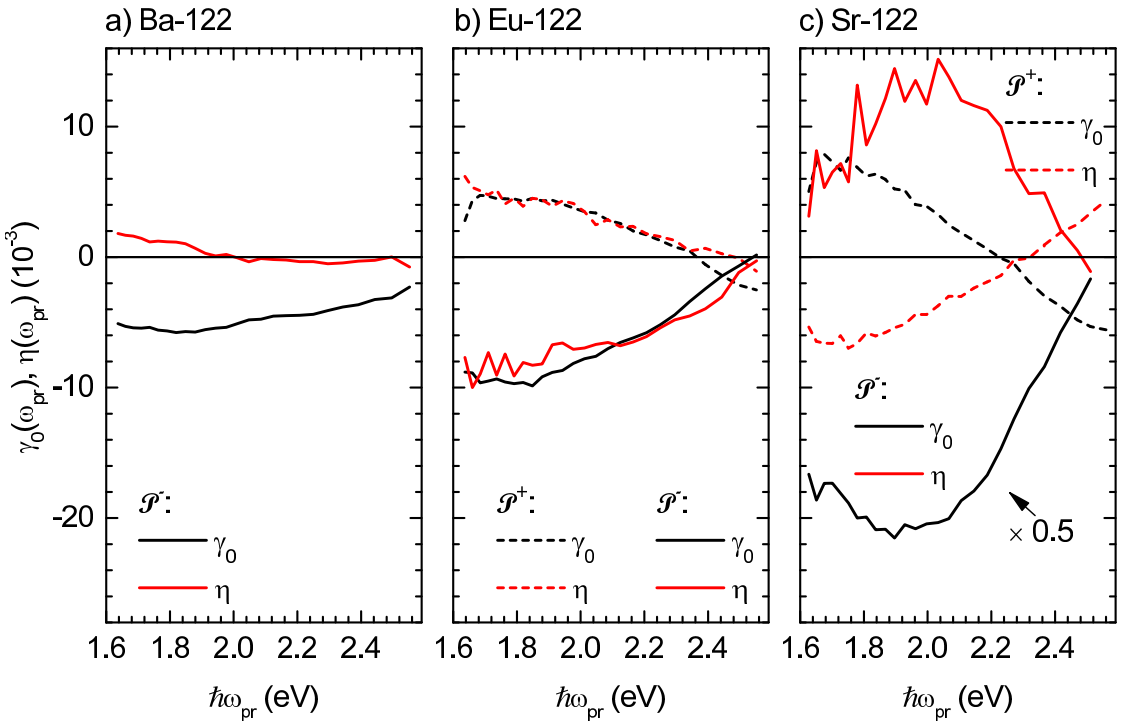


Figure 4.10: Spectral dependence of the fit amplitudes for all three samples just below the respective T_{SDW}.

a clear divergent-like behaviour, that is absent in TR-ARPES data. This indicates that either, (i) the optical probe and TR-ARPES probe different relaxation processes, or (ii) there are some unidentified surface effects that influence the relaxation near the surface probed by TR-ARPES. Since more systematic TR-ARPES investigations are needed to clarify possibility (ii) let us focus on possibility (i).

The photoinduced dielectric constant changes captured in Eq. (1.10) and taken into account in the bottleneck model are limited to the change of the non-equilibrium quasiparticle distribution function. In collectively ordered systems such as density waves, however, the collective degrees of freedom can be significantly perturbed by the photoexcitation. It was proposed recently [255], [256] that the relaxation dynamics in charge-density waves can be described by coupled dynamics of an overdamped electronic amplitude mode and phonon modes, without direct invocation of the photoinduced-quasiparticles absorption. In SDW systems a similar overdamped Raman active amplitude mode was predicted [257] but, to our best knowledge, never observed.

Despite the fact that the bottleneck relaxation model discussed above rather consistently describes the data below T_{SDW}, there exists a possibility that the observed optical relaxation is due to the order parameter relaxation, the SDW *amplitude mode*. Indeed, the gap dynamics from TR-ARPES [21] shows 100-200 fs risetime and a sub-picosecond decay consistent with the slower optical relaxation timescales. Moreover, the optical response shows a dominant single-component relaxation over a broad spectral range with the spectral dependence (Fig. 4.5) similar to the phase transition induced reflectivity change.[247] Since the SDW transition induced reflectivity change would be hardly explained just by T-induced change of the quasiparticle distribution function at a 15-20 K temperature difference, it should correspond to the characteristic order parameter spectral change. As a result, the spectral shape of the transient reflectivity is suggesting the transient order-parameter modulation origin of the optical response.

The characteristic frequency of the pure electronic SDW amplitude mode is predicted [257] to be $2\Delta/\hbar$. Taking $2\Delta \sim 200$ meV would lead to ~ 20 fs timescale which is much faster than the experimental observations. In the iron-based pnictides, however, the SDW order is clearly related to the structural transition, so it would not be surprising if the amplitude mode effective mass was renormalized due to coupling with the lattice, just like in charge density wave systems, explaining the slower observed relaxation timescales. The divergent behaviour of the relaxation time near T_{SDW} is also consistent with critical slowing down of the amplitude mode at the transition.

The spectral signature of the response, that remains above T_{SDW}, clearly breaking the tetragonal symmetry, is the same as in the SDW state. It was previously assigned [22], [258] to the bottleneck due to the normal-state pseudogap and related to the nematic fluctuations. However, the same reasoning as above can be applied and assigned to the fluctuations of the magneto-structural order parameter.

Despite the clear absence of more than one distinct slower relaxation component in the data, a simultaneous presence of both, the direct-bottleneck-quasiparticles and the order-parameter contributions to $\Delta R/R$ can not be excluded. The order parameter is directly linked to the quasiparticle distribution function by a gap equation. Since the observed dynamics is not too fast for the lattice timescales, the magneto-structural order parameter dynamics can be governed by the bottleneck dynamics of the photoexcited quasiparticle distribution function, resulting in the presence of a single relaxation timescale in the response.

4.7 Summary and conclusions

A systematic all-optical spectrally-resolved transient reflectivity study in $A\mathrm{Fe_2As_2}$ is presented. Two distinct relaxation components are identified.

(i) The fast one, is faster or similar to our temporal resolution of ~ 200 fs is consistent with recent TR-ARPES [21] results and could be associated with relaxation at the Fermi surface.

(ii) The slower one on the timescale of $0.6-1.5$ ps, with strong sensitivity to the magneto-structural transition, contrary to TR-ARPES, slows down near the magneto-structural transition. It can be well quantitatively described by a magnon-bottleneck model with zero temperature gap magnitudes $2\Delta(0)/T_{\mathrm{SDW}} \sim 10$, that are consistent with steady state optical spectroscopy results.

(iii) Alternative assignment to the relaxation of the SDW magneto-structural order-parameter amplitude mode is proposed and can not be excluded on the basis of the current data. Further TR-ARPES experiments and infrared all-optical broad-band experiments might be able to select among the two possibilities.

Chapter 5

Spin density wave destruction

5.1 SDW destruction

The fact that intense laser pulses can nonthermally destroy the collective state has been known for a long time and the interest of scientists in non-equilibrium photoinduced phenomena in solids increases every year [29], [198]. The main reason for the high attention to photoinduced phase transitions is explained by the potential application of the principles for controlling collective states with femtosecond laser pulses in ultrafast memory devices. Partly this interest is explained also by the possibility to reveal some fundamental insight into the mechanism of high-temperature superconductivity.

In [29] it is shown that the superconducting state can be destroyed in the copper oxides by an ultrafast laser pulse. Authors suggest the saturation model for determining the energy required to vaporize the superconducting condensate. In the report [198] the mechanisms of the non-thermal destruction of the superconducting state and CDW states are discussed in more details. Authors find that the vaporization of the superconducting state is relatively slow (∼1 ps) and inefficient, exhibiting a strong systematic dependence of the vaporization energy on T_c. In contrast, melting of the CDW order proceeds rapidly (∼50–200 fs) and more efficiently. A quantitative model describing the observed systematic behaviour in superconductors is proposed based on a phonon-mediated quasiparticle bottleneck mechanism. In contrast, the Fermi-surface disruption by hot QPs is proposed to be responsible for CDW state melting.

To our best knowledge, there are no reports on non-thermal destruction of the SDW state in iron pnictides by ultrafast laser pulses. In this chapter we present a systematic study on energy density needed for a non-thermal ultrafast destruction of the SDW state in iron pnictides.

5.2 Pump fluence dependence

In the experiments described here, we perturbed the SDW state with 50 femtosecond laser pulses in the same samples as described in previous chapter $EuFe_2As_2$, $SrFe_2As_2$ and $BaFe_2As_2$. The experiments were performed on freshly cleaved surfaces of high quality single crystals. The laser pulses were linearly polarized and incident along the c axis of the crystal with a 1.5 eV photon energy. We used a range of excitation fluences from $\mathcal{F} = 5$ μJ/cm^2 to 1.8 mJ/cm^2. As in the previous chapters we denote polarizations $\mathcal{P}^+$ and $\mathcal{P}^-$ according to the sign of the response.

We found that the amplitude of the SDW response strongly changes with the pump power for all samples. The amplitude of the signal shows saturation behaviour with increasing pump beam fluence (Fig. 5.1, 5.2, 5.3). In a low excitation regime the amplitude

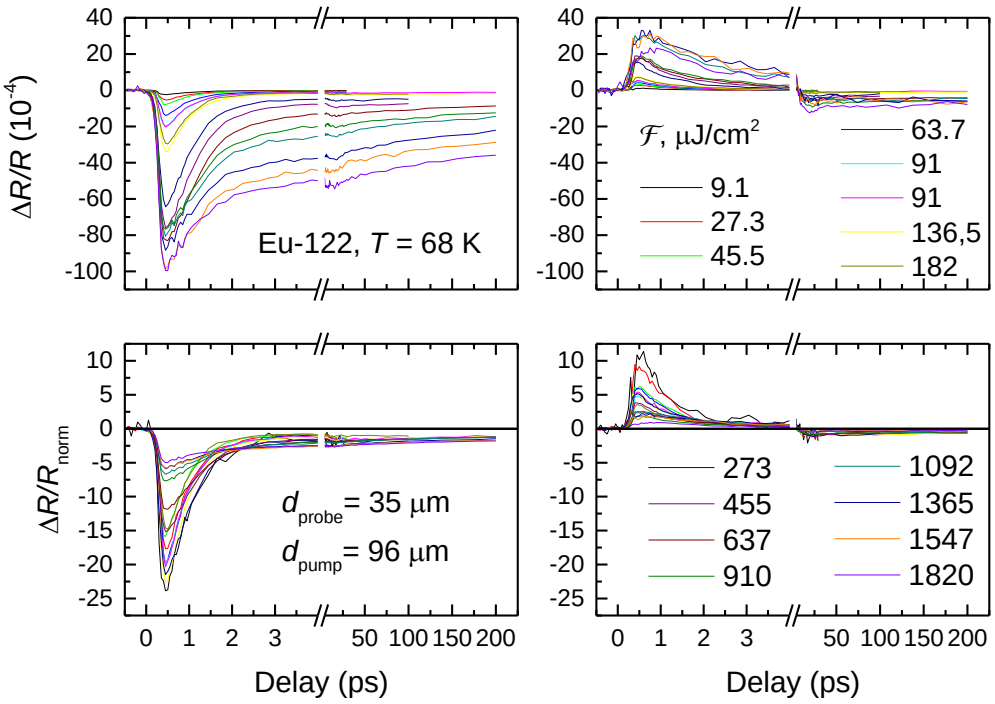


Figure 5.1: The photoinduced reflectivity $\Delta R/R$ in $EuFe_2As_2$ at various photoexcitation fluences. The data in the bottom row are normalized by the fluence. a), c) and b), d) correspond to $\mathcal{P}^+$ and $\mathcal{P}^-$ polarizations of the probe beam, respectively. The beam sizes were precisely measured using pinholes [259].

of the transient reflectivity linearly depends on the number of photoexcited quasiparticles. So the signal increases with increasing the pump power. For collective states the gap energy depends on the number of condensated electrons (electron pairs in the case of superconductor). With photoexcitation the gap decreases and can be closed if absorbed energy reaches the threshold limit. As it was shown in [29] the saturation of the signal with the pump fluence could be associated with the situation when the gapped state is destroyed.

5.3 Saturation model

To accurately determine the fluence at which the gap is destroyed, one should take into account the geometrical aspects of the experiment, such as the penetration depth, and the area of the sample irradiated by the pump and the probe beams. For that we will use the saturation model, proposed in [29]. In this model the local response is assumed to be proportional to the number of photoexcited quasiparticle n_{qp}, and n_{qp} to be proportional to excitation density up to the threshold excitation fluence. The photoinduced change in reflectivity is then given by:

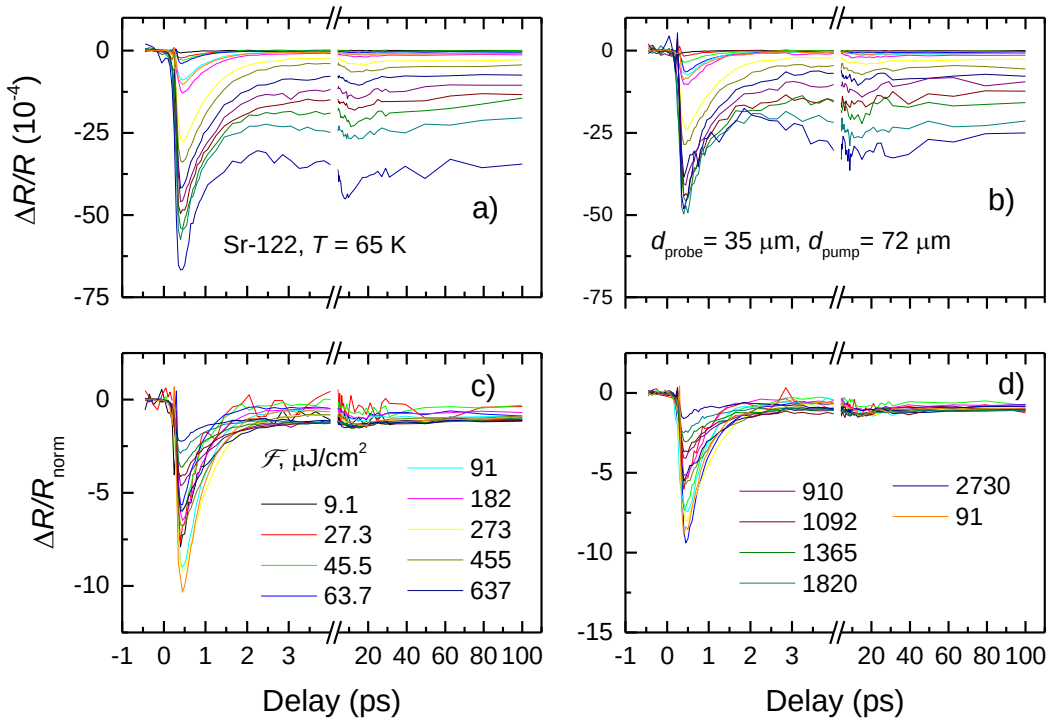


Figure 5.2: The photoinduced reflectivity $\Delta R/R$ in $SrFe_2As_2$ as a function of the pump fluence a), b) measured for two orthogonal polarizations of probe fluence $\mathcal{P}^+$ and $\mathcal{P}^-$, respectively. The traces in the bottom row are normalized by the fluence c), d).

$$\frac{\Delta R}{R} \propto \int_0^\infty \int_0^\infty \exp\left(-2\frac{z}{\lambda_{\rm op}}\right) \exp\left(-\frac{2r^2}{\rho_{\rm pr}^2}\right) n_{\rm qp}(r,z) r dr dz \tag{5.1}$$

where z is the depth coordinate and r is the radial coordinate, $\lambda_{\rm op}$ is the optical penetration depth and $2\rho_{\rm pr}$ is the probe beam diameter on the sample. Here the factor of 2 in the first exponent takes into account that the probe beam passes the sample volume twice.

If the pump laser fluence within the sample is: $\mathcal{F}(r,z) = \mathcal{F}_0 \exp\left(-\frac{z}{\lambda_{\rm op}}\right) \exp\left(-\frac{r^2}{\rho_{\rm pu}^2}\right)$, where $\rho_{\rm pu}$ is the radius of the pump beam on the surface, then the integration will give the following results: for $\mathcal{F}_0 < \mathcal{F}_{\rm sat}$ the dependence is linear with $\mathcal{F}_0$:

$$\frac{\triangle R}{R} = \frac{2(1+\rho^{-2})}{3f} \tag{5.2}$$

while for $\mathcal{F}_0 > \mathcal{F}_{\rm sat}$:

$$\frac{\triangle R}{R} = 1 - f^2 + \frac{2\left(f^{\rho^2} - f^2\right)}{\rho^2 - 2} + \frac{6f^{\rho^2}/(1+\rho^{-2}) - 2f^2\rho^2}{6 - 3\rho^2} \tag{5.3}$$

where $f = \frac{F_{\rm sat}}{F_0}$ and $\rho = \frac{\rho_{\rm pu}}{\rho_{\rm pr}}$.

In Fig. 5.4 we plot the fluence dependence of the maximum SDW amplitude for parent $SrFe_2As_2$ and $BaFe_2As_2$. The data are fitted with the saturation model described above.

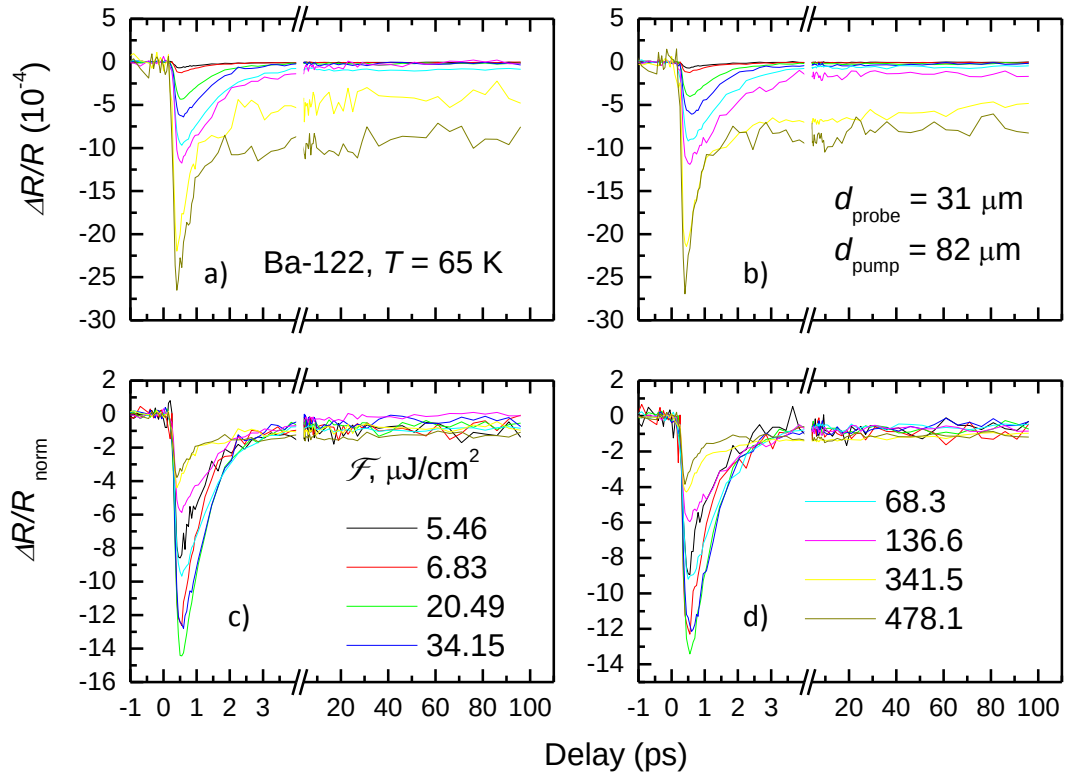


Figure 5.3: The photoinduced reflectivity $\Delta R/R$ in $BaFe_2As_2$ as a function of the photoexcitation fluence. The data in the bottom row are normalized by the pump fluence. a), c) and b), d) correspond to $\mathcal{P}^+$ and $\mathcal{P}^-$ polarizations of the probe beam, respectively.

The obtained threshold fluences are $\mathcal{F}_{\rm sat} = 191$ and 180 μJ/cm^2 for $EuFe_2As_2$ for $\mathcal{P}^+$ and $\mathcal{P}^-$, respectively. For $SrFe_2As_2$ and $BaFe_2As_2$ the saturation fluences are indicated in Figs. 5.4a,b. In fit for $BaFe_2As_2$ we did not take into account the two points at the highest pump fluence.

5.4 Calculation of the destruction energy

For convenience we express the energy density in units of Kelvin per iron atom. For that we take into account the penetration depth of the pump beam λ_p and the structural parameters of the material:

$$U_{\rm destr} = \frac{\mathcal{F}_{\rm sat}(1-R)}{\lambda_{\rm p} k_{\rm B}} \frac{V}{n} \tag{5.4}$$

where $U_{\rm destr}$ - destruction energy [K/Fe], $\mathcal{F}_{\rm sat}$ - the saturation fluence [J/cm^2], R – the reflectivity (for 1.5 eV $R = 0.22$ [103]), V – the volume of the unit cell, $k_{\rm B}$ - the Bolzman constant ($k_{\rm B} = 1.38\,10^{-23}$ J/K), $n = 8$ – the number of Fe atoms in the unit cell. The results are presented in Tab. 5.1. We observe a systematic increase of $U_{\rm distr}$ with $T_{\rm SDW}$, giving an approximate square power-law dependence (Fig 5.5).

In the BCS theory the condensation energy depends on the gap size as:

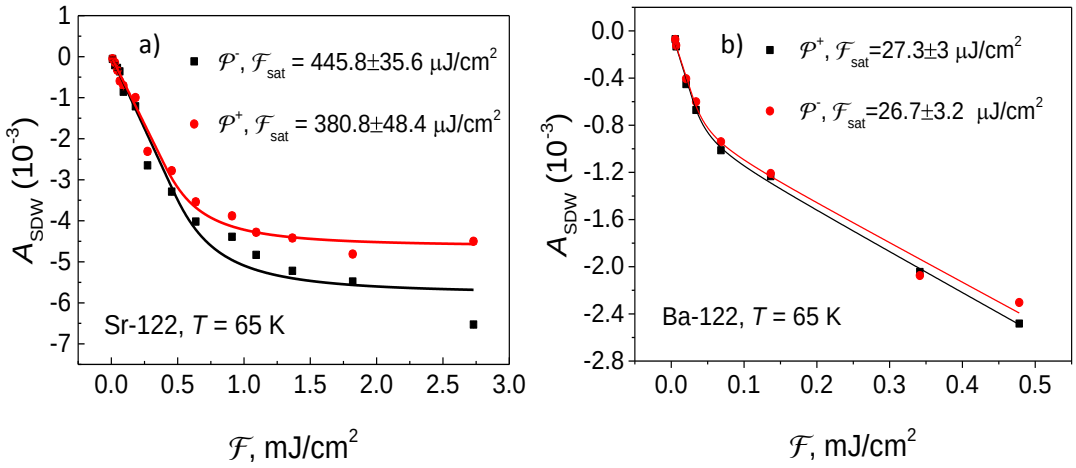


Figure 5.4: The amplitude of the SDW response as a function of the pump fluence, measured at 65 K for Sr-122 and Ba-122 for two orthogonal polarizations of the probe beam. The curves are the result of the fit of experimental data points with the saturation model.

	T_{SDW}	T (K)	Polariz.	U_{destr} (K/Fe)
Eu-122	190 K	4	$\mathcal{P}^+$	84.47±2.7
			$\mathcal{P}^-$	69.04±13.8
		20	$\mathcal{P}^+$	64.45±2.5
			$\mathcal{P}^-$	59.32±10.1
		65	$\mathcal{P}^+$	92.01±3.2
			$\mathcal{P}^-$	99.22±23.1
Ba-122	134 K	65	$\mathcal{P}^+$	30.2±1.2
			$\mathcal{P}^-$	30.2±1.2
Sr-122	203 K	65	$\mathcal{P}^+$	171.6±15.1
			$\mathcal{P}^-$	146.57±13.7

Table 5.1: The destruction energy of the SDW state in $EuFe_2As_2$, $SrFe_2As_2$ and $BaFe_2As_2$ for different temperatures and polarizations.

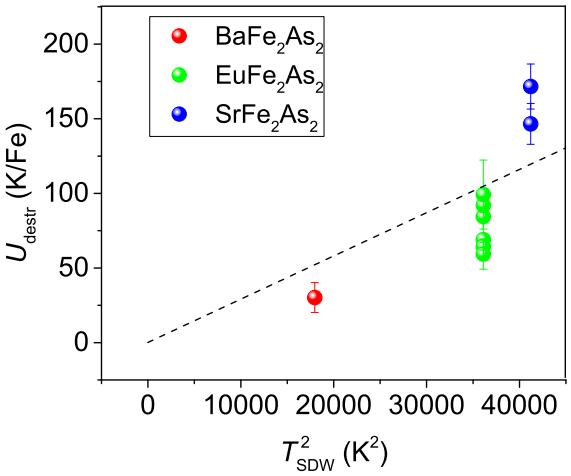


Figure 5.5: The planar destruction energy of SDW order in parent undoped 122 iron pnictides as a function of square of transition temperature.

$$U_c = \frac{1}{2} N(0) \Delta^2, \tag{5.5}$$

where $N(0)$ is the density of states at the Fermi energy.

Let us compare the destruction energy ratio with the square gap ratio for the parent Ba-122 and superconducting $BaFe_2(As_{0.7}P_{0.3})_2$ (BaP) (see Chapter 7): $U^{\rm SDW}_{\rm destr}/U^{\rm SC}_{\rm destr} \sim 100.6$ and $\Delta^{SDW}_{\rm Ba122}/\Delta^{SC}_{\rm BaP} \sim 84$. The difference can be explained by the fact the condensation and destruction energies are not equal, because not all the energy is used for the destruction [29]. Another reason of discrepancy is different mechanisms of SDW and SC states destruction. The energy needed to destroy the SDW state is much larger than the energy needed to destroy the superconducting state. The destruction time for SC state in iron pnictides is 0.5 ps [22], while the destruction of SDW state is very fast $\sim$ 50 fs. In analogy with [198] we suggest that the destruction of superconducting order can be described by the established QP recombination mechanism. While the SDW state is destroyed by the disruption of the Fermi surface nesting.

5.5 Thermal destruction energy

The thermal destruction energy energy is the energy needed for warming up the sample above the transition temperature, which correspond to the changes of internal energy. To estimate it we take from the literature the temperature dependence of the heat capacity $C_{\rm P}(T)$ in [J/moleK] (see inset of Fig. 5.6 [260]) and integrate it over the temperature. The result of the integration is shown in Fig. 5.6 as the temperature dependence of internal energy $U_{\rm mol} = \int C_{\rm P}(T) dT$ in [J/mole]. The thermal destruction energy then is given by:

$$U_{\rm th} = \frac{1}{n N_{\rm a} k_{\rm B}} [U_{\rm mol}(T_{\rm SDW}) - U_{\rm mol}(T_0)] \tag{5.6}$$

where $N_{\rm a} = 6.022 \cdot 10^{23}$ 1/mole is the Avogadro number, n is the number of Fe per unit cell, T_0 is the initial temperature of the sample, $T_{\rm SDW}$ is the transition temperature. We obtain that the energy needed for the thermal destruction of the SDW state $U_{\rm th} \sim 200$ K/Fe is higher than the one calculated in the previous section. It suggests that the mechanism of

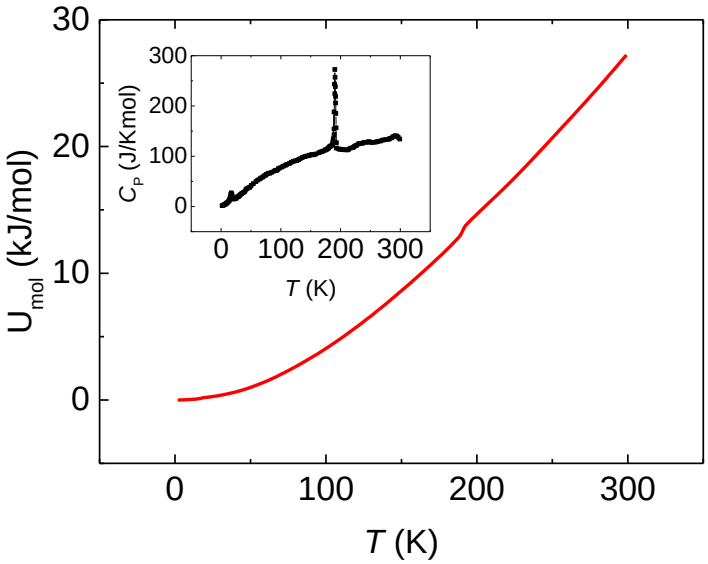


Figure 5.6: The change of the internal energy with T calculated for $EuFe_2As_2$ from the specific heat data. [260]

the destruction of the SDW state by laser pulses can not be described only by the thermal heating of all degrees of freedom and its nature is strongly non-thermal.

5.6 Relaxation time behaviour

To see how the relaxation time of the SDW response behaves with pump fluence, we normalize the transient reflectivity traces to the maximum of the signal (see Fig. 6.6a). The slowing down of the relaxation dynamics of the SDW response is well observed with increasing the pump fluence. Such a behaviour is consistent with the bottleneck mechanism of the relaxation.

To show that the amplitude and relaxation time describe the same processes of QP relaxation, we compare the behaviour of the amplitude A_{SDW} with relaxation rate $\gamma_{\mathrm{relax}} = 1/\tau_{\mathrm{relax}}$ (Figs. 6.6b,c) for Eu-122 and Ba-122, respectively.

5.7 Summary and conclusions

The non-equilibrium destruction of SDW ordering in AFe_2As_2 (A = Eu, Sr , Ba) was studied.

(i) We have shown that the SDW state in 122 pnictides can be destroyed nonthermally by an ultrafast optical laser pulses.

(ii) The energy needed to destroy the SDW order by ultrafast laser pulses and by the heating is calculated.

(ii) The analysis of energy and time needed to destroy the order suggests the electronic mechanism of destruction, which involves the disruption of the Fermi surface nesting.

(iii) The critical slowing down is observed in proximity to the phase transition.

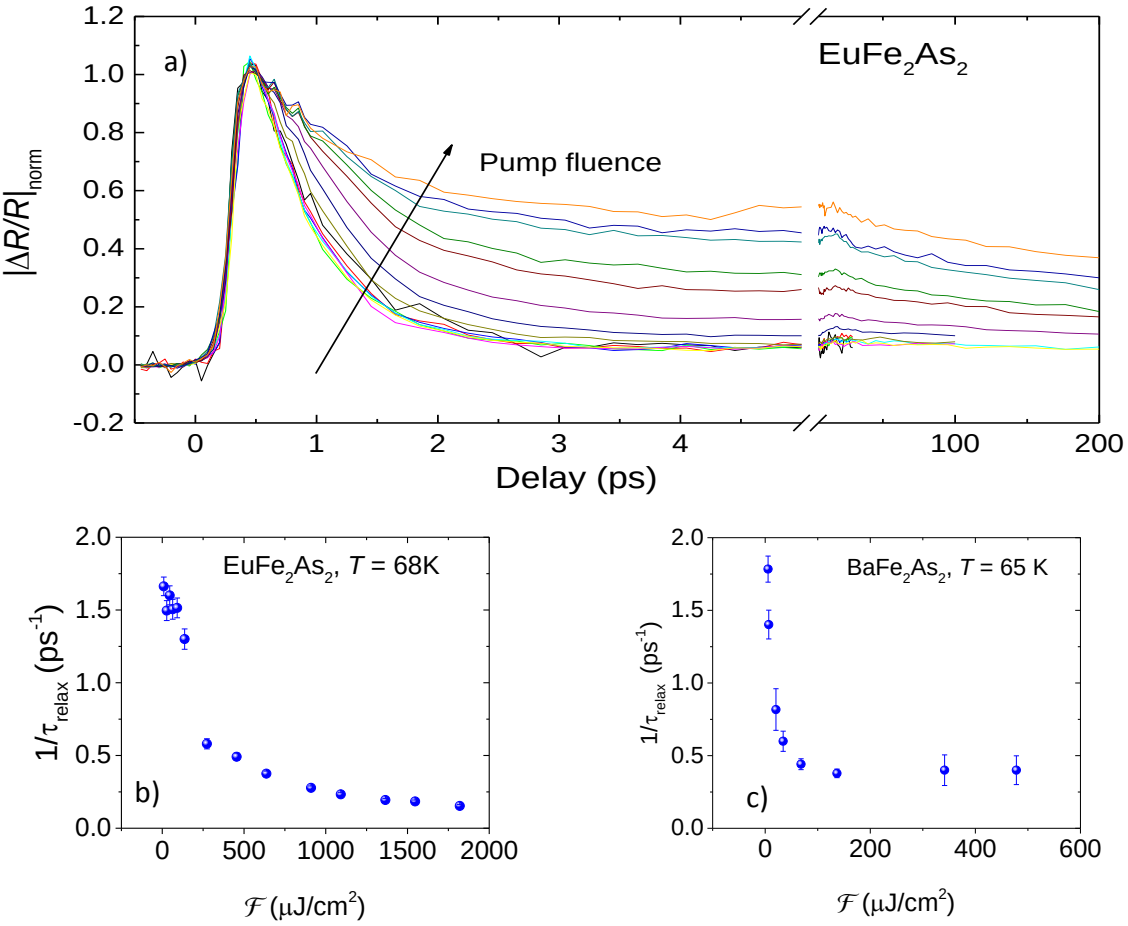


Figure 5.7: a) Normalized transient reflectivity measured for $EuFe_2As_2$ at 68 K as a function of the pump fluence. The black arrow denotes the direction of increasing the pump fluence. b), c) The relaxation rate as a function of the pump fluence compared with the transient amplitude for Eu-122 and Ba-122, respectively. As the amplitude of SDW response A_{SDW} we consider the maximal amplitude of the fast component (see Fig. 5.1).

Chapter 6

Amplitude recovery dynamics through the photoinduced SDW phase transition

The benefit of the novel three-pulse technique (see Experimental chapter for details) is a possibility for real-time observation of the evolution of the order parameter through a photoinduced phased transition. As it was shown above, the SDW state can be non-thermally destroyed by ultrafast laser pulses by applying a reasonably low destruction energy density, so the systems recovers to the ground state after a while by dissipating the exess energy to the phonon bath. In this chapter we report a systematic study of the SDW state recovery dynamics in parent $EuFe_2As_2$ iron pnictide, which possesses the SDW transition at T_{SDW}.

6.1 Destruction pulse arrives after pump

In Fig. 6.1 the transient reflectivity measured during the arrival of the destruction pulse is shown. The curves plotted in Figs. 6.1a-c are the same as the signal in the two-pulse experiments until the moment indicated with dots, when the D-pulse arrives and destroys the SDW state, so the signal drops to zero. The D-pulse fluence was kept above the threshold, which is about ~ 140 μJ/cm^2 for $EuFe_2As_2$ (see previous chapter), while the pump and probe beams were in linear regime.

As the destruction time we denote the time needed for the reflectivity signal to drop to the value of the normal state response after the D-pulse arrived. The plotted values of the destruction time are obtained by fitting the signal with a single exponent relaxation starting at the moment D-pulse arrived and until the state is completely destroyed. As one can see from Fig. 6.1d, the destruction time coincides with the raise time of the SDW signal and does not depend on the delay between the D and P pulses, neither on the fluence of the destruction beam. Independence on the D-fluence suggests the non-thermal destruction.

6.2 Destruction pulse arrives before pump

If the destruction pulse comes *after* the pump pulse, then the destruction dynamics can be studied. However, if the destruction pulse arrives to the sample *before* the pump, then the recovery of the system after the photoinduced destruction of the electronic order can be observed. In Fig. 6.2 we show a set of raw data for the case when the D pulse arrives before P, measured at different values of the destruction fluence. Reader should keep in

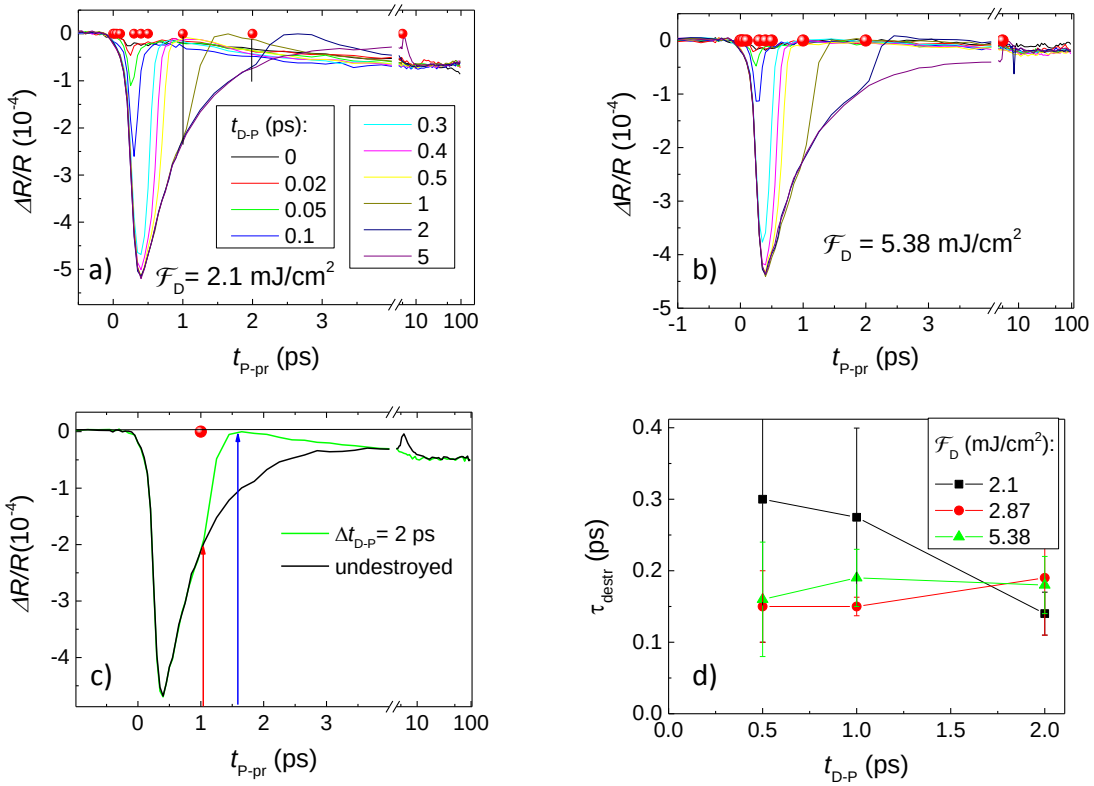


Figure 6.1: a), b) The transient reflectivity as a function of the time delay between pump (P) and probe (pr) pulses, $t_{\mathrm{P-pr}}$, measured as a function of the delay between the destruction (D) and pump pulses $t_{\mathrm{D-P}}$ for different D fluences. The moment of D pulse arrival is indicated with the red dots. c) The destruction time we define as the time between the moment, when the signal starts to deviate from the undestructed one (the red arrow), and the moment, when the destructed signal reaches the minima (the blue arrow). d) The destruction time as a function of D-P delay is shown for a few different D fluences. All the curves are measured at $T = 75$ K, much below T_{SDW}.

mind, that every single curve on these graphs is measured as a function of the pump-probe delay (the same as in the two-pulse experiments), while different curves in the same graph correspond to different delays between the destruction and pump pulses.

For example, let us look first at the graphs measured at $\mathcal{F}_{\mathrm{D}} = 2.15$ μJ/cm^2. The curve which corresponds to $t_{\mathrm{D-P}} = 0$ ps shows no SDW signal at all, because the state is completely destroyed (the remaining signal corresponds to the normal state response, described in Chapter 3). When the transient reflectivity is measured at some delay after the destruction, the system slightly recovers and one can observe the SDW peak for $t_{\mathrm{D-P}} > 0$ ps, which increases when the D-P delay is increased.

For the lowest destruction power $\mathcal{F}_{\mathrm{D}} = 0.56$ μJ/cm^2 (Fig. 6.2a) the signal does not go to zero even at $t_{\mathrm{D-P}} = 0$ ps, because the SDW state is not completely destroyed. For the highest destruction power (Fig. 6.2f) the signal does not recover completely even after $t_{\mathrm{D-P}} = 0$ ps delay.

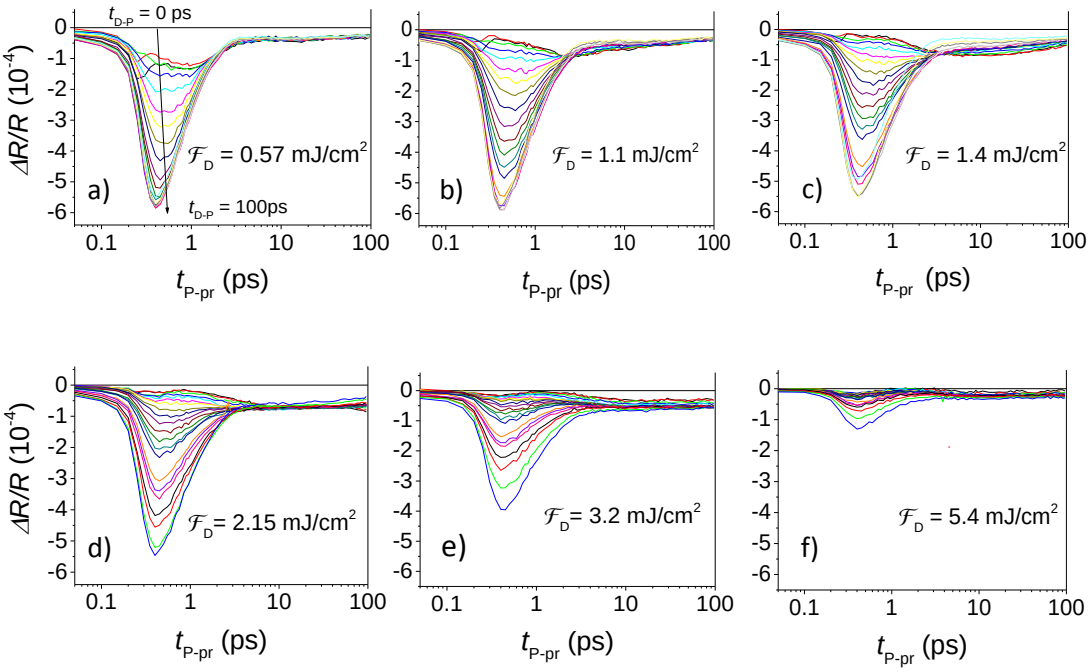


Figure 6.2: The transient reflectivity as a function of $t_{\mathrm{P-pr}}$ measured for different delays between D and P pulses, when the D pulse arrives before P. Different panels correspond to different destruction fluences indicated on each graph. The pump and probe fluences are kept in the linear regime 18 and 3 μJ/cm^2, respectively. The temperature of the sample was $T = 75$ K.

6.3 Recovery dynamics

To make the further analysis clear and figures more illustrative, we plot the transient reflectivity as a function of the delay between destruction and probe pulse, as it is shown in Fig. 6.3. The maximum amplitude for every trace is indicated with a red dot. At negative delays, before the destruction pulse arrives, we observe the signal with a constant amplitude as in the standard two-pulse experiment. At the moment, when the D-pulse arrives, the SDW order is destroyed, so the amplitude drops to zero. Afterwards, two distinct recovery dynamics of the amplitude are observed. First, it increases fast in ∼1 ps, then recovery slows down, and it completely recovers only after 200 ps.

While every separate curve in Figs. 6.3a,b should be understood as the QP relaxation dynamics, the curve produced by connecting red dots of maximum amplitudes (Fig. 6.3) is tentatively assigned to the dynamics of the order parameter, as explained in more details in the next sections.

6.3.1 Destruction fluence dependence

In Fig. 6.4 we present the destruction fluence dependence of the recovery of the maximum amplitude in the three-pulse experiment. At low D pulse fluences, when the SDW order is only partially suppressed, the amplitude recovery is fast on the 220 fs timescale. Above ~ 0.88 mJ/cm^2 the initial fast recovery, is followed by a slower one, which is attributed to the slow thermal cooling of the excited volume by heat diffusion.

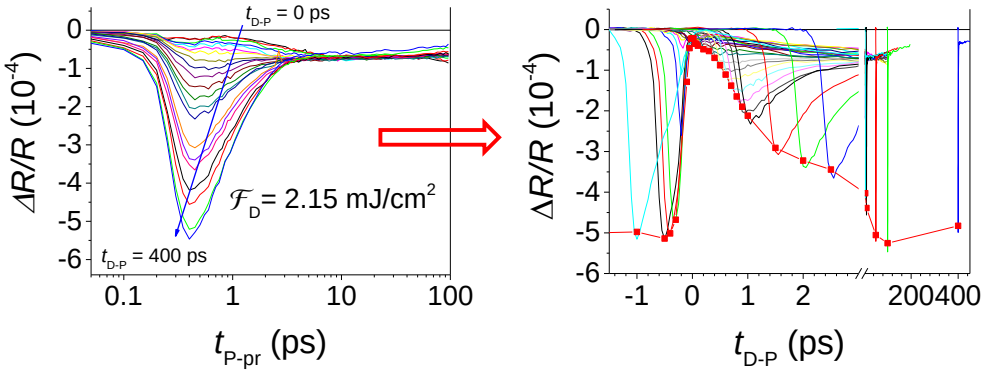


Figure 6.3: In the left panel the transient reflectivity in three-pulse experiment as a function of pump-probe delay, measured for different D-P delays. In the right panel the same data set is presented, but plotted as a function of the time delay between destruction and probe pulse. The red dots indicate the maximum of amplitude A_{fast} for every curve.

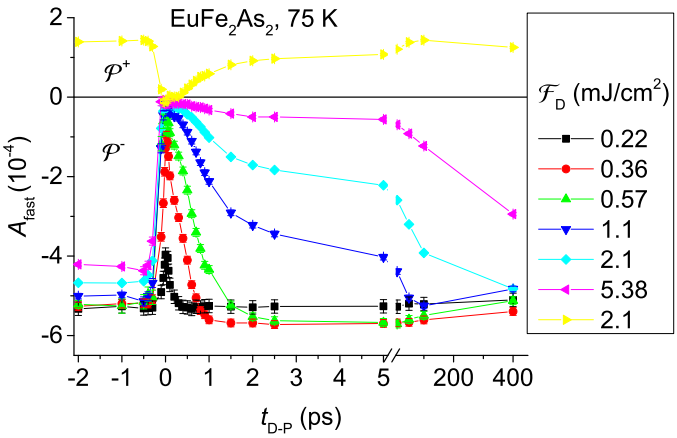


Figure 6.4: The maximum amplitude in the three-pulse experiment as a function of $t_{\text{D}-\text{P}}$ delay, plotted for different destruction fluences.

6.3.2 Recovery time

To analyze the amplitude of the recovery dynamics we fit the data with the single exponent on the limited region of $t_{\text{D}-\text{P}}$ delays (see Fig. 6.5a). In Fig. 6.5b we plot the results of the fit. The recovery time strongly depends on the destruction fluence. The recovery slows down with increasing the destruction energy and finally saturates at ∼1 ps. At the highest destruction fluence the recovery is dominated by the diffusion processes, which is pretty natural if we pay attention to the fact that the fluence of $\mathcal{F}_{\text{D}} = 5$ mJ/cm^2 corresponds to the energy of the thermal destruction of SDW state ($U_{\text{D}} \sim 1600$ K/Fe).

For strongly non-equilibrium processes the dynamics of the order parameter (OP) can differ from the dynamics of photoexcited quasiparticles. For comparison, in the same figure (Fig. 6.5b) we plot also the quasiparticle relaxation time as a function of the pump fluence in two-pulse experiments. It is well seen that the QP relaxation is much slower than the recovery dynamics observed by the three-pulse technique. This fact illustrates very well that the recovery dynamics can not be described only to the relaxation of photoinduced

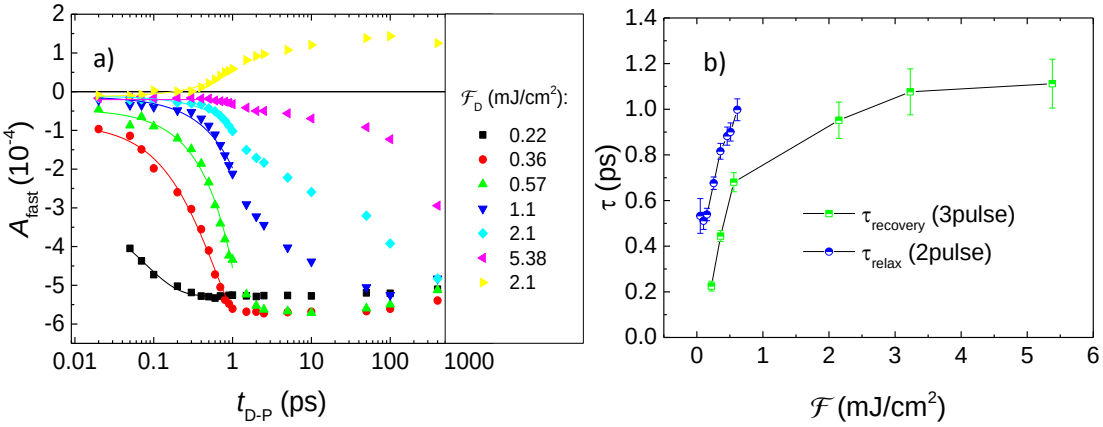


Figure 6.5: a) The same destruction fluence dependence of the fast recovery for Eu-122, which was plotted in Fig. 6.4. In the right panel b) the comparison of the recovery time and the relaxation time as a function of destruction and pump fluence, respectively.

electrons, but the signal we observe corresponds to the order parameter dynamics, which can be faster.

6.4 Amplitude dynamics and QP relaxation rate

In Fig. 6.6 we plot the amplitude A_{fast} in comparison to the relaxation rate, obtained by the single exponential fit of the reflectivity changes, measured in the same tree-pulse experiments. If we consider that the relaxation rate is proportional to the gap size, and as a consequence to the order parameter, then their dynamics should coincide [178]. However, we see that it works well only for the lowest destruction fluence. For higher fluences they do not coincide after a certain delay, when the diffusion processes prevail.

6.5 Thermal diffusion model

As it was shown in Chapter 3 for parent iron pnictides the amplitude of the SDW response strongly depends on the temperature (see Fig. 3.7b). If the signal observed in the three-pulse experiments corresponded to the QP dynamics, then the recovery dynamics would follow the temperature evolution of the SDW QP relaxation. To compare these two processes we use the thermal diffusion model (TDM) as it was described in [261], and assume that the temperature of the sample is a function of the time delay after destruction.

If we consider the one-dimensional case, then the temperature at the surface as a function of time can be approximately[1] described as:

$$T(t) = T_{0+} \frac{\Delta T}{\sqrt{1 + \left(\frac{t}{t_0}\right)^2}}, \tag{6.1}$$

where $T(t)$ is the non-equilibrium temperature of the excited sample, t is the time delay after the perturbation pulse, T_0 is the initial (cryostat) temperature, ΔT is the photoinduced

[1] For Gaussian profile of the initial energy distribution in the excited volume.

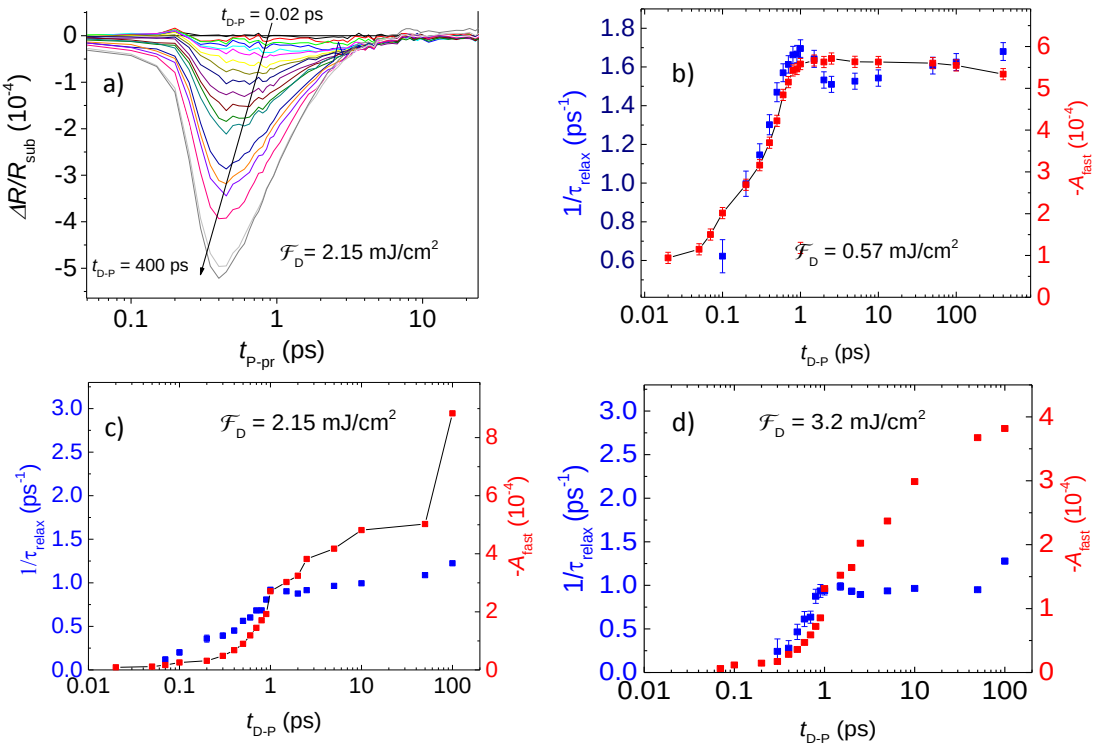


Figure 6.6: a) Three-pulse response for $EuFe_2As_2$ obtained by the subtraction of the transient reflectivity measured at $t_{D-P} = 0$ ps with the 2.15 mJ/cm^2 destruction fluence. b)-d) The QP relaxation rates (blue) and the amplitude recovery dynamics (red) as a function of delay t_{D-P} for a few different destruction fluences. The relaxation rates are superimposed from a single exponential fits on the data, obtained in the same way as in a) with respective destruction fluences. The amplitudes are obtained by the parabola fit.

change of the volume temperature[2], t_0 is the value which depends on the heat diffusion constant.

In Fig. 6.7 we plot the amplitude recovery dynamics as a function of time (blue), measured in the three-pulse experiment. After the initial fast recovery on a few picoseconds timescale the signal continues to grow. At 100 ps the modulus of a recovered amplitude is larger than it was before the destruction. In the same graph with the red line we plot the $\Delta R(t) = \Delta R(T(t))$, where $T(t)$ obtained from the Eq. (6.1), and ΔR is measured in the two-pulse experiment (see Fig. 3.7) as a function of time. ΔT was calculated as described in Sec. 5.5, t_0 was taken 100 ps.

6.6 Temperature dependence

In Fig. 6.8 we show the destruction fluence dependence measured for the SDW amplitude in $EuFe_2As_2$ at four different temperatures. The traces at 75 K were measured with a higher time resolution, but otherwise the evolution of order parameter is qualitatively the

[2]Depends on the T_0 and the pulse power, and can be estimated, if the heat capacity and the optical penetration depth are taken into account.

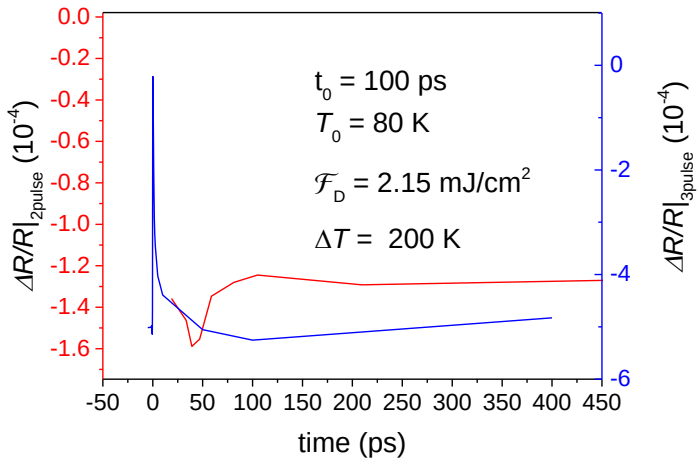


Figure 6.7: The comparison of the amplitude recovery dynamics (the blue line) and the adiabatic amplitude dynamics (the red line) obtained by means of thermal diffusion model, discussed in the text.

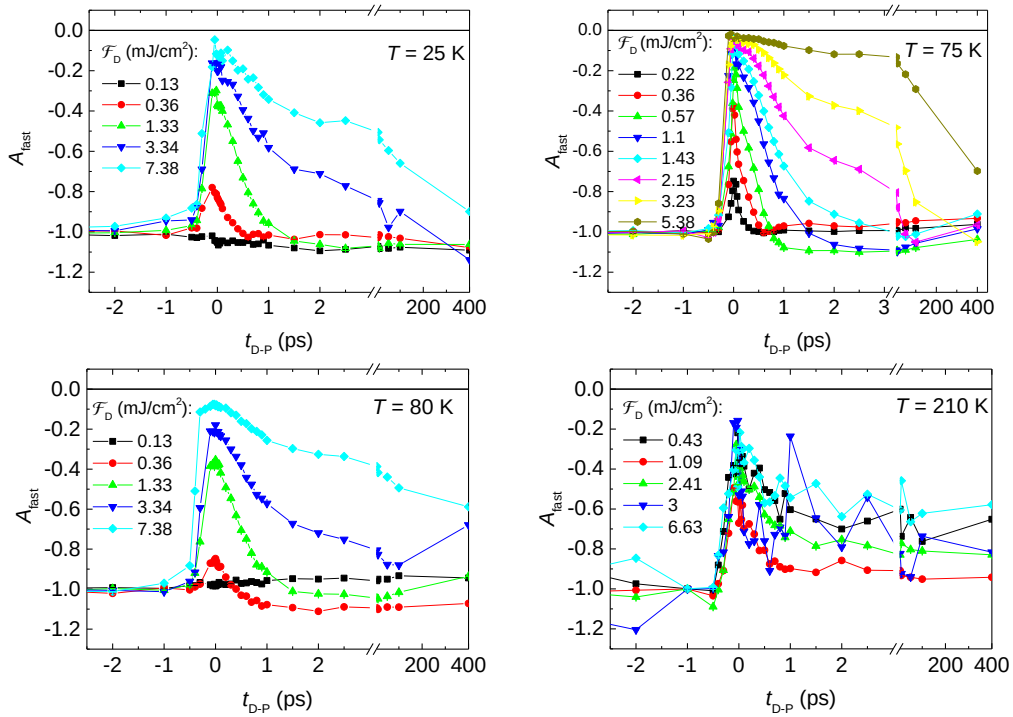


Figure 6.8: The SDW order parameter dynamics as a function of destruction fluence measured at different temperatures.

same below the transition temperature $T_{\mathrm{SDW}} = 190$ K.

Surprisingly, above the SDW transition, we also observe some change of the amplitude. These changes cannot be explained by the metallic response, because, as we have shown in previous chapters, the normal state transient reflectivity linearly depends on the excitation fluence. We think that the observed dynamic corresponds to the pseudogap dynamic, which opens due to the presence of nematic fluctuations.

6.7 Summary and outlook

The three-pulse technique allows to probe directly the real time dynamics of the SDW evolving through a non-equilibrium phase transition.

(i) The recovery of the SDW after destruction evolves in two steps. First, electronic system recovers on a ps timescale, after that the heat diffusion follows.

(ii) The comparison of the transient reflectivity relaxation time with the amplitude recovery time suggests a coherently driven order parameter excitation.

(iii) The overlap of the relaxation rate and amplitude recovery suggests the observation of the order parameter dynamics through the photoinduced phase transition.

(iv) The recovery dynamics through the nematic fluctuations phase transition can be observed.

Chapter 7

Superconducting gap in $BaFe_2(As_{1-x}P_x)_2$ from temperature dependent transient optical reflectivity

In $BaFe_2(As_{1-x}P_x)_2$ the SC is induced by the isovalent substitution of P by arsenic As and the superconducting state is induced by means of the induced chemical strain. In the optimally doped $BaFe_2(As_{0.7}P_{0.3})_2$, where the critical temperature reaches $T_c = 30$ K, the SC gaps where analyzed by means of ARPES [262]. In contrast to the optimally doped $Ba(Fe_{1-x}Co_x)_2As_2$[59], where there is little indication of nodes, nodes in the SC gap were clearly observed by ARPES in $BaFe_2(As_{1-x}P_x)_2$.

To study the possible effect of the nodes on the photoexcited quasiparticle relaxation we therefore conducted a systematic 1.55 eV optical transient reflectivity study in the optimally doped $BaFe_2(As_{0.7}P_{0.3})_2$.

7.1 Fluence dependence

In Fig. 7.1 we compare the reflectivity transients measured as a function of excitation pump fluence in the superconducting and in normal state. The signals show no significant pump and probe polarization dependence. At low fluence the amplitude of the superconducting signal increases linearly and saturates with increasing the fluence of the pump beam above 3 μJ/cm^2 (Figs. 7.1a). The saturation of the transient reflectivity signal is associated with a non-thermal destruction of the ground state and a complete closure of the gap.

The normal-state response shown in Fig. 7.1b appears much weaker at low fluencies with a different sign and a faster relaxation time in comparison to the SC response. At high fluencies, above 10 μJ/cm^2, the magnitude of the normal state response becomes comparable to the SC-response magnitude due to the saturation of the SC-response.

Below the saturation fluence in a weak excitation regime the SC signal relaxes on a few picosecond timescale and can be fitted by a single exponential fit. The relaxation time is constant at low temperature and increases near the transition temperature. Above 1 μJ/cm^2 of the pump fluence, in the strong excitation regime, the reflectivity transients are more complicated: the relaxation is delayed and can not be fitted by a single exponent.

The relaxation at higher $\mathcal{F}$ is clearly non-exponential and the faster part can be associated with the Rothwarf-Taylor bottleneck, while the slower one corresponds to the cooling after all degrees of freedom have been thermalized [209]. At excitation densities above a

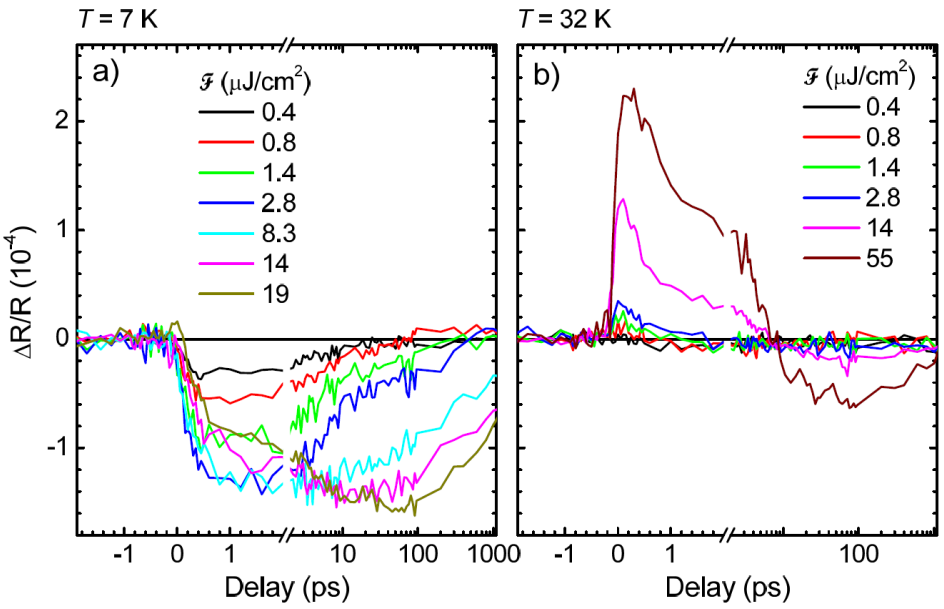


Figure 7.1: The photoinduced reflectivity transients $\Delta R/R$ in $BaFe_2(As_{0.7}P_{0.3})_2$ measured as a function of pump fluence in the superconducting a) and normal b) state.

few J/cm^2 the amount of absorbed optical energy is large enough to heat the phonon bath above T_c and the SC state recovery is governed by the energy escape from the probed volume.

7.2 Destruction energy

As described in previous chapters, we use the inhomogeneous saturation model [29] to fit fluence dependence of the transient reflectivity amplitude and determine the SC state destruction threshold fluence $\mathcal{F}_{th} = 1 \pm 0.35$ μJ/cm^2. The bulk SC state destruction energy density required to completely destroy the superconducting state can be obtained by $U_d = \mathcal{F}_{th}(1-R)/\lambda_p = 0.42$ K/Fe, where $\lambda_p = 31$nm is the penetration depth and $R = 0.22$ [103] is the reflectivity at 1.55 eV photon energy. This value is much smaller than the energy $U_{th} \approx 2.4$ K/Fe needed to heat the sample thermally above T_c [22] indicating that the SC destruction is highly non-thermal.

In Fig. 7.3 we compare the SC-condensate optical destruction energy in iron pnictides with some other superconductors. As discussed previously [198], U_d is roughly proportional to T_c^2. The actual value for each compound depends on the thermodynamic condensation energy and the amount of the energy lost by transfer to the non-pairbreaking subgap phonons [198]. We obtain the in-plane destruction-energy densities by normalizing the energy density to a single FeAs , CuO_2, Mg or Nd plane by multiplying the volume density by the interplane distances for very different layered compounds. It is therefore somewhat surprising that the destruction energy densities lie rather close to the same line with the exception of the three-dimensional NbN. Within the iron pnictide class the accuracy of the scaling with T_c^2 is enhanced if one considers the optical destruction energy normalized to the Fe content (see inset to Fig. 7.3). This suggests that the differences of the detailed gap structure, for example, the presence of nodes in $BaFe_2(As,P)_2$, between different members contribute only a small correction to the free-energy gain in the SC state.

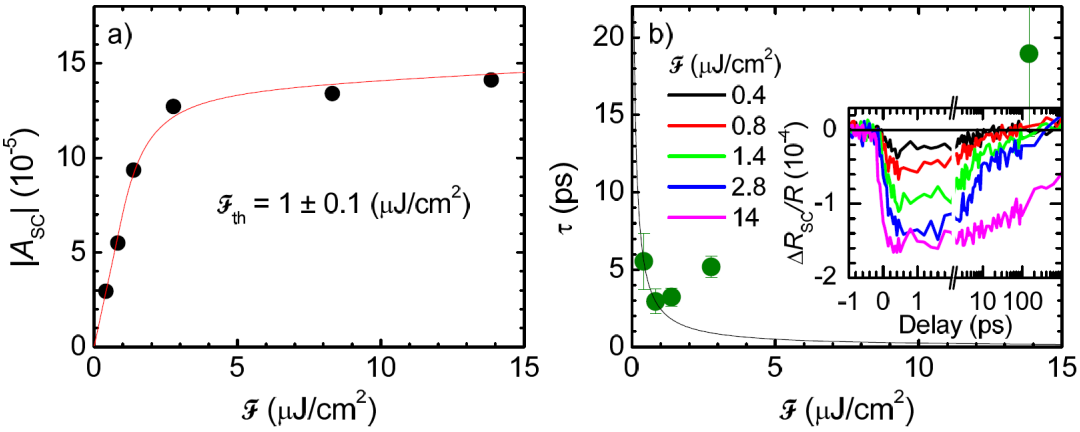


Figure 7.2: a) The fluence dependence of the transient amplitude. The thin line is the saturation model fit discussed in text. b) The dominant relaxation time in the superconducting state. The thin line is the Rothwarf-Taylor fit [177]. The inset to b) shows the 7-K transients with the 32-K normal state response subtracted.

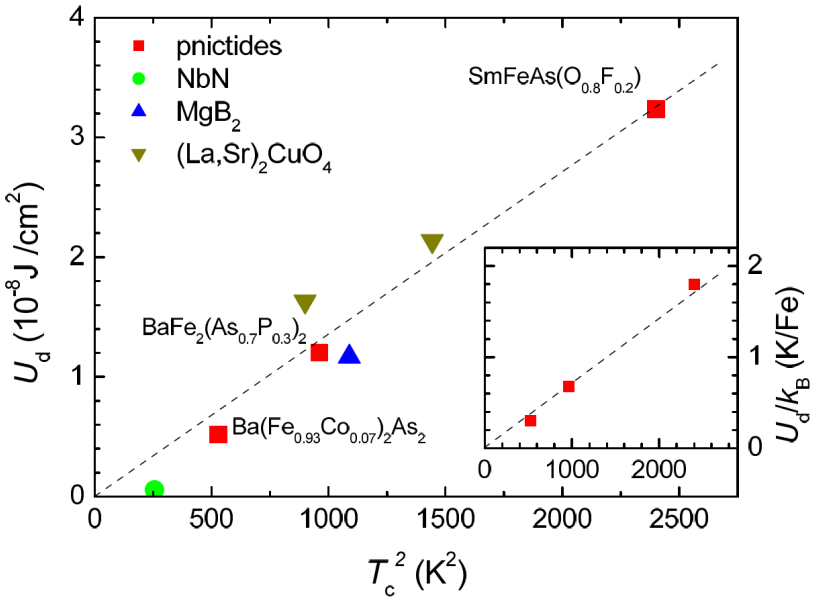


Figure 7.3: The in-plane SC-state optical destruction energy density as a function of T_c^2 for some iron based pnictides compared to NbN [263], MgB_2 [177] and $(La,Sr)_2CuO_4$ [29]. The inset shows U_d in the pnictides normalized to the Fe content.

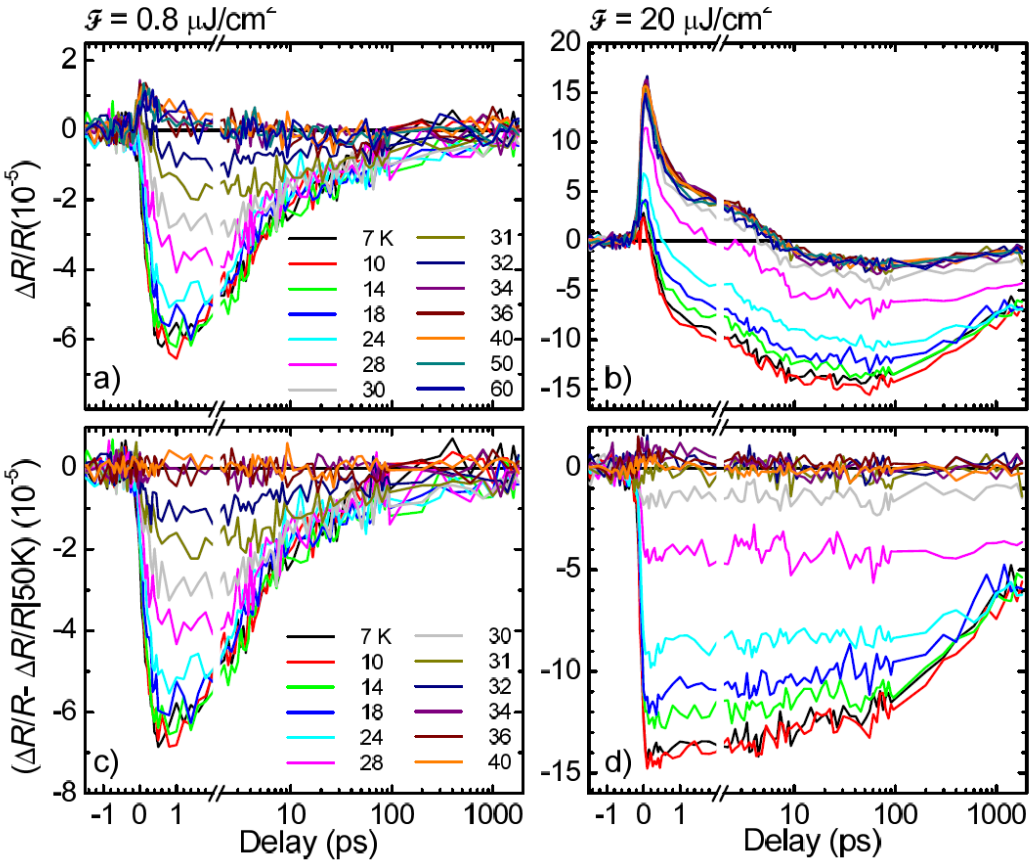


Figure 7.4: Temperature dependence of the transient reflectivity $\Delta R/R$ at low $\mathcal{F} = 0.8$ μJ/cm^2 a) and high $\mathcal{F} = 20$ μJ/cm^2 b) fluence. Note that the data above the critical temperature collapses onto a single curve in a wide temperature range at both fluencies. The superconducting state response obtained by subtracting the average of the transients from the 34 K-50 K interval at low c) and high d) fluence.

7.3 Temperature dependence in strong and weak excitation regimes

In Fig. 7.4 we show the temperature dependence of the transient reflectivity at two selected fluences. The lower was chosen to be in the $\mathcal{F}$-linear SC-response region in most of the T range while the higher corresponds to the strongly saturated SC-response fluence. In both cases the data in the normal state collapses onto a single curve in a wide T range up to twice T_c suggesting a T-independent background response present also in the SC state. We subtract this normal-state background response to obtain the SC-state response, as shown in Figs. 7.4c,d. At the low fluence the subtraction does not significantly change the shape of the response, while at the high fluence it leads to the complete removal of the picosecond timescale dynamics, which is associated with the normal state response, justifying the subtraction procedure. The SC-response shows a 0.5 ps risetime followed by 5 decay time at the low excitation. At the high excitation the risetime is faster on 0.2 ps timescale while the relaxation slows down to nanosecond timescale. In both cases the relaxation slows down when approaching T_c from below.

The transient optical response of superconductors was shown to be governed by the phonon bottleneck effects [178]. As it was mentioned in the introduction, one speaks about

weak excitation regime, if the number of photoexcited quasiparticles is much smaller than the number of thermal quasiparticles $n \ll n_{\mathrm{T}}$, and opposite for a strong excitation regime. In the weak perturbation limit the dynamics is usually discussed in the framework of simple effective two-electronic-level models, such is the Rothwarf-Taylor [190] model and the related Kabanov bottleneck model [178]. Both enable determination of the characteristic SC gap energy from the T-dependent transient response amplitude. The weak excitation limit is difficult to achieve in the case of iron pnictides due to rather small transient reflectivity magnitudes and low optical destruction thresholds. In the present case the lowest fluence of 0.8 J/cm^2 used for T-scans appears to be near the limit of the $\mathcal{F}$-linear response region. The $\mathcal{F}$-dependent dominant relaxation time shown in Fig. 7.2b shows the expected Rothwarf-Taylor behaviour, $\tau = \tau_0(\mathcal{F}+\mathcal{F}_{\mathrm{T}})^{-1}$, below $\mathcal{F} = 0.8$ μJ/cm^2 only, with $\mathcal{F}_{\mathrm{T}} = 0.05$ μJ/cm^2 at 7K, where $\mathcal{F}_{\mathrm{T}}$ corresponds to the fluence at which the density of the photoexcited quasiparticles is comparable to the thermally excited quasiparticle density.

On the other hand, the amplitude of the response appears almost linear up to $\mathcal{F} \sim 1.4$ μJ/cm^2 at the lowest T while the $\mathcal{F} = 0.8$ μJ/cm^2 amplitude reaches the saturation value only above $T = 28$ K (see Fig. 7.5b). We therefore assume that for $T = 25$ K the response is $\mathcal{F}$-linear and the T-dependent amplitude, $A(T)$, is proportional to the low-$\mathcal{F}$ limit and follows the bottleneck model from Kabanov, described in the introduction.

7.4 Superconducting gap

By increasing the temperature the amplitude of the transient reflectivity decreases and becomes zero near T_{c} in both regimes of the strong and weak excitation. In the strong excitation regime, when the amount of destroyed Cooper pairs is large enough to close the SC gap, the SC response saturates. Far above the saturation the transient reflectivity can be understood as a difference between the SC and normal state and can be described by the Mattis-Bardeen formula Eq. (1.5.5), described in the introduction. Using the approximation to the superconducting BCS gap $\Delta(T) = \Delta_0 \tanh((1.75)\sqrt{T/T_{\mathrm{c}} - 1})$, where Δ_0 is superconducting gap at $T = 0$ K, the model fits well the temperature dependence of the reflectivity changes amplitude measured in a strong excitation regime Fig. 7.5b.

Fitting $A(T)$ in Fig. 7.4a using Eq. (1.21) with the BCS temperature dependent gap, $\Delta(T)$, we obtain $2\Delta(0)/k_{\mathrm{B}}T_{\mathrm{c}} = 4 \pm 1$ with $\Delta(0) = 5$ meV. This value is consistent with the gap on the hole Fermi surface and smaller than the gap on the electron Fermi surfaces as obtained by ARPES [264] in the samples from the same batch. The relaxation dynamics detected by means of 1.55-eV probe photons in $BaFe_2(As_{1-x}P_x)_2$ can therefore be attributed to the hole Fermi surfaces as also suggested for K and Co doped $BaAs_2Fe_2$ [20].

Despite the presence of several bands with different gaps in the case of iron-based pnictides and the presence of the gap node [264] on the hole Fermi surface in $BaFe_2(As_{1-x}P_x)_2$ the amplitude of the weak-excitation response in the SC state seems to be reasonably well described by the bottleneck model similarly to the cuprate superconductors [191].

The divergence of the relaxation time of SC signal at weak excitation (see Fig. 7.5c) can also be well described by the bottleneck model. In proximity to the transition temperature the SC gap becomes smaller, which means that the probability to find a boson with the energy higher than the gap size becomes higher and this slows down the relaxation of photoexcited quasiparticles.

At low excitation fluences we observe a measurable response up to 2 K above $T_{\mathrm{c}} = 30$ K, which vanishes at the highest fluence. From the fit $T_{\mathrm{c}} = 31 \pm 0.2$ K was obtained, which is 1 K higher than the maximum bulk T_{c} in this system. The difference can not be attributed to the thermal gradient due to the laser excitation and the room radiation

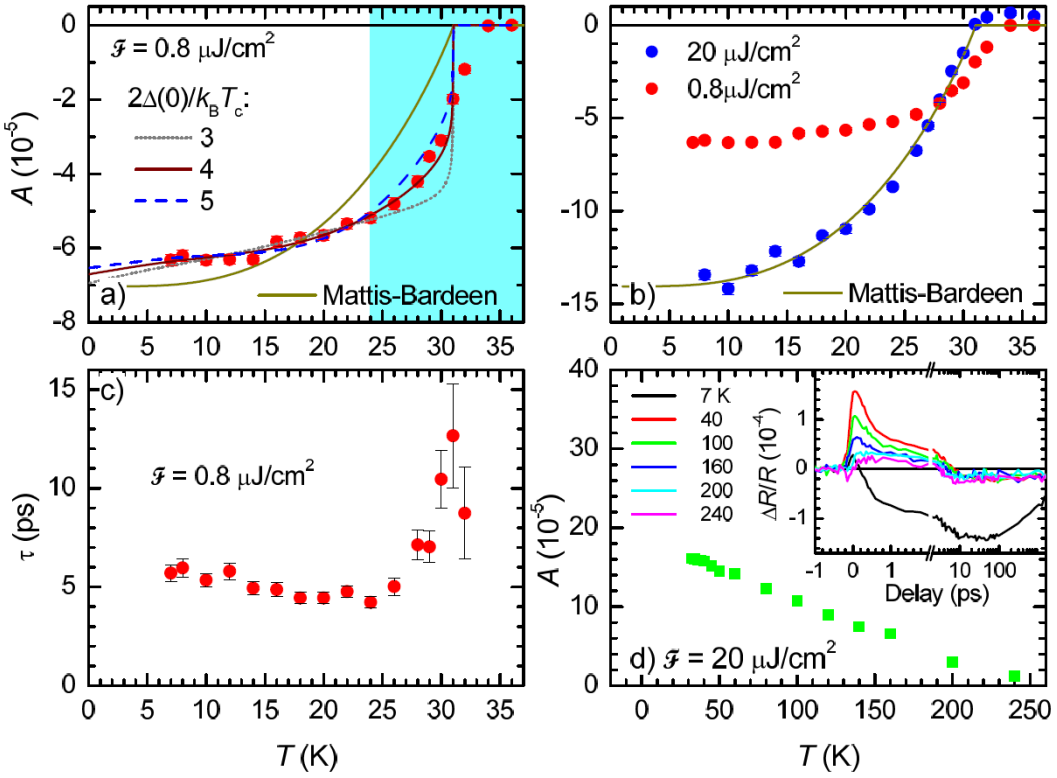


Figure 7.5: The temperature dependence of the SC response amplitude for low a) and high b) excitation density. The lines are fits discussed in text, where the shaded region in (a) was excluded from the bottleneck model fits. c) The low-excitation SC-response relaxation time as a function of temperature. d) Temperature dependence of the normal state transient reflectivity amplitude. Transients at a few characteristic temperatures are shown in the inset.

thermal-load since it should decrease the apparent T_c, but to an error in the cryostat T calibration, which was checked later by means of a calibrated diode temperature sensor mounted at the sample position to be ±1 K. We attribute this response to SC fluctuations [265]. This error does not significantly affect the gap determination from the fit above.

The normal state sub-ps transient response, which shows a vanishing amplitude with increasing temperature disappearing around $T = 250$ K (see Fig. 7.5d), is very similar to the behaviour in Co-doped Ba-122 [22], where it was associated with the presence of the pseudogap due to the nematic fluctuations. In the present case it can also be attributed to the presence of the pseudogap. The temperature range of vanishing pseudogap is about 100 K above the pseudogap formation temperature based on ARPES results [62]. Contrary to Co-doped Ba-122 it does not show any 4-fold axis symmetry breaking. Since a global external symmetry breaking (strain) field is necessary to orient the fluctuations across the whole experimental volume along one direction, this observation indicates the absence of the global field, but it does not rule out a local field with varying orientation enhancing the nematic fluctuations.

7.5 Summary and conclusions

Conducting a systematic wide-fluence-range optical time-resolved pump-probe study in optimally isovalently doped $BaFe_2(As_{0.7}P_{0.3})_2$ we find a similar behaviour to previously studied $Ba(Fe,Co)_2As_2$.

(i) In the low excitation regime the transient reflectivity changes are dominated by the bottleneck relaxation processes. The temperature dependence of the amplitude can be well fitted by the bottleneck formula and the relaxation time behaviour also supports this scenario. The superconducting gap magnitude of $2\Delta(0)/k_BT_c = 4 \pm 1$ is consistent with the gap on the hole Fermi surface. The relaxation dynamics detected by means of 1.55-eV probe photons in Ba-122 can therefore be attributed to the hole Fermi surfaces as suggested previously by Torchinsky *et al.* [20].

(ii) In the strong excitation regime the pump-probe response is due to the difference between the normal and the gapped state. The temperature dependence of the amplitude can be described well by the Mattis-Bardeen formula.

(iii)The normal state response indicates the presence of a pseudogap related to the nematic fluctuation up to $T = 250$ K as generally observed in the electron doped iron-based pnictide superconductors.

(iv) The in-plane non-thermal optical-destruction volume energy densities are found to scale linearly with T_c^2 and lie close to the same line for a range of different layered superconductors.

Chapter 8

Eu^{2+} spin dynamics

8.1 Peculiarities of Eu-based 122 compounds

Eu-based 122 compounds stand out from the other iron pnictides due to the presence of a ferromagnetic order of Eu^{2+} spins at low temperature. The iron-based $EuFe_2(As,P)_2$ and $Eu(Fe,Co)_2As_2$ offer an interesting experimental possibility to study the competition between the ferromagnetic and superconducting order parameters that can lead to nonuniform magnetic and SC states [156], [172], [266], [267], since the optimal superconducting critical temperature $T_c \sim 20.5$ K [268] is comparable to the FM Eu^{2+}-spin ordering temperatures 19 K [17], [269].

The strength and nature of the coupling between the carriers in the FeAs planes, responsible for superconductivity, and the localized Eu^{2+} f-orbital spins, responsible for ferromagnetism, is expected to strongly influence any possible magnetic as well as SC modulated state [156]. To enable coexistence of the singlet superconductivity with ferromagnetism in the case of strong exchange-interaction-dominated coupling, the magnetization modulation period should be short, on the scale below the SC coherence length [156], [266], which is a few [171], [270] tens of nm in 122 iron-based compounds. On the other hand, in the case of a weaker long-range magnetic-dipole dominated coupling a longer scale FM domain structure can effectively minimize the internal magnetic field enabling coexistence of the singlet superconductivity and FM state [271]. Alternatively, a spontaneous SC vortex state might form in $EuFe_2(As,P)_2$ as proposed recently [33]. Opposing claims regarding the coupling between the carriers in the FeAs planes and localized Eu^{2+} spins exist in the literature. A weak coupling between Fe and Eu magnetic orders was initially suggested by Xiao *et al.* [272], while recently a strong coupling was suggested from the in-plane magnetoresistance [273] and NMR [274].

The strength of the coupling between the carriers in the FeAs planes and localized Eu^{2+} f-orbital spins should be reflected also in the energy transfer speed between the two subsystems upon photoexcitation. The optical time-resolved spectroscopy can directly access the quasiparticle and spin relaxation dynamics and shed some light on Eu^{2+} f-spin Fe d-carrier interaction. We therefore systematically investigated the ultrafast transient reflectivity dynamics in $EuFe_2(As,P)_2$ and $Eu(Fe,Co)_2As_2$ for a wide range of dopings. In addition to the relaxation components, that were observed earlier in the related non-FM iron pnictides, [22], [213] and described in previous chapters, we observe another slow-relaxation component associated with the Eu^{2+}-magnetization dynamics.

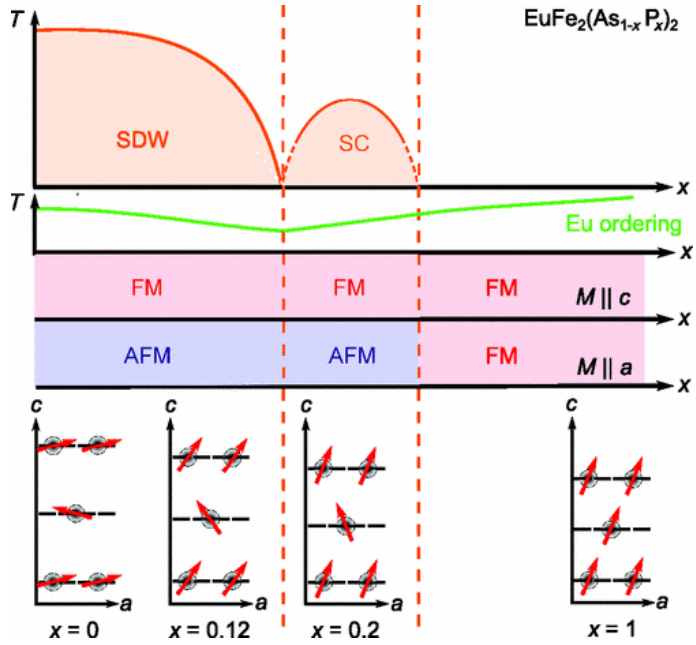


Figure 8.1: Schematic phase diagram of $EuFe_2(As_{1-x}P_x)_2$ indicating the SDW and SC phase. Proposed in [34]. In the preceding panels, we show the Eu^{2+} ordering. The scheme of the Eu^{2+} spin alignment is also shown. In the parent compound, *A*-type AFM is found with the spins being slightly canted. With pressure/doping, the canting angle increases, when the SDW is completely suppressed. At an even higher pressure, the AFM interlayer coupling turns into a FM one.

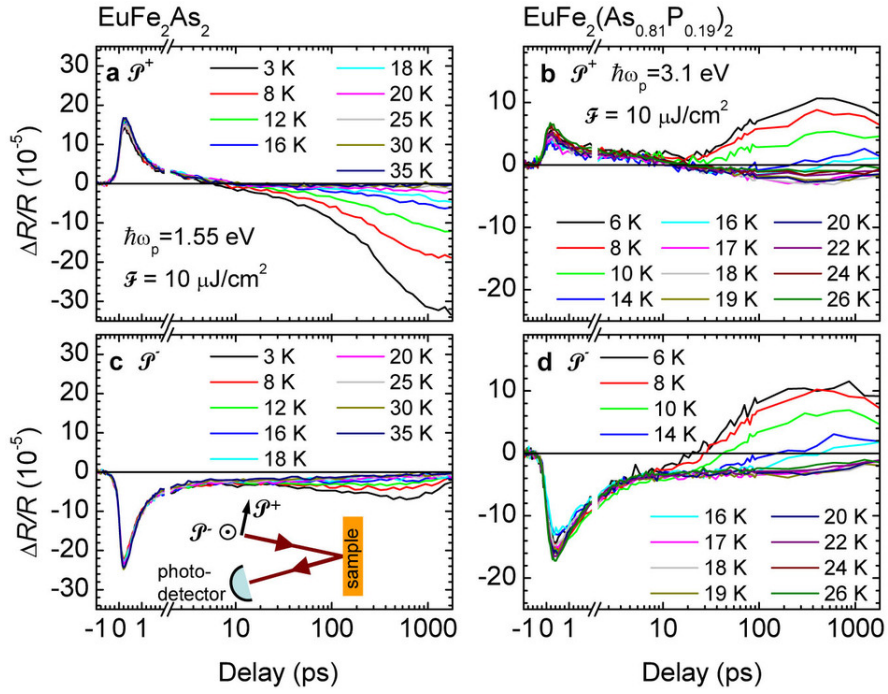


Figure 8.2: Photoinduced reflectivity transients at low-T in $EuFe_2As_2$ a), c) and $EuFe_2(As_{0.81}P_{0.19})_2$ b), d) for two probe-photon polarizations. The inset in c) represents a schematic of the probe beam configuration and corresponds to the two orthogonal in-plane probe-photon polarizations.

8.2 Low-T response in Eu-based 122 iron pnictides

In Fig. 8.2 we show temperature dependence of the transient reflectivity ($\Delta R/R$) measured with the probe pulses polarized in the *ab*-plane in undoped non-superconducting $EuFe_2As_2$ (Eu-122) and doped superconducting $EuFe_2(As_{0.81}P_{0.19})_2$ (EuP-122). The transient reflectivity is anisotropic in the *ab*-plane, consistent with the orthorhombic crystal structure. We indicate the two orthogonal polarizations according to the sign of the sub-picosecond transient reflectivity as it was done in Chapters 3 and 4.

In addition to the anisotropic fast component associated with the SDW order discussed in previous chapters, concurrently with the Eu^{2+}-spin magnetic ordering [34], [260], [272] below $\sim 17-19$ K we observe, in both samples, the appearance of another much slower relaxation component with the risetime of ~ 1 ns in Eu-122 and ~ 0.5 ns in EuP-122 (at $T = 1.5$ K) and the decay time beyond the experimental delay range (see Fig. 8.3). In the vicinity of the Eu^{2+} magnetic ordering a marked increase of the risetime is observed in both samples. It suggests that the slow component is associated with the dynamics of Eu^{2+} spins.

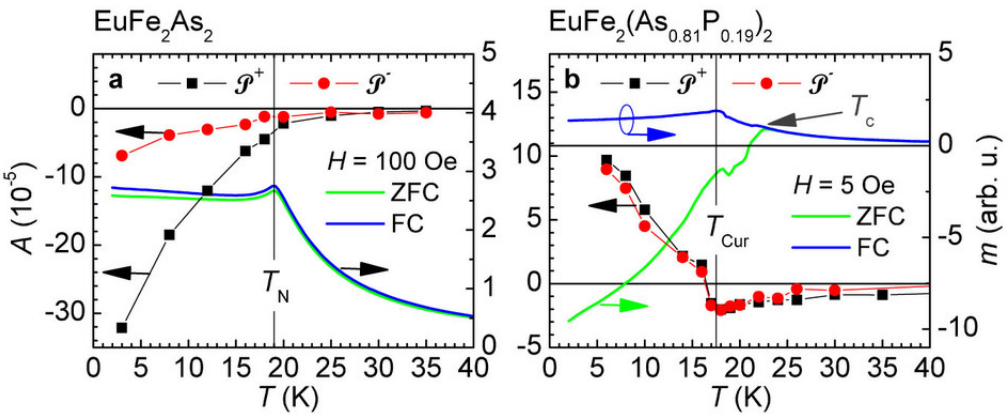


Figure 8.3: The amplitude of the transient reflectivity at long delays as a function of temperature in $EuFe_2As_2$ a), and $EuFe_2(As_{0.81}P_{0.19})_2$ b), compared to the magnetic moment along the *c*-axis and corresponding to two orthogonal in-plane probe-photon polarizations, while zero field cooling (ZFC) and field cooling (FC) correspond to cooling in the presence and absence of magnetic field, respectively.

In Eu-122 the slow component is rather anisotropic, while in EuP-122 it appears almost isotropic at the chosen pump fluence.

The probe-photon energy dependence of the transients in Eu-122 is shown in Fig. 8.4. The dispersion of the fast component (see Chapter 4) is much broader than that of the slow one, which shows a relatively narrow resonance around ~1.7 eV.

Eu^{2+} ions have $[Xe]4f^7 6s^2$ ($^8S_{7/2}$) electronic configuration. The lowest excited states of a free Eu^{2+} ion are ~ 3.5 eV above the ground state [275]. In oxides, however, this splitting can be reduced down to ~ 1 eV [275], [276]. In Eu-122 the position of f-derived states was calculated to be ~ 2 eV below the Fermi energy [77], close to the observed Eu^{2+}-spin ordering related slow-component resonance around 1.7 eV (see Fig. 8.4). It is therefore plausible that the Eu^{2+} magnetism and the dielectric constant at the probe-photon energy of 1.55 eV are coupled through the resonant magneto-optic Cotton-Mouton effect with the location of the Eu^{2+}-$4f$ states at ~1.7 eV below the Fermi level.

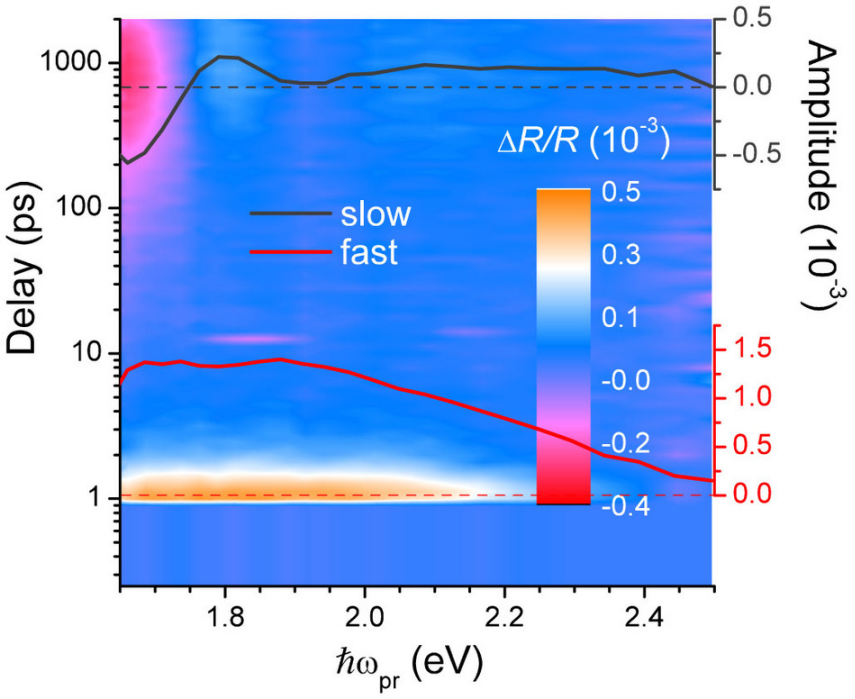


Figure 8.4: The transient reflectivity at low-T in $EuFe_2As_2$ as a function of probe-photon energy for the $\mathcal{P}^+$ polarization. The spectral dependencies of the fast and slow response amplitude are shown as red and dark-grey lines, respectively.

8.3 Magnetic field dependence of response

Upon application of magnetic field lying in the *ab*-plane the Eu^{2+} AFM order in Eu-122 is destroyed above $\mu_0 H \sim 0.8$ T in favor of an in-plane field-aligned FM state [174], [175], [274]. In EuP-122 a similar field-induced spin reorientation from the out-of-plane FM into the in-plane field-aligned FM state was observed around $\mu_0 H \sim 0.6$ T [33]. These metamagnetic transitions have remarkable influence on the transient reflectivity. The dependence of $\Delta R/R$ on the in-plane magnetic field is shown in Fig. 8.5. In both samples the fast picosecond response shows virtually no dependence on the magnetic field. Contrary, the slow response shows a marked change at the metamagnetic transition [33], [174], [175], [269].

In undoped Eu-122 in the $\mathcal{P}^+$ polarization the slow response is suppressed above the metamagnetic transition (Fig. 8.5a) and is magnetic-field independent above 2 T. Concurrently, in the $\mathcal{P}^-$ polarization (Fig. 8.5b) the slow response is first enhanced at low magnetic field above the transition, resembling a rotation of the asymmetry by $\pi/2$, and then slightly suppressed upon increasing the field up to 7 T.

In EuP-122 the initially rather isotropic slow response (Fig. 8.5c,d) switches to an anisotropic one along the $\mathcal{P}^-$ polarization. Similar to Eu-122 the response is slightly suppressed at the highest field with a faster relaxation (see Fig. 8.6).

Here we should also note, that the realignment of the twin structure [174] was not observed in our experiment, since the anisotropy of fast component, that is associated with the structural twin domains [22], shows no dependence on the magnetic field in both samples (see Fig. 8.5) up to $\mu_0 H = 7$ T. Moreover, the realignment of the twin structure observed in [174] might be related to the Fe spin ordering as indicated by observation of a partial magnetic field detwinning in $Ba(Fe_{1-x}Co_x)_2As_2$.[277]

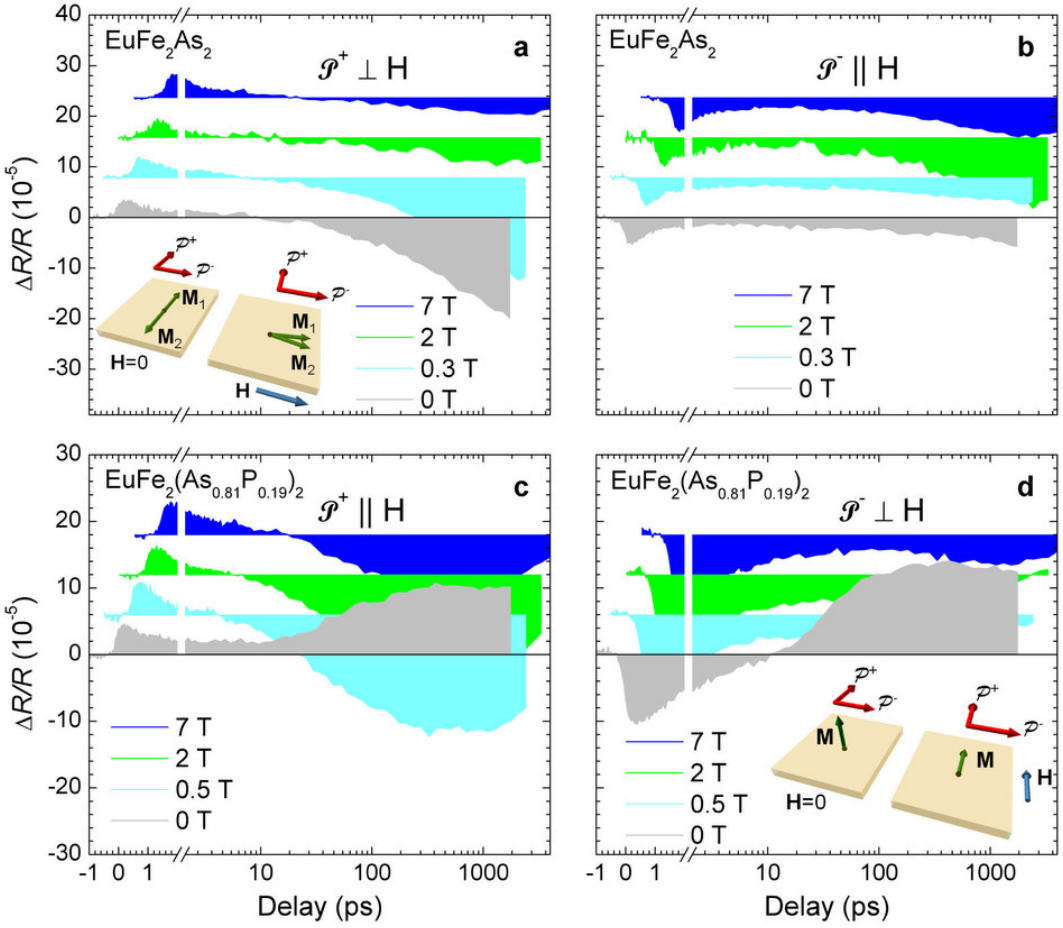


Figure 8.5: a), b) The reflectivity transients in $EuFe_2As_2$ with the magnetic field parallel to the $\mathcal{P}^-$ polarization. c), d) The reflectivity transients in $EuFe_2(As_{0.81}P_{0.19})_2$ with the magnetic field field parallel to the $\mathcal{P}^+$ polarization. All transients were measured at $T = 2$ K, $\mathcal{F} = 3$ μJ/cm^2 and 1.55-eV pump-photon energy. Insets show schematically magnetization reorientation in magnetic field.

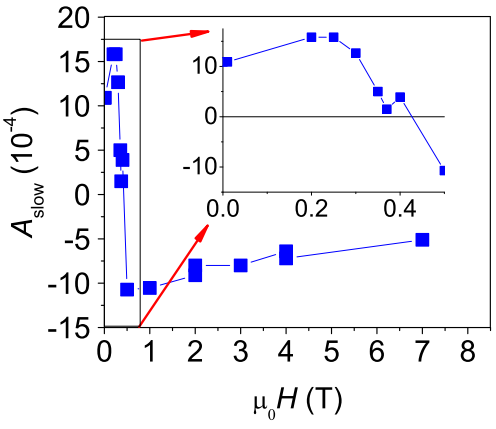


Figure 8.6: The amplitude of the slow component as the function of the applied magnetic field measured in EuP-122 at $T = 1.5$ K.

8.4 Coherent oscillations

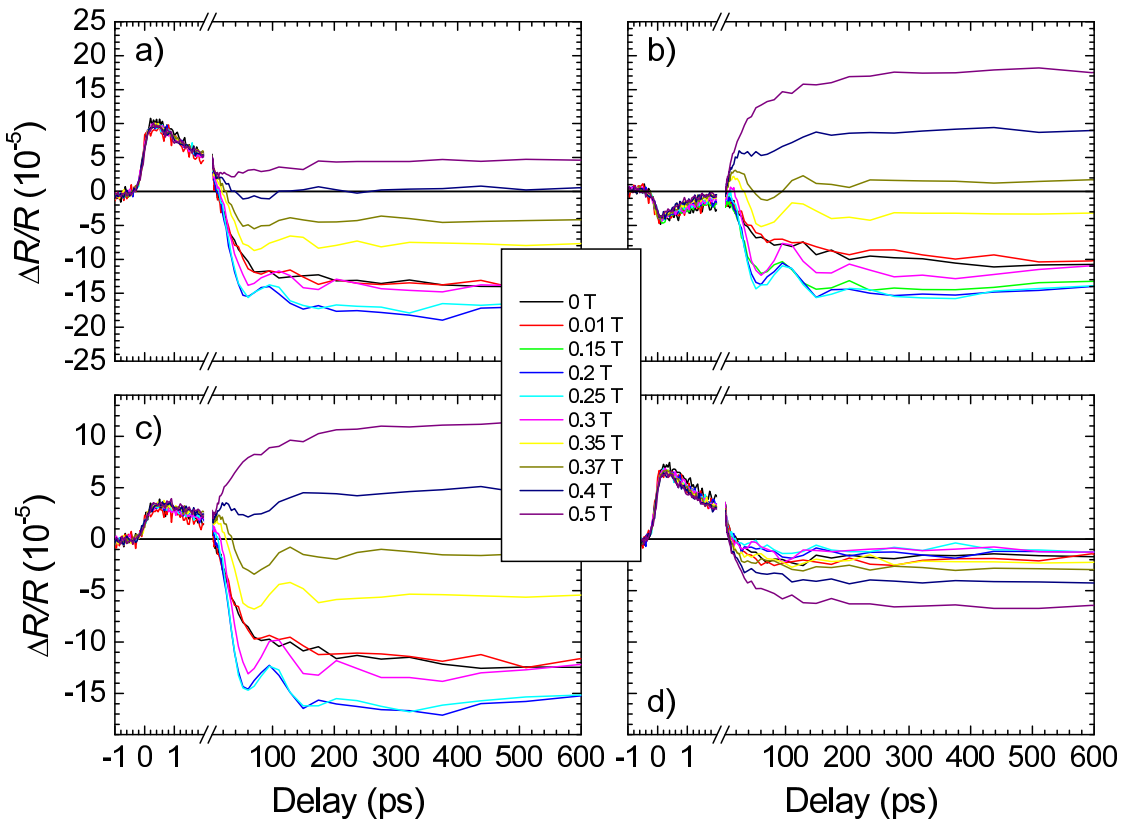


Figure 8.7: The reflectivity transients in $EuFe_2(As_{0.81}P_{0.19})_2$ for $\mathcal{P}^+$ and $\mathcal{P}^-$ probe polarizations a) and b), respectively, and the corresponding isotropic, c), and anisotropic, d), transient components in low magnetic fields at $T = 2$ K, $\mathcal{F} = 3$ μJ/cm^2 and 1.55-eV pump photon energy.

In EuP-122 at low magnetic fields below ∼0.5 T damped oscillations appear on top of the slow relaxation in $\Delta R/R$ (see Fig. 8.7a,b). These oscillations appear rather isotropic as indicated by plotting the sum, $1/2[(\Delta R/R)_{\mathcal{P}^+}+(\Delta R/R)_{\mathcal{P}^-}]$, and the difference, $1/2[(\Delta R/R)_{\mathcal{P}^+}-(\Delta R/R)_{\mathcal{P}^-}]$, in Fig. 8.7c,d, respectively. The amplitude of the oscillations, shown in Fig. 8.8d, is strongly peaked around ~ 0.25 T and vanishes at 0.5 T. The frequency of the oscillations, as determined by a damped oscillator fit, $\Delta R_{\rm osc}/R = A_{\rm osc}\exp(-t/\tau)\cos(\omega_0 t)$, shown in Fig. 8.8a, is H independent at low field and starts to decrease with the increasing field above $\mu_0 H \sim 0.3$ T. The damping, on the other hand, is magnetic-field independent at $\tau^{-1} \sim 10$ GHz.

Another oscillation with a higher frequency (~ 14.5 GHz at 0.3 T) is revealed by the transient magnetooptical Kerr effect (TR-MOKE) shown in Fig. 8.9. The oscillatory part of the TR-MOKE response is almost even with respect to the reversal of the magnetic field (see Fig. 8.10).

In a constant magnetic field the oscillations soften with increasing T and vanish at a significantly lower temperature (~ 12 K at $\mu_0 H = 0.3$ T) than the slow component (~ 20 K at $\mu_0 H = 0.3$ T) as shown in Fig. 8.11a. The comparison of this observation with the phase diagram [33] suggests the metamagnetic transition from AFM to FM ordering around 12 K, when the slow component changes the sign, and the transition to paramagnetic state, when the component is completely suppressed (above 20 K). In Section 8.7 we have mentioned

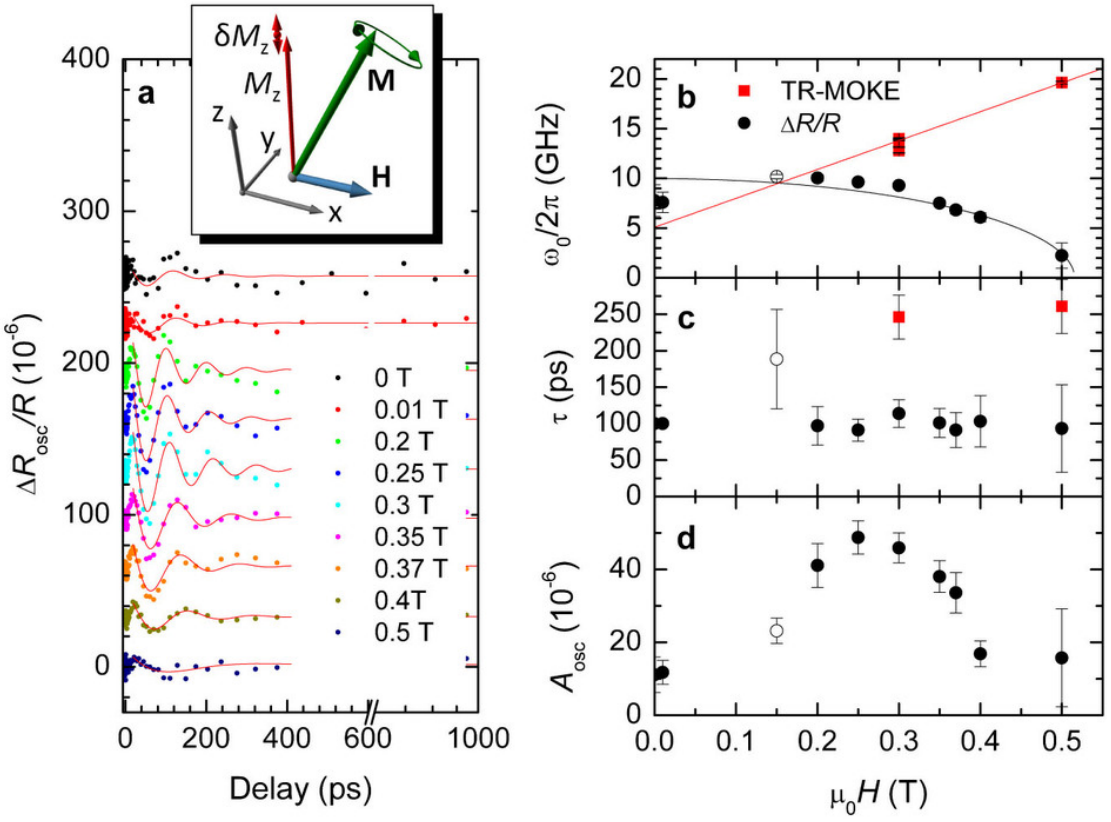


Figure 8.8: a) The oscillatory part of the isotropic $\Delta R/R$ component in $EuFe_2(As_{0.81}P_{0.19})_2$ at low magnetic fields, $\mathcal{F} = 3\ \mu J/cm^2$ and 1.5-eV pump photon energy. Thin lines represent the damped oscillator fits discussed in text. The frequency b), decay time c) and amplitude e) of the oscillations as functions of the magnetic field. The points (open symbols) at $B = 0.15$ T were obtained from the $\mathcal{P}^-$ polarization fit due to the lack of data at the $\mathcal{P}^+$ polarization. The red squares were obtained from the TR-MOKE fits. The lines in b) are uniaxial ferromagnet fits discussed in text. The inset to a) schematically shows magnetization precession in small magnetic fields with corresponding projections onto the z-axis.

that the sign of the slow component in $Eu(Fe,Co)_2As_2$ remains the same for all dopings, which suggests no transition to the FM ordering in Co-doped samples.

Softening of oscillations is observed also with increasing pump fluence (see Fig. 8.11b), where the oscillations disappear together with the saturation of the slow component above $\sim 50\ \mu J/cm^2$.

8.5 Polarization analysis of coherent oscillations

To understand the change of the anisotropy between weak and strong magnetic fields in EuP-122 let us look at the symmetric part of the in-plane dielectric tensor components ϵ_{ii}. Within the orthorhombic point symmetry ϵ can be expanded in terms of the magnetization to the lowest order as:

$$\epsilon_{ii} = \epsilon_{0,ii} + a_{iizz}M_z^2 + a_{iixx}M_x^2 + a_{iiyy}M_{iiyy}^2 \tag{8.1}$$

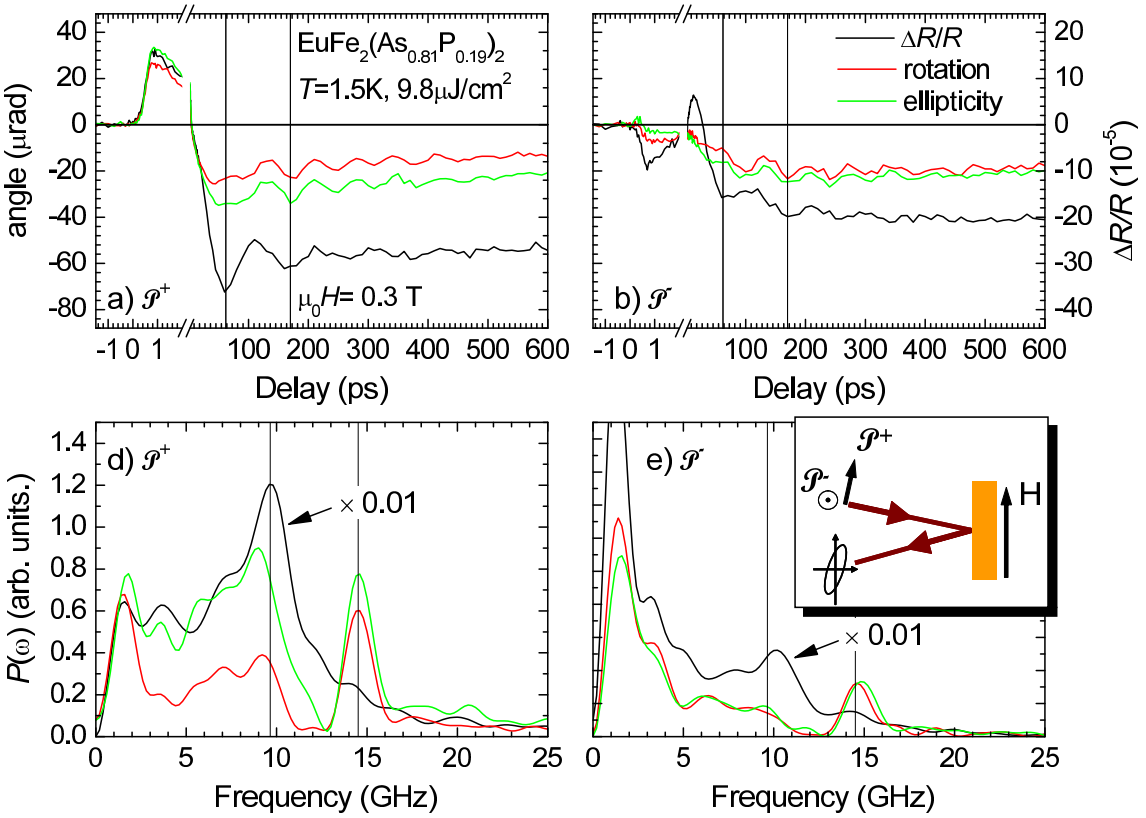


Figure 8.9: $\Delta R/R$, rotation and ellipticity in $\mu_0 H = 0.3$ T magnetic field for the $\mathcal{P}^+$ (a) and $\mathcal{P}^-$ polarization b). The corresponding Fourier-transform power spectra of traces in the top panels are shown in d) and f). The zero-frequency peak was suppressed before the Fourier transformation to reduce the finite time-window artefacts. The inset shows a schematic of the TR-MOKE measurement geometry.

with $i \in x, y$. Here M would correspond to the Eu^{2+} sublattice magnetization in the case of a canted AFM ordering, or the total Eu^{2+} magnetization in the case of FM ordering. In EuP-122 in low magnetic fields M is predominantly oriented along the c-axis [33], [278] leading to the nearly isotropic response, since $a_{xxzz} \sim a_{yyzz}$ due to the small orthorhombic lattice distortion. In the field-induced FM state and the zero-field AFM state of Eu-122 M lies in the ab-plane leading to an anisotropic response since it is quite unlikely that $a_{iiii} \sim a_{jjii}$, with $i \neq j$.

The light penetration depth at the probe-photon energy of $\hbar\omega_{\mathrm{pr}} = 1.55$ eV is ~ 27 nm [249], while the beam diameters are in a 100 μ m range. Irrespectively, of the excitation mechanism, which can be either non-thermal impulsive [279] inverse Cotton-Mouton effect or thermal displacive non-Raman [280] like, it can be assumed that the relevant wavevectors are $q \lesssim 1/30$ nm^{-1} and dominantly a uniform coherent magnetization precession is excited and detected.[1]

The low frequency mode observed in the transient reflectivity response softens with increasing temperature and vanishes in the field-induced in-plane FM state so it can definitely be assigned to a magnetic mode. The high-frequency mode has also a magnetic origin since it appears in the TR-MOKE configuration only.

Analyzing contributions of the magnetization displacements, δM_i, to the symmetric

[1] In the case of helical magnetic order with the propagation vector q_0, spin waves at $q = \pm m q_0$, $m \in \mathbb{Z}$ also need to be considered [281].

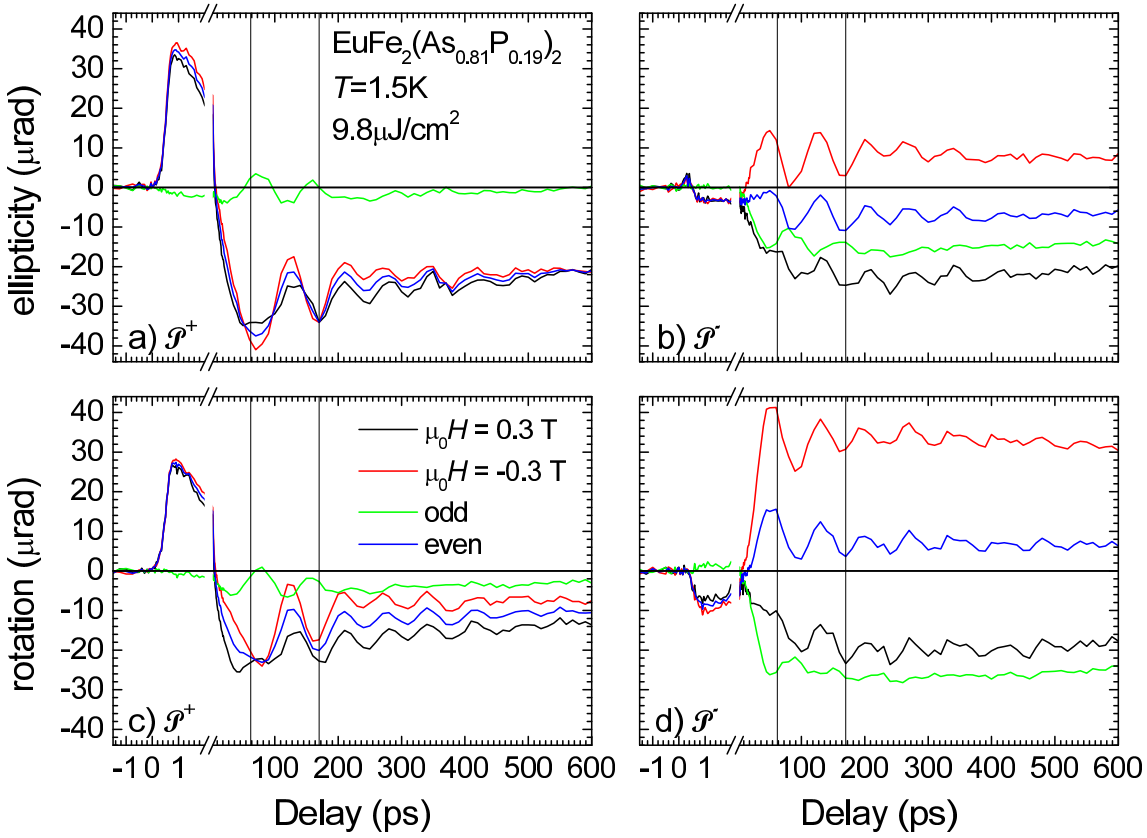


Figure 8.10: Ellipticity a), b) and rotation, c), d) upon reversal of the magnetic field for the $\mathcal{P}^+$, a), c), and $\mathcal{P}^-$ b), d), polarizations.

part of the optical response it follows from Eq. (8.1):

$$\delta\epsilon_{ii} = 2a_{iizz}M_z\delta M_z + 2a_{iixx}M_x\delta M_x + 2a_{iiyy}M_y\delta M_y. \tag{8.2}$$

The low-frequency mode is very strong in $\Delta R/R$ and rather isotropic in the ab-plane indicating that it is either associated with the out-of-plane terms (i) $2a_{iizz}M_z\delta M_z$ or (ii) both, M_x and M_y, are finite such as in the case of a helimagnetic ordering. In the latter case the local magnetization needs to be considered since the average of the terms $\langle M_i\delta M_i\rangle$, $i \in x, y$, over Eu^{2+} planes is finite despite $\langle M_i\rangle = 0$ (see Appendix). Concurrently, it is weak in the TR-MOKE configuration, which is sensitive to δM_z. Since $\delta M_z \neq 0$ for both (i) and (ii) (see Appendix information for case (ii)) this indicates that the measured volume is composed from the "up" and "down" magnetic domains magnetized along the c-axis. The sign of δM_z varies in different magnetic domains leading to a vanishing TR-MOKE response averaged over many magnetic domains, while the sign of $M_z\delta M_z$ does not depend on the domain orientation and averages to a finite value.

For the high-frequency mode observed in the TR-MOKE configuration, on the other hand, the averaged δM_z is finite while the averaged $M_z\delta M_z$ is rather small in comparison to the low frequency mode. This indicates that in addition to the c-axis magnetized domains in-plane magnetized regions exist with $M_z \sim 0$. The in-plane magnetization leads to an out-of-plane magnetization displacement with $\delta M_z \neq 0$ and $M_z\delta M_z \sim 0$, consistent with the observed magnetic field dependence of the mode frequency. The invariance of the oscillatory TR-MOKE response (see Fig. 8.10) with respect to the inversion of the magnetic field is also consistent with the in-plane magnetization orientation.

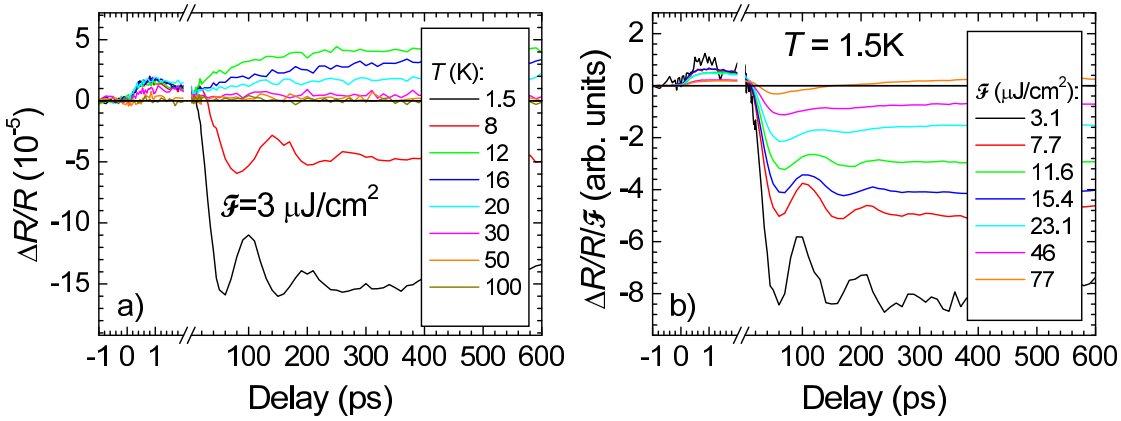


Figure 8.11: The isotropic component ($^1/_2[(\Delta R/R)_{\mathcal{P}^+} + (\Delta R/R)_{\mathcal{P}^-}]$) in $EuFe_2(As_{0.81}P_{0.19})_2$ at different T a), and $\mathcal{F}$ b), in $\mu_0 H = 0.3$ T and 1.55-eV pump photon energy. Note that the scans in b) are normalized by $\mathcal{F}$.

A fit of the frequency magnetic-field dependence (see Fig. 8.8b) using the standard uniaxial ferromagnet formula for a parallel magnetic field [282] ignoring demagnetization factors, $\omega = \gamma_{ab}(H_{ab} + H)$, yields $\mu_0 H_{ab} = 0.3$ T and $\gamma_{ab}/\mu_0 = 182$ GHz/T. The obtained gyromagnetic ratio $g_{ab} = 2.06$ is consistent with $^8S_{7/2}$ state of Eu^{2+} ions. The absence of demagnetization factors suggests that the response does not originate from the domain walls between the c-axis oriented domains but rather from planar shaped domains. Due to surface sensitivity (∼30 nm) of the optical probe these are very likely surface domains, however, the bulk nature of these domains can not be entirely excluded.

8.6 Magnetic order of Eu^{2+} spins

The observed behaviour is compatible with the simple ferromagnetic order (within the domains) proposed by Nandi *et al.* [33]. In the absence of the in-plane magnetic field the static magnetization in the c-axis domains is along the c-axis and $\delta M_z = 0$, consistent with the vanishing amplitude of the low frequency mode near the zero field. Upon application of the in-plane magnetic field the magnetization is tilted away from the c-axis (see inset to Fig. 8.8) leading to a finite δM_z and the observed decrease of the mode frequency [282]. The decrease of the transient-reflectivity amplitude, when approaching to the metamagnetic transition, can be associated with the vanishing M_z.

A fit of the frequency magnetic-field dependence using the standard uniaxial ferromagnet formula for the perpendicular magnetic field [282] ignoring demagnetization factors, $\omega = \gamma_c\sqrt{H_c^2 - H^2}$, results in $\mu_0 H_c = 0.52$ T and $\gamma_c/\mu_0 = 119$ GHz/T. The small value of γ_c leading to a small gyromagnetic ratio ($g_c = 1.35$) can be attributed to the ignored unknown demagnetization factors of the c-axis magnetized domains. Moreover, it suggests that the c-axis magnetized domains have a flat shape with the normal perpendicular to the c-axis.

On the other hand, the presence of two distinct modes and the magnetic field dependence of the mode frequencies (see Fig. 8.8b) resembles the standard uniaxial AFM cases with the magnetic field perpendicular to the easy/hard axis [282], [283] indicating a possible canted AFM [34] (CAFM) order. The polarization dependence of the modes is, however, not compatible with the CAFM picture since both, the quasi-AFM mode [284] and the quasi-FM mode, contribute to δM_z and should, contrary to the observations, contribute concurrently to the transient reflectivity and the TR-MOKE with identical relative

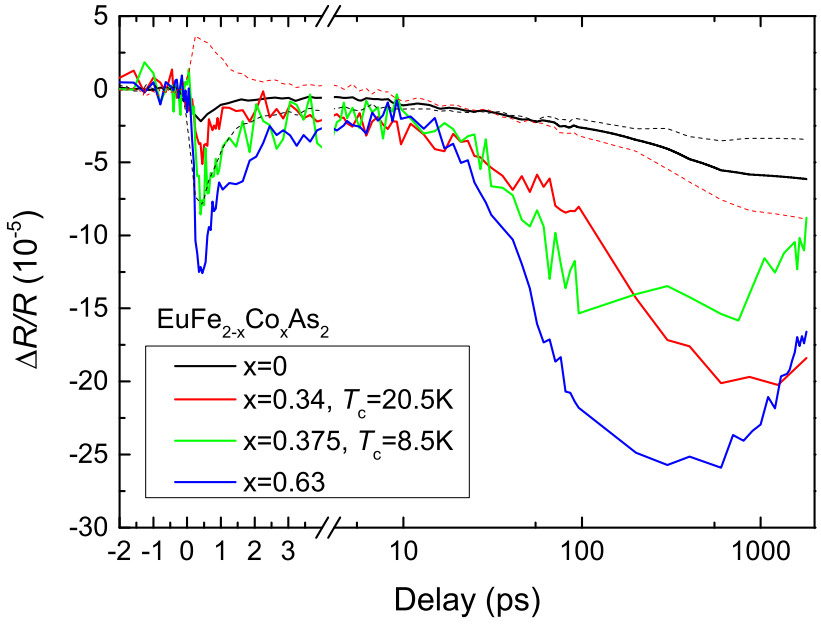


Figure 8.12: The doping dependence of the transient reflectivity response in $EuFe_{2-x}Co_xAs_2$ measured at 7 K with 7 μJ/cm^2 pump fluence. The transient reflectivity signal was isotropic with respect to the probe polarization for all $x > 0$ samples. The black line for $x = 0$ is obtained by averaging two dashed lines, which represent transient reflectivity, measured for $\mathcal{P}^+$ and $\mathcal{P}^-$ polarizations.

amplitudes.

In the case of the conical helimagnetic ordering [172], [278], [285] the in-plane isotropy naturally appears for certain modes (see Appendix). However, since, as in the case of the CAFM state, contributions of more than one magnetic mode to δM_z are expected, our data do not support the conical helimagnetic ordering.

8.7 Strength of the coupling between Eu and FeAs layers

As it was mentioned above, the strength of the coupling between Eu^{2+} f-spin Fe d-carriers plays a key role in understanding the mechanism of the coexistence of AFM and SC states in Eu-based iron pnictides. In the pump-probe experiments the photoexcited electron-hole pairs rather quickly relax by emitting optical phonons, magnons and creating lower energy electron-hole pairs, leading in general to non-equilibrium phonon (magnon) and quasiparticle distributions [183]. These distributions are non-thermal and can not be described by a single parameter such as temperature within a certain thermalization timescale. The thermalization timescale strongly depends on the electronic density of states structure near the Fermi energy and can extend to several tens of picoseconds when the quasiparticle excitation spectrum is fully gapped, as, for example, in superconductors [177].

In the case of iron-based pnictides in the SDW state the charge gap is only partial and the thermalization occurs on the picosecond timescale (see Chapter 4). One can therefore assume that the quasiparticle and lattice degrees of freedom are fully thermalized beyond ~ 10 ps when the slow component starts to emerge. This suggests that the energy transfer

a)

Co doping	τ_{rise} (ps)
$x = 0$	192 ± 16
$x = 0.34$	190 ± 13
$x = 0.37$	50 ± 7
$x = 0.63$	38 ± 5

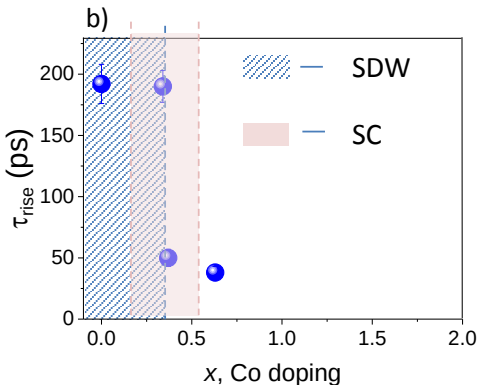


Figure 8.13: The doping dependence of the rise time of the slow component in $EuFe_{2-x}Co_xAs_2$.

from the excited quasiparticles in Fe *d*-bands to the Eu^{2+} magnons is rather inefficient. The Eu^{2+} magnons are excited indirectly *via* the spin-lattice coupling (see Fig. 8.14) only after the initial excitation energy was thermally distributed between the quasiparticles and phonons. The Eu^{2+} *f*-spins therefore appear only weakly coupled to the Fe *d*-derived-band quasiparticles.

The doping dependence of the low-temperature response from $Eu(Fe_{1-x}Co_x)_2As_2$ is shown in Fig. 8.12. The decrease of the rise time of Eu^{2+}component indicates that the energy transfer from the Fe *d*-band QP to the Eu^{2+} spins becomes more efficient when the amount of Co is increased. Moreover, a detailed analysis of the rise time as a function of doping (see Fig. 8.13) reveals a sharp drop at the doping where the SDW order is completely suppressed. Here we should also note, that in contrast to $EuFe_2(As,P)_2$, where the signal changes the sign with doping, in $Eu(Fe,Co)_2As_2$ the sign of the slow component remains the same in the whole range of doping.

The weak coupling enables a coexistence of SC and FM without the necessity of a magnetic order modulation on a lengthscale shorter than the SC coherence length. In this case a longer lengthscale FM domain structure can effectively minimize the internal magnetic field enabling coexistence of the singlet superconductivity and FM state [271].

8.8 Summary and conclusions

This chapter is dedicated to ultrafast magnetooptic studies on Eu^{2+} magnetization dynamics.

(i) The observed weak coupling between the FeAs-plane quasiparticles and Eu^{2+} spins indicates a weak magnetic-dipole dominated coupling between the SC and FM order parameters in Eu-122.

(ii) This indicates that the coexistence of the singlet superconductivity with ferromagnetism in $EuFe_2(As_{1-x}P_x)_2$ and $Eu(Fe_{1-x}Co_x)_2As_2$ is possible without the necessity of the magnetic structure modulation on the lengthscale shorter than the SC coherence-length. The presence of the FM domain structure on longer lengthscales, which is inferred from the coherent-spin-wave response, might additionally contribute to stability of the coexisting

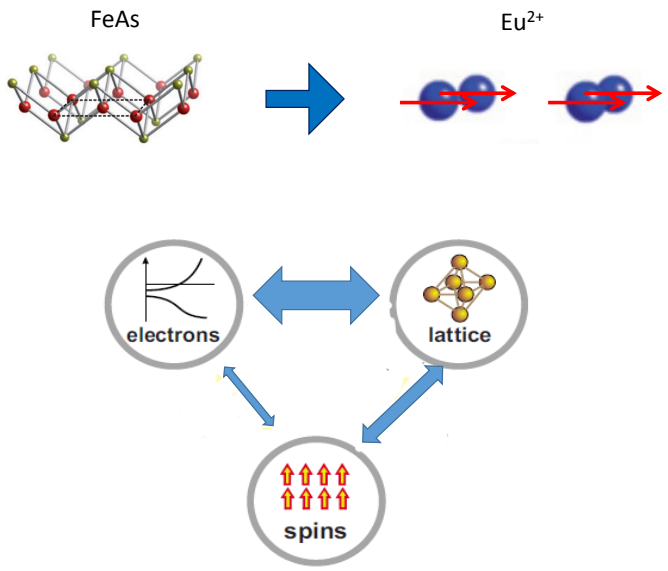


Figure 8.14: The photoexcitation of Eu^{2+}spins in iron-based pnictides is enabled through the indirect spin-lattice mechanism. The arrows in a bottom plane schematically illustrate the strength of coupling between subsystems.

state.

(iii) The coupling between FeAs and Eu planes abruptly increases, when the SDW order of Fe is suppressed.

(iv) In conclusion, our data points towards the simple FM Eu^{2+}-spin order in superconducting $EuFe_2(As,P)_2$ proposed by Nandi *et al.* [33].

Chapter 9

Conclusions

The present thesis is dedicated to the study of the ultrafast quasiparticle and collective dynamics in $A\mathrm{Fe_2As_2}$ iron pnictide high-temperature superconductors. The investigation of the dynamical processes related with the electron-phonon, electron-spin interactions and the structure of the quasiparticle density of states within the system allows deeper insight into the complex physics governing the emergence of a rich and sometimes contradictory phase diagram of the iron pnictides. Therefore, a systematic temperature, doping and anisotropy analysis of the transient reflectivity was performed in order to reveal the relaxation processes which take place in these materials after the photoexcitation.

Employing a broadband ultrafast transient optical spectroscopy we investigated quasiparticle relaxation in normal and SDW states of $\mathrm{BaFe_2As_2}$, $\mathrm{EuFe_2As_2}$ and $\mathrm{SrFe_2As_2}$ iron-based-pnictide parent compounds in a 1.6-2.6 eV spectral region. With decreasing temperature all samples start to show a twofold in-plane rotational symmetry already in the tetragonal phase, significantly above the SDW/structural transition temperature, suggesting the presence of nematic fluctuations. In the SDW state the reflectivity transients across the full spectral range can be described by just two distinct relaxation components. One is faster or similar to our temporal resolution of $\sim$ 200 fs is consistent with recent TR-ARPES [21] results and could be associated with relaxation at the Fermi surface. The second component is absent at high temperature and shows a critical-like slowing down near the SDW transition temperature. The slower component relaxes on the timescale of $0.6-1.5$ ps, with strong sensitivity to the magneto-structural transition, contrary to the TR-ARPES, slows down near the SDW transition. It can be quantitatively well described by a magnon-bottleneck model with zero temperature gap magnitudes $2\Delta(0)/T_{\mathrm{SDW}} \sim 10$, that are consistent with the steady state optical spectroscopy results. Alternative assignment to the relaxation of the SDW magneto-structural order-parameter amplitude mode is proposed and can not be excluded on the basis of the current data. Further TR-ARPES experiments and infrared all-optical broad-band experiments might be able to select among the two possibilities.

We have shown that the SDW state in the 122 iron pnictides can be destroyed nonthermally by an ultrafast optical laser pulses. The energy density required for the photodestruction of the order is temperature independent and one order of magnitude less than the energy density required for thermal destruction. In proximity to the transition the slowing down of the relaxation is observed. The analysis of the time and energy density required to destroy the SDW order suggests that the electronic mechanism dominates in the destruction process.

The recovery dynamics of non-thermally destroyed SDW state is studied by means of the ultrafast time-resolved optical three-pulse technique. The recovery of the SDW after the destruction evolves in two steps. First, electronic system recovers on a ps timescale,

after that the heat diffusion follows. At the first step the overlap of the relaxation rate and amplitude recovery suggests proportionality of the pump-probe response to the order parameter. Importantly we discovered the significant difference in the transient reflectivity relaxation time with the amplitude recovery time.

A systematic wide-fluence-range optical time-resolved pump-probe studies were conducted in optimally isovalently doped $BaFe_2(As_{0.7}P_{0.3})_2$. It is shown that the presence of nodes does not influence the relaxation dynamics in $BaFe_2(As_{0.7}P_{0.3})_2$. In the low excitation regime the transient reflectivity changes are dominated by the bottleneck relaxation processes. Temperature dependence of the amplitude can be well fitted by the bottleneck formula and the relaxation time behaviour also supports this scenario. The superconducting gap magnitude of $2\Delta(0)/k_BT_c = 4 \pm 1$ is consistent with the gap on the hole Fermi surface. The relaxation dynamics detected by means of 1.55-eV probe photons in Ba-122 can therefore be attributed to the hole Fermi surfaces as suggested previously by Torchinsky *et al.* [20]. In the strong excitation regime the pump-probe response is defined by the difference in the reflectivity of the normal and gapped state. The temperature dependence of the amplitude can be described well by the Mattis-Bardeen formula. The in-plane non-thermal optical-destruction volume energy densities are found to scale linearly with T_c^2 in a close correspondence to the trend previously reported for other layered superconductors.

We investigated the transient reflectivity relaxation dynamics in $EuFe_2(As,P)_2$ and $Eu(Fe,Co)_2As_2$ at different dopings in the temperature region of Eu^{2+} spin ordering. Two relaxation components with different dynamics were observed at low temperatures. The anisotropic subpicosecond relaxation corresponding to the SDW state appeared below $T_{SDW} = 189$ K consistently with previous results in related compounds. Another component with a long rise time on nanosecond timescale was observed below 19 K, which proves that this component corresponds to the dynamics of Eu^{2+} AFM order. The dynamics of this component suggests a weak coupling between quasiparticles in Fe-d derived bands and Eu^{2+}-f spins in SDW state, and stronger coupling, when the SDW order is suppressed by doping. The weak coupling in the optimally doped sample indicates that the coexistence of the singlet superconductivity with ferromagnetism in $EuFe_2(As_{1-x}P_x)_2$ and $Eu(Fe_{1-x}Co_x)_2As_2$ is possible without the necessity of the magnetic structure modulation on the lengthscale shorter than the SC coherence-length. In conclusion, our data imply the simple FM Eu^{2+}-spin order in superconducting $EuFe_2(As,P)_2$ proposed by Nandi *et al.* [33].

Appendix A

Appendix

Optical response in the conical helimagnetic state

Assuming that within a single plane Eu^{2+} spins are ordered ferromagnetically Eq. (8.1) can be applied to each plane separately. Neglecting for simplicity the crystallographic details and assuming a conical helimagnetic phase with $M = M_0[\cos(q_0 z)\sin(\theta), \sin(q_0 z)\sin(\theta), \cos(\theta)]$, where q_0 represents the helix propagation wavevector and θ the local magnetization angle relative to the c-axis, according to [286] we introduce a local coordinate system:

$$\hat{x}' = [\hat{x}\cos(q_0 z) + \hat{y}\sin(q_0 z)]\cos(\theta) - \hat{z}\sin(\theta),$$

$$\hat{z}' = [\hat{x}\cos(q_0 z) + \hat{y}\sin(q_0 z)]\sin(\theta) + \hat{z}\cos(\theta).$$

Here $\hat{}$ represents the Cartesian unit vectors. The modes of a spin-operator linearized Hamiltonian are then represented by[287]:

$$\begin{aligned} \delta M_{x'}(z) &\propto \sum_m s_{x'}(\mathbf{q} + mq_0\hat{z}) e^{i[(\mathbf{q}+mq_0\hat{z})^*\mathbf{r} - \omega(\mathbf{q})t]}, \\ \delta M_{y'}(z) &\propto \sum_m s_{y'}(\mathbf{q} + mq_0\hat{z}) e^{i[(\mathbf{q}+mq_0\hat{z})^*\mathbf{r} - \omega(\mathbf{q})t]}, \end{aligned} \tag{A.1}$$

where m are integers and $s_{i\prime}(\mathbf{q})$ and $\omega(\mathbf{q})$ depend on the particular choice of Hamiltonian.[286], [287] Here nonzero m terms need to be introduced because in the presence of an in-plane external magnetic field higher harmonics appear in the modulation.[287] An in-plane anisotropy also introduces higher harmonic terms. Transforming back to the crystal coordinate system and taking into account only the oscillating part by omitting the terms containing $\delta M_{z'}$ we obtain:

$$\begin{aligned} \delta M_x(z) \propto e^{-i\omega(\mathbf{q})t}\cos(\theta)[\cos(q_0\hat{z}) \sum_m s_{x'}(\mathbf{q} + mq_0\hat{z}) e^{i(\mathbf{q}+mq_0\hat{z})^*\mathbf{r}} - \\ - \sin(q_0\hat{z}) \sum_m s_{y'}(\mathbf{q} + mq_0\hat{z}) e^{i(\mathbf{q}+mq_0\hat{z})^*\mathbf{r}}], \end{aligned}$$

$$\begin{aligned} \delta M_y(z) \quad \propto \quad & e^{-i\omega(\mathbf{q})t}\cos(\theta)[\sin(q_0\hat{z}) \sum_m s_{x'}(\mathbf{q} + mq_0\hat{z}) e^{i(\mathbf{q}+mq_0\hat{z})^*\mathbf{r}} + \\ & + \cos(q_0\hat{z}) \sum_m s_{y'}(\mathbf{q} + mq_0\hat{z}) e^{i(\mathbf{q}+mq_0\hat{z})^*\mathbf{r}}], \end{aligned}$$

$$\delta M_z(z) \propto e^{-i\omega(\mathbf{q})t}\sin(\theta)\sum_m s_{x'}(\mathbf{q}+mq_0\hat{z})e^{i(\mathbf{q}+mq_0\hat{z})^*\mathbf{r}}. \quad \text{(A.2)}$$

$\langle M_i\delta M_i\rangle$ therefore contains terms:

$$\langle M_x\delta M_x\rangle \propto \cos^2(\theta)\sum_m s_{x'}(q_z\hat{z}+mq_0\hat{z})\left\langle\cos^2(q_0z)e^{i(q_z+mq_0)z}\right\rangle,$$
$$\langle M_y\delta M_y\rangle \propto \cos^2(\theta)\sum_m s_{x'}(q_z\hat{z}+mq_0\hat{z})\left\langle\sin^2(q_0z)e^{i(q_z+mq_0)z}\right\rangle,$$
$$\langle M_z\delta M_z\rangle \propto \cos(\theta)\sin(\theta)\sum_m s_{x'}(q_z\hat{z}+mq_0\hat{z})\left\langle e^{i(q_z+mq_0)z}\right\rangle. \quad \text{(A.3)}$$

Here $\langle\rangle$ represents the average over Eu^{2+} planes. $\langle M_x\delta M_x\rangle$ and $\langle M_y\delta M_y\rangle$ are nonzero only when (i) $q_z+mq_0=\pm 2q_0$ or (ii) $q_z+mq_0=0$. In case (i) $\langle M_x\delta M_x\rangle = -\langle M_y\delta M_y\rangle$ leading to an anisotropic in-plane response while in case (ii) $\langle M_x\delta M_x\rangle = \langle M_y\delta M_y\rangle$ leading to the isotropic response. The frequencies present in the in-plane isotropic response are therefore $\omega(0+mq_0)$.

Due to terms $e^{i(q_z+mq_0)z}$ the term $\langle M_z\delta M_z\rangle$ also leads to isotropic response at frequencies $\omega(0+mq_0)$.

The TR-MOKE response, on the other hand, is determined by $\delta\epsilon_{xy}\propto i\,(\delta M_z)$ and contains terms $e^{i(q_z+mq_0)z}$ that are nonzero for $q_z+mq_0=0$, which is identical to (ii). In a single magnetic domain sample the in-plane isotropic modes should therefore appear also in the c-axis TR-MOKE response.

Optical response in the canted antiferromagnetic state

For convenience we switch to the standard definition of the order parameters in weak ferromagnets.[282] Assuming that the magnetization at $H=0$ is oriented along the c axis, the total magnetization displacement, δM, of the quasi-FM mode would lie on an ellipse perpendicular to M with the AFM vector displacements, δL, linear along M, [284] while for the quasi-AFM mode δM would be linear along M and δL on an ellipse lying in the xy plane. Looking at the symmetric part of the dielectric tensor for the orthorhombic case following Iida *et al.* [4] and assuming $L||a$ and $H||b$ it follows:

$$\epsilon_{ii} = \epsilon_{0,ii} + a_{iizz}M_z^2 + a_{iiyy}M_y^2 + b_{iixx}L_x^2 + c_{iizx}M_zL_x. \quad \text{(A.4)}$$

Here the terms $c_{iizx}M_zL_x$ are due to the Dzyaloshinskii-Moriya interaction and are incompatible with our samples' crystallographic structure ($Fmmm$).[33] The modulation of the dielectric tensor obtained from A.4 to the linear order in displacements is given by:

$$\delta\epsilon_{ii} = 2a_{iizz}M_z\delta M_z + 2a_{iiyy}M_y\delta M_y + +2b_{iixx}L_x\delta L_x + c_{iizx}(L_x\delta M_z + M_z\delta L_x). \quad \text{(A.5)}$$

For both magnetic modes the nearly-isotropic response can come from the term $2a_{iizz}M_z\delta M_z$ only since $a_{xxzz}\sim a_{yyzz}$ due to the small orthorhombicity. The nearly isotropic in-plane response can therefore only be associated with δM_z. Since both modes contribute to δM_z at a finite in-plane magnetic field, when M is tilted away from the c-axis along the magnetic field, both should occur concurrently in the transient reflectivity response.

References

[1] J. Bednorz and K. Muller, "Possible high T_c superconductivity in the Ba-La-Cu-O system," *Zeitschrift fur Phys, B Condens. Matter*, vol. 64, pp. 189–193, 1986, ISSN: 0722-3277. DOI: 10.1007/BF01303701.

[2] P. W. Anderson, "Twenty-five years of high-temperature superconductivity - A personal review," *J. Phys. Conf. Ser.*, vol. 449, p. 012 001, 2013, ISSN: 1742-6596. DOI: 10.1088/1742-6596/449/1/012001. [Online]. Available: http://stacks.iop.org/1742-6596/449/i=1/a=012001?key=crossref.19ee78e29509b9bff9aa6f9886ac5451.

[3] H. Hosono and K. Kuroki, "Iron-Based Superconductors: current status of materials and pairing mechanism," *Phys. C Supercond. its Appl.*, 2015, ISSN: 09214534. DOI: 10.1016/j.physc.2015.02.020. [Online]. Available: http://linkinghub.elsevier.com/retrieve/pii/S0921453415000477.

[4] J. R. Gavaler, "Superconductivity in Nb-Ge films above 22 K," *Appl. Phys. Lett.*, vol. 23, no. 8, pp. 480–482, 1973, ISSN: 00036951. DOI: 10.1063/1.1654966.

[5] K. Tanigaki, T. W. Ebbesen, S. Saito, J. Mizuki, J. S. Tsai, Y. Kubo, and S. Kuroshima, "Superconductivity at 33 K in $Cs_xRb_yC_{60}$," *Nature*, vol. 352, no. 6332, pp. 222–223, 1991, ISSN: 0028-0836. DOI: 10.1038/352222a0.

[6] P. Canfield, P. Gammell, and D. Bishop, "New magnetic superconductors: A toy box fo solid-state physicists," *Phys. Today*, 1988. DOI: S-0031-9228-9810-030-3.

[7] F.-C. Hsu, J.-Y. Luo, K.-W. Yeh, T.-K. Chen, T.-W. Huang, P. M. Wu, Y.-C. Lee, Y.-L. Huang, Y.-Y. Chu, D.-C. Yan, and M.-K. Wu, "Superconductivity in the PbO-type structure α-FeSe.," *Proc. Natl. Acad. Sci. U. S. A.*, vol. 105, no. 38, pp. 14 262–14 264, 2008, ISSN: 0027-8424. DOI: 10.1073/pnas.0807325105. arXiv: 0807.2369.

[8] J. L. Sarrao, L. A. Morales, J. D. Thompson, B. L. Scott, G. R. Stewart, F. Wastin, J. Rebizant, P. Boulet, E. Colineau, and G. H. Lander, "Plutonium-based superconductivity with a transition temperature above 18 K," *Nature*, vol. 420, no. 6913, pp. 297–299, 2002, ISSN: 0028-0836. DOI: 10.1038/nature01212.

[9] Y. Kamihara, H. Hiramatsu, M. Hirano, R. Kawamura, H. Yanagi, T. Kamiya, and H. Hosono, "Iron-based layered superconductor: LaOFeP," *JACS Commun.*, pp. 3296–3297, 2006. arXiv: arXiv:0803.3286v1.

[10] K.-J. Zhou, Y.-B. Huang, C. Monney, X. Dai, V. N. Strocov, N.-L. Wang, Z.-G. Chen, C. Zhang, P. Dai, L. Patthey, J. van den Brink, H. Ding, and T. Schmitt, "Persistent high-energy spin excitations in iron-pnictide superconductors," *Nat. Commun.*, vol. 4, p. 1470, 2013, ISSN: 2041-1723. DOI: 10.1038/ncomms2428. arXiv: 1301.1289. [Online]. Available: http://www.ncbi.nlm.nih.gov/pubmed/23403571.

[11] E. C. Blomberg, M. A. Tanatar, R. M. Fernandes, I. I. Mazin, B. Shen, H.-H. Wen, M. D. Johannes, J. Schmalian, and R. Prozorov, "Sign-reversal of the in-plane resistivity anisotropy in hole-doped iron pnictides.," *Nat. Commun.*, vol. 4, no. May, p. 1914, 2013, ISSN: 2041-1723. DOI: 10.1038/ncomms2933. arXiv: 1202.4430. [Online]. Available: http://www.ncbi.nlm.nih.gov/pubmed/23715273.

[12] P. J. W. Moll, L. Balicas, V. Geshkenbein, G. Blatter, J. Karpinski, N. D. Zhigadlo, and B. Batlogg, "Transition from slow Abrikosov to fast moving Josephson vortices in iron pnictide superconductors.," *Nat. Mater.*, vol. 12, no. 2, pp. 134–8, 2013, ISSN: 1476-1122. DOI: 10.1038/nmat3489. [Online]. Available: http://www.ncbi.nlm.nih.gov/pubmed/23178267.

[13] S. Lee, C. Tarantini, P. Gao, J. Jiang, J. D. Weiss, F. Kametani, C. M. Folkman, Y. Zhang, X. Q. Pan, E. E. Hellstrom, D. C. Larbalestier, and C. B. Eom, "Artificially engineered superlattices of pnictide superconductors.," *Nat. Mater.*, vol. 12, no. 5, pp. 392–6, 2013, ISSN: 1476-1122. DOI: 10.1038/nmat3575. [Online]. Available: http://www.ncbi.nlm.nih.gov/pubmed/23455850.

[14] M. Yi, Y. Zhang, Z.-K. Liu, X. Ding, J.-H. Chu, A. F. Kemper, N. Plonka, B. Moritz, M. Hashimoto, S.-K. Mo, Z. Hussain, T. P. Devereaux, I. R. Fisher, H. H. Wen, Z.-X. Shen, and D. H. Lu, "Dynamic competition between spin-density wave order and superconductivity in underdoped $Ba_{1-x}K_xFe_2As_2$," *Nat. Commun.*, vol. 5, p. 3711, 2014, ISSN: 2041-1723. DOI: 10.1038/ncomms4711. [Online]. Available: http://www.ncbi.nlm.nih.gov/pubmed/24762657.

[15] A. Patz, T. Li, S. Ran, R. M. Fernandes, J. Schmalian, S. L. Bud'ko, P. C. Canfield, I. E. Perakis, and J. Wang, "Ultrafast observation of critical nematic fluctuations and giant magnetoelastic coupling in iron pnictides.," *Nat. Commun.*, vol. 5, p. 3229, 2014, ISSN: 2041-1723. DOI: 10.1038/ncomms4229. arXiv: arXiv:1402.4890v1. [Online]. Available: http://www.ncbi.nlm.nih.gov/pubmed/24499997.

[16] R. M. Fernandes, A. V. Chubukov, and J. Schmalian, "What drives nematic order in iron-based superconductors?" *Nat. Phys.*, vol. 10, no. 2, pp. 97–104, Jan. 2014, ISSN: 1745-2473. DOI: 10.1038/nphys2877. [Online]. Available: http://www.nature.com/doifinder/10.1038/nphys2877.

[17] Z. Ren, Q. Tao, S. Jiang, C. Feng, C. Wang, J. Dai, G. Cao, and Z. Xu, "Superconductivity induced by phosphorus doping and its coexistence with ferromagnetism in $EuFe_2(As_{0.7}P_{0.3})_2$," *Phys. Rev. Lett.*, vol. 102, no. April, pp. 5–8, 2009, ISSN: 00319007. DOI: 10.1103/PhysRevLett.102.137002. arXiv: 0811.2390.

[18] Y. Kamihara, T. Watanabe, M. Hirano, and H. Hosono, "Iron-based layered superconductor $La(O_{1-x}F_x)FeAs$ ($x = 0.05$-0.12) with $T_c = 26$ K," *J. Am. Chem. Soc.*, vol. 130, no. 11, pp. 3296–7, Mar. 2008, ISSN: 1520-5126. DOI: 10.1021/ja800073m. [Online]. Available: http://www.ncbi.nlm.nih.gov/pubmed/18293989.

[19] J. Demsar, K. Biljakovic, and D. Mihailovic, "Single particle and collective excitations in the one-dimensional charge density wave solid $K_{0.3}MoO_3$ probed in real time by femtosecond spectroscopy," *Phys. Rev. Lett.*, p. 5, 1999, ISSN: 0031-9007. DOI: 10.1103/PhysRevLett.83.800. arXiv: 9906316 [cond-mat]. [Online]. Available: http://arxiv.org/abs/cond-mat/9906316.

[20] D. H. Torchinsky, J. W. McIver, D. Hsieh, G. F. Chen, J. L. Luo, N. L. Wang, and N. Gedik, "Nonequilibrium quasiparticle relaxation dynamics in single crystals of hole and electron doped $BaFe_2As_2$," *Phys. Rev. B*, vol. 104518, pp. 1–11, 2011. DOI: 10.1103/PhysRevB.84.104518. arXiv: 1108.1411. [Online]. Available: http://arxiv.org/abs/1108.1411.

[21] L. Rettig, R. Cortes, S. Thirupathaiah, P. Gegenwart, H. S. Jeevan, M. Wolf, J. Fink, and U. Bovensiepen, "Ultrafast momentum-dependent response of electrons in antiferromagnetic $EuFe_2As_2$ driven by optical excitation," *Phys. Rev. Lett.*, vol. 108, p. 097 002, 9 Feb. 2012. DOI: 10.1103/PhysRevLett.108.097002. [Online]. Available: http://link.aps.org/doi/10.1103/PhysRevLett.108.097002.

[22] L. Stojchevska, T. Mertelj, J. H. Chu, I. R. Fisher, and D. Mihailovic, "Doping dependence of femtosecond quasiparticle relaxation dynamics in $Ba(Fe,Co)_2As_2$ single crystals: Evidence for normal-state nematic fluctuations," *Phys. Rev. B - Condens. Matter Mater. Phys.*, vol. 86, pp. 1–12, 2012, ISSN: 10980121. DOI: 10.1103/PhysRevB.86.024519. eprint: 1107.5934.

[23] K. W. Kim, A. Pashkin, H. Schafer, M. Beyer, M. Porer, T. Wolf, C. Bernhard, J. Demsar, R. Huber, and A. Leitenstorfer, "Ultrafast transient generation of spin-density-wave order in the normal state of $BaFe_2As_2$ driven by coherent lattice vibrations," *Nat. Mater.*, vol. 11, no. 6, pp. 497–501, 2012, ISSN: 1476-1122. DOI: 10.1038/nmat3294. [Online]. Available: http://dx.doi.org/10.1038/nmat3294.

[24] F. Ning, K. Ahilan, T. Imai, A. S. Sefat, R. Jin, M. A. McGuire, B. C. Sales, and D. Mandrus, "Spin susceptibility, phase diagram, and quantum criticality in the eelctron-doped high T_c superconductor $Ba(Fe_{1-x}Co_x)_2As_2$," *J. Phys. Soc. Japan*, vol. 78, no. 1, pp. 4–7, 2009, ISSN: 00319015. DOI: 10.1143/JPSJ.78.013711. arXiv: 0811.1617.

[25] H. Fukazawa, N. Takeshita, T. Yamazaki, K. Kondo, K. Hirayama, Y. Kohori, K. Miyazawa, H. Kito, H. Eisaki, and A. Iyo, "Suppression of magnetic order by pressure in $BaFe_2As_2$," *J. Phys. Soc. Japan*, vol. 77, no. 10, pp. 1–2, 2008, ISSN: 00319015. DOI: 10.1143/JPSJ.77.105004. arXiv: 0808.0718.

[26] A. Dusza, A. Lucarelli, F. Pfuner, J.-H. Chu, I. R. Fisher, and L. Degiorgi, "Anisotropic charge dynamics in detwinned $Ba(Fe_{1-x}Co_x)_2As_2$," *EPL (Europhysics Lett.*, vol. 93, no. 3, p. 37 002, 2011, ISSN: 0295-5075. DOI: 10.1209/0295-5075/93/37002. arXiv: arXiv:1007.2543v1. [Online]. Available: http://stacks.iop.org/0295-5075/93/i=3/a=37002?key=crossref.028fd264670dcf1c32e38473a7e0b5b7.

[27] C. Mirri, A. Dusza, S. Bastelberger, J.-H. Chu, H.-H. Kuo, I. R. Fisher, and L. Degiorgi, "Nematic-driven anisotropic electronic properties of underdoped detwinned $Ba(Fe_{1-x}Co_x)_2As_2$ revealed by optical spectroscopy," *Phys. Rev. B*, vol. 90, no. 15, pp. 1–7, 2014, ISSN: 1098-0121. DOI: 10.1103/PhysRevB.90.155125. [Online]. Available: http://link.aps.org/doi/10.1103/PhysRevB.90.155125.

[28] L. Stojchevska, P. Kusar, T. Mertelj, V. V. Kabanov, X. Lin, G. H. Cao, Z. A. Xu, and D. Mihailovic, "Electron-phonon coupling and the charge gap of spin-density wave iron-pnictide materials from quasiparticle relaxation dynamics," *Phys. Rev. B - Condens. Matter Mater. Phys.*, vol. 82, pp. 1–4, 2010, ISSN: 10980121. DOI: 10.1103/PhysRevB.82.012505.

[29] P. Kusar, V. V. Kabanov, J. Demsar, T. Mertelj, S. Sugai, and D. Mihailovic, "Controlled vaporization of the superconducting condensate in cuprate superconductors by femtosecond photoexcitation," *Phys. Rev. Lett.*, vol. 101, no. November, pp. 1–4, 2008, ISSN: 00319007. DOI: 10.1103/PhysRevLett.101.227001. arXiv: 0805.0536.

[30] R. Yusupov, T. Mertelj, V. V. Kabanov, S. Brazovskii, P. Kusar, J.-H. Chu, I. R. Fisher, and D. Mihailovic, "Coherent dynamics of macroscopic electronic order through a symmetry-breaking transition," *Nat. Phys.*, vol. 6, no. 9, pp. 681–684, 2010, ISSN: 1745-2473. DOI: 10.1038/nphys1738. arXiv: 1006.1815. [Online]. Available: http://arxiv.org/abs/1006.1815.

[31] G. Coslovich, C. Giannetti, F. Cilento, S. Dal Conte, T. Abebaw, D. Bossini, G. Ferrini, H. Eisaki, M. Greven, A. Damascelli, and F. Parmigiani, "Competition between the pseudogap and superconducting states of $Bi_2Sr_2Ca_{0.92}Y_{0.08}Cu_2O_{8+d}$ single crystals revealed by ultrafast broadband optical reflectivity," *Phys. Rev. Lett.*, vol. 110, no. March, pp. 1–5, 2013, ISSN: 00319007. DOI: 10.1103/PhysRevLett.110.107003.

[32] Z. R. Ye, Y. Zhang, F. Chen, M. Xu, Q. Q. Ge, J. Jiang, B. P. Xie, and D. L. Feng, "Doping dependence of the electronic structure in phosphorus-doped ferropnictide superconductor $BaFe_2(As_{1-x}P_x)_2$ studied by angle-resolved photoemission spectroscopy," *Phys. Rev. B - Condens. Matter Mater. Phys.*, vol. 86, no. 3, pp. 1–8, 2012, ISSN: 10980121. DOI: 10.1103/PhysRevB.86.035136. arXiv: 1105.5242.

[33] S. Nandi, W. T. Jin, Y. Xiao, Y. Su, S. Price, D. K. Shukla, J. Strempfer, H. S. Jeevan, P. Gegenwart, and T. Bruckel, "Coexistence of superconductivity and ferromagnetism in P-doped $EuFe_2As_2$," *Phys. Rev. B - Condens. Matter Mater. Phys.*, vol. 89, pp. 1–7, 2014, ISSN: 10980121. DOI: 10.1103/PhysRevB.89.014512. arXiv: 1407.3711.

[34] S. Zapf, D. Wu, L. Bogani, H. S. Jeevan, P. Gegenwart, and M. Dressel, "Varying Eu^{2+} magnetic order by chemical pressure in $EuFe_2(As_{1-x}P_x)_2$," *Phys. Rev. B - Condens. Matter Mater. Phys.*, vol. 84, pp. 2–5, 2011, ISSN: 10980121. DOI: 10.1103/PhysRevB.84.140503.

[35] T. Stürzer, G. Derondeau, and D. Johrendt, "Role of different negatively charged layers in $Ca_{10}(FeAs)_{10}(Pt_4As_8)$ and superconductivity at 30 K in electron-doped $(Ca_{0.8}La_{0.2})_{10}(FeAs)_{10}(Pt_3As_8)$," *Phys. Rev. B - Condens. Matter Mater. Phys.*, vol. 86, pp. 4–7, 2012, ISSN: 10980121. DOI: 10.1103/PhysRevB.86.060516.

[36] C. W. Chu, "High-temperature superconductivity: Alive and kicking," *Nat. Phys.*, vol. 5, no. 11, pp. 787–789, Nov. 2009, ISSN: 1745-2473. DOI: 10.1038/nphys1449. [Online]. Available: http://www.nature.com/doifinder/10.1038/nphys1449.

[37] D. J. Singh, "Electronic structure and doping in $BaFe_2As_2$ and LiFeAs: Density functional calculations," *Phys. Rev. B*, vol. 78, no. 9, p. 094 511, Sep. 2008, ISSN: 1098-0121. DOI: 10.1103/PhysRevB.78.094511. [Online]. Available: http://link.aps.org/doi/10.1103/PhysRevB.78.094511.

[38] M. Rotter, M. Pangerl, M. Tegel, and D. Johrendt, "Superconductivity and crystal structures of $(Ba_{1-x}K_x)Fe_2As_2$ (x = 0-1)," *Angew. Chem. Int. Ed. Engl.*, vol. 47, no. 41, pp. 7949–7952, Jan. 2008, ISSN: 1521-3773. DOI: 10.1002/anie.200803641. [Online]. Available: http://www.ncbi.nlm.nih.gov/pubmed/18780403.

[39] S. Kasahara, H. J. Shi, K. Hashimoto, S. Tonegawa, Y. Mizukami, T. Shibauchi, K. Sugimoto, T. Fukuda, T. Terashima, A. H. Nevidomskyy, and Y. Matsuda, "Electronic nematicity above the structural and superconducting transition in $BaFe_2(As_{1-x}P_x)_2$," *Nature*, vol. 486, no. 7403, pp. 382–385, 2012, ISSN: 0028-0836. DOI: 10.1038/nature11178. arXiv: 1207.1045. [Online]. Available: http://dx.doi.org/10.1038/nature11178.

[40] N. Ni, M. E. Tillman, J. .-.-Q. Yan, A. Kracher, S. T. Hannahs, S. L. Bud'ko, and P. C. Canfield, "Effects of Co substitution on thermodynamic and transport properties and anisotropic H_{c2} in $Ba(Fe_{1-x}Co_x)_2As_2$ single crystals," *Phys. Rev. B*, pp. 1–9, 2008, ISSN: 1098-0121. DOI: 10.1103/PhysRevB.78.214515. arXiv: 0811.1767. [Online]. Available: http://arxiv.org/abs/0811.1767.

[41] D. K. Pratt, W. Tian, A. Kreyssig, J. L. Zarestky, S. Nandi, N. Ni, S. L. Bud'Ko, P. C. Canfield, A. I. Goldman, and R. J. McQueeney, "Coexistence of competing antiferromagnetic and superconducting phases in the underdoped $Ba(Fe_{0.953}Co_{0.047})_2As_2$ compound using X-ray and neutron scattering techniques," *Phys. Rev. Lett.*, vol. 103, no. August, pp. 1–4, 2009, ISSN: 00319007. DOI: 10.1103/PhysRevLett.103.087001.

[42] T. Chuang, M. P. Allan, J. Lee, Y. Xie, N. Ni, S. L. Bud'ko, G. S. Boebinger, P. C. Canfield, and J. C. Davis, "Nematic electronic structure in the parent state of the iron-based superconductor $Ca(Fe_{1-x}Co_x)_2As_2$.," *Science*, vol. 327, no. January, pp. 181–184, 2010, ISSN: 0036-8075. DOI: 10.1126/science.1181083. arXiv: 1005.1761.

[43] J. J. Ying, X. F. Wang, T. Wu, Z. J. Xiang, R. H. Liu, Y. J. Yan, A. F. Wang, M. Zhang, G. J. Ye, P. Cheng, J. P. Hu, and X. H. Chen, "Measurements of the anisotropic in-plane resistivity of underdoped feas-based pnictide superconductors," *Phys. Rev. Lett.*, vol. 107, p. 067 001, 6 Aug. 2011. DOI: 10.1103/PhysRevLett.107.067001. [Online]. Available: http://link.aps.org/doi/10.1103/PhysRevLett.107.067001.

[44] S. Kasahara, T. Shibauchi, K. Hashimoto, K. Ikada, S. Tonegawa, R. Okazaki, H. Shishido, H. Ikeda, H. Takeya, K. Hirata, T. Terashima, and Y. Matsuda, "Evolution from non-Fermi- to Fermi-liquid transport via isovalent doping in $BaFe_2(As_{1-x}P_x)_2$ superconductors," *Phys. Rev. B - Condens. Matter Mater. Phys.*, vol. 81, pp. 1–5, 2010, ISSN: 10980121. DOI: 10.1103/PhysRevB.81.184519. arXiv: 0905.4427.

[45] M. A. McGuire, A. D. Christianson, A. S. Sefat, B. C. Sales, M. D. Lumsden, R. Jin, E. A. Payzant, D. Mandrus, Y. Luan, V. Keppens, V. Varadarajan, J. W. Brill, R. P. Hermann, M. T. Sougrati, F. Grandjean, and G. J. Long, "Phase transitions in LaFeAsO: structural, magnetic, elastic, and transport properties, heat capacity and Mossbauer spectra," *Phys. Rev. B*, pp. 1–10, 2008, ISSN: 1098-0121. DOI: 10.1103/PhysRevB.78.094517. arXiv: 0806.3878. [Online]. Available: http://arxiv.org/abs/0806.3878.

[46] C. Fang, H. Yao, W. F. Tsai, J. Hu, and S. A. Kivelson, "Theory of electron nematic order in LaFeAsO," *Phys. Rev. B - Condens. Matter Mater. Phys.*, vol. 77, pp. 3–8, 2008, ISSN: 10980121. DOI: 10.1103/PhysRevB.77.224509. arXiv: 0804.3843.

[47] C. Xu, M. Müller, and S. Sachdev, "Ising and spin orders in the iron-based superconductors," *Phys. Rev. B - Condens. Matter Mater. Phys.*, vol. 78, pp. 1–4, 2008, ISSN: 10980121. DOI: 10.1103/PhysRevB.78.020501. arXiv: 0804.4293.

[48] J.-H. Chu, J. G. Analytis, K. De Greve, P. L. McMahon, Z. Islam, Y. Yamamoto, and I. R. Fisher, "In-plane resistivity anisotropy in an underdoped iron arsenide superconductor.," *Science*, vol. 329, pp. 824–826, 2010, ISSN: 0036-8075. DOI: 10.1126/science.1190482. arXiv: 1002.3364.

[49] R. M. Fernandes, E. Abrahams, and J. Schmalian, "Anisotropic in-plane resistivity in the nematic phase of the iron pnictides," *Phys. Rev. Lett.*, vol. 107, no. November, pp. 1–5, 2011, ISSN: 00319007. DOI: 10.1103/PhysRevLett.107.217002. arXiv: 1105.3906.

[50] J. Teng, C. Chen, Y. Xiong, J. Zhang, R. Jin, and E. W. Plummer, "Anomalous surface lattice dynamics in the low-temperature phase of $Ba(Fe_{1-x}Co_x)_2As_2$," *Proc. Natl. Acad. Sci. U. S. A.*, vol. 110, p. 898, 2013. DOI: 10.1073/pnas.1220170110/-/DCSupplemental.www.pnas.org/cgi/doi/10.1073/pnas.1220170110.

[51] M. Allan, T. Chuang, F. Massee, and Y. Xie, "Anisotropic impurity states, quasiparticle scattering and nematic transport in underdoped $Ca(Fe_{1-x}Co_x)_2As_2$," *Nat. Phys.*, vol. 9, no. 4, pp. 220–224, 2013, ISSN: 1745-2473. DOI: 10.1038/nphys2544. arXiv: 1211.6454. [Online]. Available: http://www.nature.com/doifinder/10.1038/nphys2544.

[52] E. P. Rosenthal, E. F. Andrade, C. J. Arguello, R. M. Fernandes, L. Y. Xing, X. C. Wang, C. Q. Jin, A. Millis, and A. N. Pasupathy, "Visualization of electron nematicity and unidirectional antiferroic fluctuations at high temperatures in NaFeAs," *Nat. Phys.*, vol. 10, no. February, pp. 225–232, 2014, ISSN: 1745-2473. DOI: 10.1038/nphys2870. arXiv: 1307.3526.

[53] M. Yi, D. Lu, J.-H. Chu, J. G. Analytis, A. P. Sorini, A. F. Kemper, and B. Moritz, "Symmetry-breaking orbital anisotropy observed for detwinned $Ba(Fe_{1-x}Co_x)_2As_2$ above the spin density wave transition," *Proc. Natl. Acad. Sci. U. S. A.*, 2011. DOI: 10.1073/pnas.1015572108/-/DCSupplemental.www.pnas.org/cgi/doi/10.1073/pnas.1015572108.

[54] R. M. Fernandes, A. V. Chubukov, J. Knolle, I. Eremin, and J. Schmalian, "Preemptive nematic order, pseudogap, and orbital order in the iron pnictides," *Phys. Rev. B - Condens. Matter Mater. Phys.*, vol. 85, no. 2, pp. 1–31, 2012, ISSN: 10980121. DOI: 10.1103/PhysRevB.85.024534. arXiv: arXiv:1110.1893v2.

[55] R. M. Fernandes, L. H. VanBebber, S. Bhattacharya, P. Chandra, V. Keppens, D. Mandrus, M. A. McGuire, B. C. Sales, A. S. Sefat, and J. Schmalian, "Effects of nematic fluctuations on the elastic properties of iron arsenide superconductors," *Phys. Rev. Lett.*, vol. 105, no. 15, p. 157 003, Oct. 2010. DOI: 10.1103/PhysRevLett.105.157003.

[56] G.-M. Zhang, Y.-H. Su, Z.-Y. Lu, Z.-Y. Weng, D.-H. Lee, and T. Xiang, "Universal linear-temperature dependence of static magnetic susceptibility in iron-pnictides," *EPL (Europhysics Lett.*, vol. 37006, no. 86, p. 4, 2009, ISSN: 0295-5075. DOI: 10.1209/0295-5075/86/37006. arXiv: 0809.3874. [Online]. Available: http://arxiv.org/abs/0809.3874.

[57] S. J. Moon, Y. S. Lee, A. A. Schafgans, A. V. Chubukov, S. Kasahara, T. Shibauchi, T. Terashima, Y. Matsuda, M. A. Tanatar, R. Prozorov, A. Thaler, P. C. Canfield, S. L. Bud'Ko, a. S. Sefat, D. Mandrus, K. Segawa, Y. Ando, and D. N. Basov, "Infrared pseudogap in cuprate and pnictide high-temperature superconductors," *Phys. Rev. B - Condens. Matter Mater. Phys.*, vol. 90, no. 1, pp. 1–16, 2014, ISSN: 1550235X. DOI: 10.1103/PhysRevB.90.014503. arXiv: 1404.7233.

[58] T. Valla, A. V. Fedorov, J. Lee, J. C. Davis, and G. D. Gu, "The ground state of the pseudogap in cuprate superconductors," *Science*, vol. 314, no. 5807, pp. 1914–1916, 2006, ISSN: 0036-8075. DOI: 10.1126/science.1134742. arXiv: 0612672 [cond-mat].

[59] Z. P. Yin, K. Haule, and G. Kotliar, "Magnetism and charge dynamics in iron pnictides," *Nat. Phys.*, vol. 7, no. 4, pp. 294–297, Feb. 2011, ISSN: 1745-2473. DOI: 10.1038/nphys1923. [Online]. Available: http://www.nature.com/doifinder/10.1038/nphys1923.

[60] A. V. Boris, N. N. Kovaleva, S. S. Seo, J. S. Kim, P. Popovich, Y. Matiks, R. K. Kremer, and B. Keimer, "Signatures of electronic correlations in optical properties of $LaFeAsO_{1-x}F_x$," *Phys. Rev. Lett.*, vol. 102, no. January, pp. 1–4, 2009, ISSN: 00319007. DOI: 10.1103/PhysRevLett.102.027001. arXiv: 0806.1732.

[61] S. J. Moon, A. A. Schafgans, S. Kasahara, T. Shibauchi, T. Terashima, Y. Matsuda, M. a. Tanatar, R. Prozorov, A. Thaler, P. C. Canfield, A. S. Sefat, D. Mandrus, and D. N. Basov, "Infrared measurement of the pseudogap of P-doped and Co-doped high-temperature $BaFe_2As_2$ superconductors," *Phys. Rev. Lett.*, vol. 109, no. July, pp. 1–6, 2012, ISSN: 00319007. DOI: 10.1103/PhysRevLett.109.027006. arXiv: 1207.3567.

[62] T. Shimojima, T. Sonobe, W. Malaeb, K. Shinada, A. Chainani, S. Shin, T. Yoshida, S. Ideta, A. Fujimori, H. Kumigashira, K. Ono, Y. Nakashima, H. Anzai, M. Arita, A. Ino, H. Namatame, M. Taniguchi, M. Nakajima, S. Uchida, Y. Tomioka, T. Ito, K. Kihou, C. H. Lee, A. Iyo, H. Eisaki, K. Ohgushi, S. Kasahara, T. Terashima, H. Ikeda, T. Shibauchi, Y. Matsuda, and K. Ishizaka, "Pseudogap formation above the superconducting dome in iron pnictides," *Phys. Rev. B - Condens. Matter Mater. Phys.*, vol. 89, no. 4, pp. 32–40, 2014, ISSN: 10980121. DOI: 10.1103/PhysRevB.89.045101. arXiv: 1305.3875v2.

[63] T. Mertelj, V. V. Kabanov, C. Gadermaier, N. D. Zhigadlo, S. Katrych, J. Karpinski, and D. Mihailovic, "Distinct pseudogap and quasiparticle relaxation dynamics in the superconducting state of nearly optimally doped $SmFeAsO_{0.8}F_{0.2}$ single crystals," *Phys. Rev. Lett.*, vol. 102, no. March, pp. 3–6, 2009, ISSN: 00319007. DOI: 10.1103/PhysRevLett.102.117002.

[64] C. de la Cruz, Q. Huang, J. W. Lynn, J. Li, W. Ratcliff, J. L. Zarestky, H. A. Mook, G. F. Chen, J. L. Luo, N. L. Wang, and P. Dai, "Magnetic order close to superconductivity in the iron-based layered $LaO_{1-x}F_xFeAs$ systems," *Nature*, vol. 453, no. 7197, pp. 899–902, Jun. 2008, ISSN: 1476-4687. DOI: 10.1038/nature07057. [Online]. Available: http://www.ncbi.nlm.nih.gov/pubmed/18509333.

[65] J. Paglione and R. L. Greene, "High-temperature superconductivity in iron-based materials," *Nat. Phys.*, vol. 6, no. 9, pp. 645–658, Aug. 2010, ISSN: 1745-2473. DOI: 10.1038/nphys1759. [Online]. Available: http://www.nature.com/doifinder/10.1038/nphys1759.

[66] M. Kim, R. Fernandes, A. Kreyssig, J. Kim, A. Thaler, S. Budko, P. Canfield, R. McQueeney, J. Schmalian, and A. Goldman, *Character of the structural and magnetic phase transitions in the parent and electron-doped $BaFe_2As_2$ compounds*, 2011. DOI: 10.1103/PhysRevB.83.134522.

[67] M. Kovacic, M. H. Christensen, M. N. Gastiasoro, and B. M. Andersen, "Spin excitations in the nematic phase and the metallic stripe spin-density wave phase of iron pnictides," *Phys. Rev. B*, vol. 91, no. 6, pp. 1–10, 2015, ISSN: 1098-0121. DOI: 10.1103/PhysRevB.91.064424. [Online]. Available: http://link.aps.org/doi/10.1103/PhysRevB.91.064424.

[68] I. I. Mazin, D. J. Singh, M. D. Johannes, and M. H. Du, "Unconventional superconductivity with a sign reversal in the order parameter of $LaFeAsO_{1-x}F_x$," *Phys. Rev. Lett.*, vol. 101, no. 5, p. 057003, Jul. 2008, ISSN: 00319007. DOI: 10.1103/PhysRevLett.101.057003. [Online]. Available: http://link.aps.org/doi/10.1103/PhysRevLett.101.057003.

[69] J. Dong, H. J. Zhang, G. Xu, Z. Li, G. Li, W. Z. Hu, D. Wu, G. F. Chen, X. Dai, J. L. Luo, Z. Fang, and N. L. Wang, "Competing orders and spin-density-wave instability in $La(O_{1-x}F_x)FeAs$," *EPL (Europhysics Lett.*, vol. 83, no. 2, p. 27006, Jul. 2008, ISSN: 0295-5075. DOI: 10.1209/0295-5075/83/27006. [Online]. Available: http://stacks.iop.org/0295-5075/83/i=2/a=27006?key=crossref.4f6b14c71217d793b478c2f2d9ee332c.

[70] C. Ning, W. Yan-Feng, Z. Ji-Min, Z. Shi-Ping, Y. Qian-Sheng, Z. Zhi-Guo, and F. Pan-Ming, "Femtosecond optical detection of quasiparticle dynamics in single-crystal $Bi_2Sr_2CaCu_2O_{8+d}$," *Chinese Phys. Lett.*, vol. 25, no. 6, pp. 2257–2260, 2008, ISSN: 0256-307X. DOI: 10.1088/0256-307X/25/6/092. [Online]. Available: http://stacks.iop.org/0256-307X/25/i=6/a=092?key=crossref.bea429646678acc6413e204d6aff2b69.

[71] K. Igawa, H. Okada, H. Takahashi, S. Matsuishi, Y. Kamihara, M. Hirano, H. Hosono, K. Matsubayashi, and Y. Uwatoko, "Pressure-induced superconductivity in iron pnictide compound $SrFe_2As_2$," *J. Phys. Soc. Japan*, vol. 78, no. 2, pp. 1–2, 2009, ISSN: 00319015. DOI: 10.1143/JPSJ.78.025001. arXiv: 0810.1377.

[72] E. Colombier, S. Budko, N. Ni, and P. Canfield, "Complete pressure-dependent phase diagrams for $SrFe_2As_2$ and $BaFe_2As_2$," *Phys. Rev. B*, vol. 79, no. June, pp. 1–9, 2009, ISSN: 1098-0121. DOI: 10.1103/PhysRevB.79.224518.

[73] P. L. Alireza, Y. T. C. Ko, J. Gillett, C. M. Petrone, J. M. Cole, G. G. Lonzarich, and S. E. Sebastian, "Superconductivity up to 29 K in $SrFe_2As_2$ and BaF_2As_2 at high pressures.," *J. Phys. Condens. Matter*, vol. 21, p. 012 208, 2009, ISSN: 0953-8984. DOI: 10.1088/0953-8984/21/1/012208. arXiv: 0807.1896.

[74] S. Medvedev, T. M. McQueen, I. A. Troyan, T. Palasyuk, M. I. Eremets, R. J. Cava, S. Naghavi, F. Casper, V. Ksenofontov, G. Wortmann, and C. Felser, "Electronic and magnetic phase diagram of β-$Fe_{1.01}Se$ with superconductivity at 36.7 K under pressure," *Nat. Mater.*, vol. 8, no. 8, pp. 630–633, 2009, ISSN: 1476-1122. DOI: 10.1038/nmat2491. arXiv: 0903.2143. [Online]. Available: http://dx.doi.org/10.1038/nmat2491.

[75] K. Mydeen, E. Lengyel, Z. Deng, X. C. Wang, C. Q. Jin, and M. Nicklas, "Temperature-pressure phase diagram of the superconducting iron pnictide LiFeP," *Phys. Rev. B - Condens. Matter Mater. Phys.*, vol. 82, pp. 2–5, 2010, ISSN: 10980121. DOI: 10.1103/PhysRevB.82.014514. arXiv: 1003.0785.

[76] S. Jiang, H. Xing, G. Xuan, C. Wang, Z. Ren, C. Feng, J. Dai, Z. Xu, and G. Cao, "Superconductivity up to 30 K in the vicinity of the quantum critical point in $BaFe_2(As_{1-x}P_x)_2$," *J. Phys. Condens. Matter*, vol. 21, p. 382 203, 2009, ISSN: 1361-648X. DOI: 10.1088/0953-8984/21/38/382203. arXiv: arXiv:0901.3227v2.

[77] Z. Li, R. Zhou, Y. Liu, D. L. Sun, J. Yang, C. T. Lin, and G. Q. Zheng, "Microscopic coexistence of antiferromagnetic order and superconductivity in $Ba_{0.77}K_{0.23}Fe_2As_2$," *Phys. Rev. B - Condens. Matter Mater. Phys.*, vol. 86, pp. 21–24, 2012, ISSN: 10980121. DOI: 10.1103/PhysRevB.86.180501. arXiv: 1204.2434.

[78] D. Van Delft and P. Kes, "The discovery of superconductivity," *Phys. Today*, vol. 63, no. 9, pp. 38–43, 2010, ISSN: 00319228. DOI: 10.1063/1.3490499.

[79] H. K. Onnes, "The resistance of pure mercury at helium temperatures," *ommun. Phys. Lab. Univ. Leiden*, vol. 12, p. 1911, 1911.

[80] F. Giustino, M. L. Cohen, and S. G. Louie, "Small phonon contribution to the photoemission kink in the copper oxide superconductors.," *Nature*, vol. 452, no. 7190, pp. 975–978, 2008, ISSN: 0028-0836. DOI: 10.1038/nature06874.

[81] R. Heid, K. P. Bohnen, R. Zeyher, and D. Manske, "Momentum dependence of the electron-phonon coupling and self-energy effects in superconducting $YBa_2Cu_3O_7$ within the local density approximation," *Phys. Rev. Lett.*, vol. 100, no. 13, pp. 2–5, 2008, ISSN: 00319007. DOI: 10.1103/PhysRevLett.100.137001. arXiv: 0707.4429.

[82] K. Haule, J. H. Shim, and G. Kotliar, "Correlated electronic structure of $LaO_{1-x}F_xFeAs$," *Phys. Rev. Lett.*, vol. 100, no. June, pp. 3–6, 2008, ISSN: 00319007. DOI: 10.1103/PhysRevLett.100.226402. arXiv: arXiv:0803.1279v1.

[83] G. Wu, Y. L. Xie, H. Chen, M. Zhong, R. H. Liu, B. C. Shi, Q. J. Li, X. F. Wang, T. Wu, Y. J. Yan, J. J. Ying, and X. H. Chen, "Superconductivity at 56 K in samarium-doped SrFeAsF," *J. Phys. Condens. Matter*, vol. 21, no. 14, p. 142 203, 2009, ISSN: 0953-8984. DOI: 10.1088/0953-8984/21/14/142203. arXiv: 0811.0761.

[84] P. B. Allen, "Theory of thermal relaxation of electrons in metals," *Phys. Rev. Lett.*, vol. 59, no. 13, pp. 1460–1463, 1987, ISSN: 00319007. DOI: 10.1103/PhysRevLett.59.1460.

[85] S. D. Brorson, A. Kazeroonian, J. S. Moodera, D. W. Face, T. K. Cheng, E. P. Ippen, M. S. Dresselhaus, and G. Dresselhaus, "Femtosecond room-temperature measurement of the electron-phonon coupling constant γ in metallic superconductors," *Phys. Rev. Lett.*, vol. 64, no. 18, pp. 2172–2175, 1990, ISSN: 0031-9007. DOI: 10.1103/PhysRevLett.64.2172.

[86] L. Boeri, O. V. Dolgov, and A. A. Golubov, "Electron-phonon properties of pnictide superconductors," *Phys. C Supercond. its Appl.*, vol. 469, no. 9-12, pp. 628–634, 2009, ISSN: 09214534. DOI: 10.1016/j.physc.2009.03.020. arXiv: 0902.0288. [Online]. Available: http://dx.doi.org/10.1016/j.physc.2009.03.020.

[87] C. Gadermaier, V. V. Kabanov, A. S. Alexandrov, L. Stojchevska, T. Mertelj, C. Manzoni, G. Cerullo, N. D. Zhigadlo, J. Karpinski, Y. Q. Cai, X. Yao, Y. Toda, M. Oda, S. Sugai, and D. Mihailovic, "Strain-induced enhancement of the electron energy relaxation in strongly correlated superconductors," *Phys. Rev. X*, vol. 4, no. 1, pp. 1–6, 2014, ISSN: 21603308. DOI: 10.1103/PhysRevX.4.011056.

[88] Q. Si, "Iron pnictide superconductors: Electrons on the verge," *Nat. Phys.*, vol. 5, no. 9, p. 5, 2009, ISSN: 1745-2473. DOI: 10.1038/nphys1394. arXiv: 0912.4989. [Online]. Available: http://arxiv.org/abs/0912.4989.

[89] M. M. Qazilbash, J. J. Hamlin, R. E. Baumbach, L. Zhang, D. J. Singh, M. B. Maple, and D. N. Basov, "Electronic correlations in the iron pnictides," *Nat. Phys.*, vol. 5, no. 9, pp. 647–650, 2009, ISSN: 1745-2473. DOI: 10.1038/nphys1343. [Online]. Available: http://dx.doi.org/10.1038/nphys1343.

[90] L. Craco, M. S. Laad, S. Leoni, and H. Rosner, "Self-doping induced orbital-selective Mott transition in $Hg_2Ru_2O_7$," *Phys. Rev. B - Condens. Matter Mater. Phys.*, vol. 79, pp. 1–5, 2009, ISSN: 10980121. DOI: 10.1103/PhysRevB.79.075125. arXiv: arXiv:0901.4658v1.

[91] Q. Si and E. Abrahams, "Strong correlations and magnetic frustration in the high T_c iron pnictides," *Phys. Rev. Lett.*, vol. 101, no. August, pp. 1–4, 2008, ISSN: 00319007. DOI: 10.1103/PhysRevLett.101.076401. arXiv: 0804.2480.

[92] L. De Medici, G. Giovannetti, and M. Capone, "Selective Mott physics as a key to iron superconductors," *Phys. Rev. Lett.*, vol. 112, no. May, pp. 1–5, 2014, ISSN: 10797114. DOI: 10.1103/PhysRevLett.112.177001. arXiv: 1212.3966.

[93] L. Boeri, O. V. Dolgov, and A. A. Golubov, "Is $LaFeAsO_{1-x}F_x$ an electron-phonon superconductor?" *Phys. Rev. Lett.*, vol. 101, no. 2, pp. 1–4, 2008, ISSN: 00319007. DOI: 10.1103/PhysRevLett.101.026403. arXiv: 0803.2703.

[94] A. D. Christianson, E. A. Goremychkin, R. Osborn, S. Rosenkranz, M. D. Lumsden, C. D. Malliakas, I. S. Todorov, H. Claus, D. Y. Chung, M. G. Kanatzidis, R. I. Bewley, and T. Guidi, "Unconventional superconductivity in $Ba_{0.6}K_{0.4}Fe_2As_2$ from inelastic neutron scattering.," *Nature*, vol. 456, no. 7224, pp. 930–932, 2008, ISSN: 0028-0836. DOI: 10.1038/nature07625. [Online]. Available: http://dx.doi.org/10.1038/nature07625.

[95] T. Imai, K. Ahilan, F. L. Ning, T. M. McQueen, and R. J. Cava, "Why does undoped FeSe become a high-T_c superconductor under pressure?" *Phys. Rev. Lett.*, vol. 102, no. 17, pp. 1–4, 2009, ISSN: 00319007. DOI: 10.1103/PhysRevLett.102.177005. arXiv: 0902.3832.

[96] Y. Tsuge, A. Iyo, Y. Tanaka, H. Eisaki, and T. Nishio, "Inverse iron isotope effect in $FeSe_{0.35}Te_{0.65}$," *Phys. Procedia*, vol. 36, pp. 731–734, 2012, ISSN: 18753892. DOI: 10.1016/j.phpro.2012.06.276.

[97] Y. Tsuge, T. Nishio, A. Iyo, Y. Tanaka, and H. Eisaki, "Iron isotope effect in the iron arsenide superconductor $(Ca_{0.4}Na_{0.6})Fe_2As_2$," *J. Phys. Conf. Ser.*, vol. 507, no. 1, p. 012 037, 2014, ISSN: 1742-6596. DOI: 10.1088/1742-6596/507/1/012037. [Online]. Available: http://stacks.iop.org/1742-6596/507/i=1/a=012037?key=crossref.f81b3c405d8187dfbaf8b51a82ae8e64.

[98] P. M. Shirage, K. Miyazawa, K. Kihou, H. Kito, Y. Yoshida, Y. Tanaka, H. Eisaki, and A. Iyo, "Absence of an appreciable iron isotope effect on the transition temperature of the optimally doped $SmFeAsO_{1-y}$ superconductor," *Phys. Rev. Lett.*, vol. 105, no. 3, pp. 16–19, 2010, ISSN: 00319007. DOI: 10.1103/PhysRevLett.105.037004.

[99] S. L. Bud'ko, G. Lapertot, C. Petrovic, C. E. Cunningham, N. Anderson, and P. C. Canfield, "Boron isotope effect in superconducting MgB_2," *Phys. Rev. Lett.*, vol. 86, no. 9, pp. 1877–1880, 2001, ISSN: 00319007. DOI: 10.1103/PhysRevLett.86.1877. arXiv: 0101463 [cond-mat].

[100] A. Hinojosa, R. M. Fernandes, and A. V. Chubukov, "Time-reversal symmetry breaking superconductivity in the coexistence phase with magnetism in Fe-pnictides," *Phys. Rev. Lett.*, vol. 167001, no. October, p. 9, 2014, ISSN: 10797114. DOI: 10.1103/PhysRevLett.113.167001. [Online]. Available: http://journals.aps.org/prl/pdf/10.1103/PhysRevLett.113.167001.

[101] M. Marciani, L. Fanfarillo, C. Castellani, and L. Benfatto, "Leggett modes in iron-based superconductors as a probe of time-reversal symmetry breaking," *Phys. Rev. B - Condens. Matter Mater. Phys.*, vol. 88, pp. 1–20, 2013, ISSN: 10980121. DOI: 10.1103/PhysRevB.88.214508.

[102] S. Maiti and A. V. Chubukov, "$s + is$ state with broken time-reversal symmetry in Fe-based superconductors," *Phys. Rev. B - Condens. Matter Mater. Phys.*, vol. 87, no. April, pp. 1–14, 2013, ISSN: 10980121. DOI: 10.1103/PhysRevB.87.144511. arXiv: arXiv:1302.2964v2.

[103] D. Wu, N. Barišić, P. Kallina, A. Faridian, B. Gorshunov, N. Drichko, L. J. Li, X. Lin, G. H. Cao, Z. A. Xu, N. L. Wang, and M. Dressel, "Optical investigations of the normal and superconducting states reveal two electronic subsystems in iron pnictides," *Phys. Rev. B - Condens. Matter Mater. Phys.*, vol. 81, pp. 1–4, 2010, ISSN: 10980121. DOI: 10.1103/PhysRevB.81.100512.

[104] V. Stanev, "Model of collective modes in three-band superconductors with repulsive interband interactions," *Phys. Rev. B - Condens. Matter Mater. Phys.*, vol. 85, no. 17, pp. 1–5, 2012, ISSN: 10980121. DOI: 10.1103/PhysRevB.85.174520.

[105] C. C. Tsuei and J. R. Kirtley, "Phase-sensitive evidence for d-wave pairing symmetry in electron-doped cuprate superconductors," *Phys. Rev. Lett.*, vol. 85, no. 1, pp. 182–185, 2000, ISSN: 00319007. DOI: 10.1103/PhysRevLett.85.182. arXiv: 0002341 [cond-mat].

[106] C. Tsuei and J. Kirtley, "Pairing symmetry in cuprate superconductors," *Rev. Mod. Phys.*, vol. 72, no. 4, pp. 969–1016, 2000, ISSN: 0034-6861. DOI: 10.1103/RevModPhys.72.969.

[107] C.-T. Chen, C. C. Tsuei, M. B. Ketchen, Z.-A. Ren, and Z. X. Zhao, "Integer and half-integer flux-quantum transitions in a niobium/iron-pnictide loop," *Nat. Phys.*, vol. 6, no. 4, p. 23, 2010, ISSN: 1745-2473. DOI: 10.1038/nphys1531. arXiv: 0905.3571. [Online]. Available: http://arxiv.org/abs/0905.3571.

[108] K. Kuroki, S. Onari, R. Arita, H. Usui, Y. Tanaka, H. Kontani, and H. Aoki, "Unconventional pairing originating from the disconnected Fermi surfaces of superconducting $LaFeAsO_{1-x}F_x$," *Phys. Rev. Lett.*, vol. 101, no. August, pp. 1–4, 2008, ISSN: 00319007. DOI: 10.1103/PhysRevLett.101.087004. arXiv: 0803.3325.

[109] A. V. Chubukov, D. V. Efremov, and I. Eremin, "Magnetism, superconductivity, and pairing symmetry in iron-based superconductors," *Phys. Rev. B - Condens. Matter Mater. Phys.*, vol. 78, pp. 1–10, 2008, ISSN: 10980121. DOI: 10.1103/PhysRevB.78.134512. arXiv: 0807.3735.

[110] H. Kontani and S. Onari, "Orbital-fluctuation-mediated superconductivity in iron pnictides: Analysis of the five-orbital hubbard-holstein model," *Phys. Rev. Lett.*, vol. 104, no. 15, pp. 1–4, 2010, ISSN: 00319007. DOI: 10.1103/PhysRevLett.104.157001. arXiv: 0912.1975.

[111] W. C. Lee, S. C. Zhang, and C. Wu, "Pairing state with a time-reversal symmetry breaking in FeAs-based superconductors," *Phys. Rev. Lett.*, vol. 102, no. May, pp. 1–4, 2009, ISSN: 00319007. DOI: 10.1103/PhysRevLett.102.217002. arXiv: 0810.0887.

[112] Z. Chen, R. Yuan, T. Dong, N. Wang, S. Ce, N. Pr, *et al.*, "Optical spectroscopy study on single crystalline LaFeAsO," *Arxiv preprint arXiv:0910.1318*, 2009.

[113] J. E. Hirsch, M. B. Maple, and F. Marsiglio, "Superconducting materials classes: introduction and overview," *arxiv*, 2015. arXiv: 1504.03318v1.

[114] A. Charnukha, "Optical conductivity of iron-based superconductors.," *J. Phys. Condens. Matter*, vol. 26, p. 253 203, 2014, ISSN: 1361-648X. DOI: 10.1088/0953-8984/26/25/253203. arXiv: 1406.1879. [Online]. Available: http://www.ncbi.nlm.nih.gov/pubmed/24899620.

[115] I. R. Shein and A. L. Ivanovskii, "Electronic structure of oxygen-free 38 K superconductor $Ba_{1-x}K_xFe_2As_2$ in comparison with $BaFe_2As_2$ from first principles," *JEPT Lett.*, vol. 88, no. 2, p. 11, 2008, ISSN: 0021-3640. DOI: 10.1134/S0021364008140087. arXiv: 0806.0750. [Online]. Available: http://arxiv.org/abs/0806.0750.

[116] C. Krellner, N. Caroca-Canales, A. Jesche, H. Rosner, A. Ormeci, and C. Geibel, "Magnetic and structural transitions in layered iron arsenide systems: AFe_2As_2 versus RFeAsO," *Phys. Rev. B - Condens. Matter Mater. Phys.*, vol. 78, pp. 1–4, 2008, ISSN: 10980121. DOI: 10.1103/PhysRevB.78.100504.

[117] I. A. Nekrasov, Z. V. Pchelkina, and M. V. Sadovskii, "Electronic structure of new LiFeAs high-T_c superconductor," *JEPT Lett.*, vol. 88, no. 8, p. 4, 2008. DOI: 10.1134/S0021364008200150. arXiv: 0807.1010. [Online]. Available: http://arxiv.org/abs/0807.1010.

[118] F. J. Ma, Z. Y. Lu, and T. Xiang, "Electronic structures of ternary iron arsenides $A\mathrm{Fe_2As_2}$ (A = Ba, Ca, or Sr)," *Front. Phys. China*, vol. 5, no. 2, pp. 150–160, 2010, ISSN: 16733487. DOI: 10.1007/s11467-009-0076-9. arXiv: 0806.3526.

[119] A. Charnukha, P. Popovich, Y. Matiks, D. L. Sun, C. T. Lin, A. N. Yaresko, B. Keimer, and A. V. Boris, "Superconductivity-induced optical anomaly in an iron arsenide," *Nat. Commun.*, vol. 2, p. 219, 2011, ISSN: 2041-1723. DOI: 10.1038/ncomms1223. arXiv: 1009.5915. [Online]. Available: http://dx.doi.org/10.1038/ncomms1223.

[120] M. Nakajima, S. Ishida, T. Tanaka, K. Kihou, Y. Tomioka, T. Saito, C.-H. Lee, H. Fukazawa, Y. Kohori, T. Kakeshita, A. Iyo, T. Ito, H. Eisaki, and S.-i. Uchida, "Strong electronic correlations in iron pnictides: comparison of optical spectra for $\mathrm{BaFe_2As_2}$-related compounds," *J. Phys. Soc. Japan*, vol. 83, no. 10, p. 104 703, Oct. 2014, ISSN: 0031-9015. DOI: 10.7566/JPSJ.83.104703. arXiv: arXiv:1308.6113v1. [Online]. Available: http://journals.jps.jp/doi/abs/10.7566/JPSJ.83.104703.

[121] M. Nakajima, T. Liang, S. Ishida, Y. Tomioka, K. Kihou, C. H. Lee, A. Iyo, H. Eisaki, T. Kakeshita, T. Ito, and S. Uchida, "Unprecedented anisotropic metallic state in undoped iron arsenide $\mathrm{BaFe_2As_2}$ revealed by optical spectroscopy.," *Proc. Natl. Acad. Sci. U. S. A.*, vol. 108, no. 30, pp. 12 238–12 242, 2011, ISSN: 0027-8424. DOI: 10.1073/pnas.1100102108. arXiv: 1106.4967.

[122] S. L. Drechsler, M. Grobosch, K. Koepernik, G. Behr, A. Köhler, J. Werner, A. Kondrat, N. Leps, C. Hess, R. Klingeler, R. Schuster, B. Büchner, and M. Knupfer, "Optical study of $\mathrm{LaO_{0.9}F_{0.1}FeAs}$: Evidence for a weakly coupled superconducting state," *Phys. Rev. Lett.*, vol. 101, no. December, pp. 2–5, 2008, ISSN: 00319007. DOI: 10.1103/PhysRevLett.101.257004.

[123] G. Li, W. Z. Hu, J. Dong, Z. Li, P. Zheng, G. F. Chen, J. L. Luo, and N. L. Wang, "Probing the superconducting energy gap from infrared spectroscopy on a $\mathrm{Ba_{0.6}K_{0.4}Fe_2As_2}$ single rystal with T_c = 37 K," *Phys. Rev. Lett.*, vol. 101, no. September, pp. 1–4, 2008, ISSN: 00319007. DOI: 10.1103/PhysRevLett.101.107004.

[124] A. P. Litvinchuk, V. G. Hadjiev, M. N. Iliev, B. Lv, A. M. Guloy, and C. W. Chu, "Raman-scattering study of $\mathrm{K}_x\mathrm{Sr}_{1-x}\mathrm{Fe}_2\ \mathrm{As}_2$ (x=0.0,0.4)," *Phys. Rev. B - Condens. Matter Mater. Phys.*, vol. 78, pp. 4–7, 2008, ISSN: 10980121. DOI: 10.1103/PhysRevB.78.060503.

[125] K. Y. Choi, D. Wulferding, P. Lemmens, N. Ni, S. L. Bud'Ko, and P. C. Canfield, "Lattice and electronic anomalies of $\mathrm{CaFe_2As_2}$ studied by Raman spectroscopy," *Phys. Rev. B - Condens. Matter Mater. Phys.*, vol. 78, pp. 2–5, 2008, ISSN: 10980121. DOI: 10.1103/PhysRevB.78.212503.

[126] P. Kumar, D. V. S. Muthu, L. Harnagea, S. Wurmehl, B. Büchner, and A. K. Sood, "Phonon anomalies, orbital-ordering and electronic raman scattering in iro-pnictide $\mathrm{Ca(Fe_{0.97}Co_0.03)_2As_2}$: temperature-dependent Raman study," *J. Phys. Condens. Matter*, vol. 26, p. 305 403, 2014, ISSN: 1361-648X. DOI: 10.1088/0953-8984/26/30/305403. arXiv: 1406.5844. [Online]. Available: http://arxiv.org/abs/1406.5844.

[127] G. Gruener, *Density waves in solids*. 1994, ISBN: 0201626543.

[128] T. Egami, B. V. Fine, D. Parshall, A. Subedi, and D. J. Singh, "Spin-lattice coupling and superconductivity in Fe pnictides," *Adv. Condens. Matter Phys.*, vol. 2010, pp. 1–7, 2010, ISSN: 1687-8108. DOI: 10.1155/2010/164916. [Online]. Available: http://www.hindawi.com/journals/acmp/2010/164916/.

[129] G. Gruener, "The dynamics of spin-density waves," *Rev. Mod. Phys.*, vol. 66, no. 1, 1994. DOI: 0034-6861/94/66(1)/1.

[130] P. Littlewood and C. Varna, "Amplitude collective modes in superconductors and their coupling to charge-density waves," *Phys. Rev. B*, vol. 26, no. 9, pp. 4883–4893, 1982.

[131] P. J. Hirschfeld, M. M. Korshunov, and I. I. Mazin, "Gap symmetry and structure of Fe-based superconductors," *Reports Prog. Phys.*, vol. 124508, p. 81, 2011, ISSN: 0034-4885. DOI: 10.1088/0034-4885/74/12/124508. arXiv: 1106.3712. [Online]. Available: http://arxiv.org/abs/1106.3712.

[132] A. Chubukov, "Pairing mechanism in multiband superconductors," p. 7, 2011. arXiv: 1107.1796. [Online]. Available: http://arxiv.org/abs/1107.1796.

[133] M. Liu, L. W. Harriger, H. Luo, M. Wang, R. A. Ewings, T. Guidi, H. Park, K. Haule, G. Kotliar, S. M. Hayden, and P. Dai, "Nature of magnetic excitations in superconducting $BaFe_{1.9}Ni_{0.1}As_2$," *Nat. Phys.*, vol. 8, no. March, pp. 376–381, 2012, ISSN: 1745-2473. DOI: 10.1038/nphys2268. arXiv: 1202.2827.

[134] I. I. Mazin and M. D. Johannes, "A key role for unusual spin dynamics in ferropnictides," *Nat. Phys.*, vol. 5, no. 2, pp. 141–145, 2008, ISSN: 1745-2473. DOI: 10.1038/nphys1160. arXiv: 0807.3737. [Online]. Available: http://arxiv.org/abs/0807.3737.

[135] S. J. Moon, J. H. Shin, D. Parker, W. S. Choi, I. I. Mazin, Y. S. Lee, J. Y. Kim, N. H. Sung, B. K. Cho, S. H. Khim, J. S. Kim, K. H. Kim, and T. W. Noh, "Dual character of magnetism in $EuFe_2As_2$: Optical spectroscopic and density-functional calculation study," *Phys. Rev. B - Condens. Matter Mater. Phys.*, vol. 81, pp. 1–5, 2010, ISSN: 10980121. DOI: 10.1103/PhysRevB.81.205114.

[136] P. Hansmann, R. Arita, A. Toschi, S. Sakai, G. Sangiovanni, and K. Held, "Dichotomy between large local and small ordered magnetic moments in iron-based superconductors," *Phys. Rev. Lett.*, vol. 104, no. May, pp. 14–17, 2010, ISSN: 00319007. DOI: 10.1103/PhysRevLett.104.197002. arXiv: 1003.2162.

[137] L. Ortenzi, H. Gretarsson, S. Kasahara, T. Shibauchi, K. D. Finkelstein, W. Wu, S. R. Julian, Y.-j. Kim, I. I. Mazin, and L. Boeri, "Structural origin of the anomalous temperature dependence of the local magnetic moments in the $CaFe_2As_2$ family of materials," *Phys. Rev. Lett.*, vol. 2, no. January, pp. 1–7, 2015, ISSN: 10797114. DOI: 10.1103/PhysRevLett.114.047001. arXiv: 1408.4058. [Online]. Available: http://arxiv.org/abs/1408.4058v1.

[138] T. Shimojima, K. Ishizaka, Y. Ishida, N. Katayama, K. Ohgushi, T. Kiss, M. Okawa, T. Togashi, X. Y. Wang, C. T. Chen, S. Watanabe, R. Kadota, T. Oguchi, A. Chainani, and S. Shin, "Orbital-dependent modifications of electronic structure across the magnetostructural transition in $BaFe_2As_2$," *Phys. Rev. Lett.*, vol. 104, no. February, pp. 3–6, 2010, ISSN: 00319007. DOI: 10.1103/PhysRevLett.104.057002. arXiv: 0904.1632.

[139] W. Malaeb, T. Yoshida, A. Fujimori, M. Kubota, K. Ono, K. Kihou, P. M. Shirage, H. Kito, A. Iyo, H. Eisaki, Y. Nakajima, T. Tamegai, and R. Arita, "Three-dimensional electronic structure of superconducting iron pnictides observed by angle-resolved photoemission spectroscopy," *J. Phys. Soc. Japan*, vol. 78, no. 12, pp. 12–15, 2009, ISSN: 00319015. DOI: 10.1143/JPSJ.78.123706. arXiv: 0906.1846.

[140] J. Fink, S. Thirupathaiah, R. Ovsyannikov, H. Dürr, R. Follath, Y. Huang, S. de Jong, M. Golden, Y.-Z. Zhang, H. Jeschke, R. Valentí, C. Felser, S. Dastjani Farahani, M. Rotter, and D. Johrendt, "Electronic structure studies of $BaFe_2As_2$ by angle-resolved photoemission spectroscopy," *Phys. Rev. B*, vol. 79, pp. 18–20, 2009, ISSN: 1098-0121. DOI: 10.1103/PhysRevB.79.155118. arXiv: arXiv:0903.0967v1.

[141] C. Liu, T. Kondo, N. Ni, A. D. Palczewski, A. Bostwick, G. D. Samolyuk, R. Khasanov, M. Shi, E. Rotenberg, S. L. Bud'Ko, P. C. Canfield, and A. Kaminski, "Three- to two-dimensional transition of the electronic structure in $CaFe_2As_2$: A parent compound for an iron arsenic high-temperature superconductor," *Phys. Rev. Lett.*, vol. 102, no. April, pp. 2–5, 2009, ISSN: 00319007. DOI: 10.1103/PhysRevLett.102.167004. arXiv: 0903.4388.

[142] S. V. Borisenko, V. B. Zabolotnyy, D. V. Evtushinsky, T. K. Kim, I. V. Morozov, A. N. Yaresko, A. A. Kordyuk, G. Behr, A. Vasiliev, R. Follath, and B. Büchner, "Superconductivity without nesting in LiFeAs," *Phys. Rev. Lett.*, vol. 105, no. AUGUST, pp. 2–5, 2010, ISSN: 00319007. DOI: 10.1103/PhysRevLett.105.067002.

[143] L. Rettig, R. Cortés, H. S. Jeevan, P. Gegenwart, T. Wolf, J. Fink, and U. Bovensiepen, "Electron-phonon coupling in 122 Fe pnictides analyzed by femtosecond time-resolved photoemission," *New J. Phys.*, vol. 15, 2013, ISSN: 13672630. DOI: 10.1088/1367-2630/15/8/083023. arXiv: 1304.5355.

[144] H. Ding, P. Richard, K. Nakayama, T. Sugawara, T. Arakane, Y. Sekiba, A. Takayama, S. Souma, T. Sato, T. Takahashi, Z. Wang, X. Dai, Z. Fang, G. F. Chen, J. L. Luo, and N. L. Wang, "Observation of Fermi-surface-dependent nodeless superconducting gaps in $Ba_{0.6}K_{0.4}Fe_2As_2$," *Europhys. Lett.*, vol. 47001, pp. 0295–5075, 2008, ISSN: 0295-5075. DOI: 10.1209/0295-5075/83/47001. arXiv: 0807.0419. [Online]. Available: http://arxiv.org/abs/0807.0419.

[145] D. V. Evtushinsky, D. S. Inosov, V. B. Zabolotnyy, A. Koitzsch, M. Knupfer, B. Büchner, M. S. Viazovska, G. L. Sun, V. Hinkov, A. V. Boris, C. T. Lin, B. Keimer, A. Varykhalov, A. A. Kordyuk, and S. V. Borisenko, "Momentum dependence of the superconducting gap in $Ba_{1-x}K_xFe_2As_2$," *Phys. Rev. B - Condens. Matter Mater. Phys.*, vol. 79, pp. 1–13, 2009, ISSN: 10980121. DOI: 10.1103/PhysRevB.79.054517.

[146] C. Liu, G. D. Samolyuk, Y. Lee, N. Ni, T. Kondo, A. F. Santander-Syro, S. L. Bud'Ko, J. L. McChesney, E. Rotenberg, T. Valla, A. V. Fedorov, P. C. Canfield, B. N. Harmon, and A. Kaminski, "K-doping dependence of the Fermi surface of the iron-arsenic $Ba_{1-x}K_xFe_2As_2$ superconductor using angle-resolved photoemission spectroscopy," *Phys. Rev. Lett.*, vol. 101, no. October, pp. 1–4, 2008, ISSN: 00319007. DOI: 10.1103/PhysRevLett.101.177005. arXiv: 0806.3453.

[147] R. Yoshida, T. Wakita, H. Okazaki, Y. Mizuguchi, S. Tsuda, Y. Takano, H. Takeya, K. Hirata, T. Muro, M. Okawa, K. Ishizaka, S. Shin, H. HArima, M. Hirai, Y. Muraoka, and T. Yokoya, "Electronic structure of superconducting FeSe studied by high-resolution photoemission spectroscopy," *J. Phys. Soc. Japan*, vol. 78, no. 3, pp. 1–4, 2009, ISSN: 00319015. DOI: 10.1143/JPSJ.78.034708. arXiv: 0811.1507.

[148] S. E. Sebastian, J. Gillett, N. Harrison, P. H. C. Lau, C. H. Mielke, and G. G. Lonzarich, "Quantum oscillations in the parent magnetic phase of an iron arsenide high temperature superconductor," *J. Phys. Condens. Matter*, vol. 422203, 2008, ISSN: 0953-8984. DOI: 10.1088/0953-8984/20/42/422203. arXiv: 0806.4726. [Online]. Available: http://arxiv.org/abs/0806.4726.

[149] S. Thirupathaiah, E. D. L. Rienks, H. S. Jeevan, R. Ovsyannikov, E. Slooten, J. Kaas, E. Van Heumen, S. De Jong, H. a. Dürr, K. Siemensmeyer, R. Follath, P. Gegenwart, M. S. Golden, and J. Fink, "Dissimilarities between the electronic structure of chemically doped and chemically pressurized iron pnictides from an angle-resolved photoemission spectroscopy study," *Phys. Rev. B - Condens. Matter Mater. Phys.*, vol. 84, pp. 1–7, 2011, ISSN: 10980121. DOI: 10.1103/PhysRevB.84.014531. arXiv: 1007.5205.

[150] J. G. Analytis, C. M. J. Andrew, A. I. Coldea, A. McCollam, J. H. Chu, R. D. McDonald, I. R. Fisher, and A. Carrington, "Fermi surface of $SrFe_2P_2$ determined by the de Haas-van Alphen effect," *Phys. Rev. Lett.*, vol. 103, no. August, pp. 1–4, 2009, ISSN: 00319007. DOI: 10.1103/PhysRevLett.103.076401. arXiv: 0904.2405.

[151] W. Z. Hu, J. Dong, G. Li, Z. Li, P. Zheng, G. F. Chen, J. L. Luo, and N. L. Wang, "Origin of the spin density wave instability in AFe_2As_2 (A=Ba,Sr) as revealed by optical spectroscopy," *Phys. Rev. Lett.*, vol. 101, no. 25, p. 257 005, Dec. 2008, ISSN: 0031-9007. DOI: 10.1103/PhysRevLett.101.257005. [Online]. Available: http://link.aps.org/doi/10.1103/PhysRevLett.101.257005.

[152] Y. Nakai, T. Iye, S. Kitagawa, K. Ishida, H. Ikeda, S. Kasahara, H. Shishido, T. Shibauchi, Y. Matsuda, and T. Terashima, "Unconventional superconductivity and antiferromagnetic quantum critical behavior in the isovalent-doped $BaFe_2(As_{1-x}P_x)_2$," *Phys. Rev. Lett.*, vol. 105, no. September, pp. 31–34, 2010, ISSN: 00319007. DOI: 10.1103/PhysRevLett.105.107003. arXiv: 1005.2853.

[153] J. Murphy, C. P. Strehlow, K. Cho, M. A. Tanatar, N. Salovich, R. W. Giannetta, T. Kobayashi, S. Miyasaka, S. Tajima, and R. Prozorov, "Nodal superconductivity in isovalently substituted $SrFe_2(As_{1-x}P_x)_2$ pnictide superconductor at the optimal doping $x = 0.35$," *Phys. Rev. B - Condens. Matter Mater. Phys.*, vol. 87, pp. 1–5, 2013, ISSN: 10980121. DOI: 10.1103/PhysRevB.87.140505. arXiv: 1301.5622.

[154] Z. Wang, H. Yang, C. Ma, H. Tian, H. Shi, J. Lu, L. Zeng, and J. Li, "The structural and physical properties of $Ba_{1-x}Sr_xFe_2As_2$ ($0<x<1$) and $Ba_{1-x}Sr_xFe_{1.8}Co_{0.2}As_2$ ($0<x<1$)," *J. Phys. Condens. Matter*, vol. 21, p. 495 701, 2009, ISSN: 1361-648X. DOI: 10.1088/0953-8984/21/49/495701.

[155] V. Ginzburg, "Experimental manifestation of instability of the normal phase in superconductors," *Sov. Phys. - JETP*, vol. 4, 1957. [Online]. Available: http://www.osti.gov/scitech/biblio/7354408.

[156] A. Buzdin, L. Bulaevskii, M. Kulich, and S. Panyukov, "Magnetic superconductors," *Uspekhi Fiz. Nauk*, vol. 144, p. 597, 1984, ISSN: 0042-1294. DOI: 10.3367/UFNr.0144.198412b.0597.

[157] Q. Huang, Y. Qiu, W. Bao, M. A. Green, J. W. Lynn, Y. C. Gasparovic, T. Wu, G. Wu, and X. H. Chen, "Neutron-diffraction measurements of magnetic order and a structural transition in the parent $BaFe_2As_2$ compound of FeAs-based high-temperature superconductors," *Phys. Rev. Lett.*, vol. 101, no. December, pp. 2–5, 2008, ISSN: 00319007. DOI: 10.1103/PhysRevLett.101.257003.

[158] N. F. Berk and J. R. Schrieffer, "Effect of ferromagnetic spin correlations on superconductivity," *Phys. Rev. Lett.*, vol. 69, no. 8, pp. 168–171, 1966.

[159] J. R. Schrieffer, X. G. Wen, and S. C. Zhang, "Dynamic spin fluctuations and the bag mechanism of high-T_c superconductivity," *Phys. Rev. B*, vol. 39, no. 16, pp. 11 663–11 679, 1989, ISSN: 01631829. DOI: 10.1103/PhysRevB.39.11663.

[160] W. Li, J. X. Zhu, Y. Chen, and C. S. Ting, "First-principles calculations of the electronic structure of iron-pnictide $EuFe_2(As,P)_2$ superconductors: Evidence for antiferromagnetic spin order," *Phys. Rev. B - Condens. Matter Mater. Phys.*, vol. 86, pp. 1–5, 2012, ISSN: 10980121. DOI: 10.1103/PhysRevB.86.155119.

[161] A. A. Aczel, E. Baggio-Saitovitch, S. L. Budko, P. C. Canfield, J. P. Carlo, G. F. Chen, P. Dai, T. Goko, W. Z. Hu, G. M. Luke, J. L. Luo, N. Ni, D. R. Sanchez-Candela, F. F. Tafti, N. L. Wang, T. J. Williams, W. Yu, and Y. J. Uemura, "Muon-spin-relaxation studies of magnetic order and superfluid density in antiferromagnetic NdFeAsO, $BaFe_2As_2$, and superconducting $Ba_{1-x}K_xFe_2As_2$," *Phys. Rev. B - Condens. Matter Mater. Phys.*, vol. 78, no. 21, pp. 1–5, 2008, ISSN: 10980121. DOI: 10.1103/PhysRevB.78.214503.

[162] T. Goko, A. A. Aczel, E. Baggio-Saitovitch, S. L. Budko, P. C. Canfield, J. P. Carlo, G. F. Chen, P. Dai, A. C. Hamann, W. Z. Hu, H. Kageyama, G. M. Luke, J. L. Luo, B. Nachumi, N. Ni, D. Reznik, D. R. Sanchez-Candela, A. T. Savici, K. J. Sikes, N. L. Wang, C. R. Wiebe, T. J. Williams, T. Yamamoto, W. Yu, and Y. J. Uemura, "Superconducting state coexisting with a phase-separated static magnetic order in $(Ba,K)Fe_2As_2$, $(Sr,Na)Fe_2As_2$, and $CaFe_2As_2$," *Phys. Rev. B - Condens. Matter Mater. Phys.*, vol. 80, no. 2, pp. 1–6, 2009, ISSN: 10980121. DOI: 10.1103/PhysRevB.80.024508.

[163] J. T. Park, D. S. Inosov, C. Niedermayer, G. L. Sun, D. Haug, N. B. Christensen, R. Dinnebier, A. V. Boris, A. J. Drew, L. Schulz, T. Shapoval, U. Wolff, V. Neu, X. Yang, C. T. Lin, B. Keimer, and V. Hinkov, "Electronic phase separation in the slightly underdoped iron pnictide superconductor $Ba_{1-x}K_xFe_2As_2$," *Phys. Rev. Lett.*, vol. 102, no. 11, pp. 1–4, 2009, ISSN: 00319007. DOI: 10.1103/PhysRevLett.102.117006. arXiv: 0811.2224.

[164] C. Bernhard, A. J. Drew, L. Schulz, V. K. Malik, M. Rössle, C. Niedermayer, T. Wolf, G. D. Varma, G. Mu, H.-H. Wen, H. Liu, G. Wu, and X. H. Chen, "Muon spin rotation study of magnetism and superconductivity in $BaFe_{2-x}Co_xAs_2$ and $Pr_{1-x}Sr_xFeAsO$," *New J. Phys.*, vol. 11, no. 5, p. 055 050, 2009. DOI: 10.1088/1367-2630/11/5/055050.

[165] P. Marsik, K. W. Kim, A. Dubroka, M. Rössle, V. K. Malik, L. Schulz, C. N. Wang, C. Niedermayer, A. J. Drew, M. Willis, T. Wolf, and C. Bernhard, "Coexistence and competition of magnetism and superconductivity on the nanometer scale in underdoped $BaFe_{1.89}Co_{0.11}As_2$," *Phys. Rev. Lett.*, vol. 105, no. 5, pp. 1–4, 2010, ISSN: 00319007. DOI: 10.1103/PhysRevLett.105.057001. arXiv: 1004.4860.

[166] Y. Laplace, J. Bobroff, F. Rullier-Albenque, D. Colson, and A. Forget, "Atomic coexistence of superconductivity and incommensurate magnetic order in the pnictide $Ba(Fe_{1-x}Co_x)_2As_2$," *Phys. Rev. B - Condens. Matter Mater. Phys.*, vol. 80, no. 14, pp. 1–4, 2009, ISSN: 10980121. DOI: 10.1103/PhysRevB.80.140501. arXiv: 0906.2125.

[167] F. Massee, Y. Huang, R. Huisman, S. De Jong, J. B. Goedkoop, and M. S. Golden, "Nanoscale superconducting-gap variations and lack of phase separation in optimally doped $BaFe_{1.86}Co_{0.14}As_2$," *Phys. Rev. B - Condens. Matter Mater. Phys.*, vol. 79, no. 22, pp. 1–4, 2009, ISSN: 10980121. DOI: 10.1103/PhysRevB.79.220517. arXiv: 0812.4539.

[168] H. Mayaffre, S. Krämer, M. Horvatić, C. Berthier, K. Miyagawa, K. Kanoda, and V. F. Mitrović, "Evidence of Andreev bound states as a hallmark of the FFLO phase in k-(BEDT-TTF)$_2$Cu(NCS)$_2$," *Nat. Phys.*, vol. 10, no. October, 2014, ISSN: 1745-2473. DOI: 10.1038/nphys3121.

[169] L. P. Gorkov and G. B. Teitelbaum, "Spatial inhomogeneities in iron pnictide superconductors: The formation of charge stripes," *Phys. Rev. B - Condens. Matter Mater. Phys.*, vol. 82, no. 2, pp. 1–4, 2010, ISSN: 10980121. DOI: 10.1103/PhysRevB.82.020510.

[170] K. Cho, H. Kim, M. A. Tanatar, Y. J. Song, Y. S. Kwon, W. A. Coniglio, C. C. Agosta, A. Gurevich, and R. Prozorov, "Anisotropic upper critical field and possible Fulde-Ferrel-Larkin- Ovchinnikov state in the stoichiometric pnictide superconductor LiFeAs," *Phys. Rev. B - Condens. Matter Mater. Phys.*, vol. 83, no. 6, pp. 1–4, 2011, ISSN: 10980121. DOI: 10.1103/PhysRevB.83.060502. arXiv: 1011.5126.

[171] L. Shan, Y.-L. Wang, B. Shen, B. Zeng, Y. Huang, A. Li, D. Wang, H. Yang, C. Ren, Q.-H. Wang, S. Pan, and H.-H. Wen, "Observation of lattice and Andreev bound states of vortices in $Ba_{0.6}K_{0.4}Fe_2As_2$ single crystals with scanning tunneling microscopy/spectroscopy," *Nat. Phys.*, vol. 7, no. 4, p. 18, 2010, ISSN: 1745-2473. DOI: 10.1038/nphys1908. arXiv: 1005.4038. [Online]. Available: http://arxiv.org/abs/1005.4038.

[172] S. Jiang, H. Xing, G. Xuan, Z. Ren, C. Wang, Z.-a. Xu, and G. Cao, "Superconductivity and local-moment magnetism in $Eu(Fe_{0.89}Co_{0.11})_2As_2$," *Phys. Rev. B*, no. November, p. 8, 2009, ISSN: 1098-0121. DOI: 10.1103/PhysRevB.80.184514. arXiv: 0911.0273. [Online]. Available: http://arxiv.org/abs/0911.0273.

[173] S. Zapf, H. S. Jeevan, T. Ivek, F. Pfister, F. Klingert, S. Jiang, D. Wu, P. Gegenwart, R. K. Kremer, and M. Dressel, "$EuFe_2(As_{1-x}P_x)_2$: Reentrant spin glass and superconductivity," *Phys. Rev. Lett.*, vol. 110, no. 23, pp. 1–5, 2013, ISSN: 00319007. DOI: 10.1103/PhysRevLett.110.237002. arXiv: arXiv:1305.5672v1.

[174] Y. Xiao, Y. Su, W. Schmidt, K. Schmalzl, C. M. N. Kumar, S. Price, T. Chatterji, R. Mittal, L. J. Chang, S. Nandi, N. Kumar, S. K. Dhar, A. Thamizhavel, and T. Brueckel, "Field-induced spin reorientation and giant spin-lattice coupling in $EuFe_2As_2$," *Phys. Rev. B - Condens. Matter Mater. Phys.*, vol. 81, no. 22, p. 220 406, Jun. 2010, ISSN: 10980121. DOI: 10.1103/PhysRevB.81.220406. arXiv: 1004.0145. [Online]. Available: http://link.aps.org/doi/10.1103/PhysRevB.81.220406.

[175] S. Jiang, Y. Luo, Z. Ren, Z. Zhu, C. Wang, X. Xu, Q. Tao, G. Cao, and Z. Xu, "Metamagnetic transition in $EuFe_2As_2$ single crystals," *New J. Phys.*, vol. 11, 2009, ISSN: 13672630. DOI: 10.1088/1367-2630/11/2/025007. arXiv: arXiv:0808.0325v1.

[176] U. Keller, G. W. 'Thooft, W. H. Knox, and J. E. Cunningham, "Femtosecond pulses from a continuously self-starting passively mode-locked Ti:sapphire laser," *Opt. Lett.*, vol. 16, no. 13, pp. 1022–1024, 1991, ISSN: 0146-9592. DOI: 10.1364/OL.16.001022.

[177] J. Demsar, R. D. Averitt, A. J. Taylor, V. V. Kabanov, W. N. Kang, H. J. Kim, E. M. Choi, and S. I. Lee, "Pair-breaking and superconducting state recovery dynamics in MgB_2," *Phys. Rev. Lett.*, vol. 91, no. 26 Pt 1, p. 267 002, 2003, ISSN: 0031-9007. DOI: 10.1103/PhysRevLett.91.267002. arXiv: 0310379 [cond-mat].

[178] V. V. Kabanov, J. Demsar, B. Podobnik, and D. Mihailovic, "Quasiparticle relaxation dynamics in superconductors with different gap structures: Theory and experiments on $YBa_2Cu_3O_{7-\delta}$," *Phys. Rev. B*, vol. 59, no. 2, p. 12, 1999, ISSN: 1098-0121. DOI: 10.1103/PhysRevB.59.1497. arXiv: 9809333 [cond-mat]. [Online]. Available: http://arxiv.org/abs/cond-mat/9809333.

[179] D. Dvorsek, V. V. Kabanov, J. Demsar, S. M. K. J. Karpinski, and D. Mihailovic, "Femtosecond quasiparticle relaxation dynamics and probe polarization anisotropy in $YBa_2Cu_4O_8$," *Phys. Rev. B*, vol. 66, p. 4, 2002, ISSN: 0163-1829. DOI: 10.1103/PhysRevB.66.020510. arXiv: 0203614 [cond-mat]. [Online]. Available: http://arxiv.org/abs/cond-mat/0203614.

[180] S. Anisimov, B. Kapeliovich, and T. Perel-man, "Electron emission from metal surfaces exposed to ultrashort laser pulses," *J. Exp. Theor. Phys.*, vol. 66, pp. 375–377, 1974.

[181] P. Jacobsson and B. Sundqvist, "Thermal conductivity and electrical resistivity of gadolinium as functions of pressure and temperature," *Phys. Rev. B*, vol. 40, no. 14, 1989. DOI: http://dx.doi.org/10.1103/PhysRevB.40.9541.

[182] V. V. Baranov and V. V. Kabanov, "Theory of electronic relaxation in a metal excited by an ultrashort optical pump," *Phys. Rev. B - Condens. Matter Mater. Phys.*, vol. 89, no. August 2013, pp. 1–11, 2014, ISSN: 10980121. DOI: 10.1103/PhysRevB.89.125102.

[183] V. V. Kabanov and A. S. Alexandrov, "Electron relaxation in metals: Theory and exact analytical solutions," *Phys. Rev. B - Condens. Matter Mater. Phys.*, vol. 78, no. 17, pp. 1–8, 2008, ISSN: 10980121. DOI: 10.1103/PhysRevB.78.174514. arXiv: 0809.0818.

[184] R. H. M. Groeneveld, R. Sprik, and A. Lagendijk, "Femtosecond spectroscopy of electron-electron and electron-phonon energy relaxation in Ag and Au," *Phys. Rev. B*, vol. 51, no. 17, pp. 11 433–11 445, 1995, ISSN: 01631829. DOI: 10.1103/PhysRevB.51.11433.

[185] L. Perfetti, P. A. Loukakos, M. Lisowski, U. Bovensiepen, H. Eisaki, and M. Wolf, "Ultrafast electron relaxation in superconducting $Bi_2Sr_2CaCu_2O_{8+d}$ by time-resolved photoelectron spectroscopy," *Phys. Rev. Lett.*, vol. 99, no. NOVEMBER, pp. 1–4, 2007, ISSN: 00319007. DOI: 10.1103/PhysRevLett.99.197001.

[186] C. Gadermaier, A. S. Alexandrov, V. V. Kabanov, P. Kusar, T. Mertelj, X. Yao, C. Manzoni, D. Brida, G. Cerullo, and D. Mihailovic, "Electron-phonon coupling in high-temperature cuprate superconductors determined from electron relaxation rates," *Phys. Rev. Lett.*, vol. 105, no. 25, pp. 1–4, 2010, ISSN: 00319007. DOI: 10.1103/PhysRevLett.105.257001. arXiv: 0902.1636.

[187] J. Bardeen, L. N. Cooper, and J. R. Schrieffer, "Theory of superconductivity," *Phys. Rev.*, vol. 108, no. 5, pp. 1175–1204, 1957, ISSN: 0031899X. DOI: 10.1103/PhysRev.108.1175.

[188] B. Mansart, D. Boschetto, A. Savoia, F. Rullier-Albenque, F. Bouquet, E. Papalazarou, A. Forget, D. Colson, A. Rousse, and M. Marsi, "Ultrafast transient response and electron-phonon coupling in the iron-pnictide superconductor $Ba(Fe_{1-x}Co_x)_2As_2$," *Phys. Rev. B - Condens. Matter Mater. Phys.*, vol. 82, pp. 1–5, 2010, ISSN: 10980121. DOI: 10.1103/PhysRevB.82.024513.

[189] A. Lanzara, P. V. Bogdanov, X. J. Zhou, S. A. Kellar, D. L. Feng, E. D. Lu, T. Yoshida, H. Eisaki, A. Fujimori, K. Kishio, J. I. Shimoyama, T. Noda, S. Uchida, Z. Hussain, and Z. X. Shen, "Evidence for ubiquitous strong electron-phonon coupling in high-temperature superconductors.," *Nature*, vol. 412, no. 6846, pp. 510–514, 2001, ISSN: 0028-0836. DOI: 10.1038/35087518. arXiv: 0102227 [cond-mat].

[190] A. Rothwarf and B. N. Taylor, "Measurement of recombination lifetimes in superconductors," *Phys. Rev. Lett.*, vol. 19, no. 1, pp. 27–30, 1967, ISSN: 00319007. DOI: 10.1103/PhysRevLett.19.27.

[191] V. V. Kabanov, J. Demsar, and D. Mihailovic, "Kinetics of a superconductor excited with a femtosecond optical pulse," *Phys. Rev. Lett.*, vol. 95, no. 14, pp. 1–4, 2005, ISSN: 00319007. DOI: 10.1103/PhysRevLett.95.147002. arXiv: 0501711 [cond-mat].

[192] L. Perfetti, P. A. Loukakos, M. Lisowski, U. Bovensiepen, H. Berger, S. Biermann, P. S. Cornaglia, A. Georges, and M. Wolf, "Time evolution of the electronic structure of $1T$-TaS_2 through the insulator-metal transition," *Phys. Rev. Lett.*, vol. 97, no. 6, pp. 1–4, 2006, ISSN: 00319007. DOI: 10.1103/PhysRevLett.97.067402.

[193] R. V. Yusupov, T. Mertelj, J. H. Chu, I. R. Fisher, and D. Mihailovic, "Single-particle and collective mode couplings associated with 1- and 2-directional electronic ordering in metallic RTe$_3$ (R=Ho,Dy,Tb)," *Phys. Rev. Lett.*, vol. 101, no. 24, pp. 1–4, 2008, ISSN: 00319007. DOI: 10.1103/PhysRevLett.101.246402. arXiv: 0807.1022.

[194] N. Gedik, P. Blake, R. C. Spitzer, J. Orenstein, R. Liang, D. A. Bonn, and W. N. Hardy, "Single-quasiparticle stability and quasiparticle-pair decay in YBa $_2$Cu$_3$O$_{6.5}$," *Phys. Rev. B - Condens. Matter Mater. Phys.*, vol. 70, pp. 1–13, 2004, ISSN: 01631829. DOI: 10.1103/PhysRevB.70.014504. arXiv: 0309121 [cond-mat].

[195] J. Demsar, B. Podobnik, V. V. Kabanov, D. Mihailovic, and T. Wolf, "The superconducting gap Δ_c, the pseudogap Δ_p and pair fluctuations above T_c in overdoped $Y_{1-x}Ca_xBa_2Cu_3O_{7-d}$ from femtosecond time-domain spectroscopy," *Phys. Rev. Lett.*, p. 4, 1999, ISSN: 0031-9007. DOI: 10.1103/PhysRevLett.82.4918. arXiv: 9905026 [cond-mat]. [Online]. Available: http://arxiv.org/abs/cond-mat/9905026.

[196] D. C. Mattis and J. Bardeen, "Theory of the anomalous skin effect in normal and superconducting metals," *Phys. Rev.*, vol. 111, no. 2, pp. 412–417, 1958, ISSN: 0031899X. DOI: 10.1103/PhysRev.111.412.

[197] V. M. Krasnov, A. Yurgens, D. Winkler, P. Delsing, and T. Claeson, "Evidence for coexistence of the superconducting gap and the pseudogap in Bi-2212 from intrinsic tunneling spectroscopy," *Phys. Rev. Lett.*, vol. 84, pp. 5860–5863, 2000, ISSN: 00319007. DOI: 10.1103/PhysRevLett.84.5860. arXiv: 0102252 [cond-mat].

[198] L. Stojchevska, P. Kusar, T. Mertelj, V. V. Kabanov, Y. Toda, X. Yao, and D. Mihailovic, "Mechanisms of nonthermal destruction of the superconducting state and melting of the charge-density-wave state by femtosecond laser pulses," *Phys. Rev. B - Condens. Matter Mater. Phys.*, vol. 84, no. 18, pp. 1–5, 2011, ISSN: 10980121. DOI: 10.1103/PhysRevB.84.180507. arXiv: 1109.5546.

[199] F. Schmitt, P. S. Kirchmann, U. Bovensiepen, R. G. Moore, L. Rettig, M. Krenz, J.-H. Chu, N. Ru, L. Perfetti, D. H. Lu, M. Wolf, I. R. Fisher, and Z.-X. Shen, "Transient electronic structure and melting of a charge density wave in $TbTe_3$," *Science*, vol. 321, no. 5896, pp. 1649–1652, 2008, ISSN: 0036-8075. DOI: 10.1126/science.1160778.

[200] P. Kusar, T. Mertelj, V. V. Kabanov, and D. Mihailovic, "Coherent trajectory through the normal-to-superconducting transition reveals ultrafast vortex dynamics in a superconductor.," *ArXive*, pp. 1–5, 2012. arXiv: arXiv:1207.2879v2.

[201] E. Beaurepaire, J.-C. Merle, A. Daunois, and J.-Y. Bigot, "Ultrafast spin dynamics in ferromagnetic nickel," *Phys. Rev. Lett.*, no. 22, p. 4, 1996, ISSN: 0163-1829. DOI: 10.1103/PhysRevB.58.R5920. arXiv: 9709264 [cond-mat]. [Online]. Available: http://arxiv.org/abs/cond-mat/9709264.

[202] A. Scholl, L. Baumgarten, R. Jacquemin, and W. Eberhardt, "Ultrafast spin dynamics of ferromagnetic thin films observed by fs spin-resolved two-photon photoemission," *Phys. Rev. Lett.*, vol. 79, no. 25, pp. 5146–5149, 1997, ISSN: 0031-9007. DOI: 10.1103/PhysRevLett.79.5146.

[203] T. Ostler, J. Barker, R. Evans, R. Chantrell, U. Atxitia, O. Chubykalo-Fesenko, S. El Moussaoui, L. Le Guyader, E. Mengotti, L. Heyderman, F. Nolting, A. Tsukamoto, A. Itoh, D. Afanasiev, B. Ivanov, A. Kalashnikova, K. Vahaplar, J. Mentink, A. Kirilyuk, T. Rasing, and A. Kimel, "Ultrafast heating as a sufficient stimulus for magnetization reversal in a ferrimagnet," *Nat. Commun.*, vol. 3, p. 666, 2012, ISSN: 2041-1723. DOI: 10.1038/ncomms1666. [Online]. Available: http://dx.doi.org/10.1038/ncomms1666.

[204] P. Prelovsek, J. Kokalj, Z. Lenarcic, and R. H. McKenzie, "Holon-doublon binding as the mechanism for the Mott transition," *ArXive*, pp. 2–6, 2015. arXiv: arXiv:1505.01498v1.

[205] J. Kogoj, Z. Lenarcic, D. Golez, M. Mierzejewski, P. Prelovsek, and J. Bonca, "Multistage dynamics of the spin-lattice polaron formation," *Phys. Rev. B*, vol. 90, no. 12, pp. 1–6, 2014, ISSN: 1098-0121. DOI: 10.1103/PhysRevB.90.125104. [Online]. Available: http://link.aps.org/doi/10.1103/PhysRevB.90.125104.

[206] A. V. Kimel, A. Kirilyuk, A. Tsvetkov, R. V. Pisarev, and T. Rasing, "Laser-induced ultrafast spin reorientation in the antiferromagnet $TmFeO_3$," *Nature*, vol. 429, no. 6994, pp. 850–853, 2004, ISSN: 0028-0836. DOI: 10.1038/nature02659.

[207] A. V. Kimel, A. Kirilyuk, P. A. Usachev, R. V. Pisarev, A. M. Balbashov, and T. Rasing, "Ultrafast non-thermal control of magnetization by instantaneous photomagnetic pulses," *Nature*, vol. 435, no. 7042, pp. 655–657, 2005, ISSN: 0028-0836. DOI: 10.1038/nature03564.

[208] A. V. Kimel, A. Kirilyuk, F. Hansteen, R. V. Pisarev, and T. Rasing, "Nonthermal optical control of magnetism and ultrafast laser-induced spin dynamics in solids," *J. Phys. Condens. Matter*, vol. 19, no. 4, p. 043 201, 2007, ISSN: 0953-8984. DOI: 10.1088/0953-8984/19/4/043201.

[209] T. Mertelj, P. Kusar, V. V. Kabanov, L. Stojchevska, N. D. Zhigadlo, S. Katrych, Z. Bukowski, J. Karpinski, S. Weyeneth, and D. Mihailovic, "Quasiparticle relaxation dynamics in spin-density-wave and superconducting $SmFeAsO_{1-x}F_x$ single crystals," *Phys. Rev. B - Condens. Matter Mater. Phys.*, vol. 81, pp. 1–9, 2010, ISSN: 10980121. DOI: 10.1103/PhysRevB.81.224504. arXiv: arXiv:1001.1047v2.

[210] S. Kumar, L. Harnagea, S. Wurmehl, B. Buchner, and A. K. Sood, "Acoustic and optical phonon dynamics from femtosecond time-resolved optical spectroscopy of superconducting iron pnictide $Ca(Fe_{0.944}Co_{0.056})_2As_2$," *Europhys. Lett.*, vol. 57007, p. 6, 2012, ISSN: 0295-5075. DOI: 10.1209/0295-5075/100/57007. arXiv: 1209.3174. [Online]. Available: http://arxiv.org/abs/1209.3174.

[211] E. E. M. Chia, D. Talbayev, J. X. Zhu, H. Q. Yuan, T. Park, J. D. Thompson, C. Panagopoulos, G. F. Chen, J. L. Luo, N. L. Wang, and A. J. Taylor, "Ultrafast pump-probe study of phase separation and competing orders in the underdoped (Ba,K)Fe_2As_2 superconductor," *Phys. Rev. Lett.*, vol. 104, no. January, pp. 1–4, 2010, ISSN: 00319007. DOI: 10.1103/PhysRevLett.104.027003. arXiv: 0809.4097.

[212] D. H. Torchinsky, G. F. Chen, J. L. Luo, N. L. Wang, and N. Gedik, "Band-dependent quasiparticle dynamics in single crystals of the $Ba_{0.6}K_{0.4}Fe_2As_2$ superconductor revealed by pump-probe spectroscopy," *Phys. Rev. Lett.*, vol. 105, no. July, pp. 1–4, 2010, ISSN: 00319007. DOI: 10.1103/PhysRevLett.105.027005.

[213] D. H. Torchinsky, J. W. McIver, D. Hsieh, G. F. Chen, J. L. Luo, N. L. Wang, and N. Gedik, "Band-dependent quasiparticle dynamics in the hole-doped Ba-122 iron pnictides," *J. Phys. Chem. Solids*, vol. 72, no. 5, pp. 519–522, 2011, ISSN: 00223697. DOI: 10.1016/j.jpcs.2010.10.066. [Online]. Available: http://dx.doi.org/10.1016/j.jpcs.2010.10.066.

[214] S. Kumar, L. Harnagea, S. Wurmehl, B. Buchner, and A. K. Sood, "Ultrafast quasiparticle relaxation dynamics in superconducting iron pnictide $Ca(Fe_{0.944}Co_{0.056})_2As_2$," *Solid State Commun.*, vol. 160, pp. 8–12, 2013, ISSN: 00381098. DOI: 10.1016/j.ssc.2013.02.008. [Online]. Available: http://dx.doi.org/10.1016/j.ssc.2013.02.008.

[215] D. C. Johnston, "The puzzle of high-temperature superconductivity in layered iron pnictides and chalcogenides," *Adv. Phys.*, no. April 2015, pp. 803–1061, 2010, ISSN: 0001-8732. DOI: 10.1080/00018732.2010.513480. arXiv: 1005.4392. [Online]. Available: http://arxiv.org/abs/1005.4392.

[216] L. Rettig, S. O. Mariager, A. Ferrer, S. Grübel, J. A. Johnson, J. Rittmann, T. Wolf, S. L. Johnson, G. Ingold, P. Beaud, and U. Staub, "Ultrafast structural dynamics of the Fe-pnictide parent compound $BaFe_2As_2$," *Phys. Rev. Lett.*, vol. 114, no. 6, pp. 1–5, 2015, ISSN: 0031-9007. DOI: 10.1103/PhysRevLett.114.067402. [Online]. Available: http://link.aps.org/doi/10.1103/PhysRevLett.114.067402.

[217] I. Avigo, R. Cortes, L. Rettig, S. Thirupathaiah, H. S. Jeevan, P. Gegenwart, T. Wolf, M. Ligges, M. Wolf, J. Fink, and U. Bovensiepen, "Coherent excitations and electron-phonon coupling in Ba/$EuFe_2As_2$ compounds investigated by femtosecond time- and angle-resolved photoemission spectroscopy," *J. Phys. Condens. Matter*, vol. 25, p. 094 003, 2013, ISSN: 0953-8984. DOI: 10.1088/0953-8984/25/9/094003. arXiv: 1204.4069.

[218] L. X. Yang, G. Rohde, T. Rohwer, A. Stange, K. Hanff, C. Sohrt, L. Rettig, R. Cortés, F. Chen, D. L. Feng, T. Wolf, B. Kamble, I. Eremin, T. Popmintchev, M. M. Murnane, H. C. Kapteyn, L. Kipp, J. Fink, M. Bauer, U. Bovensiepen, and K. Rossnagel, "Ultrafast modulation of the chemical potential in $BaFe_2As_2$ by coherent phonons," *Phys. Rev. Lett.*, vol. 112, no. May, pp. 1–6, 2014, ISSN: 10797114. DOI: 10.1103/PhysRevLett.112.207001. arXiv: arXiv:1312.6025v1.

[219] P. K. Dixon and L. Wu, "Broadband digital lock-in amplifier techniques," *Rev. Sci. Instrum.*, vol. 60, no. 10, pp. 3329–3336, 1989, ISSN: 00346748. DOI: 10.1063/1.1140523.

[220] L. Stojchevska, P. Kusar, T. Mertelj, V. V. Kabanov, X. Lin, G. H. Cao, Z. A. Xu, and D. Mihailovic, "Electron-phonon coupling and the charge gap of spin-density wave iron-pnictide materials from quasiparticle relaxation dynamics," *Phys. Rev. B*, vol. 82, no. 1, p. 012 505, Jul. 2010. DOI: 10.1103/PhysRevB.82.012505.

[221] T. Mertelj, R. Mamin, R. Yusupov, and D. Mihailovic, "Ultrafast phase separation dynamics in $La_{0.875}Sr_{0.125}MnO_3$ single crystals," *Phys. Rev. B*, vol. 83, no. 11, pp. 1–4, 2011, ISSN: 1098-0121. DOI: 10.1103/PhysRevB.83.113103.

[222] W.-H. Jiao, Q. Tao, J.-K. Bao, Y.-L. Sun, C.-M. Feng, Z.-A. Xu, I. Nowik, I. Felner, and G.-H. Cao, "Anisotropic superconductivity in $Eu(Fe_{0.75}Ru_{0.25})_2As_2$ ferromagnetic superconductor," *EPL (Europhysics Lett.*, vol. 95, no. 6, p. 67 007, Sep. 2011, ISSN: 0295-5075. DOI: 10.1209/0295-5075/95/67007. [Online]. Available: http://stacks.iop.org/0295-5075/95/i=6/a=67007?key=crossref.6747a408e118e4a60640b682e0d74b01.

[223] J. H. Chu, J. G. Analytis, C. Kucharczyk, and I. R. Fisher, "Determination of the phase diagram of the electron-doped superconductor $Ba(Fe_{1-x}Co_x)_2As_2$," *Phys. Rev. B - Condens. Matter Mater. Phys.*, vol. 79, no. 1, pp. 1–6, 2009, ISSN: 10980121. DOI: 10.1103/PhysRevB.79.014506.

[224] K. H. Ahn, M. J. Graf, S. A. Trugman, J. Demsar, R. D. Averitt, J. L. Sarrao, and A. J. Taylor, "Ultrafast quasiparticle relaxation dynamics in normal metals and heavy fermion materials," *Phys. Rev. B*, no. August 2003, p. 10, 2003, ISSN: 1098-0121. DOI: 10.1103/PhysRevB.69.045114. arXiv: 0308213 [cond-mat]. [Online]. Available: http://arxiv.org/abs/cond-mat/0308213.

[225] R. H. M. Groeneveld, R. Sprik, and A. Lagendijk, "Effect of a nonthermal electron distribution on the electron-phonon energy relaxation process in noble metals," *Phys. Rev. B*, vol. 45, no. 9, pp. 5079–5082, 1992, ISSN: 01631829. DOI: 10.1103/PhysRevB.45.5079.

[226] M. Rahlenbeck, G. L. Sun, D. L. Sun, C. T. Lin, B. Keimer, and C. Ulrich, "Phonon anomalies in pure and underdoped $R_{1-x}K_xFe_2$ As_2 (R=Ba, Sr) investigated by Raman light scattering," *Phys. Rev. B - Condens. Matter Mater. Phys.*, vol. 80, no. 6, pp. 1–5, 2009, ISSN: 10980121. DOI: 10.1103/PhysRevB.80.064509. arXiv: 0907.0560.

[227] T. Stevens, J. Kuhl, and R. Merlin, "Coherent phonon generation and the two stimulated Raman tensors," *Phys. Rev. B*, vol. 65, no. 14, pp. 3–6, 2002, ISSN: 0163-1829. DOI: 10.1103/PhysRevB.65.144304.

[228] K. Ishioka and O. V. Misochko, "Coherent lattice oscillations in solids and their optical control Part I. Fundamentals and optical detection techniques," *Springer Ser. Chem. Phys.*, vol. 98, pp. 23–46, 2010, ISSN: 01726218. DOI: 10.1007/978-3-642-03825-9_2.

[229] I. Bozovic, M. Schneider, Y. Xu, R. Sobolewski, Y. H. Ren, G. Lüpke, J. Demsar, A. J. Taylor, and M. Onellion, "Long-lived coherent acoustic waves generated by femtosecond light pulses," *Phys. Rev. B - Condens. Matter Mater. Phys.*, vol. 69, no. 13, pp. 3–6, 2004, ISSN: 01631829. DOI: 10.1103/PhysRevB.69.132503.

[230] D. Lim, R. D. Averitt, J. Demsar, A. J. Taylor, N. Hur, and S. W. Cheong, "Coherent acoustic phonons in hexagonal manganite $LuMnO_3$," *Appl. Phys. Lett.*, vol. 83, no. 23, pp. 4800–4802, 2003, ISSN: 00036951. DOI: 10.1063/1.1630847.

[231] M. Hase, K. Ishioka, J. Demsar, K. Ushida, and M. Kitajima, "Ultrafast dynamics of coherent optical phonons and nonequilibrium electrons in transition metals," *Phys. Rev. B - Condens. Matter Mater. Phys.*, vol. 71, no. 18, pp. 1–2, 2005, ISSN: 10980121. DOI: 10.1103/PhysRevB.71.184301. arXiv: 0504540 [cond-mat].

[232] K. Kuroki, H. Usui, S. Onari, R. Arita, and H. Aoki, "Pnictogen height as a possible switch between high-T_c nodeless and low-T_c nodal pairings in the iron-based superconductors," *Phys. Rev. B - Condens. Matter Mater. Phys.*, vol. 79, no. 22, pp. 33–36, 2009, ISSN: 10980121. DOI: 10.1103/PhysRevB.79.224511. arXiv: 0904.2612.

[233] W. Hu, S. Kaiser, D. Nicoletti, C. R. Hunt, I. Gierz, M. C. Hoffmann, M. Le Tacon, T. Loew, B. Keimer, and A. Cavalleri, "Optically enhanced coherent transport in $YBa_2Cu_3O_{6.5}$ by ultrafast redistribution of interlayer coupling.," *Nat. Mater.*, vol. 13, no. May, pp. 705–711, 2014, ISSN: 1476-1122. DOI: 10.1038/nmat3963. arXiv: 1308.3204. [Online]. Available: http://www.ncbi.nlm.nih.gov/pubmed/24813422.

[234] P. Kusar, J. Demsar, D. Mihailovic, and S. Sugai, "A systematic study of femtosecond quasiparticle relaxation processes in $La_{2-x}Sr_xCuO_4$," *Phys. Rev. B - Condens. Matter Mater. Phys.*, vol. 72, no. 1, pp. 1–6, 2005, ISSN: 10980121. DOI: 10.1103/PhysRevB.72.014544.

[235] M. .-.-H. Julien, H. Mayaffre, M. Horvatic, C. Berthier, X. D. Zhang, W. Wu, G. F. Chen, N. L. Wang, and J. L. Luo, "Homogeneous vs. inhomogeneous coexistence of magnetic order and superconductivity probed by NMR in Co and K doped iron pnictides," *EPL (Europhysics Lett.*, vol. 37001, 2009, ISSN: 0295-5075. DOI: 10.1209/0295-5075/87/37001. arXiv: 0906.3708. [Online]. Available: http://arxiv.org/abs/0906.3708.

[236] R. A. Kaindl, M. Woerner, T. Elsaesser, D. Smith, J. Ryan, G. Farnan, M. McCurry, and D. Walmsley, "Ultrafast mid-infrared response of $YBa_2Cu_3O_{7-d}$," *Science (80- .)*., vol. 287, no. 5452, pp. 470–473, Jan. 2000, ISSN: 00368075. DOI: 10.1126/science.287.5452.470. [Online]. Available: http://www.sciencemag.org/cgi/doi/10.1126/science.287.5452.470.

[237] R. D. Averitt, G. Rodriguez, A. I. Lobad, J. L. W. Siders, S. A. Trugman, and A. J. Taylor, "Nonequilibrium superconductivity and quasiparticle dynamics in $YBa_2Cu_3O_{7-d}$," *Phys. Rev. B*, vol. 63, no. 14, p. 140 502, 2001, ISSN: 0163-1829. DOI: 10.1103/PhysRevB.63.140502. [Online]. Available: http://link.aps.org/doi/10.1103/PhysRevB.63.140502.

[238] G. P. Segre, N. Gedik, J. Orenstein, D. A. Bonn, R. Liang, and W. N. Hardy, "Photoinduced changes of reflectivity in single crystals of $YBa_2Cu_3O_{6.5}$ (ortho II)," *Phys. Rev. Lett.*, vol. 88, no. 13, p. 137 001, 2002, ISSN: 0031-9007. DOI: 10.1103/PhysRevLett.88.137001. arXiv: 0107325 [cond-mat].

[239] E. E. M. Chia, J. X. Zhu, H. J. Lee, N. Hur, N. O. Moreno, E. D. Bauer, T. Durakiewicz, R. D. Averitt, J. L. Sarrao, and A. J. Taylor, "Quasiparticle relaxation across the spin-density-wave gap in the itinerant antiferromagnet $UNiGa_5$," *Phys. Rev. B - Condens. Matter Mater. Phys.*, vol. 74, no. 14, pp. 5–8, 2006, ISSN: 10980121. DOI: 10.1103/PhysRevB.74.140409. arXiv: 0605240 [cond-mat].

[240] Y. H. Liu, Y. Toda, K. Shimatake, N. Momono, M. Oda, and M. Ido, "Direct observation of the coexistence of the pseudogap and superconducting quasiparticles in $Bi_2Sr_2CaCu_2O_{8+y}$ by time-resolved optical spectroscopy," *Phys. Rev. Lett.*, vol. 101, no. 13, pp. 1–4, 2008, ISSN: 00319007. DOI: 10.1103/PhysRevLett.101.137003. arXiv: 0802.2994.

[241] G. Coslovich, C. Giannetti, F. Cilento, S. Dal Conte, G. Ferrini, P. Galinetto, M. Greven, H. Eisaki, M. Raichle, R. Liang, A. Damascelli, and F. Parmigiani, "Evidence for a photoinduced nonthermal superconducting-to-normal-state phase transition in overdoped $Bi_2Sr_2Ca_{0.92}Y_{0.08}Cu_2O_{8+d}$," *Phys. Rev. B - Condens. Matter Mater. Phys.*, vol. 83, no. 6, pp. 1–9, 2011, ISSN: 10980121. DOI: 10.1103/PhysRevB.83.064519. arXiv: 1005.4320.

[242] J. Demsar, R. D. Averitt, K. H. Ahn, M. J. Graf, S. A. Trugman, V. V. Kabanov, J. L. Sarrao, and A. J. Taylor, "Quasiparticle relaxation dynamics in heavy fermion compounds," *Phys. Rev. Lett.*, vol. 91, no. 2, p. 027 401, 2003, ISSN: 0031-9007. DOI: 10.1103/PhysRevLett.91.027401. arXiv: 0305597 [cond-mat].

[243] R. Cortés, L. Rettig, Y. Yoshida, H. Eisaki, M. Wolf, and U. Bovensiepen, "Momentum-resolved ultrafast electron dynamics in superconducting $Bi_2Sr_2CaCu_2O_{8+d}$," *Phys. Rev. Lett.*, vol. 107, no. August, pp. 1–4, 2011, ISSN: 0031-9007. DOI: 10.1103/PhysRevLett.107.097002.

[244] C. L. Smallwood, J. P. Hinton, C. Jozwiak, W. Zhang, J. D. Koralek, H. Eisaki, D.-H. Lee, J. Orenstein, and A. Lanzara, "Tracking Cooper pairs in a cuprate superconductor by ultrafast angle-resolved photoemission," *Science (80-.).*, vol. 336, pp. 1137–1139, 2012, ISSN: 0036-8075. DOI: 10.1126/science.1217423. arXiv: 1206.2300.

[245] C. Gadermaier, A. S. Alexandrov, V. V. Kabanov, P. Kusar, T. Mertelj, X. Yao, C. Manzoni, D. Brida, G. Cerullo, and D. Mihailovic, "Electron-phonon coupling in high-temperature cuprate superconductors determined from electron relaxation rates," *Phys. Rev. Lett.*, vol. 105, no. 25, p. 257 001, Dec. 2010. DOI: 10.1103/PhysRevLett.105.257001.

[246] C. Giannetti, F. Cilento, S. Dal Conte, G. Coslovich, G. Ferrini, H. Molegraaf, M. Raichle, R. Liang, H. Eisaki, M. Greven, A. Damascelli, D. van der Marel, and F. Parmigiani, "Revealing the high-energy electronic excitations underlying the onset of high-temperature superconductivity in cuprates.," *Nat. Commun.*, vol. 2, no. May, p. 353, 2011, ISSN: 2041-1723. DOI: 10.1038/ncomms1354. arXiv: 1105.2508. [Online]. Available: http://dx.doi.org/10.1038/ncomms1354.

[247] A. Charnukha, D. Pröpper, T. I. Larkin, D. L. Sun, Z. W. Li, C. T. Lin, T. Wolf, B. Keimer, and A. V. Boris, "Spin density wave induced anomalies in the optical conductivity of AFe_2As_2, (A=Ca, Sr, Ba) single-crystalline iron pnictides," *Phys. Rev. B - Condens. Matter Mater. Phys.*, vol. 88, pp. 1–11, 2013, ISSN: 10980121. DOI: 10.1103/PhysRevB.88.184511. arXiv: 1402.0325.

[248] J. G. Analytis, R. D. McDonald, J. H. Chu, S. C. Riggs, A. F. Bangura, C. Kucharczyk, M. Johannes, and I. R. Fisher, "Quantum oscillations in the parent pnictide $BaFe_2As_2$: Itinerant electrons in the reconstructed state," *Phys. Rev. B - Condens. Matter Mater. Phys.*, vol. 80, no. 6, pp. 1–5, 2009, ISSN: 10980121. DOI: 10.1103/PhysRevB.80.064507. arXiv: 0902.1172.

[249] D. Wu, N. Barišić, N. Drichko, S. Kaiser, A. Faridian, M. Dressel, S. Jiang, Z. Ren, L. J. Li, G. H. Cao, Z. A. Xu, H. S. Jeevan, and P. Gegenwart, "Effects of the magnetic orderings on the dynamical conductivity: optical investigations of $EuFe_2As_2$ single crystals," *Phys. Rev. B*, vol. 75, no. 155103, p. 10, 2009. DOI: 10.1103/PhysRevB.79.155103. arXiv: 0903.0575. [Online]. Available: http://arxiv.org/abs/0903.0575.

[250] C. Gadermaier, V. Kabanov, A. Alexandrov, L. Stojchevska, T. Mertelj, C. Manzoni, G. Cerullo, N. Zhigadlo, J. Karpinski, Y. Cai, *et al.*, "High superconducting critical temperatures depend universally on the electron-phonon interaction strength," *Arxiv preprint arXiv:1205.4978*, 2012.

[251] M. Zbiri, R. Mittal, S. Rols, Y. Su, Y. Xiao, H. Schober, S. L. Chaplot, M. R. Johnson, T. Chatterji, Y. Inoue, S. Matsuishi, H. Hosono, and T. Brueckel, "Magnetic lattice dynamics of the oxygen-free FeAs pnictides: how sensitive are phonons to magnetic ordering?" *J. Phys. Condens. Matter*, vol. 22, p. 315 701, 2010, ISSN: 0953-8984. DOI: 10.1088/0953-8984/22/31/315701. arXiv: 1007.1711.

[252] R. A. Ewings, T. G. Perring, R. I. Bewley, T. Guidi, M. J. Pitcher, D. R. Parker, S. J. Clarke, and A. T. Boothroyd, "High-energy spin excitations in $BaFe_2As_2$ observed by inelastic neutron scattering," *Phys. Rev. B - Condens. Matter Mater. Phys.*, vol. 78, pp. 2–5, 2008, ISSN: 10980121. DOI: 10.1103/PhysRevB.78.220501.

[253] R. A. Ewings, T. G. Perring, J. Gillett, S. D. Das, S. E. Sebastian, a. E. Taylor, T. Guidi, and A. T. Boothroyd, "Itinerant spin excitations in $SrFe_2As_2$ measured by inelastic neutron scattering," *Phys. Rev. B - Condens. Matter Mater. Phys.*, vol. 83, pp. 1–6, 2011, ISSN: 10980121. DOI: 10.1103/PhysRevB.83.214519. arXiv: 1011.3831.

[254] S. Sugai, Y. Mizuno, R. Watanabe, T. Kawaguchi, K. Takenaka, H. Ikuta, K. Kiho, M. Nakajima, C. H. Lee, A. Iyo, H. Eisaki, and S. Uchida, "Selective Raman scattering detection of the Dirac node and theaAnti-node of the spin density wave gap and magnetic excitations in $BaFe_2As_2$," *J. Supercond. Nov. Magn.*, vol. 26, pp. 1179–1183, 2013, ISSN: 1557-1939. DOI: 10.1007/s10948-012-1966-6. [Online]. Available: http://link.springer.com/10.1007/s10948-012-1966-6.

[255] H. Schäfer, V. V. Kabanov, M. Beyer, K. Biljakovic, and J. Demsar, "Disentanglement of the electronic and lattice parts of the order parameter in a 1D charge density wave system probed by femtosecond spectroscopy," *Phys. Rev. Lett.*, vol. 105, no. August, pp. 1–4, 2010, ISSN: 00319007. DOI: 10.1103/PhysRevLett.105.066402. arXiv: 1007.2267.

[256] H. Schaefer, V. V. Kabanov, and J. Demsar, "Collective modes in quasi-one-dimensional charge-density wave systems probed by femtosecond time-resolved optical studies," *Phys. Rev. B - Condens. Matter Mater. Phys.*, vol. 89, pp. 1–13, 2014, ISSN: 10980121. DOI: 10.1103/PhysRevB.89.045106.

[257] G. C. Psaltakis, "Phase and amplitude collective modes of an incommensurate spin density wave," *Solid State Commun.*, vol. 51, pp. 535–538, 1984. DOI: 10.1016/0038-1098(84)91028-7.

[258] T. Mertelj, L. Stojchevska, N. D. Zhigadlo, J. Karpinski, and D. Mihailovic, "Normal state bottleneck and nematic fluctuations from femtosecond quasiparticle relaxation dynamics in Sm(Fe,Co)AsO," *Phys. Rev. B - Condens. Matter Mater. Phys.*, vol. 87, pp. 1–6, 2013, ISSN: 10980121. DOI: 10.1103/PhysRevB.87.174525. arXiv: 1304.2866.

[259] P. Kusar, V. Kabanov, J. Demsar, T. Mertelj, S. Sugai, and D. Mihailovic, "Controlled vaporization of the superconducting condensate in cuprate superconductors by femtosecond photoexcitation," *Physical Review Letters*, vol. 101, no. 22, p. 227 001, 2008.

[260] J. Herrero-Martín, V. Scagnoli, C. Mazzoli, Y. Su, R. Mittal, Y. Xiao, T. Brueckel, N. Kumar, S. Dhar, A. Thamizhavel, and L. Paolasini, "Magnetic structure of $EuFe_2As_2$ as determined by resonant x-ray scattering," *Phys. Rev. B*, vol. 80, pp. 1–5, 2009, ISSN: 1098-0121. DOI: 10.1103/PhysRevB.80.134411.

[261] T. Mertelj, A. Ošlak, J. Dolinšek, I. R. Fisher, V. V. Kabanov, and D. Mihailovic, "Fine structure in the electronic density of states near the fermi energy of Al-Ni-Co decagonal quasicrystal from ultrafast time-resolved optical reflectivity," *Phys. Rev. Lett.*, vol. 102, no. 8, p. 86 405, 2009, ISSN: 00319007. DOI: 10.1103/PhysRevLett.102.086405.

[262] Y. Zhang, C. He, Z. R. Ye, J. Jiang, F. Chen, M. Xu, Q. Q. Ge, B. P. Xie, J. Wei, M. Aeschlimann, X. Y. Cui, M. Shi, J. P. Hu, and D. L. Feng, "Symmetry breaking via orbital-dependent reconstruction of electronic structure in detwinned nafeas," *Phys. Rev. B*, vol. 85, p. 085 121, 8 Feb. 2012. DOI: 10.1103/PhysRevB.85.085121. [Online]. Available: http://link.aps.org/doi/10.1103/PhysRevB.85.085121.

[263] M. Beck, M. Klammer, S. Lang, P. Leiderer, V. V. Kabanov, G. N. Gol'Tsman, and J. Demsar, "Energy-gap dynamics of superconducting NbN thin films studied by time-resolved terahertz spectroscopy," *Phys. Rev. Lett.*, vol. 107, no. 17, pp. 19–22, 2011, ISSN: 00319007. DOI: 10.1103/PhysRevLett.107.177007. arXiv: 1102.5616.

[264] Y. Zhang, Z. R. Ye, Q. Q. Ge, F. Chen, J. Jiang, M. Xu, B. P. Xie, and D. L. Feng, "Nodal superconducting gap structure in ferropnictide superconductor $BaFe_2(As_{0.7}P_{0.3})_2$," *Nat. Phys.*, vol. 8, no. March, p. 6, 2011, ISSN: 1745-2473. DOI: 10.1038/nphys2248. arXiv: 1109.0229. [Online]. Available: http://arxiv.org/abs/1109.0229.

[265] I. Madan, T. Kurosawa, Y. Toda, M. Oda, T. Mertelj, P. Kusar, and D. Mihailovic, "Separating pairing from quantum phase coherence dynamics above the superconducting transition by femtosecond spectroscopy.," *Sci. Rep.*, vol. 4, p. 5656, 2014, ISSN: 2045-2322. DOI: 10.1038/srep05656. arXiv: arXiv:1404.2707v1.

[266] P. W. Anderson and H. Suhl, "Spin alignment in the superconducting state," *Phys. Rev.*, vol. 116, no. 3, pp. 898–900, 1959, ISSN: 0031899X. DOI: 10.1103/PhysRev.116.898.

[267] A. Blachowski, K. Ruebenbauer, J. Zukrowski, Z. Bukowski, K. Rogacki, P. J. W. Moll, and J. Karpinski, "Interplay between magnetism and superconductivity in $EuFe_{2-x}Co_xAs_2$ studied by ^{57}Fe and ^{151}Eu Mossbauer spectroscopy," *Phys. Rev. B*, vol. 174503, p. 13, 2011, ISSN: 1098-0121. DOI: 10.1103/PhysRevB.84.174503. arXiv: 1107.5271. [Online]. Available: http://arxiv.org/abs/1107.5271.

[268] H. S. Jeevan, D. Kasinathan, H. Rosner, and P. Gegenwart, "Interplay of antiferromagnetism, ferromagnetism, and superconductivity in $EuFe_2(As_{1-x}P_x)_2$ single crystals," *Phys. Rev. B - Condens. Matter Mater. Phys.*, vol. 83, pp. 1–6, 2011, ISSN: 10980121. DOI: 10.1103/PhysRevB.83.054511. arXiv: arXiv:1011.4481v1.

[269] Z. Ren, Z. Zhu, S. Jiang, X. Xu, Q. Tao, C. Wang, C. Feng, G. Cao, and Z. Xu, "Antiferromagnetic transition in $EuFe_2As_2$: A possible parent compound for superconductors," *Phys. Rev. B - Condens. Matter Mater. Phys.*, vol. 78, pp. 2–5, 2008, ISSN: 10980121. DOI: 10.1103/PhysRevB.78.052501. arXiv: 0806.2591.

[270] Y. Yin, M. Zech, T. L. Williams, X. F. Wang, G. Wu, X. H. Chen, and J. E. Hoffman, "Scanning tunneling spectroscopy and vortex imaging in the iron pnictide superconductor $BaFe_{1.8}Co_{0.2}As_2$," *Phys. Rev. Lett.*, vol. 102, no. March, pp. 1–4, 2009, ISSN: 00319007. DOI: 10.1103/PhysRevLett.102.097002. arXiv: arXiv:0810.1048v2.

[271] M. Fauré and A. I. Buzdin, "Domain structure in a superconducting ferromagnet," *Phys. Rev. Lett.*, vol. 94, no. May, pp. 2–5, 2005, ISSN: 00319007. DOI: 10.1103/PhysRevLett.94.187202.

[272] Y. Xiao, Y. Su, M. Meven, R. Mittal, C. M. N. Kumar, T. Chatterji, S. Price, J. Persson, N. Kumar, S. K. Dhar, A. Thamizhavel, and T. Brueckel, "Magnetic structure of $EuFe_2As_2$ determined by single crystal neutron diffraction," *Phys. Rev. B*, p. 7, 2009. DOI: 10.1103/PhysRevB.80.174424. arXiv: 0908.3142. [Online]. Available: http://arxiv.org/abs/0908.3142.

[273] Y. Xiao, Y. Su, S. Nandi, S. Price, B. Schmitz, C. M. N. Kumar, R. Mittal, T. Chatterji, N. Kumar, S. K. Dhar, A. Thamizhavel, and T. Brückel, "Anomalous in-plane magnetoresistance in a $EuFe_2As_2$ single crystal: Evidence of strong spin-charge-lattice coupling," *Phys. Rev. B - Condens. Matter Mater. Phys.*, vol. 85, pp. 1–7, 2012, ISSN: 10980121. DOI: 10.1103/PhysRevB.85.094504.

[274] Z. Guguchia, J. Roos, A. Shengelaya, S. Katrych, Z. Bukowski, S. Weyeneth, F. Murányi, S. Strässle, A. Maisuradze, J. Karpinski, and H. Keller, "Strong coupling between Eu^{2+} spins and Fe_2As_2 layers in $EuFe_{1.9}Co_{0.1}As_2$ observed with NMR," *Phys. Rev. B - Condens. Matter Mater. Phys.*, vol. 83, pp. 1–7, 2011, ISSN: 10980121. DOI: 10.1103/PhysRevB.83.144516. arXiv: 1010.5948.

[275] P. Dorenbos, "Energy of the first $4f^7$->$4f^6$ $5d$ transition of Eu^{2+} in inorganic compounds," *J. Lumin.*, vol. 104, pp. 239–260, 2003, ISSN: 00222313. DOI: 10.1016/S0022-2313(03)00078-4.

[276] J. Feinleib, W. J. Scouter, J. O. Dimmock, J. Hanus, and T. B. Reed, "Spin polarized splittings in the temperature dependent reflectance of EuO," *Phys. Rev. Lett.*, vol. 22, no. 25, pp. 2–5, 1969. DOI: http://dx.doi.org/10.1103/PhysRevLett.22.1385.

[277] J. H. Chu, J. G. Analytis, D. Press, K. De Greve, T. D. Ladd, Y. Yamamoto, and I. R. Fisher, "In-plane electronic anisotropy in underdoped $Ba(Fe_{1-x}Co_x)_2As_2$ revealed by partial detwinning in a magnetic field," *Phys. Rev. B - Condens. Matter Mater. Phys.*, vol. 81, pp. 1–5, 2010, ISSN: 10980121. DOI: 10.1103/PhysRevB.81.214502. arXiv: arXiv:0911.3878v1.

[278] I. Nowik, I. Felner, Z. Ren, G. H. Cao, and Z. A. Xu, "Coexistence of ferromagnetism and superconductivity: magnetization and Mossbauer studies of $EuFe(As_{1-x}P_x)$," *J. Phys. Condens. Matter*, vol. 23, p. 065 701, 2011, ISSN: 0953-8984. DOI: 10.1088/0953-8984/23/6/065701.

[279] F. Hansteen, A. Kimel, A. Kirilyuk, and T. Rasing, "Femtosecond photomagnetic switching of spins in ferrimagnetic garnet films," *Phys. Rev. Lett.*, vol. 95, no. July, pp. 1–4, 2005, ISSN: 00319007. DOI: 10.1103/PhysRevLett.95.047402.

[280] A. M. Kalashnikova, A. V. Kimel, R. V. Pisarev, V. N. Gridnev, P. A. Usachev, A. Kirilyuk, and T. Rasing, "Impulsive excitation of coherent magnons and phonons by subpicosecond laser pulses in the weak ferromagnet $FeBO_3$," *Phys. Rev. B - Condens. Matter Mater. Phys.*, vol. 78, pp. 1–21, 2008, ISSN: 10980121. DOI: 10.1103/PhysRevB.78.104301.

[281] B. Cooper, "Magnetoelastic effects and the magnetic properties of rare-earth metals," *Phys. Rev. Lett.*, vol. 19, Jun. 1967, ISSN: 0031-9007. [Online]. Available: http://link.aps.org/doi/10.1103/PhysRevLett.22.1320.

[282] E. A. Turov, Tybulewicz, A., and S. Chomet, "Physical properties of magnetically ordered crystals.," *Phys. Prop. Magn. ordered Cryst.*, vol. 23, pp. 184–184, 1965, ISSN: 0365-110X. DOI: 10.1107/S0365110X67004529.

[283] R. R. Subkhangulov, A. B. Henriques, P. H. O. Rappl, E. Abramof, T. Rasing, and A. V. Kimel, "All-optical manipulation and probing of the $d - f$ exchange interaction in EuTe.," *Sci. Rep.*, vol. 4, p. 4368, 2014, ISSN: 2045-2322. DOI: 10.1038/srep04368. [Online]. Available: http://www.nature.com/srep/2014/140324/srep04368/pdf/srep04368.pdf.

[284] R. Iida, T. Satoh, T. Shimura, K. Kuroda, B. A. Ivanov, Y. Tokunaga, and Y. Tokura, "Spectral dependence of photoinduced spin precession in $DyFeO_3$," *Phys. Rev. B - Condens. Matter Mater. Phys.*, vol. 84, pp. 1–11, 2011, ISSN: 10980121. DOI: 10.1103/PhysRevB.84.064402. eprint: 1009.4743.

[285] I. Nowik, I. Felner, Z. Ren, G. H. Cao, and Z. A. Xu, "^{57}Fe and ^{151}Eu Mossbauer spectroscopy and magnetization studies of $Eu(Fe_{0.89}Co_{0.11})_2As_2$ and $Eu(Fe_{0.9}Ni_{0.1})_2As_2$," *New J. Phys.*, vol. 13, 2011, ISSN: 13672630. DOI: 10.1088/1367-2630/13/2/023033.

[286] B. R. Cooper, R. J. Elliott, S. J. Nettel, and H. Suhl, "Theory of magnetic resonance in the heavy rare-earth metals," *Phys. Rev.*, vol. 127, no. 1, pp. 57–68, 1962, ISSN: 0031899X. DOI: 10.1103/PhysRev.127.57.

[287] R. J. Cooper and B. R. Elliott, "Spin-wave theory of magnetic resonance in spiral spin structures: effect of an applied field," *Phys. Rev.*, vol. 153, no. 654, 1963. DOI: http://dx.doi.org/10.1103/PhysRev.131.1043.

Bibliography

Original scientific article

1. Anna Pogrebna, Tomaz Mertelj, Natasa Vujicic, Guozhong Cao, Z. A. Xu, Dragan Mihailovic, Coexistence of ferromagnetism and superconductivity in iron based pnictides: a time resolved magnetooptical study, Scientific reports **5** (2015).

2. Anna Pogrebna, Natasa Vujicic, Tomaz Mertelj, Tetiana Borzda, Guozhong Cao, Z. A. Xu, Jiun-Haw Chu, Ian R. Fisher, Dragan Mihailovic, Spectrally resolved femtosecond reflectivity relaxation dynamics in undoped spin-density wave 122-structure iron-based pnictides, Physical review B - Condensed matter physics **89**, no. 16 (2014).

3. Tomaz Mertelj, Natasa Vujicic Tetiana Borzda, Igor Vaskivskyi, Anna Pogrebna, Dragan Mihailovic, Multichannel photodiode detector for ultrafast optical spectroscopy, Review scientific instruments **85**, no. 12 (2014).

4. Anna Pogrebna, Tomaz Mertelj, Guozhong Cao, Z. A. Xu, Dragan Mihailovic, Photoexcited Eu^{2+} spin dynamics in $EuFe_2As_2$, Optics and spectroscopy **116**, no. 6 (2014).

5. A. Pogrebna, T. Mertelj, Z. R. Ye, D. L. Feng, D. Mihailovic, Superconducting gap in $BaFe_2(As_{1-x}P_x)_2$ from temperature dependent transient optical reflectivity, submitted to PRB (2015).

Published scientific conference contribution abstract (invited lecture)

1. Anna Pogrebna, Tomaz Mertelj, Natasa Vujicic, Guozhong Cao, Z. A. Xu, Z. Bukowski, Dragan Mihailovic, Femtosecond quasi-particle and Eu^{2+}-spin relaxation dymanics in $EuFe_2(As,P)_2$ and $Eu(Fe,Co)_2As_2$, Tenth International Conference on New Theories: Discoveries and Applications of Superconductors and Related Materials, Chonhqing, China (2014).

Published scientific conference contribution abstract

1. Anna Pogrebna, Tomaz Mertelj, Z. Bukowski, Dragan Mihailovic, Spin-lattice coupling in superconductive pnictide $Eu(Fe_{(1-x)}Co_x)_2As_2$, 4th International Conference on Superconductivity and Magnetism, Antalya, Turkey (2014).

2. Tomaz Mertelj, Anna Pogrebna, Ljupka Stojchevska, Dragan Mihailovic, Femtosecond quasi-particle relaxation dynamics in electron doped iron-based pnictides, 4th International Conference on Superconductivity and Magnetism, Antalya, Turkey (2014).

3. Anna Pogrebna, Z. A. Xu, Tomaz Mertelj, Dragan Mihailovic, Nothermal destruction of SDW order in iron based pnictides by ultrashort laser pulses, 5th International Conference on Photoinduced Phase Transitions and Cooperative Phenomena, Bled, Slovenija (2014).

4. Anna Pogrebna, Tomaz Mertelj, Igor Vaskivskyi, Z. A. Xu, Guozhong Cao, Dragan Mihailovic, Magnetooptical time-resolved study of Eu^{2+} spin dynamics in $EuFe_2(As_{1-x}P_x)_2$

pnictide superconductor, Moscow International Symposium on Magnetism, Moscow, M. V. Lomonosov Moscow University, Faculty of Physics (2014).

5. Anna Pogrebna, Natasa Vujicic, Tomaz Mertelj, Guozhong Cao, Z. A. Xu, Jiun-Haw Chu, Ian R. Fisher, Dragan Mihailovic, Spectrally-resolved femtosecond reflectivity relaxation dynamics in undoped SDW 122-structure iron based pnictides, International Research School and Workshop on Electronic Crystals, Cargese, France (2014).

6. Anna Pogrebna, Z. A. Xu, Guozhong Cao, Tomaz Mertelj, Ian R. Fisher, Dragan Mihailovic, The nonthermal destruction of SDW ordering in pnictides by ultrashort laser pulses, International Research School and Workshop on Electronic Crystals, Cargese, France (2014).

7. Anna Pogrebna, Tomaz Mertelj, Z. A. Xu, Guozhong Cao, Dragan Mihailovic, Non-thermal destruction and recovery of SDW order in iron based pnictides, Non-equilibrium dynamics of correlated electron-systems: latest theoretical and experimental advances: book of abstracts, Ambroz, Krvavec (2014).

8. Anna Pogrebna, Tomaz Mertelj, Natasa Vujicic, Guozhong Cao, Z. A. Xu, Dragan Mihailovic, Coexistence of ferromagnetism and superconductivity in iron based pnictides: a time resolved magnetooptical study, Non-equilibrium dynamics of correlated electron-systems: latest theoretical and experimental advances: book of abstracts, Ambroz, Krvavec (2014).

9. Anna Pogrebna, Tomaz Mertelj, Z. Ye, Dong-Lai Feng, Dragan Mihailovic, Bottleneck relaxation dynamics in photoexcited iron pnictide superconductor, Zbornik povzetkov, 9. konferenca fizikov v osnovnih raziskavah, Skofja Loka (2014).

10. Anna Pogrebna, Tomaz Mertelj, G. Caola, Z. A. Xu, Dragan Mihailovic, Photoexcited Eu^{2+} spin dynamics in $EuFe_2(As_{1-x}P_x)_2$, SLONANO 2013, Ljubljana, Slovenia (2013).

11. Anna Pogrebna, Z. A. Xu, Tomaz Mertelj, Dragan Mihailovic, Magnetooptical time-resolved study of Eu^{2+} spin dynamics in $EuFe_2(As_{1-x}P_x)_2$ pnictide superconductors, XV International Feofilov Symposium on Spectroscopy of Crystals doped with Rare Earth and Transition Metal Ions, Kazan, Russia (2013).

12. Anna Pogrebna, Natasa Vujicic, Z. A. Xu, Guozhong Cao, Tomaz Mertelj, Transient optical reflectivity in SDW iron-based pnictides: a supercontinuum-probe study, Non-equilibrium dynamics of correlated electron-systems: latest theoretical and experimental advance: book of abstracts, Ambroz, Krvavec, (2013).

13. Anna Pogrebna, Z. A. Xu, Tomaz Mertelj, Dragan Mihailovic, Migaku Oda, Optical and magnetooptical time-resolved study of spin dynamics in $EuFe_2(As_{1-x}P_x)_2$ pnictide superconductor, Workshop on Short-time Dynamics in Strongly Corelated Systems and Novel Superconductors, Bochum, Germany (2013).

14. Anna Pogrebna, Z. A. Xu, Toma¸ Mertelj, Dragan Mihailovic, Magnetooptical time-resolved study of Eu^{2+} spin dynamics in $EuFe_2(As_{1-x}P_x)_2$ pnictide superconductors, 5th Jozef Stefan International Postgraduate School Students Conference, Ljubljana, Slovenija (2013).

15. Anna Pogrebna, Igor Vaskivskyi, Z. A. Xu, Tomaz Mertelj, Dragan Mihailovic, Magnetooptical time-resolved study of Eu^{2+} spin dynamics in $EuFe_2(As_{1-x}P_x)_2$ pnictide superconductors, SLONANO 2012, Ljubljana, Slovenia (2012).

16. Anna Pogrebna, Igor Vaskivskyi, Z. A. Xu, Tomaz Mertelj, Dragan Mihailovic, Magnetooptical time-resolved study of Eu^{2+} spin dynamics in $EuFe_2(As_{1-x}P_x)_2$ pnictide superconductors, Nonequilibrium phenomena in complex matter: new observations and new theories: Ambroz, Krvavec (2012).

17. Anna Pogrebna, Igor Vaskivskyi, Z. A. Xu, Tomaz Mertelj, Dragan Mihailovic, Magnetoopticna casovno-locljiva raziskava dinamike spinov Eu^{2+} v pniktidnih superpre-

vodnikih $EuFe_2(As_{1-x}P_x)_2$, 8. konferenca fizikov v osnovnih raziskavah, Rimske Toplice (2012).

Biography

Personal information

Date of birth: August 31, 1988
e-mail: annapogrebna@gmail.com

Education

2011-2015 PhD, International postgraduate school, Ljubljana, Slovenia

2009-2011 M.Sc. at Taras Shevchenko National university of Kyiv (KNU), physics department, experimental physics division, specialization photonics. Title of diploma: Spectral properties of human blood and its components in presence of RNA

2009 Bachelor degree in physics, KNU. Title: Optical properties of cyanine dyes and its complexes with RNA

2005-2009 Taras Shevchenko National university of Kyiv (KNU), physics department, experimental physics division, specialization photonics.

1996-2006 Middle school in Khotiv, Kyiv region, Ukraine

Scientific career

2011-2015, Young Researcher, Department for Complex Matter, Jozef Stefan Institute, Ljubljana, Slovenia

Research activity

Current: Ultrafast spectroscopy of strongly correlated systems; iron pnictide superconductors.

Previous: Optical spectroscopy of RNA cyanine dye complexes.